INFORMATION TO USERS

This manuscript has been reproduced from the microfilm master. UMI films the text directly from the original or copy submitted. Thus, some thesis and dissertation copies are in typewriter face, while others may be from any type of computer printer.

The quality of this reproduction is dependent upon the quality of the copy submitted. Broken or indistinct print, colored or poor quality illustrations and photographs, print bleedthrough, substandard margins, and improper alignment can adversely affect reproduction.

In the unlikely event that the author did not send UMI a complete manuscript and there are missing pages, these will be noted. Also, if unauthorized copyright material had to be removed, a note will indicate the deletion.

Oversize materials (e.g., maps, drawings, charts) are reproduced by sectioning the original, beginning at the upper left-hand corner and continuing from left to right in equal sections with small overlaps. Each original is also photographed in one exposure and is included in reduced form at the back of the book.

Photographs included in the original manuscript have been reproduced xerographically in this copy. Higher quality 6" x 9" black and white photographic prints are available for any photographs or illustrations appearing in this copy for an additional charge. Contact UMI directly to order.

UMI

A Bell & Howell Information Company
300 North Zeeb Road, Ann Arbor MI 48106-1346 USA
313/761-4700 800/521-0600

Downloaded from SHAREOK. Persistent Handle URL: https://hdl.handle.net/11244/5563

THE UNIVERSITY OF OKLAHOMA

GRADUATE COLLEGE

AN EXPERIMENTAL STUDY OF FIBER MOTION AND NONWOVEN WEBS IN MELT BLOWING

A DISSERTATION

SUBMITTED TO THE GRADUATE FACULTY

in partial fulfillment of the requirements for the

degree of

DOCTOR OF PHILOSOPHY

by

RAJEEV CHHABRA

Norman, Oklahoma

1997

UMI Number: 9812252

UMI Microform 9812252
Copyright 1998, by UMI Company. All rights reserved.

This microform edition is protected against unauthorized copying under Title 17, United States Code.

UMI
300 North Zeeb Road
Ann Arbor, MI 48103

© Copyright by RAJEEV CHHABRA 1997
All Rights Reserved.

AN EXPERIMENTAL STUDY OF FIBER MOTION AND NONWOVEN WEBS IN MELT BLOWING

A Dissertation Approved for the

SCHOOL OF CHEMICAL ENGINEERING AND MATERIALS SCIENCE

BY

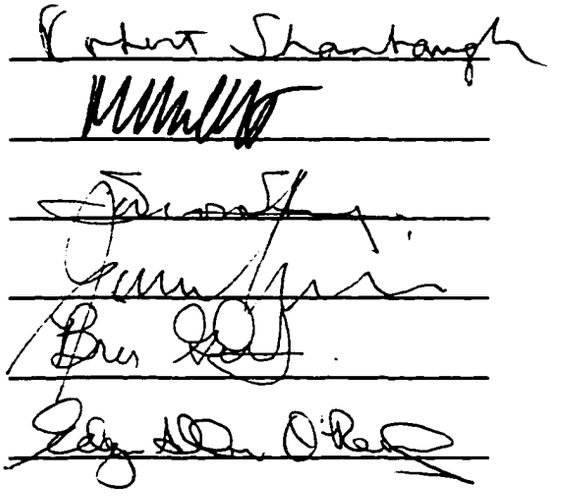

मातृ देवो भवः। पितृ देवो भवः। आचार्यो देवो भवः।

"Mother is like God, father is like God, teacher is like God."

Dedicated to My Parents and Teachers

Acknowledgements

I would like to dedicate this dissertation to my parents and teachers (from Elementary school to Graduate school), and all those who have taught me different things in life so far. I am thankful to all my friends who were there for me during all the years of my learning. To start with, I would like to sincerely thank -

Dr. Robert L. Shambaugh, for being a great research advisor and a teacher, for his thoughtful suggestions, intelligent and interesting discussions, and financial support over the last five years. I have deepest gratitude for him for giving me an opportunity to do the research I always wanted;

Dr. Faruk Civan, for being a member of my committee, and teaching me Advanced Engineering Analysis for Digital Computers course;

Dr. Simon Fung at 3M, for being a member of my committee, giving me useful suggestions, and loaning the hot-wire anemometer;

Dr. M. U. Nollert, for being a member of my committee, and teaching me Engineering Rate Operations course;

Dr. B. P. Grady and Dr. E. O'Rear III, for being members of my committee;

Dr. K. Parthasarthy, for teaching me how to use a hot-wire anemometer and the Turbulence course;

Dr. R. Harrison, for teaching me Chemical Engineering Design course and helping me as a co-instructor for Chemical Engineering Design Laboratory course;

Dr. S. Lakshmivarahan, Dr. L. Lee, Dr. L. Lobban, and Dr. D. Trytten, for teaching me various courses at the University of Oklahoma;

Dr. J. N. Kapur, for enlightening me with Kullback-Leibler principle of information theory;

Dr. R. Mallinson and Mr. Jay Liang of ECAS lab, for letting me use the IBM/RISC computer workstations;

Larry Isley, for the putting in countless hours in building equipment essential to my research, thoughtful and intelligent discussions, and for being a friend;

Thor Sheffield, for helping me in processing photographic prints, maintaining lab computers, and being a friend;

Vishal Bansal, for the insightful suggestions and discussions useful for my research, being my room-mate for last five years, and for his friendship;

Vishal Bansal, John Jacob, Anil Shenoy, and Anne de Rovere for reviewing different parts of this dissertation;

Manoj Tyagi and Uday Shivaswamy, for teaching me various skills to work with the melt blowing equipment and LDV at the Center for Polymer and Fiber Research. Brian Tate, Mike Hankinson, Steve Kelley, Anthony Harpham, Lance Canaday, and Anne de Rovere for being great colleagues. I have enjoyed working with you;

Shailesh Ekbote, Atul Joshi, Sachin Deshpande, and Balaram Bollapragada, for giving me an objective viewpoint of my research, and for being great friends;

Sameer Kalucha, Navin Chaddha, Puneet Suri, Bala Gadiyar, Vishal Singal, Sushant Parti, Sandeep Verma, Gurinder Singh, Uday Malhan, John Jacob, Aravind Salecha, Rohit Panse, Bhanu Gunturi, Firoz Ghadiali, Naval Goel, Nagendra Shivakumar, Sanjay Kunapulli, Tahir Munawar, Harry, Rashmi, Aishwarya, and Bhvya for your moral support and great friendship that has enriched my life;

Dr. V. P. Sharma for teaching me the fundamentals of science and mathematics during my high school years;

Kim Channer, Robin, Bob, and Nick Chaffee, for their emotional support and being my family in the United States of America;

My aunt Kailash Sharma and Dr. V. P. Sharma, for being a constant source of inspiration and encouragement;

My mother Santosh Chhabra, my father Sudarshan Chhabra, my sister Beenu, my brother-in-law Ajay, and most of all my niece Apoorva, for being the greatest family, encouraging me, and supporting me all the time. I could not have done this without you.

Table of Contents

Acknowledgements v

Table of Contents vii

List of Illustrations xi

List of Tables xx

Abstract xxi

Chapter 1 1
INTRODUCTION
1.1 Overview of Melt Blowing 1
1.1.1 The Melt Blowing Process 2
1.1.2 Background 5
1.1.3 Melt Blowing Models 5
1.1.4 Air Drag in Melt Blowing 6
1.1.5 Air Velocity and Temperature Flow Fields 7
1.2 Objectives 7
1.3 References 11

Chapter 2 14
EXPERIMENTAL MEASUREMENTS OF FIBER THREADLINE VIBRATIONS IN THE MELT BLOWING PROCESS
2.1 Abstract 14
2.2 Introduction 15
2.3 Experimental Equipment 17
2.4 Experimental Techniques 19
2.4.1 Cone Diameter Measurements with Multiple Image Photography 19

2.4.2 Cone Diameter Measurements with Laser Doppler Velocimetry 20
2.4.3 Fiber Threadline Frequency Measurements 22
2.5 Results and Analysis 23
2.5.1 Photographic Measurements of Cone Diameter 23
2.5.2 LDV Measurements of Cone Diameter 25
2.5.3 LDV Measurements of Fiber Frequency 26
2.5.4 Superposition of the Response Correlation (h*) on the Fiber Cone 29
2.5.5 Interpretation of LDV Data 32
2.6 Conclusions 37
2.7 Nomenclature 39
2.8 References 41

Chapter 3 72
THE STOCHASTIC NATURE OF FIBER THREADLINE MOTION IN THE MELT BLOWING PROCESS
3.1 Abstract 72
3.2 Introduction 73
3.3 Literature Review 74
3.4 The Statistics of Fiber Position 79
3.4.1 Mathematical Formulation 79
3.4.1.1 Bivariate Normal Distribution 85
3.4.2 Fitting the Data to the Distribution Function 93
3.4.3 Experimental Equipment 96
3.4.4 Experimental Technique 97
3.5 Results 100
3.6 Conclusions 106
3.7 Nomenclature 110
3.8 References 113

Chapter 4 146
AN ENTROPIC MEASURE OF SPATIAL FIBER DISTRIBUTION IN A MELT-BLOWN WEB
4.1 Abstract 146
4.2 Introduction 147

4.3 Literature Review 149
4.4 Technique Development 151
4.4.1 Origin 152
4.4.2 Mathematical Formulation 155
4.4.2.1 Evaluation of the Fiber Presence Probability Density Function of the Sample Web Image 155
4.4.2.2 Evaluation of Fiber Presence Probability Density Function using Information Entropy 166
4.4.3 Web Distribution in Multiple Filament Melt Blowing .. 178
4.5 Technique Implementation 180
4.5.1 Experimental Details 180
4.5.2 Data Analysis 182
4.6 Results 186
4.6.1 Effect of z Position on the Spread of the Web Distribution 187
4.6.2 Effect of Process Variables on the Spread of the Web Distribution 188
4.6.3 Effect on the Orientation Angle of the Web 192
4.7 Conclusions 194
4.8 Nomenclature 197
4.9 References 202

Chapter 5 232
AIR TURBULENCE STRUCTURE IN MELT BLOWING
5.1 Overview 232
5.2 Literature Review 238
5.3 Experimental Details 239
5.3.1 Experimental Equipment 239
5.3.2 Hot-wire System Calibration Procedure 241
5.3.3 Experimental Conditions 246
5.4 Results 248
5.4.1 Definitions of Terms Used 248
5.4.2 Mean Velocity Field 250
5.4.3 Turbulence Structure of the Jet Flow 255
5.4.3.1 A Comment on the Jet Spread 259
5.4.4 Mean Velocity in Oscillating Jets 261

5.5 Conclusions and Recommendations 266
5.6 Nomenclature 270
5.7 References 272

Chapter 6 295
CONCLUSIONS AND RECOMMENDATIONS
6.1 Summary of Conclusions 295
6.2 Applications and Recommendations 298

Appendix I 301
A SUPPLEMENT TO CHAPTER 2
AI.1 LDV Settings for Amplitude and Frequency Measurements .. 301

Appendix II 307
A SUPPLEMENT TO CHAPTER 3

Appendix III 312
COMPUTER PROGRAM FOR EVALUATING THE WEB DISTRIBUTION USING ENTROPIC ANALYSIS

List of Illustrations

Figure 1.1 Typical setup of single-filament melt blowing 4

Figure 2.1 Cross-section of the melt blowing die used in the experiments. 43

Figure 2.2a The photographic setup used to measure fiber cone diameter in the x direction. 44

Figure 2.2b LDV setup used to measure fiber cone diameter along the y axis and fiber crossover frequency across the x axis 45

Figure 2.3 Top view of the photographic setup used to measure cone diameter 46

Figure 2.4 The LDV arrangement for measuring cone diameter along the x axis and crossover frequency across the y axis. The two laser beams cross in the x-y plane, the probe axis is aligned parallel to the y axis, and the fringes are parallel to the y-z plane. 47

Figure 2.5 The LDV arrangement for measuring cone diameter along the y axis and crossover frequency across the x axis. The two laser beams cross in the x-y plane, the probe axis is aligned parallel to the x axis, and the fringes are parallel to the x-z plane. 48

Figure 2.6 A typical multiple image photograph of the x axis fiber cone from z=1 to z=8 cm. The operating conditions were as follows: Q_p=0.4 cm^3/min, T_p=350°C, v_{jo}=30.9m/s, and T_a=320°C. 49

Figure 2.7 A multiple image photograph of the y axis fiber cone from z = 1 to z = 8 cm. The operating conditions were the same as for Figure 2.6. 50

Figure 2.8 A comparison between the x axis and the y axis cone diameters measured using multiple image photography. Each data point represents the average from six replicate photographs, and each error bar represents a range of ± one standard deviation. 51

Figure 2.9 The x axis cone diameters measured via both LDV and multiple image photography. 52

Figure 2.10 The y axis cone diameters measured via both LDV and multiple image photography. 53

Figure 2.11 The effect of air velocity on the x axis fiber cone diameter. Each data point represents the average of six independent LDV measurements, and each error bar represents a range of ± one standard deviation. 54

Figure 2.12 The average fiber angle determined from photographs. For the y axis measurements, the angle corresponds to α. Each data point represents the average of about 50 angle measurements, and each error bar represents a range of ± one standard deviation. 55

Figure 2.13 Effect of measuring volume position on data/passage. The solid line is predicted from the fitted correlation of eq 2.3. 56

Figure 2.14 A qualitative comparison between the actual number of fiber passages and the passages measured by the laser mv. 57

Figure 2.15 Superposition of the fiber density distribution function f(x) and the laser measuring volume response function h. 58

Figure 2.16 A comparison of corrected crossover frequencies per unit length across x and y axes at z = 10 cm. 59

Figure 2.17 The fiber crossover frequency per unit length across the x axis. . 60

Figure 2.18 The fiber crossover frequency per unit length across the y axis. . 61

Figure 2.19 Effect of polymer flow rate on crossover frequency per unit length across the x axis at z = 10 cm. 62

Figure 2.20 Effect of polymer flow rate on crossover frequency per unit length across the y axis at z = 10 cm. 63

Figure 2.21 Effect of polymer temperature on crossover frequency per unit length across the x axis at z = 10 cm. 64

Figure 2.22 Effect of polymer temperature on crossover frequency per unit length across the y axis at z = 10 cm. 65

Figure 2.23 Effect of air velocity on crossover frequency per unit length across the x axis at z = 10 cm. 66

Figure 2.24 Effect of air velocity on crossover frequency per unit length across the y axis at z = 10 cm. 67

Figure 2.25 Effect of air temperature on crossover frequency per unit length across the x axis at z = 10 cm. 68

Figure 2.26 Effect of air temperature on crossover frequency per unit length across the y axis at z = 10 cm. 69

Figure 2.27 The total crossover frequency as a function of z when v_{jo} = 17.6 m/s 70

Figure 2.28 The total crossover frequency as a function of z when v_{jo} = 30.9m/s 71

Figure 3.1 Cross section of the melt blowing die used in the experiments. The origin of the coordinate system, which is shown separately, lies at the polymer orifice of the die. 119

Figure 3.2 Gridding used to group the fiber position (x, y) data. Frequencies are shown to lie at the center of each grid cell. The fiber distribution is contained in the shown ellipse. 120

Figure 3.3 Top view of the experimental setup used to measure the fiber position data. 121

Figure 3.4 Root mean square deviation between the experimental data and the fitted distribution for various values of z below the die. 122

Figure 3.5 Surface plot of experimental fiber density distribution at z = 20 mm. 123

Figure 3.6 Surface plot of fitted bivariate normal distribution at z = 20 mm. 124

Figure 3.7 Surface plot of experimental fiber density distribution at z = 40 mm. 125

Figure 3.8 Surface plot of fitted bivariate normal distribution at z = 40 mm. 126

Figure 3.9 Surface plot of experimental fiber density distribution at z = 60 mm 127

Figure 3.10 Surface plot of fitted bivariate normal distribution at z = 60 mm. 128

Figure 3.11 Surface plot of experimental fiber density distribution at z = 80 mm. 129

Figure 3.12 Surface plot of fitted bivariate normal distribution at z = 80 mm. 130

Figure 3.13 Contour plots showing the experimental and fitted bivariate normal distribution at z = 20 mm. The direction of the arrow shows that the major axis of the elliptical pattern is oriented at 20.8° with respect to the x axis. 131

Figure 3.14 Contour plots showing the experimental and fitted bivariate normal distribution at z = 40 mm. The direction of the arrow shows that the major axis of the elliptical pattern is oriented at 5.5° with respect to the x axis. 132

Figure 3.15 Contour plots showing the experimental and fitted bivariate normal distribution at z = 60 mm. The direction of the arrow shows that the major axis of the elliptical pattern is oriented at -73.4° with respect to the x axis. 133

Figure 3.16 Contour plots showing the experimental and fitted bivariate normal distribution at z = 80 mm. The direction of the arrow shows that the major axis of the elliptical pattern is oriented at 9.9° with respect to the x axis. 134

Figure 3.17 Surface plot showing the auto-correlation r_{xx} between the x components of the fiber positions in the xy planes at different z levels below the die. 135

Figure 3.18 Surface plot showing the auto-correlation r_{yy} between the y components of the fiber positions in the xy planes at different z levels below the die. 136

Figure 3.19 Correlation coefficient between the x and y components of fiber positions at different z levels below the die. 137

Figure 3.20 Orientation angle of the fiber distribution ellipse at different z levels below the die. 138

Figure 3.21 Fourier orientation angle amplitude spectra as a function of spatial separation (spatial period) along the z direction. 139

Figure 3.22 Variation in the x direction standard deviation of the fiber distribution with z position. 140

Figure 3.23 Variation in the y direction standard deviation of the fiber distribution with z position. 141

Figure 3.24 Comparison of spreading characteristics of the fiber distribution and the air jets in the z direction. 142

Figure 3.25 Variation in the x and y direction mean positions of the fiber threadline with z position below the die. 143

Figure 3.26 Top view image of the fiber pattern formed on a black wire-mesh screen placed at $z = 300$ mm. The white lines shown in the image correspond to the digitally overlaid coordinate axes. 144

Figure 3.27 Side view image of the fiber collected on a black wire-mesh screen placed at $z = 300$ mm. The white lines in the image correspond to the coordinate axes which were set on the screen before fiber collection. 145

Figure 4.1 Typical top-view image of a single filament melt-blown web. The two orthogonal white lines, corresponding to the coordinate axes, were digitally overlaid on the image. 208

Figure 4.2 Cross-section of the melt blowing die used in the experiments. The origin of the coordinate system, which is shown separately, lies at the polymer orifice of the die. 209

Figure 4.3 Typical surface plot of the observed (web image) spatial order distribution. 210

Figure 4.4 Typical surface plot of the model spatial order distribution. 211

Figure 4.5 Typical surface plot of the observed (web image) distribution of fibers in a single filament melt-blown web. 212

Figure 4.6 Typical surface plot of the model fiber presence distribution in a single filament melt-blown web. 213

Figure 4.7 Variation in the standard deviations of the web distribution with the z position. 214

Figure 4.8 Comaprison of spreading characteristics of the web distribution and the air jets in the z direction. 215

Figure 4.9 Fiber diameter at different z positions below the melt blowing die. 216

Figure 4.10 Variation in the standard deviations of the web distribution with nominal air jet velocity at z = 300 mm. 217

Figure 4.11 Effect of nominal air jet velocity on the fiber diameter at z = 300 mm 218

Figure 4.12 Centerline air velocity profile below the die. 219

Figure 4.13 Effect of discharge air temperature on the fiber diameter at z = 300 mm. 220

Figure 4.14 Variation in the standard deviations of the web distribution with discharge air temperature at z = 300 mm. 221

Figure 4.15 Effect of polymer mass flow rate on the fiber diameter at z = 300 mm. 222

Figure 4.16 Variation in the standard deviations of the web distribution with polymer mass flow rate z = 300 mm. 223

Figure 4.17 Effect of discharge polymer temperature on the fiber diameter at z = 300 mm. 224

Figure 4.18 Variation in the standard deviations of the web distribution with discharge air temperature at z = 300 mm. 225

Figure 4.19 Variation in the web orientation angle with the z position. The solid line shown on the graph is a smooth line joining the average web orientation angles. 226

Figure 4.20 Effect of nominal air jet velocity on the web orientation angle at z = 300

mm. The solid line shown on the graph is a smooth line joining the average web orientation angles. 227

Figure 4.21 Effect of discharge air temperature on the web orientation angle at z = 300 mm. The solid line shown on the graph is a smooth line joining the average web orientation angles. 228

Figure 4.22 Effect of polymer mass flow rate on the web orientation angle at z = 300 mm. The solid line shown on the graph is a smooth line joining the average web orientation angles. 229

Figure 4.23 Effect of discharge polymer temperature on the web orientation angle at z = 300 mm. The solid line shown on the graph is a smooth line joining the average web orientation angles. 230

Figure 4.24 Effect of the fiber diameter on the spread of the web distribution. Different fiber diameters were obtained by varying the melt blowing process conditions. 231

Figure 5.1 Cross-section of the melt blowing slot die used in the experiments. The origin of the coordinate system, which is shown separately, lies at the polymer orifice of the die. 277

Figure 5.2 Structure of cross-jet mixing flow below a melt blowing slot die. 278

Figure 5.3 Top view of the die face. The z axis (not shown) is perpendicular to the plane of the drawing with positive z axis direction into the plane of the drawing 279

Figure 5.4 Development of flat velocity profiles at the end of the calibration pipe for four different air flow rates. The measurements done at other air flow rates are not shown on the figure. 280

Figure 5.5 Development of the axial mean velocity profile for seven z positions below the die. All measurements were done at y = 0 with a hot-wire anemometer. 281

Figure 5.6 Nondimensional axial mean velocity profiles for different z positions studied. 282

Figure 5.7 Dimensionless centerline axial mean velocity distribution at different z positions below the die. 283

Figure 5.8 Growth of jet half-width with increasing distance from the die. 284

Figure 5.9 Centerline axial component turbulence intensity distribution at different z positions below the die. 285

Figure 5.10 Dimensionless axial component turbulence intensity distribution across the cross-jet flow. 286

Figure 5.11 Dimensionless axial component skewness factor profile. Gaussian value of zero is shown as the dotted line on the figure. 287

Figure 5.12 Dimensionless axial component flatness factor profile. Gaussian value of 3 is shown as the dotted line on the figure. 288

Figure 5.13 Dimensionless axial component turbulent intensity distribution across the jet. For nondimensionalizing the transverse position x, Harpham and Shambaugh's (1996) equation was used to calculate the jet half-width $x_{1/2}$. .. 289

Figure 5.14 Comparison of axial mean velocity profiles of oscillating flow and continuous flow through the die slots. 290

Figure 5.15 Comparison of dimensionless axial mean velocity profiles of oscillating flow and continuous flow through the die slots. 291

Figure 5.16 Comparison of dimensionless axial component turbulence intensity profiles of oscillating flow and continuous flow through the die slots. 292

Figure 5.17 Comparison of dimensionless axial component skewness factor profiles of oscillating and continuous flows through the die slots. 293

Figure 5.18 Comparison of dimensionless axial component flatness factor profiles of oscillating and continuous flows through the die slots. 294

Figure AI.1 Effect of fiber diameter and measuring-volume position on data/passage in calibration wheel experiments. The solid and dotted lines are predicted from the fitted correlation of eq 2.3. 302

Figure AI.2 Fiber crossover frequency per unit length across the x axis for an air velocity v_{jo} = 17.6 m/s. 303

Figure AI.3 Fiber crossover frequency per unit length across the y axis for an air velocity v_{jo} = 17.6 m/s. 304

Figure AI.4 Fiber crossover frequency per unit length across the y axis for a polymer flow rate Q_p = 0.60 cm^3/min. 305

Figure AI.5 Fiber crossover frequency per unit length across the y axis for a polymer flow rate Q_p = 0.80 cm^3/min. 306

Figure AII.1 Surface plots of (a) experimental and (b) fitted fiber density distribution at z = 10 mm. 308

Figure AII.2 Surface plots of (a) experimental and (b) fitted fiber density distribution at z = 30 mm. 309

Figure AII.3 Surface plots of (a) experimental and (b) fitted fiber density distribution at z = 50 mm. 310

Figure AII.4 Surface plots of (a) experimental and (b) fitted fiber density distribution at z = 70 mm. 311

List of Tables

Table 2.1 The operating conditions used in the experiments. 42

Table 3.1 Various values of q for different values of r, s_x, and s_y 117

Table 3.2 Modified values of q for case 3, Table 3.1 118

Table 4.1 Asymmetrical 5×5 neighborhood, shown as non-shaded cells, of window (i, j) in a web image. 206

Table 4.2 The operating conditions used in the experiments 207

Table 5.1 Comparison of jet half-widths and the probe sizes used in the present study and by Harpham and Shambaugh (1996) 276

Abstract

An experimental study of fiber motion and nonwoven webs in melt blowing was done. Fiber motion was characterized in terms of the fiber vibrations - amplitude and frequency of vibrations - and the fiber position distribution. Fiber amplitude was measured with both multiple image flash photography and laser Doppler velocimetry. Fiber frequency was measured with laser Doppler velocimetry. The fiber frequency experimental results were compared to the predictions of Rao and Shambaugh model for melt blowing. The fiber amplitude results showed that the fiber cone was elliptical. The elliptical nature of the fiber cone was further confirmed with the fiber position distribution study. High speed flash photography was used to determine the fiber positions in three-dimensional space below a melt blowing die. For the planes transverse to the spinning direction, the fiber distribution was found to follow a unimodal biavriate probability distribution, and the experimental data were fit to a bivariate normal distribution. Furthermore, it was found that the fiber laydown pattern or the web distribution also follows a bivariate normal distribution. An image analysis technique, based on Kullback-Leibler information principle, was developed to evaluate the distribution of fibers in a melt-blown web. The parameters of the web distribution were correlated to the melt blowing process variables - air velocity, air temperature, polymer flow rate and polymer temperature. The web distribution was found to increase (a) linearly with the axial position below the die, and (b) for process conditions that reduced the fiber diameter. To further understand the melt blowing process, the air turbulence structure of the rectangular, inclined cross-jets was studied using a hot-wire anemometer. The axial mean velocity, turbulence intensity, skewness factor, and flatness factor profiles were determined for both continuous and oscillating flows.

An Experimental Study of Fiber Motion and Nonwoven Webs in Melt Blowing

Chapter 1

INTRODUCTION

1.1 Overview of Melt Blowing

In the nonwovens industry, melt blowing has become one of the important processes for producing fine fiber webs. The fiber diameter in commercial melt-blown webs ranges from 0.1 μm to 30 μm. Because of the fineness of fibers, melt-blown webs have a large surface area per unit weight. This property of melt-

blown webs makes them excellent filtration and absorbent materials. Currently, melt-blown webs are used in a wide variety of applications like high performance filters, medical garments, industrial wipes, geo-textiles, battery separators, hygiene products, carpets, and insulators.

1.1.1 The Melt Blowing Process

In melt blowing, the molten polymer extrudes through fine capillaries (about 500 micron) into a high velocity, hot gas jet, usually an air jet. Figure 1.1 shows a typical setup of single filament melt blowing. The aerodynamic force of the high velocity hot gas jet attenuates the molten polymer filaments to microfibers. These microfibers entangle and get captured on the collection drum to form a nonwoven web. The properties of nonwoven web depend on the fineness of fibers in web. The higher the air velocity, the larger the aerodynamic drag force on the fiber, and the more the fiber attenuates. Shambaugh (1988) has shown that the melt blowing process has three main regions of air jet exit velocity. In region I, the low air velocity region, the fiber is continuous and moves almost parallel with the air flow. Typical fiber diameters in this velocity region are ≥ 10 μm. With the increase in the air jet exit velocity, region II is reached, and the fiber becomes discontinuous and forms undesirable polymer lumps, or "shots" (typically ≥ 0.3 mm in diameter). On further increasing the air velocity, the process enters region III. In this region, fiber

shots are still present, but are much finer (≤0.3 mm in diameter). The fiber diameters in this region range from 0.1 μm to 10 μm. The decrease in fiber diameter, due to increase in air velocity, changes the fiber motion characteristics. Consequently, air jet exit velocity becomes an important parameter in studying the fiber motion. In the present work, all the experiments were done in region I of air velocity.

For a given air jet exit velocity, fiber motion varies with the distance from the die. Wu and Shambaugh (1992) defined three spatial "zones" of fiber motion at the exit of melt blowing die. Zone A is close to the die exit. The fiber motion in zone A is predominantly in the axial direction, and the fibers are predominantly oriented in the axial direction. In zone C, the fibers are almost randomly oriented. Zone B is the transition region between zone A and zone C. Furthermore, in their work involving the measurement of fiber velocities with laser Doppler velocimetry, Wu and Shambaugh described that the spatial location of the three zones of melt blowing is a function of the air velocity region. Knowledge of orientation of fibers in a zone is useful in defining the fiber motion and fiber-to-fiber contact and entanglement. In the light of this, the present work concentrates on determining the two parameters of fiber motion - fiber vibrations and fiber positions - in melt blowing, and the parameters' effect on the resulting nonwoven web.

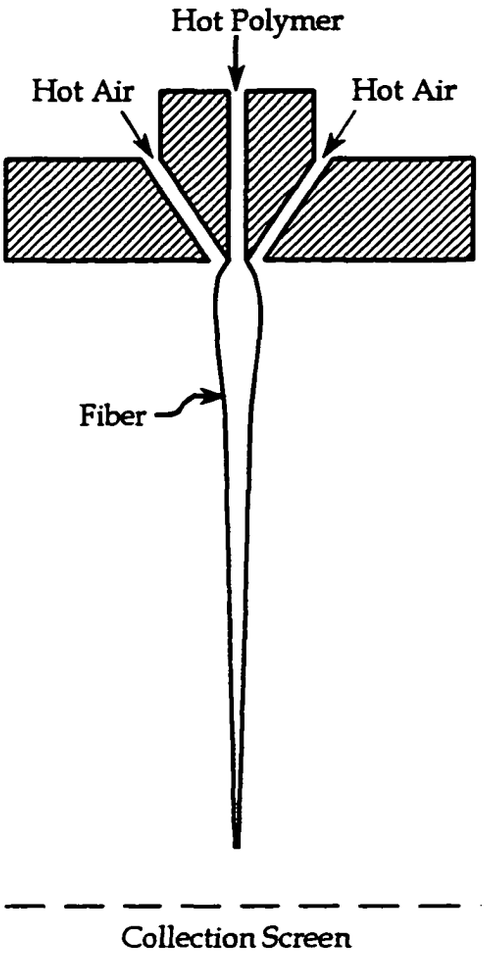

Figure 1.1 Typical setup of single-filament melt blowing

1.1.2 *Background*

The origin of melt blowing is attributed to the work of Fred W. Manning (Manning, 1946). In his method, the hot molten polymer was extruded into two consecutive air jets. The first jet heated and stretched the polymer into fiber, while the second jet further stretched the filament and directed the fiber to the collection screen. This work originated the concept of attenuating the molten polymer by high velocity gas jet. The pioneering work in setting up a melt blowing unit was done by V. A. Wente in 1950's (Wente, 1954; 1956). His unit was set up in Naval Research Laboratory to produce filters for removing radioactive contaminants formed in radioactive testing. The process was later commercialized by Exxon Corporation; they developed first commercial multiple hole slot die for producing nonwovens. Exxon has made dozens of patent claims in melt blowing, e.g., Buntin et al. (1976) and Prentice (1978). Besides Exxon, many others have produced melt blowing patents. For example, Schwarz (1983) patented a die design to improve the economics of the process in terms of air to polymer mass loading.

1.1.3 *Melt Blowing Models*

Shambaugh (1988), Kayser and Shambaugh (1990), and Milligan and Haynes (1995) have empirically modeled melt blowing to predict the fiber behavior at different

process conditions. Mathematical models of Uyttendaele and Shambaugh (1990) and Rao and Shambaugh (1993) can be used to predict the diameter, rheological stress, velocity, and temperature of the fiber. The Rao-Shambaugh model can also predict the vibrations of the fiber threadline. The Uyttendaele-Shambaugh model is one-dimensional, while the Rao-Shambaugh model is two-dimensional. Recently, Bansal (1997) extended the Rao-Shambaugh model to three dimensions. Bansal also performed online experiments to measure fiber properties in melt blowing and melt spinning.

1.1.4 Air Drag in Melt Blowing

For the mathematical modeling of melt blowing, air drag coefficient correlations were first studied by Narasimhan and Shambaugh (1986). They extended Matsui's (1976) correlation for drag coefficient in melt spinning to melt blowing. Milligan and Haynes (1987) experimentally measured the air drag acting on the fiber filament for a slot die. However, they did not evaluate a correlation for the drag coefficient which can be used in a mathematical model. Majumdar and Shambaugh (1990) experimentally measured the drag force on the fiber filament in an annular, turbulent air stream to determine the drag coefficient of a filament in a parallel flow. Later, Ju and Shambaugh (1994) developed correlations for the air drag on the fiber filament at oblique and normal angles to the flow. Their

correlation was used in the models of Rao and Shambaugh (1993) and Bansal (1997). In another work, Milligan (1991) hypothesized that the "form" drag or pressure drag is due to the "flapping" or changing shape of the fiber threadline for a melt blowing slot die.

1.1.5 Air Velocity and Temperature Flow Fields

The isothermal air velocity field of slot die were first studied by Milligan and Haynes (1987) with a hot wire anemometer. The air flow fields required for modeling the melt blowing process were experimentally measured by Uyttendaele and Shambaugh (1989) for annular dies at isothermal conditions. They used a Pitot tube for their measurements. Majumdar and Shambaugh (1991) measured velocity and temperature fields of annular jets. Mohammed and Shambaugh (1993; 1994) studied the velocity and temperature fields below a Schwarz die. Recently, Harpham and Shambaugh (1996; 1997) developed correlations for the air velocity and temperature fields below a slot die.

1.2 Objectives

The objectives of this study are (a) understanding the fiber motion in melt blowing, and (b) relating the fiber motion to melt-blown webs. Fiber motion in melt

blowing has three main parameters: fiber velocity, fiber vibrations, and fiber positions. Wu and Shambaugh (1991) measured the velocity of the fiber threadline for an annular die with laser Doppler velocimetry. Shivaswamy (1994) extended their work for the fiber motion below a slot die. Since velocity of the fiber at different process conditions has already been studied, the works presented in this study concentrate on fiber vibrations and fiber positions below a melt blowing slot die.

Rao and Shambaugh observed that fiber vibrates with a characteristic frequency in melt blowing. Tyagi and Shambaugh (1995) found that the fiber diameter could be reduced by oscillating the primary air jets of a slot die with a frequency that matches the natural frequency of the fiber. Recently, Chhabra and Shambaugh (1996) measured the amplitude and frequency of fiber vibrations below a melt blowing slot die. Their results for frequency measurements matched with the results predicted by the Rao-Shambaugh model. This work is presented in Chapter 2 of this dissertation.

Fiber positions below a melt blowing die are apparently random. Milligan (1991) concluded that, in melt blowing, the fiber motion is not periodic and exhibits the nature of a chaotic phenomena. However, in this work, it has been found that the fiber positions, while the fiber is in motion, follow a pattern. The pattern in which

fiber moves can be fitted to a probability distribution. Chapter 3 of this dissertation deals with the statistics of fiber positions below a melt blowing die. The contents of Chapter 3 have been submitted for a journal publication.

The effects of melt blowing process conditions on the morphological and mechanical properties of polypropylene webs have been studied by Lee and Wadsworth (1992). However, neither the fiber web distribution nor correlation between the process conditions and the web structure were evaluated. A detailed review of literature on the evaluation of web structure and fiber orientation in web has been presented in Chapters 3 and 4. In the work described in Chapter 3, it has been found that the fiber laydown pattern should also follow the same probability distribution as the fiber follows while in motion. Following this conclusion, a study has been done to evaluate the distribution of fibers in a melt-blown web. An image processing technique, based on information entropy, has been developed to evaluate the distribution of fibers in a single filament, melt-blown web. The statistical parameters of the web distribution have been correlated to the melt blowing process conditions. This work is presented in Chapter 4 of this dissertation. The contents of Chapter 4 will be submitted for a journal publication.

Finally, since the fiber motion is affected by the air flow fields below a melt blowing die, a one-dimensional study of the air turbulence in melt blowing has

been done. The study could not be extended to higher dimensions due to the lack of equipment. However, the conclusions obtained from the results can be taken as a starting point for two or three-dimensional study. This study is described in Chapter 5 of this dissertation.

1.3 References

Bansal, V. Online Measurement and Mathematical Modeling of Fiber Properties During the Melt Blowing and Melt Spinning Processes. Ph.D. Dissertation, University of Oklahoma, Norman, OK, 1997.

Buntin, R. R.; Keller, J. P.; Harding, J. W. Non-woven Mats by Melt Blowing. U.S. Patent 3,849,241, Nov. 19, 1974.

Chhabra, R.; Shambaugh, R. L. Experimental Measurements of Fiber Threadline Vibrations in the Melt-Blowing Process. *Ind. Eng. Chem. Res.* **1996**, *35* (11), 4366-4374.

Harpham, A. S.; Shambaugh, R. L. Flow Field of Practical Dual Rectangular Jets. *Ind. Eng. Chem. Res.* **1996**, *35* (10), 3776-3781.

Harpham, A. S.; Shambaugh, R. L. Velocity and Temperature Fields of Dual Rectangular Jets. *Ind. Eng. Chem. Res.* **1997**, *36* (9), 3937-3943.

Ju, Y. D.; Shambaugh, R. L. Air Drag on Fine Filaments at Oblique and Normal Angles to the Air Stream. *Polym. Eng. Sci.* **1994**, *34* (12), 958-964.

Kayser, J. C.; Shambaugh, R. L. The Manufacture of Continuous Polymeric Filaments by the Melt Blowing Process. *Polym. Eng. Sci.* **1990**, *30* (19), 1237-1251.

Lee, Y.; Wadsworth, L. Effects of Melt-blowing Process Conditions on Morphological and Mechanical Properties of Polypropylene Webs. *Polymer* **1992**, *33* (6), 1200-1209.

Majumdar, B.; Shambaugh, R. L. Air Drag on Filaments in the Melt Blowing Process. *J. Rheol.* **1990**, *34* (4), 591-601.

Majumdar, B.; Shambaugh, R. L. Velocity and Temperature Fields in Annular Jets. *Ind. Eng. Chem. Res.* **1991**, *30* (6), 1300-1306.

Manning, F. W. Method of Making Filter Cartridges, Abrasive Sheets, Scouring Pads, and the Like. U.S. Patent 2,411,660, Nov. 26, 1946.

Matsui, M. Air Drag on a Continuous Filament in Melt Spinning. *Trans. Soc. Rheol.* **1976**, *20* (3), 466-473.

Milligan, M. W.; Haynes, B. D. Air Drag on Monofilament Fibers - Melt Blowing Application. *ASME Ind. Appl. Fluid. Mech.* **1987**, *FED. 54*, 47-50.

Milligan, M. W. Aerodynamic Flapping Characteristics of Meltblown Fibers. *ASME Ind. Appl. Fluid. Mech.* **1991**, *FED. 132*, 1-5.

Milligan, M. W.; Haynes, B. D. Empirical Models for Melt Blowing. *J. Appl. Polym. Sci.* **1995**, *58*, 159-163.

Mohammed, A.; Shambaugh, R. L. Three-Dimensional Flow Field of a Rectangular Array of Practical Air Jets. *Ind. Eng. Chem. Res.* **1993**, *32* (5), 976-980.

Mohammed, A.; Shambaugh, R. L. Three-Dimensional Temperature Field of a Rectangular Array of Practical Air Jets. *Ind. Eng. Chem. Res.* **1994**, *33* (3), 730-735.

Narasimhan, K. M.; Shambaugh, R. L. Fiber/Gas Interaction During Melt Blowing. Society of Rheology Meeting, Tulsa, OK, 1986.

Prentice, J. S. Laminated Non-woven Sheet. U.S. Patent 4,078,124, March 7, 1978.

Rao, R. S.; Shambaugh, R. L. Vibration and Stability in the Melt Blowing Process. *Ind. Eng. Chem. Res.* **1993**, *32* (12), 3100-3111.

Schwarz, E. C. A. Apparatus and Process for Melt Blowing a Fiberforming Thermoplastic Polymer and Product Produced Thereby. U.S. Patent 4,380,570, April 19, 1983.

Shambaugh, R. L. A Macroscopic View of the Melt Blowing Process for Producing Microfibers. *Ind. Eng. Chem. Res.* **1988**, *27* (12), 2363-2372.

Shivaswamy, U. Mass Flux and Related Measurements in the Processing of Melt Blown Fibers. M.S. Thesis, University of Oklahoma, Norman, OK, 1994.

Tyagi, M. K.; Shambaugh, R. L. Use of Oscillating Gas Jets in Fiber Processing. *Ind. Eng. Chem. Res.* **1995**, *34* (2), 656-660.

Uyttendaele, M. A. J.; Shambaugh, R. L. The Flow Field of Annular Jets at Moderate Reynolds Numbers. *Ind. Eng. Chem. Res.* **1989**, *28* (11), 1735-1740.

Uyttendaele, M. A. J.; Shambaugh, R. L. Melt Blowing: General Equation Development and Experimental Verification. *AICHE J.* **1990**, *36* (2), 175-186.

Wente, V. A. Manufacture of Superfine Organic Fibers. United States Department of Commerce, Office of Technical Services, *Report No. PB 11437*, April 15, 1954.

Wente, V. A. Superfine Thermoplastic Fibers. *Ind. Eng. Chem. Res.* **1956**, *8*, 1342-1346.

Wu, T. T.; Shambaugh, R. L. Characterization of the Melt Blowing Process with Laser Doppler Velocimetry. *Ind. Eng. Chem. Res.* **1992**, *31* (1), 379-389.

Chapter 2

EXPERIMENTAL MEASUREMENTS OF FIBER THREADLINE VIBRATIONS IN THE MELT BLOWING PROCESS

(The contents of this chapter were published in the journal *Industrial & Engineering Chemistry Research*, v. 35, n. 11, 1996, pp. 4366-4374.)

2.1 Abstract

The motion of a melt blown fiber was experimentally measured. After exiting the spinning die, a melt blown fiber was found to vibrate with frequencies and amplitudes that were functions of the operating conditions (polymer flowrate, polymer temperature, air flowrate, and air temperature). Fiber amplitude was

measured with both multiple image flash photography and laser Doppler velocimetry. Fiber frequency was measured with laser Doppler velocimetry.

2.2 Introduction

In melt blowing a stream of hot polymer is extruded into a rapidly moving field of hot gas. The force of the gas upon the polymer results in the rapid attenuation of the polymer into fine filaments. The polymer filaments are collected on a screen as a nonwoven mat of fibers. Such mats have commercial value as filter media, sorbent materials, insulation, and other uses. See Shambaugh (1988) for an overview of melt blowing. Empirical models for melt blowing have been developed for annular dies (Shambaugh, 1988; Kayser and Shambaugh, 1990) and slot dies (Milligan and Haynes, 1995).

As the polymer filaments travel from the spinneret to the collection screen, the filaments exhibit vibration. The amplitude of these vibrations can be (qualitatively) observed with the naked eye. Under mild conditions (e.g., low gas velocities), the amplitude is almost imperceptible. However, as conditions become more severe (e.g., at higher gas velocities), the vibration amplitude becomes steadily larger. Shambaugh (1988) defined three regions of melt blowing which

relate to fiber breakup; these regions correspond to the severity of vibration amplitude.

Mild (small amplitude) conditions of melt blowing were modeled by Uyttendaele and Shambaugh (1990), and Kayser and Shambaugh (1990) did extensive experimental work in this area. Basically, Uyttendaele and Shambaugh assumed that the polymer stream moved in one direction only. Rao and Shambaugh (1993) extended the Uyttendaele-Shambaugh model. The Rao-Shambaugh model accounts for fiber vibrations: as conditions become more severe, the model predicts larger vibration amplitudes. The model also predicts that there are characteristic frequencies of vibrations associated with melt blowing -- i.e., though conditions along the threadline change rapidly, the threadline is a mechanical system and, as such, has a characteristic frequency of vibration.

This work involves the experimental measurement of fiber vibration amplitude and frequency. This work can be compared with the theoretical predictions of the Rao-Shambaugh model.

2.3 Experimental Equipment

The polymer was melted and pressurized with a Brabender extruder of 19.0 mm (0.75 in) diameter and 381 mm (15 in) length. After exiting the extruder, the polymer was fed to a modified Zenith pump which in turn fed a single hole melt blowing die.

Refer to Tyagi and Shambaugh (1995) for details on the polymer supply equipment; Figure 2.1 shows a cross section of the die. (Haynes and Milligan [1991] have done work with a similar single hole die.) The polymer capillary had an inside diameter of 0.407 mm and a length of 2.97 mm. The two air slots were 0.65 mm wide and 74.6 mm long. The air fields below this same melt blowing die were recently characterized by Harpham and Shambaugh (1996). The polymer used was 75 MFR (melt flow rate) Fina Dypro* polypropylene with M_w=122,500. The ranges of basic operating conditions used for the experiments are given in Table 2.1.

Multiple image photographs were taken with a Canon AE-1 camera equipped with a Tokina AT-X Macro 90 mm lens. A GenRad 1546 digital strobe provided the illumination.

The laser measurements were made with a one-dimensional, frequency shift, fiber optic LDV system assembled by TSI Incorporated. The laser was a 15-mW He-Ne laser built by Spectra Physics. A Bragg cell provided frequency shifting for measuring flow reversals. The measuring volume (mv) was produced by a backscatter probe that was at the end of a 10 meter long optic cable. This probe and cable allowed us to keep the LDV system away from the spinning machine. The small probe was 14 mm in diameter, 100 mm long, and had a working distance of 60 mm. The laser probe was mounted on a Velmex 3-D traverse system that permitted x, y, and z motions in 0.01 mm increments. Additional information on this laser system is given by Wu and Shambaugh (1992); also see Appendix I for the settings of LDV used in the experiments.

A multiple hole die as used in industry produces large numbers of filaments below the die. With such a die, it is difficult to separate the measurements (via photography and LDV) of one filament from that of another. Hence, as stated above, a single hole die was used in the experiments.

2.4 Experimental Techniques

2.4.1 Cone Diameter Measurements with Multiple Image Photography

The fiber "cone" is the volume below a melt blowing die in which a fiber travels. The apex of the cone is at the spinneret hole. Figure 2.2a shows the setup used to measure fiber cone diameter in the x direction; the coordinate system is shown in the figure. Since the cone is three-dimensional, a similar setup was used to measure cone diameter in the y direction. Figure 2.3 shows a top view of the setup shown in Figure 2.2a. The camera was focused by temporarily placing a fine metal wire directly below the die head and focusing the lens on the wire. The position of the strobe resulted in excellent illumination of the filaments. The following particulars gave photographs with excellent contrast between the filaments and the background:

Lens aperture: f/2.5 for $z \leq 10$ cm; f/4.0 for $z > 10$ cm

Exposure time: 30 seconds in darkened room

Flash rate: 300 per minute (hence, there were 150 exposures per film frame)

Field of view of lens: 12.5 cm x 8.3 cm at 25 cm

Film: Kodak T-Max 400 developed with Kodak T-Max developer

Paper: Kodak Polymax RC

To take cone photographs the camera was placed at the following five different z levels: 5.0, 7.5, 10.0, 12.5, and 15.0 cm. At each z level, 5 replicate photographs were taken. The distance between the two extreme fiber positions on the photograph was taken as the fiber cone diameter.

To measure cone size in the y direction, the positions of the camera and strobe were rotated 90° about the z-axis (see Figure 2.3). The above photographic procedure was then repeated.

2.4.2 *Cone Diameter Measurements with Laser Doppler Velocimetry*

Cone diameter measurements were also produced using laser Doppler velocimetry. This diameter measurement was based on the fact that an electronic signal occurred whenever a fiber crossed the measuring volume (mv), which is the

intersection of the two laser beams of the LDV system (see Wu and Shambaugh, 1992).

For the LDV measurements the camera and strobe (see Figure 2.2a) were replaced with the LDV probe; see Figure 2.2b. For example, consider the placement of the probe with the probe's major axis located along or parallel to the positive y axis. Consider also that the probe is rotated about its major axis such that the two laser beams lie in the x-y plane; see Figure 2.4. Now, consider the placement of the beam intersection, the mv, along the x-axis; measuring volume "A" is representative of an mv located along the x-axis. Since the fringes in this mv are parallel to the y-z plane, fiber motion in the ±x direction would be measured; this is exactly the kind of motion that occurs in a fiber cone with an x dimension. Traversing the mv along the x-axis would determine the presence or lack of fibers all along the x-axis. This fiber presence should be comparable to the presence of fibers in a cone photograph. Hence, the x-direction cone dimensions should be measurable with this technique. (The use of the measuring volume "B" will be discussed later.)

The laser system gives the data rate, which is the number of times that objects cross the mv fringes during a given time period. Since fiber crossings produce strong signals, it is easy to tell when the mv is located within the fiber-dense center of the

cone. However, the signals fall off as the mv is moved away from the center of the cone. Some arbitrary cut-off point is needed to quantify the size of the cone. The edge of the cone was arbitrarily defined as the position where the data rate fell to 10% of the maximum (cone center) value.

Figure 2.5 shows an arrangement for measuring the y dimension of the fiber cone. Here the major axis of the fiber probe is located along or parallel to the -x axis and the probe is rotated so that the laser beams both lie in the x-y plane. The fringes are thus parallel to the x-z plane. To measure the y dimension of the fiber cone, the mv is traversed along the y axis; measuring volume "A" is representative of an mv located along the y-axis.

2.4.3 *Fiber Threadline Frequency Measurements*

In their computer modeling of melt blowing, Rao and Shambaugh (1993) calculated fiber frequency by counting how many times a fiber element crossed the centerline. The frequency of vibration was found by first dividing this count by the time interval of measurement. This result was then multiplied by 1/2 (since there are two crossovers for each cycle).

In the present work, a similar line of reasoning was used to take actual measurements of crossovers. (Refer to Figure 2.4.) For the previously discussed measurement of x-direction amplitude, the fiber probe was moved in the ±x direction; measuring volume "A" illustrates a typical location of the mv for these measurements. For the measurement of crossovers of the y-z plane, the major axis of the measuring probe was kept coincident with the y axis. The probe was then translated along the y axis such that the measuring volume was always located along the y axis; measuring volume "B" is typical of these locations. The vertical fringes of these measuring volumes measured crossovers of the y-z plane.

To measure crossovers of the x-z plane, the major axis of the probe was kept coincident with the x axis. Refer to Figure 2.5. The probe was then translated along the x axis such that the measuring volume was always located along the x axis. Measuring volume "B" is typical of these locations.

2.5 Results and Analysis

2.5.1 Photographic Measurements of Cone Diameter

In the melt blowing die, the two air slots are arranged parallel to the y axis (see Figure 2.2a). Hence, the air field is not radially symmetric with respect to the z

axis. As a consequence, the fiber vibration amplitudes might not be radially symmetric. In the Cartesian system of Figure 2.2a, the amplitude in the x direction might be different than the amplitude in the y direction.

Figure 2.6 is a multiple image photograph of the fiber cone during typical melt blowing conditions. For this photograph, the camera was positioned along the +y axis as shown in Figure 2.2a. Hence, the photograph shows the fiber cone size in the x direction. Keep in mind that this photograph shows 150 separate exposures of a single threadline.

Figure 2.7 is a multiple image photograph taken with the camera located along the +x axis – i.e., from a position oriented 90° to the arrangement of Figure 2.2a. Thus, Figure 2.7 shows fiber cone size in the y-direction. As can be qualitatively observed, the cone sizes in both directions are of a similar magnitude. This implies that the cone cross-section (in a plane of constant z) is approximately circular. Thus, the non-radial symmetry of the air slots does not cause a large non-radial symmetry in the cone amplitude.

Figure 2.8 compares quantitative measurements of fiber cone diameters. The x-axis cone diameter is slightly larger than the y-axis cone diameter. Additional cone photographs (not shown) were also taken from a position 45° to both the x-axis and

the y-axis. Cone diameter measurements taken from these photographs demonstrated that, as expected, cone diameters at 45° were intermediate between the measurements taken along the x-axis and the y-axis. This suggests that the cone cross-section is an ellipse with the x-axis corresponding to the major axis of the ellipse. The ellipse becomes more circular as the distance from the die increases. This result parallels the behavior of an air field below a slot jet: a slot jet air field approaches a point source air field (which is a radially symmetric field) at large distances below the slot jet. [Refer to Harpham and Shambaugh (1996).]

2.5.2 *LDV Measurements of Cone Diameter*

Figure 2.9 shows measurements of x-axis cone diameter via LDV. For comparison, results from photography are also given. The two techniques give similar results: the slopes of the data are nearly the same and the magnitudes are fairly close. Figure 2.10 compares y-axis cone diameters determined via the two techniques. Again, the two techniques give very similar results.

As discussed by Rao and Shambaugh (1993), higher gas velocities should theoretically produce higher amplitudes. Figure 2.11 gives experimental verification of their work: as gas velocity increases, the fiber amplitude (measured via LDV) increases. Besides gas velocity, the other basic variables in melt blowing

are gas temperature, polymer temperature, and polymer throughput (Tyagi and Shambaugh, 1995). LDV measurements showed that -- for the ranges listed in Table 2.1 -- the fiber amplitude was fairly insensitive to changes in these three remaining operating variables.

2.5.3 *LDV Measurements of Fiber Frequency*

Development of an LDV Response Correlation

The Experimental Techniques section (section 2.3) described how the mv could be positioned within the fiber cone to measure fiber vibration frequency. Unfortunately, as discussed by Wu and Shambaugh (1992), there is not a one-to-one correspondence between an LDV signal and an actual crossover of the mv by a fiber. Consider the measurement of crossovers of the y-z plane (see Figure 2.4). Then, in the geometry of present experiments, Wu and Shambaugh described the following important variables which effect LDV signals:

(1) *fiber angle* α: the angle between the z direction and the projection of the fiber upon the y-z plane.

(2) *fiber angle* β: the angle between the fiber axis and the y-z plane.

(3) *fiber-mv crossover (y')*: the location within the mv where the fiber intersects the mv.

(4) *motion of fiber relative to the fringes*: the angle that the fiber motion vector makes with respect to the optical fringes of the mv.

(5) *fiber diameter (δ)*.

Similar arguments would apply for fiber crossovers of the x-z plane (see Figure 2.5).

Wu and Shambaugh found that, as long as the fiber crossed the mv, item (4) had no effect on the LDV signal. Then the LDV signal can be expressed as

$$data / passage = h(\alpha, \beta, y', \delta) \tag{2.1}$$

Wu and Shambaugh also found that the effects of the angles α and β are constant when $\alpha<40°$ and $\beta<15°$. From photographs such as Figure 2.7, the average value of α was determined for various z levels: see Figure 2.12. Obviously, $\alpha<40°$. Photographs of the x axis cone size (see Figure 2.6) were used to calculate the x axis fiber angle values shown on Figure 2.12. For small angles (e.g., angles less than

10°), these fiber angles are a good approximation for β. Hence, β<15°. In terms of the fiber zones defined by Wu and Shambaugh, Figure 2.12 represents zones A and B, not the random orientation of zone C (where the average angle is 45°).

Since angles α and β are small, the LDV signal can be represented by the simplified expression

$$data/passage = h^*(y', \delta) \tag{2.2}$$

Now, similar to the procedure followed by Wu and Shambaugh, let the h^* function be expressed empirically as

$$h^*(y', \delta) = a \cdot C \cdot D \tag{2.3}$$

where

$$C = 1 \Big/ \left[c_1 + c_2 y'^2 \exp(c_3 y') \right] \tag{2.4}$$

$$D = (\delta / 27.6)^{0.254} \tag{2.4}$$

The parameters a, c_1, c_2, and c_3 are empirical constants. These empirical constants were determined by a calibration wheel experiment wherein fibers were taped to the rim of a wheel. The wheel was rapidly rotated and the fiber was passed through the measuring volume of an LDV. The wheel (and thus fiber) speed was controlled along with the orientation of the fiber with respect to the measuring volume. Figure 2.13 resulted from this procedure. (See Wu and Shambaugh [1992] for additional details on the calibration wheel technique; also see Figure AI.1 in Appendix I for calibration experiments done with other fiber diameters.) The empirical constants were then determined by minimizing the following function with a Gauss-Newton scheme:

$$\sum_{\text{all data points}} \left[h^*(y',\delta) - \textit{data per passage at a given point} \right]^2 \qquad (2.5)$$

The best-fit values were determined to be $a = 0.987$, $c_1 = 2.457$, $c_2 = 0.489$, and $c_3 = 0.670$.

2.5.4 *Superposition of the Response Correlation (h^*) on the Fiber Cone*

Figure 2.14 illustrates the situation where the mv is moved outward in 3 mm steps from the center of the fiber cone. The fiber density in the fiber cone is highest at

the center and falls off radially. Hence, the data rate measured by the LDV system is a function of both $\dot{h}$ and of the fiber density.

Let us assume that the fiber cone density can be described by the normal distribution

$$f(x) = \frac{1}{\sqrt{2\pi\sigma^2}} e^{-(x-\mu)^2/(2\sigma^2)} \tag{2.6}$$

where μ is the mean and σ is the standard deviation of the cone density distribution.

Figure 2.15 shows the superposition of a normal fiber distribution and an arbitrarily positioned mv. Because the cone is centered over the origin of the x axis, μ=0. The center of the mv is located at x_C, and the mv limits are x_L and x_R. An arbitrary element i of length Δx lies between $x_{i,L}$ and $x_{i,R}$.

Now, for the mv, the LDV signal is

$$\begin{matrix} data \\ recorded \end{matrix} = \sum_{all\ i} \left(\begin{matrix} \%\ response\ of \\ element\ i \end{matrix} \right) \cdot \left(\begin{matrix} actual\ number \\ of\ crossovers\ of \\ element\ i \end{matrix} \right) \tag{2.7}$$

Dividing by the actual number of crossovers of the mv gives

$$\frac{\begin{matrix}\textit{data}\\ \textit{recorded}\end{matrix}}{\begin{matrix}\textit{actual number}\\ \textit{of crossovers}\\ \textit{of mv}\end{matrix}} = \sum_{\textit{all } i}\left(\begin{matrix}\textit{\% response of}\\ \textit{element } i\end{matrix}\right)\cdot\left(\frac{\begin{matrix}\textit{actual number}\\ \textit{of crossovers of}\\ \textit{element } i\end{matrix}}{\begin{matrix}\textit{actual number}\\ \textit{of crossovers}\\ \textit{of mv}\end{matrix}}\right) \tag{2.8}$$

Of the total fibers that cross the mv, the fraction that cross the element i can be expressed as

$$\frac{\textit{actual number of crossovers of element } i}{\textit{actual number of crossovers of mv}} = \frac{\left[\int_{x_{i,L}}^{x_{i,R}} f(x)\,dx\right]\cdot\left[\begin{matrix}\textit{total crossovers}\\ \textit{of cone}\end{matrix}\right]}{\left[\int_{x_L}^{x_R} f(x)\,dx\right]\cdot\left[\begin{matrix}\textit{total crossovers}\\ \textit{of cone}\end{matrix}\right]} \tag{2.9}$$

Since the percent response of element i is simply $\dot{h}$, then equation (2.3) can be used in equation (2.8). If, in addition, equation (2.9) is used in equation (2.8), the result is

$$\frac{\begin{matrix}\textit{data}\\ \textit{recorded}\end{matrix}}{\begin{matrix}\textit{actual number}\\ \textit{of crossovers}\\ \textit{of mv}\end{matrix}} = \sum_{\textit{all } i}\left[h^{\cdot}(y',\delta)\right]\cdot\left[\frac{\int_{x_{i,L}}^{x_{i,R}} f(x)\,dx}{\int_{x_L}^{x_R} f(x)dx}\right] \tag{2.10}$$

Equation (2.10) is the working equation which allows the conversion of data recorded to the actual number of fiber crossovers.

The parameters in the distribution function f(x) were determined from the cone size measurements. As stated earlier, the LDV cone size was determined by assuming that the cone boundary occurred where the fiber density fell to 10% of the centerline value. Thus, for a given cone radius x, σ=0.4660x.

For a particular set of operating conditions, the diameter δ used in equation (2.9) was found by off-line measurements of the product fiber diameter. Uyttendaele and Shambaugh (1990) determined that the final fiber diameter is reached by z = 5 cm. Hence, since all of the measurements in the present study were taken for z $\geq$ 5 cm, the use of the final (product) diameter is appropriate.

2.5.5 Interpretation of LDV Data

Figure 2.16 shows the results of using equation (2.9) to find the corrected crossover frequency from the measured data rate. Corrected frequencies are given at z = 10 cm for both crossover of the y axis and crossover of the x axis. [Equation (2.9) was used as is for calculating x axis crossover; for calculating y axis crossover, the x and f(x) in equation (2.9) were replaced with y and f(y).] Observe that the frequency

per mv length was larger across the y axis than across the x axis. Also, since the mv length is significantly less than the cone width, the ordinate value can be interpreted as the local frequency per length.

For crossovers of the x axis, Figure 2.17 shows the corrected crossover frequency at different z levels. As z increases, the center (maximum) value decreases, but crossovers occur at larger |x| values. Figure 2.18 shows similar results for crossovers of the y axis. (See Figures AI.2 through AI.5 in Appendix I for the similar experiments done at air velocity v_{jo} = 17.6 m/s and polymer mass flow rates Q_p = 0.60 and 0.80 cm^3/min.) A comparison of Figure 2.18 with Figure 2.17 shows that the frequency per length levels are higher for crossings of the y axis (as was suggested by Figure 2.16).

As discussed by Tyagi and Shambaugh (1995), there are four major operating variables in melt blowing: polymer flow rate, polymer temperature, air flow rate (or gas velocity), and air temperature. The effects of each of these variables upon the crossover frequency were examined. For x axis crossovers, Figure 2.19 shows the frequency/length as a function of polymer flowrate (Q_p). The crossover frequency stays fairly constant for Q_p values of 0.40, 0.50, and 0.60 cm^3/min, but then the frequency rises as Q_p is increased. For y axis crossovers, Figure 2.20 shows that the frequency/length values are highest at Q_p=0.60 cm^3/min. Except

for this 0.60 cm^3/min rate on Figure 2.20, the frequency/length profiles in both figures are quite similar, though the Figure 2.19 profiles are a little lower. For example, at x=0 on Figure 2.19, the average frequency/length is about 0.78 Hz/mm, while at the corresponding y=0 on Figure 2.20, the average frequency/length is about 1.20 Hz/mm.

The effect of polymer temperature (T_p) is shown in Figure 2.21 for x axis crossovers. A low polymer temperature of 300°C gave the highest frequency/length. Figure 2.22 shows the effect of polymer temperature on y axis crossovers. Again, the frequency/length is highest at 300°C.

Figures 2.23 and 2.24 show how air velocity effects the frequency/length. For the case of x axis crossover shown in Figure 2.23, the lower air velocity causes a higher frequency/length. The lower air velocity also gives a higher frequency/length for y axis crossover. However, as Figure 2.24 illustrates, the effect is much more pronounced.

Figure 2.25 shows the effect of air temperature (T_a) on frequency/length for x axis crossover. Figure 2.26 is the analogous graph for y axis crossover. A rise in air temperature T_a appears to decrease the crossover frequency. However, this

decrease is not that definitive (at least not definitive for the range of temperatures investigated).

Since, as stated previously, the frequency/length data on Figures 2.16-2.25 can be considered as local values (rates), then a particular frequency/length profile can be integrated over the cone width to give the fiber crossover frequency at a particular z level. The profiles in Figures 2.17 and 2.18 were integrated in this manner to produce Figures 2.27 and 2.28. Figure 2.27 shows results for a gas velocity of 17.6 m/s, while Figure 2.28 shows results for a gas velocity of 30.9 m/s. As suggested by earlier figures, for both Figures 2.27 and 2.28 the frequency across the y axis is higher than the frequency across the x axis. For both figures the x axis frequency is nearly constant all along the threadline, while the y axis data appear to decrease as z increases. The data scatter is probably caused by the approximations involved in calculating the points on these two figures. At v_{jo}=30.9 m/s (see Figure 2.28) the frequencies of both the x and y axis crossovers are about half as great as the corresponding frequencies at v_{jo}=17.6 m/s (see Figure 2.27).

Rao and Shambaugh (1993) developed a mathematical model for melt blowing. This model is highly complex and involves the simultaneous solution of a group of differential equations. Because of the model's complexity, some model predictions are not what one would expect from a more simplistic analysis of the

melt blowing problem. The model utilizes carefully measured input parameters such as the constants in drag force correlations (Majumdar and Shambaugh, 1990; Ju and Shambaugh, 1994).

The Rao and Shambaugh model predicts that the fiber frequency is constant along the threadline. For x axis crossovers, the present work verifies this prediction. For the more vigorous (higher frequency) y axis crossovers, the experiments in the present work showed a decrease in crossovers as z increased. However, the decrease was only about 2X, and not, for example, 10X.

For typical operating conditions, Rao and Shambaugh predicted vibration frequencies ranging from 8 to 62 Hz. In the present work, the average measured frequencies across the x axis were 14 and 6.6 Hz/mm at 17.6 and 30.9 m/s, respectively. Across the y axis, the measured frequencies were 45 and 18 Hz/mm, respectively, at 17.6 and 30.9 m/s. The correspondence between the model predictions and the measurements in the present work is very good. Rao and Shambaugh modelled an annular melt blowing die, while the present work involved a slot die. Apparently, the basic process of melt blowing -- and the associated frequencies -- is not greatly effected by whether the die is axisymmetric (annular) or two-dimensional (a slot).

As discussed earlier, the air field below the two-dimensional slot jet used in this study approximates the field of an axisymmetric jet (e.g., an annular jet) at large z values. Since the largest fiber vibrations occur at large z, then the air field configuration at large z is dominant. Thus, at large z values, the fiber motions below a slot die should be similar to the fiber motions below an annular die. Also, because the whole fiber vibrates as a unit, the vibrations at large z will effect vibrations at small z.

2.6 Conclusions

Fiber cone dimensions can be measured by either high speed photography or laser Doppler velocimetry. The results from these two techniques are comparable. The fiber cone cross-section is slightly elliptical; the x axis is the major axis in the direction across the slots. The cone cross-section becomes circular at large distances from the die.

The fiber oscillation frequency can be measured by laser Doppler velocimetry. The oscillation frequency across the y axis (in the x direction) is higher than the frequency across the x axis. For a given set of operating conditions, the frequency is roughly constant along the threadline.

The measured frequency range matches the frequency range predicted by the model of Rao and Shambaugh (1993). Knowledge of fiber oscillation and cone size can be used to predict such things as fiber laydown pattern and fiber-to-fiber contact and entanglement.

2.7 Nomenclature

a = constant in eq (2.3)

c = camera to filament distance defined in Fig 2.3, cm

c_1 = constant in eq (2.3), $mm^{½}$

c_2 = constant in eq (2.3), mm^{-2}

c_3 = constant in eq (2.3), mm^{-1}

C = quantity defined in eq (2.3)

D = quantity defined in eq (2.3)

M_w = weight average molecular weight, g/mole

Q_p = polymer flowrate, cm^3/min

s = strobe to filament distance defined in Fig 2.3, cm

T_a = air temperature, °C

T_p = polymer temperature, °C

v_{jo} = discharge air velocity, m/s

x = Cartesian coordinate defined on Fig 2.2, mm

x_C = the location of the measuring volume's center, mm

x_L = the left limit of the measuring volume, mm

x_R = the right limit of the measuring volume, mm

$x_{i,L}$ = the left limit of an element of the measuring volume, mm

$x_{i,R}$ = the right limit of an element of the measuring volume, mm

y = Cartesian coordinate defined on Fig 2.2, mm

y′ = fiber-mv crossover location, mm

z = distance below the die defined on Fig 2.2, mm

Greek Symbols

α = angle between the z direction and the projection of the fiber upon the y-z plane (or x-z plane; see text), degrees

β = angle between the fiber axis and the y-z plane (or x-z plane; see text), degrees

δ = fiber diameter, μm

θ = angle defined in Fig 2.3, degrees

μ = the mean of the cone density [see eq (2.6)], mm

σ = standard deviation of cone density [see eq (2.6)], mm

2.8 References

Harpham, A.S.; Shambaugh, R.L. The Flow Field of Practical Dual Rectangular Jets. *Ind. Eng. Chem. Res.*, **1996**, *35* (10), 3776-3781.

Haynes, B.D.; Milligan, M.W. Experimental Investigation of Melt Blowing. *INDA J. Nonwovens Res.* **1991**, *3* (4), 20-25.

Ju, Y.D.; Shambaugh, R.L. Air Drag on Fine Filaments at Oblique and Normal Angles to the Air Stream. *Polym. Eng. Sci.* **1994**, *34* (12), 958-964.

Kayser, J.C.; Shambaugh, R.L. The Manufacture of Continuous Polymeric Filaments by the Melt Blowing Process. *Polym. Eng. Sci.* **1990**, *30* (19), 1237-1251.

Majumdar, B.; Shambaugh, R.L. Air Drag on Filaments in the Melt Blowing Process. *J. Rheol.* **1990**, *34* (4), 591-601.

Milligan, M.W.; Haynes, B.D. Empirical Models for Melt Blowing. *J. Appl. Polym. Sci.* **1995**, *58*, 159-163.

Rao, R.S.; Shambaugh, R.L. Vibration and Stability in the Melt Blowing Process. *Ind. Eng. Chem. Res.* **1993**, *32* (12), 3100-3111.

Shambaugh, R.L. A Macroscopic View of the Melt Blowing Process for Producing Microfibers. *Ind. Eng. Chem. Res.* **1988**, *27* (12), 2363.

Tyagi, M.K.; Shambaugh, R.L. Use of Oscillating Gas Jets in Fiber Processing. *Ind. Eng. Chem. Res.* **1995**, *34* (2), 656-660.

Uyttendaele, M.A.J.; Shambaugh, R.L. Melt Blowing: General Equation Development and Experimental Verification. *AIChE J.*, **1990**, *36* (2), 175-186.

Wu, T.T.; Shambaugh, R.L. Characterization of the Melt Blowing Process with Laser Doppler Velocimetry. *Ind. Eng. Chem. Res.* **1992**, *31* (1), 379-389.

(1) Discharge (nominal) air velocity: 17.6, 30.9, and 39.7 m/s.
(2) Discharge air temperature: 300, 310, 320, 330, and 340°C.
(3) Polymer flow rate: 0.40, 0.50, 0.60, and 0.70 cm^3/min.
(4) Discharge polymer temperature: 300, 325, and 350°C.

Table 2.1 The operating conditions used in the experiments.

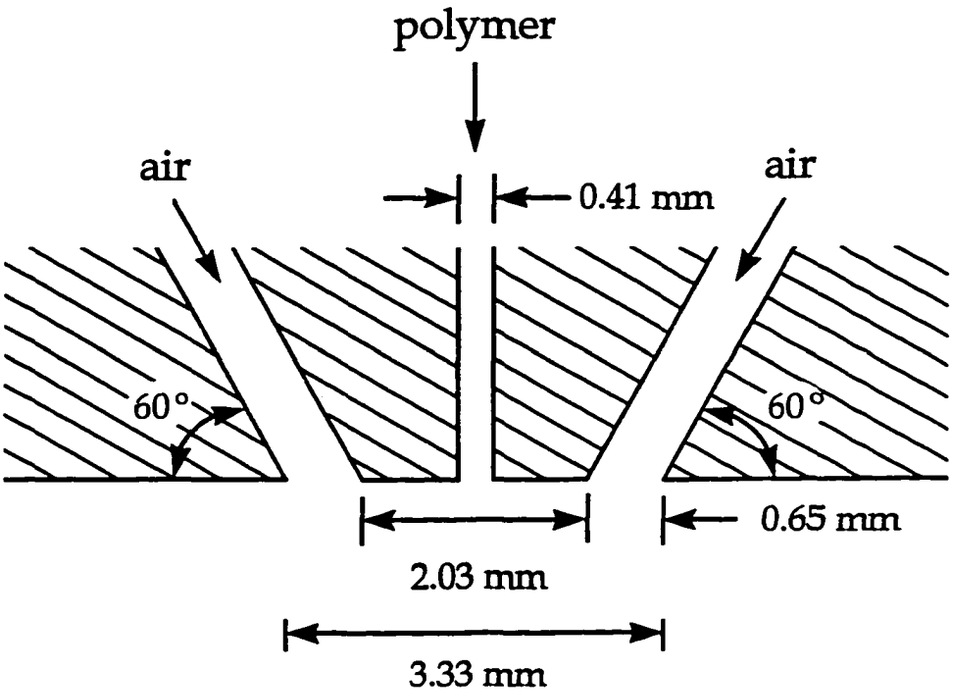

Figure 2.1 Cross-section of the melt blowing die used in the experiments.

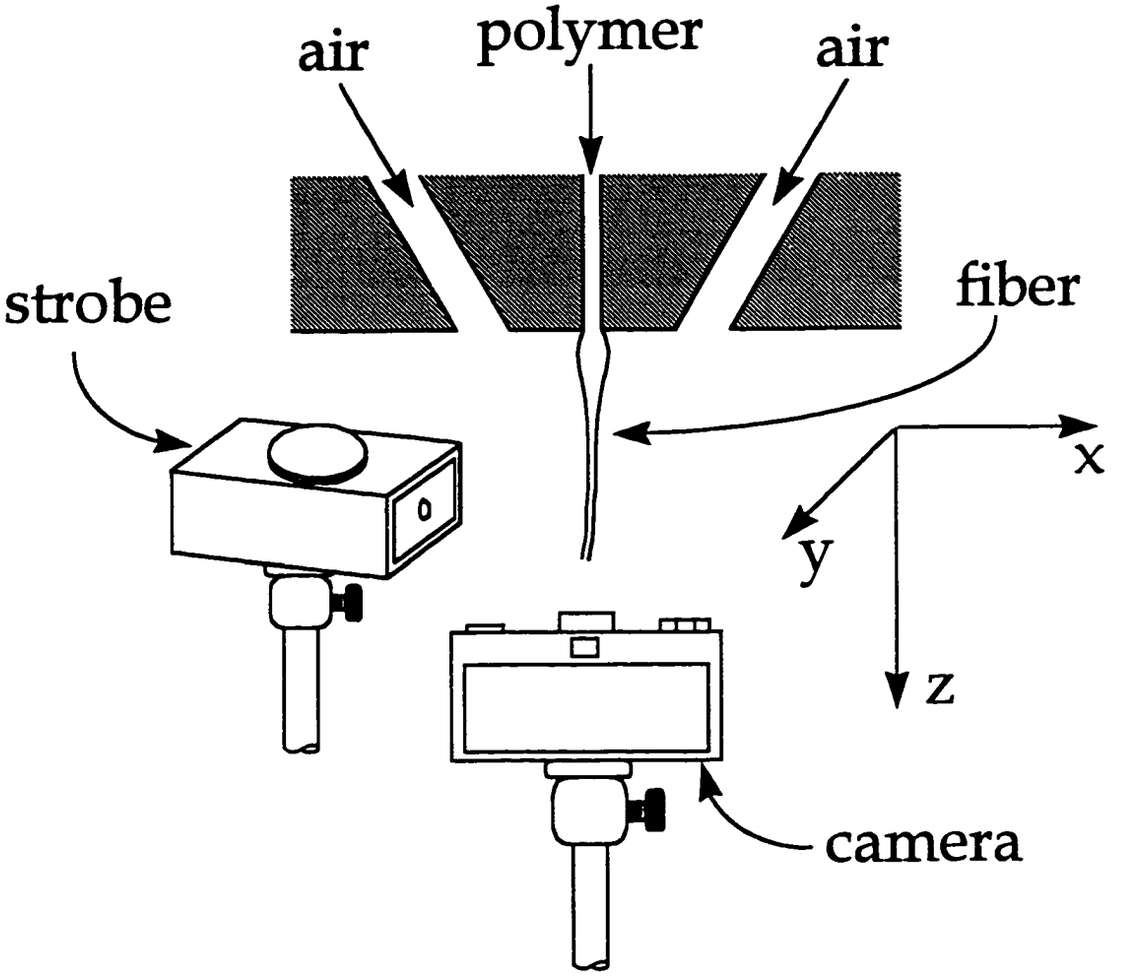

Figure 2.2a The photographic setup used to measure fiber cone diameter in the x direction.

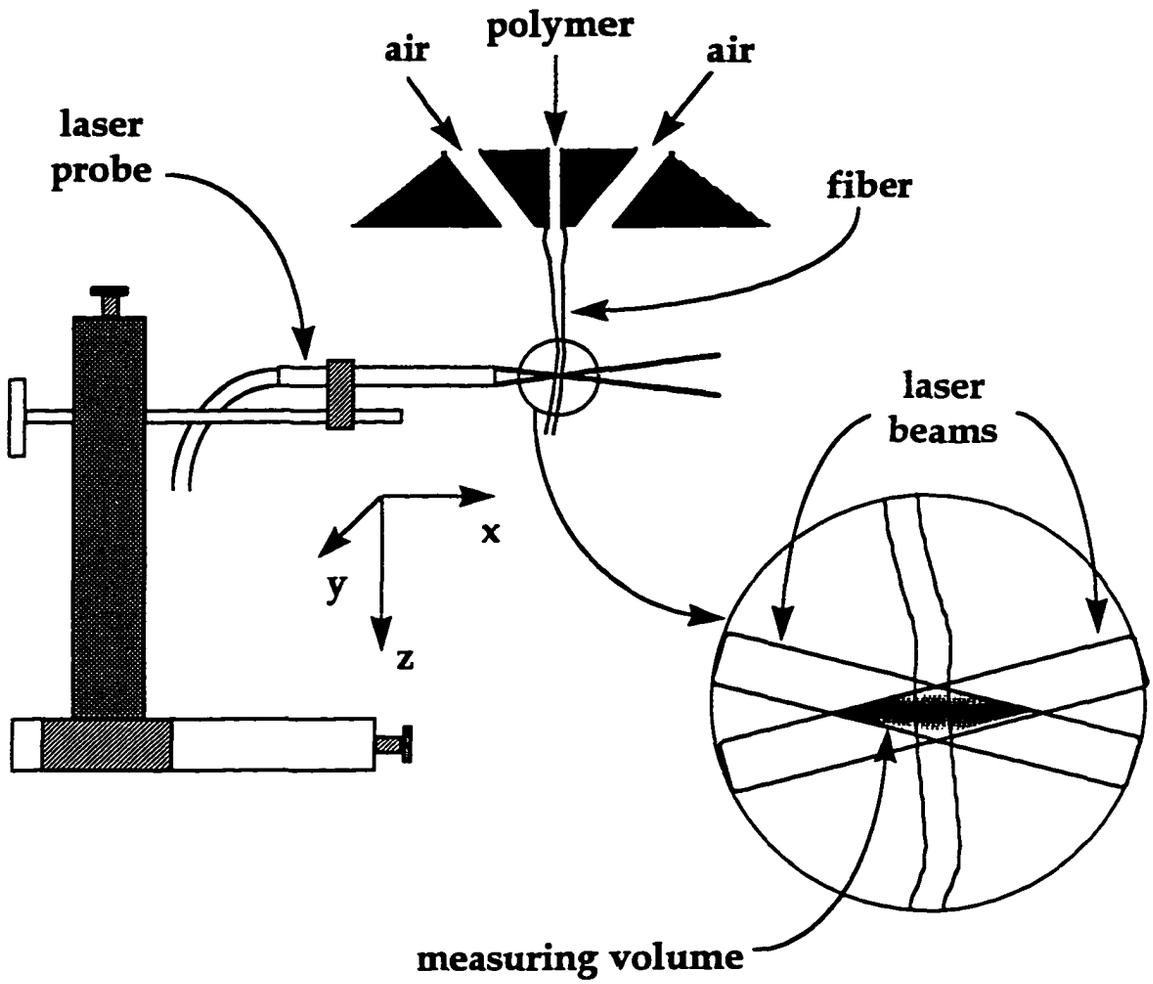

Figure 2.2b LDV setup used to measure fiber cone diameter along the y axis and fiber crossover frequency across the x axis.

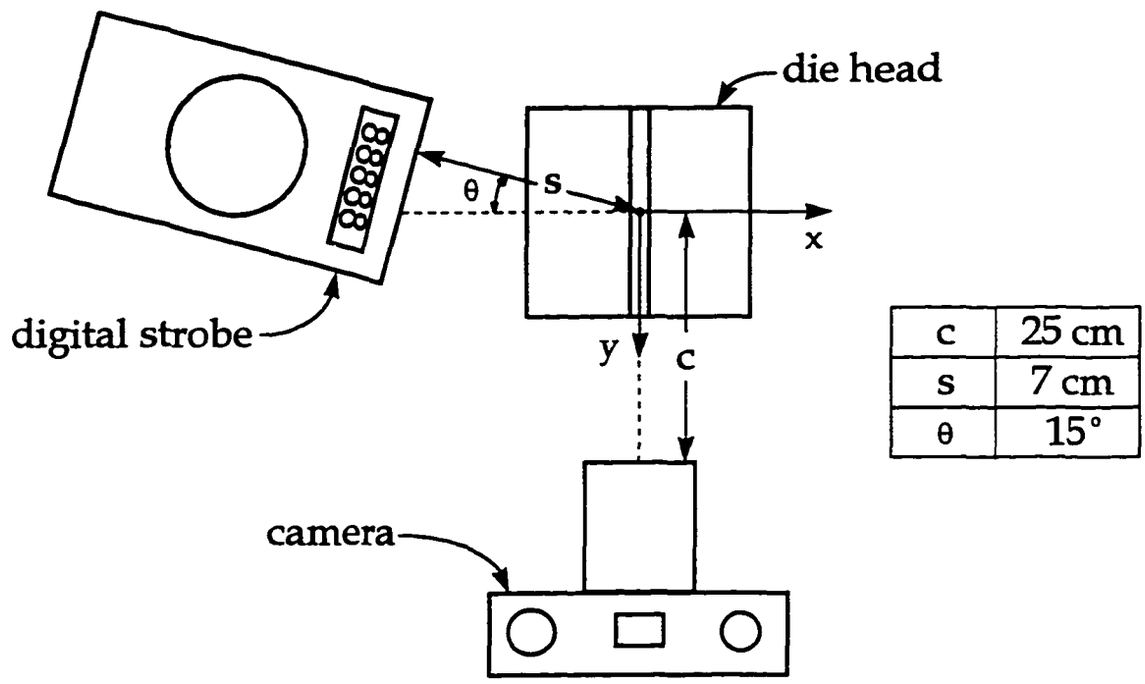

Figure 2.3 Top view of the photographic setup used to measure cone diameter.

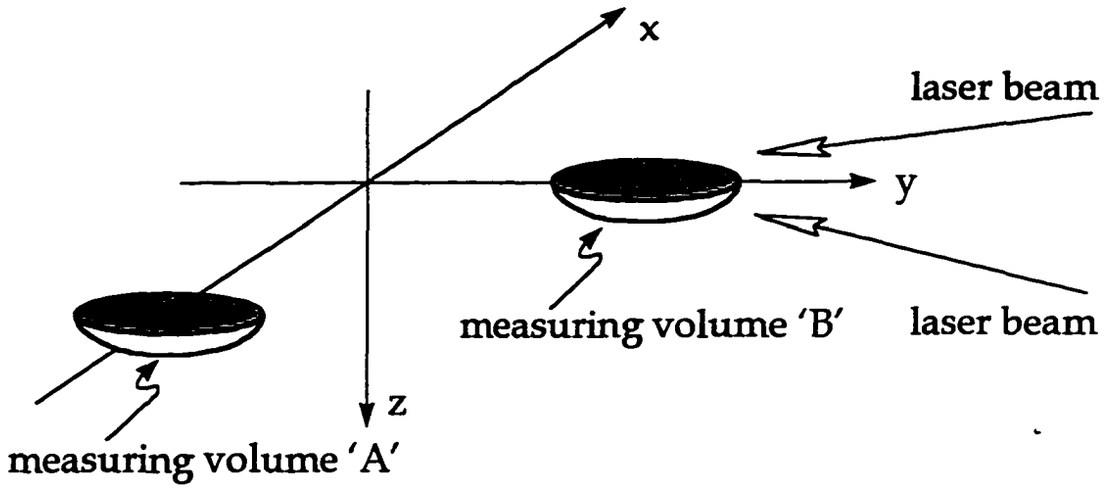

Figure 2.4 The LDV arrangement for measuring cone diameter along the x axis and crossover frequency across the y axis. The two laser beams cross in the x-y plane, the probe axis is aligned parallel to the y axis, and the fringes are parallel to the y-z plane.

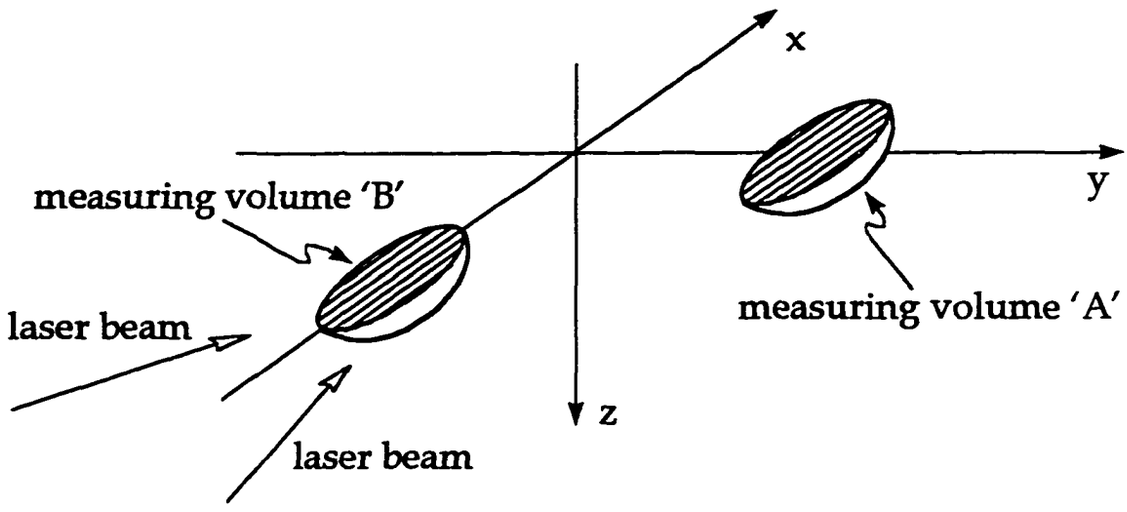

laser beams crossing in x-y plane with probe aligned along x axis

Figure 2.5 The LDV arrangement for measuring cone diameter along the y axis and crossover frequency across the x axis. The two laser beams cross in the x-y plane, the probe axis is aligned parallel to the x axis, and the fringes are parallel to the x-z plane.

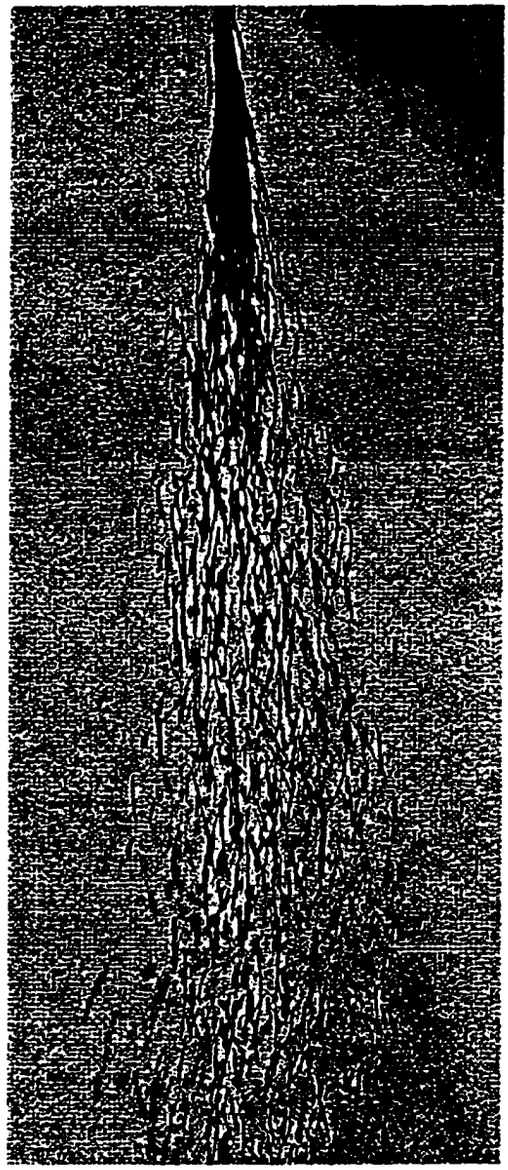

Figure 2.6 A typical multiple image photograph of the x axis fiber cone from z=1 to z=8 cm. The operating conditions were as follows: Q_p=0.4 cm^3/min, T_p=350°C, v_{jo}=30.9 m/s, and T_a=320°C.

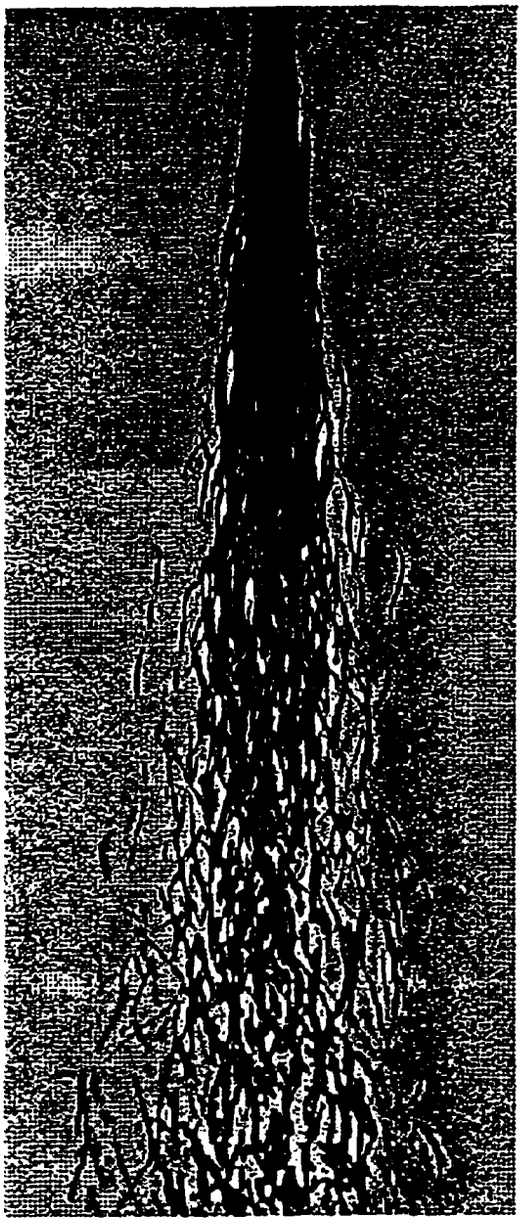

Figure 2.7 A multiple image photograph of the y axis fiber cone from z = 1 to z = 8 cm. The operating conditions were the same as for Figure 2.6.

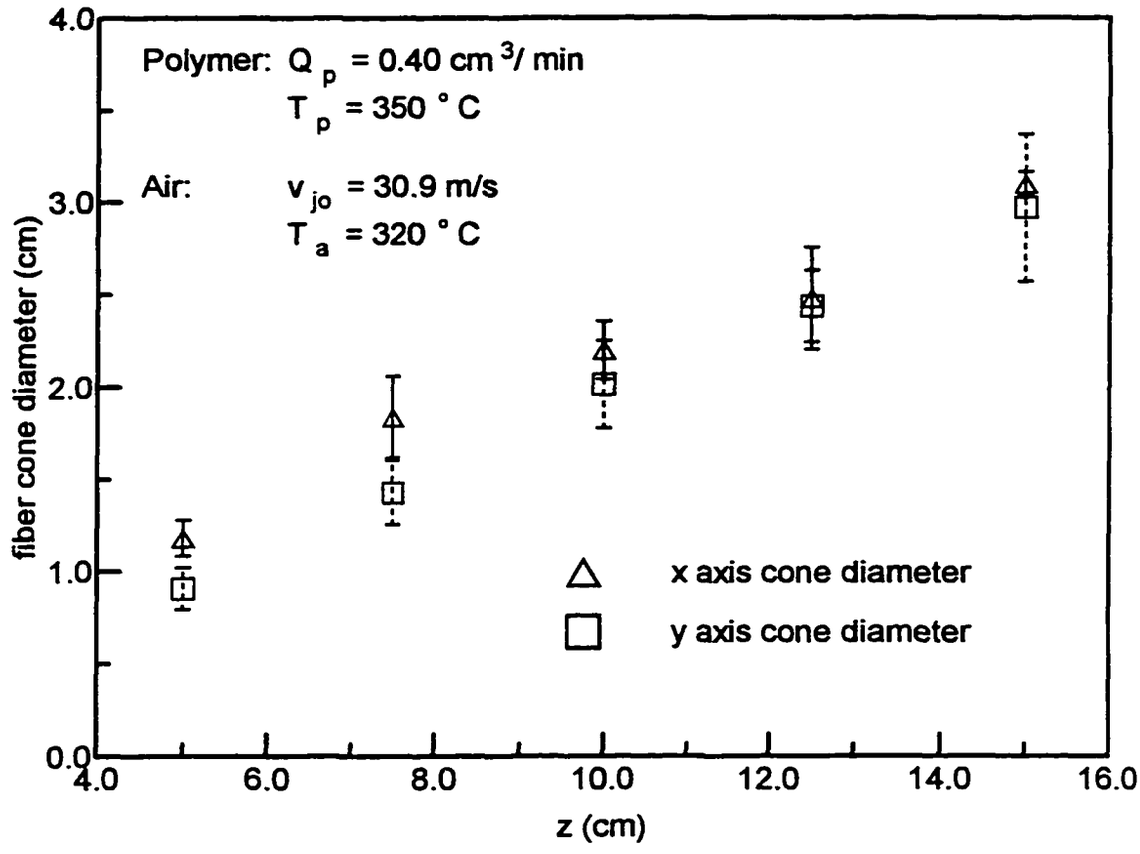

Figure 2.8 A comparison between the x axis and the y axis cone diameters measured using multiple image photography. Each data point represents the average from six replicate photographs, and each error bar represents a range of ± one standard deviation.

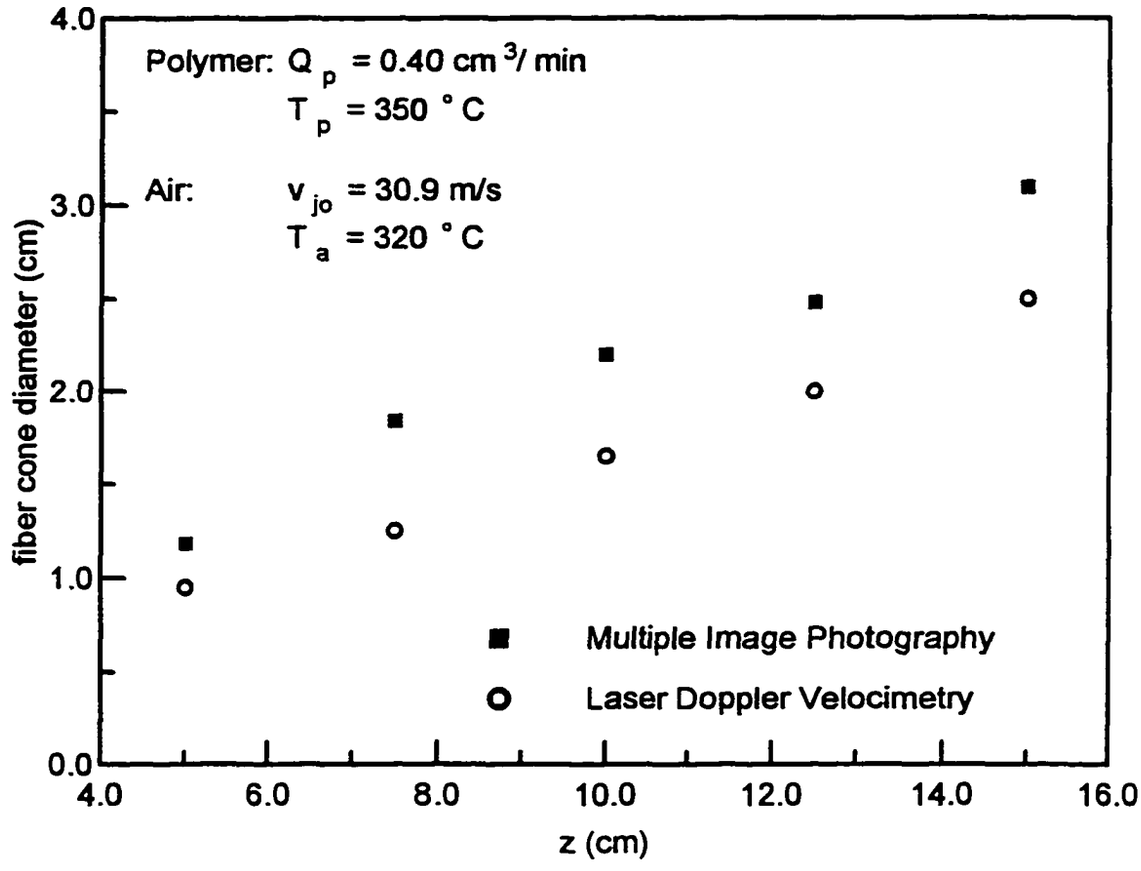

Figure 2.9 The x axis cone diameters measured via both LDV and multiple image photography.

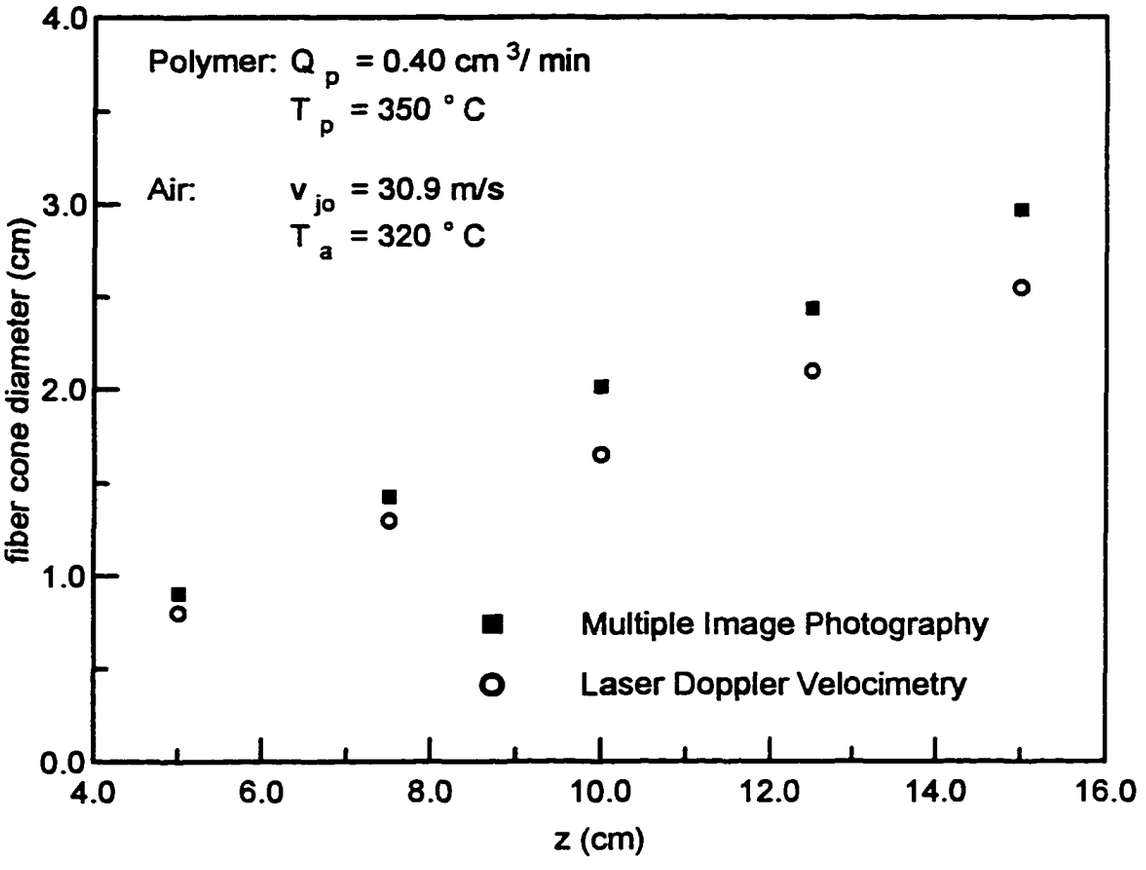

Figure 2.10 The y axis cone diameters measured via both LDV and multiple image photography.

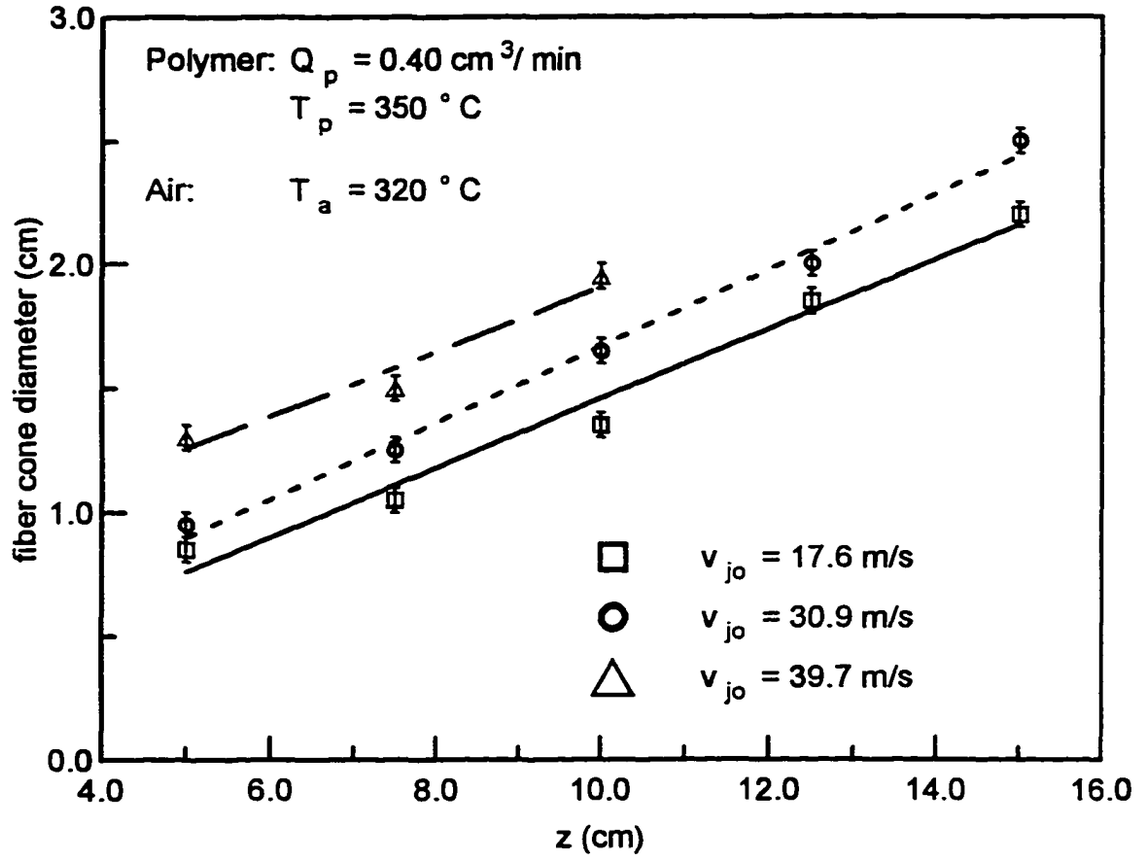

Figure 2.11 The effect of air velocity on the x axis fiber cone diameter. Each data point represents the average of six independent LDV measurements, and each error bar represents a range of ± one standard deviation.

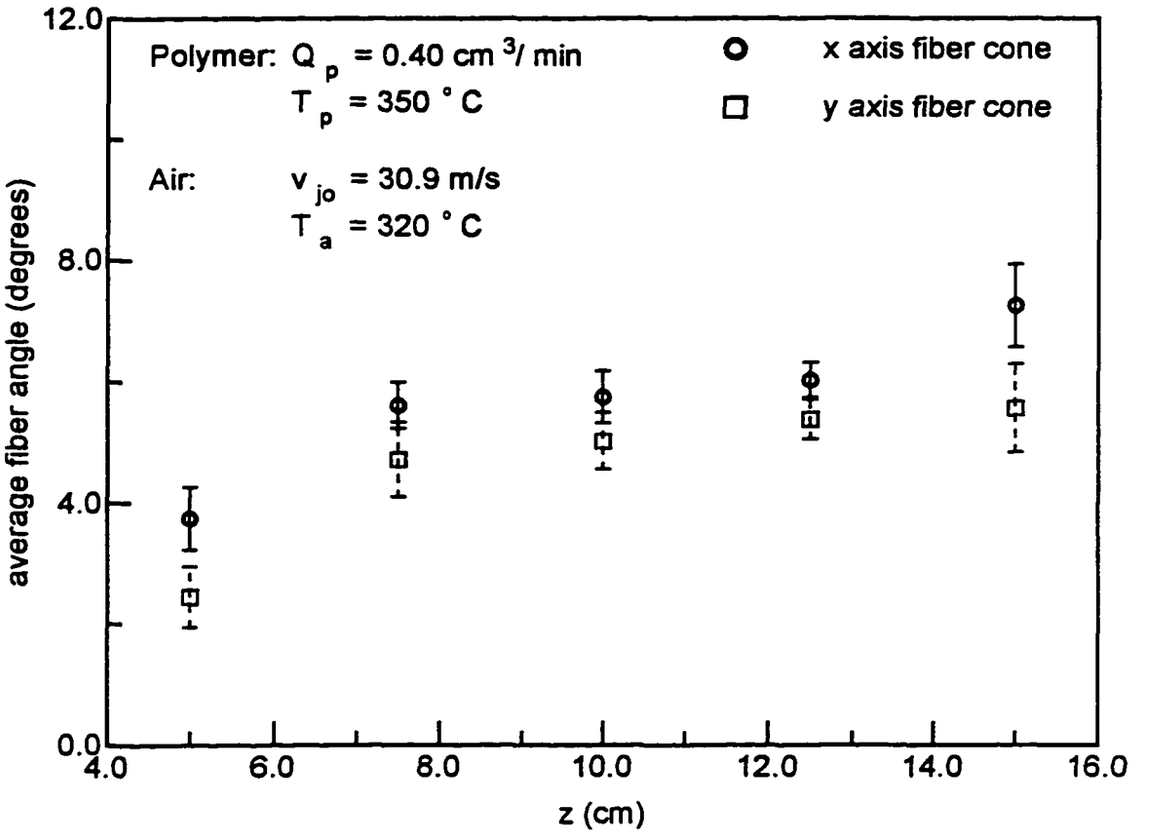

Figure 2.12 The average fiber angle determined from photographs. For the y axis measurements, the angle corresponds to α. Each data point represents the average of about 50 angle measurements, and each error bar represents a range of ± one standard deviation.

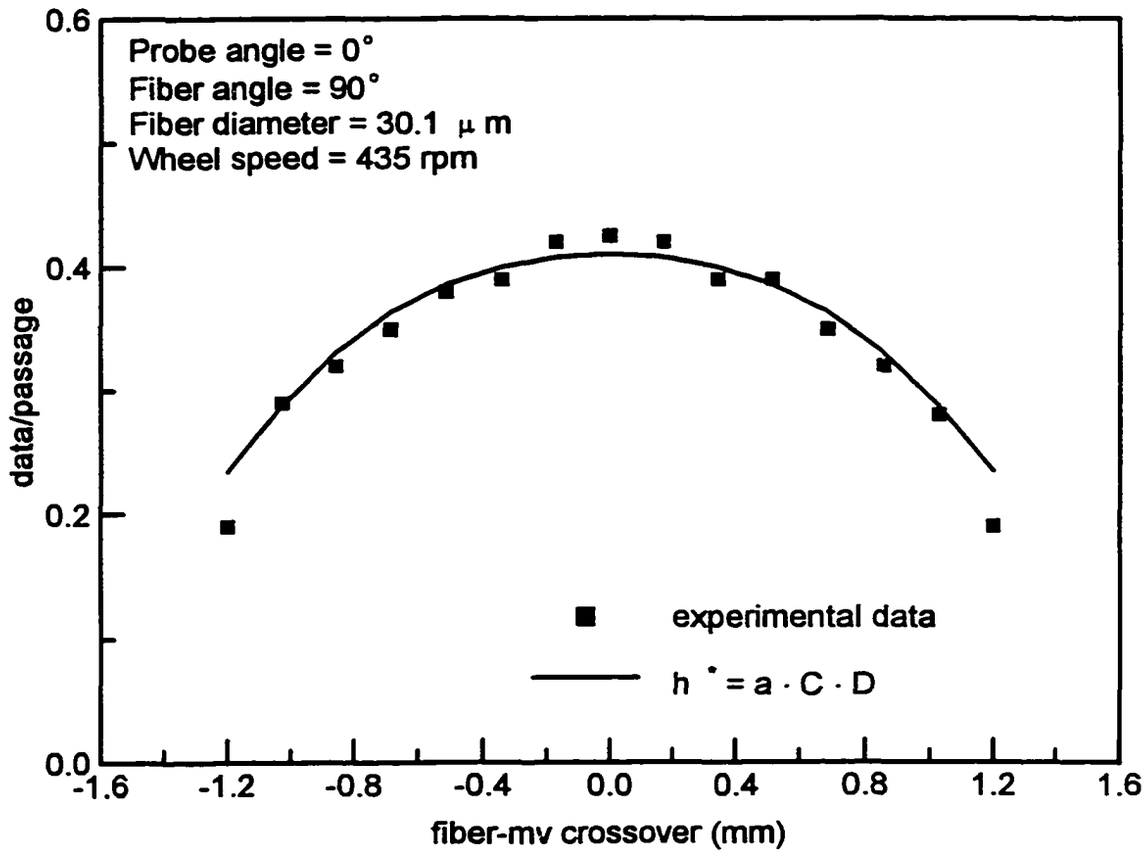

Figure 2.13 Effect of measuring volume position on data/passage. The solid line is predicted from the fitted correlation of eq 2.3.

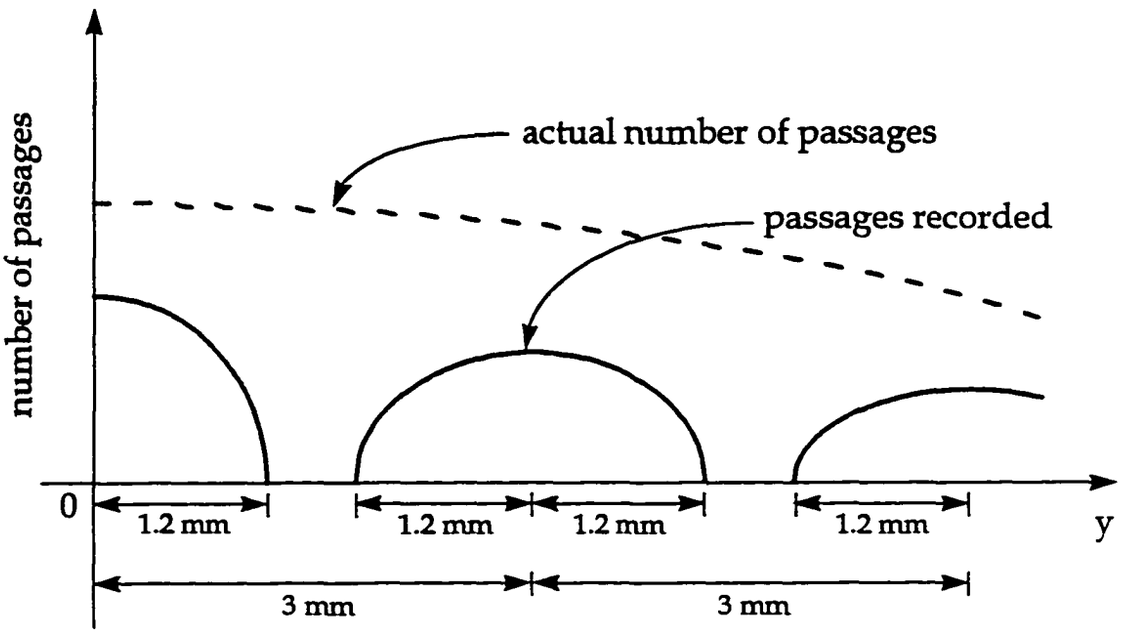

Figure 2.14 A qualitative comparison between the actual number of fiber passages and the passages measured by the laser mv.

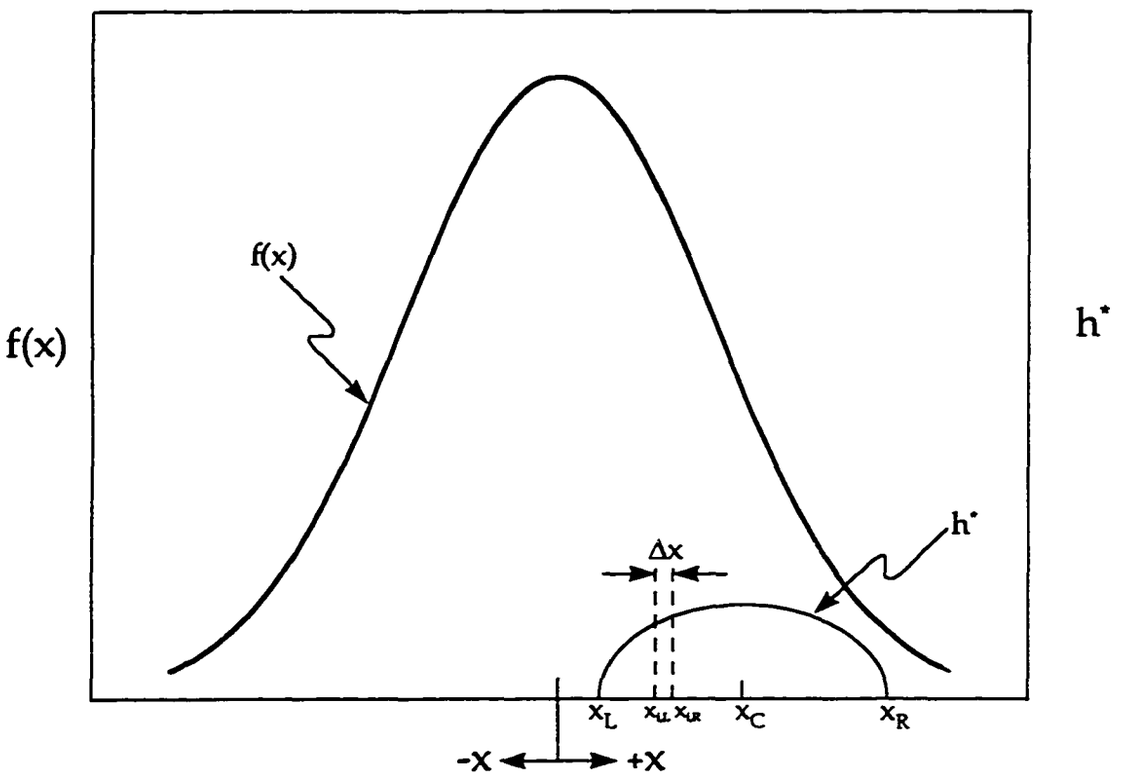

Figure 2.15 Superposition of the fiber density distribution function f(x) and the laser measuring volume response function h^*.

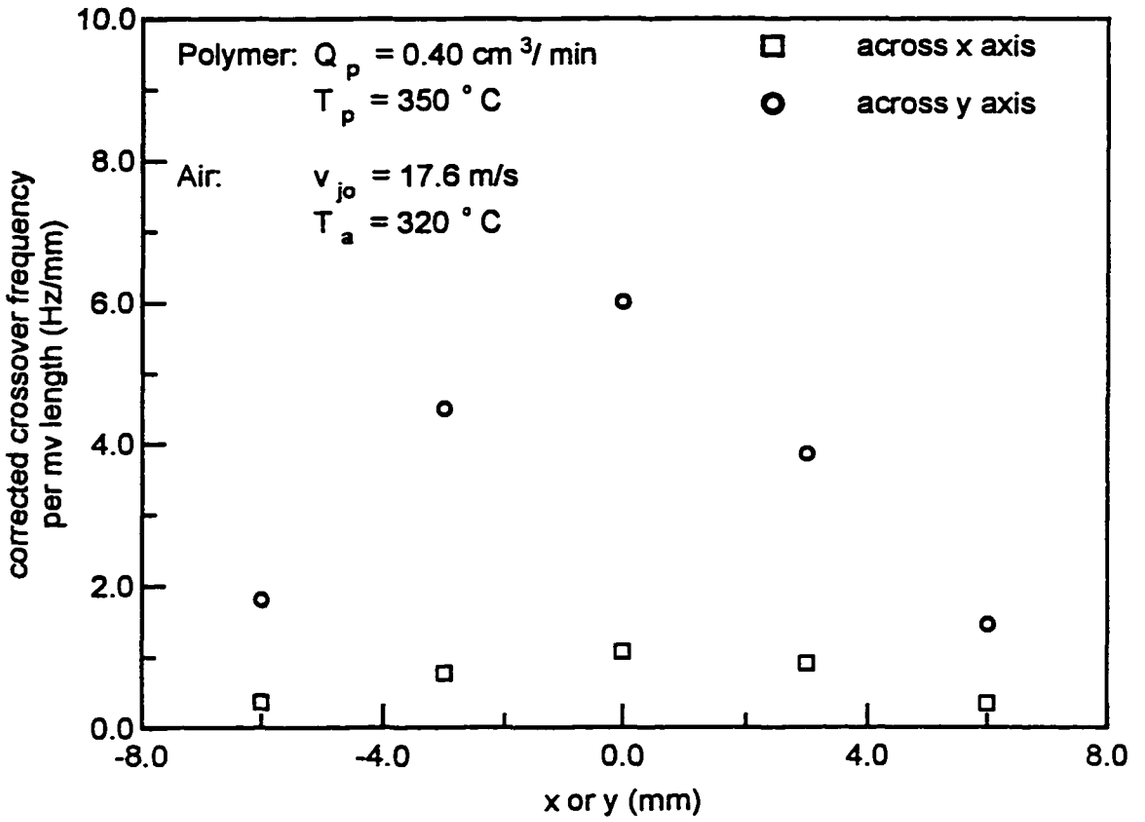

Figure 2.16 A comparison of corrected crossover frequencies per unit length across x and y axes at z = 10 cm.

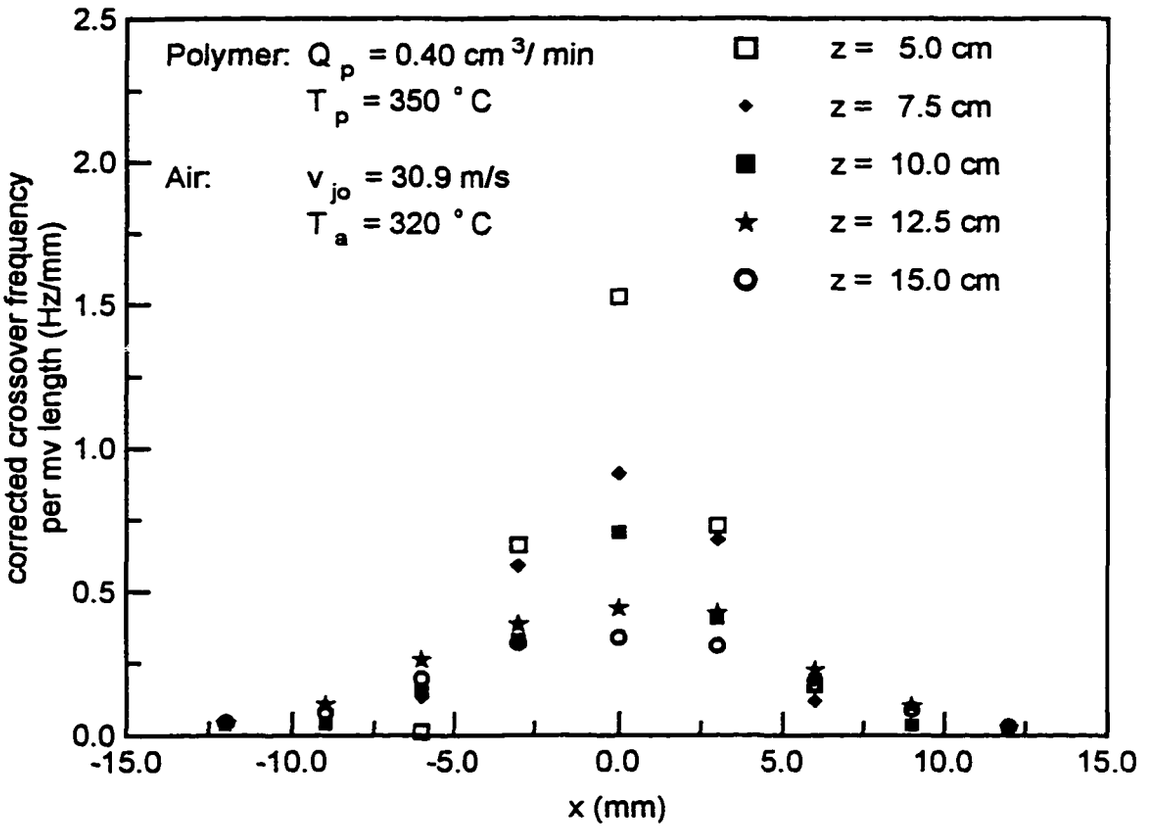

Figure 2.17 The fiber crossover frequency per unit length across the x axis.

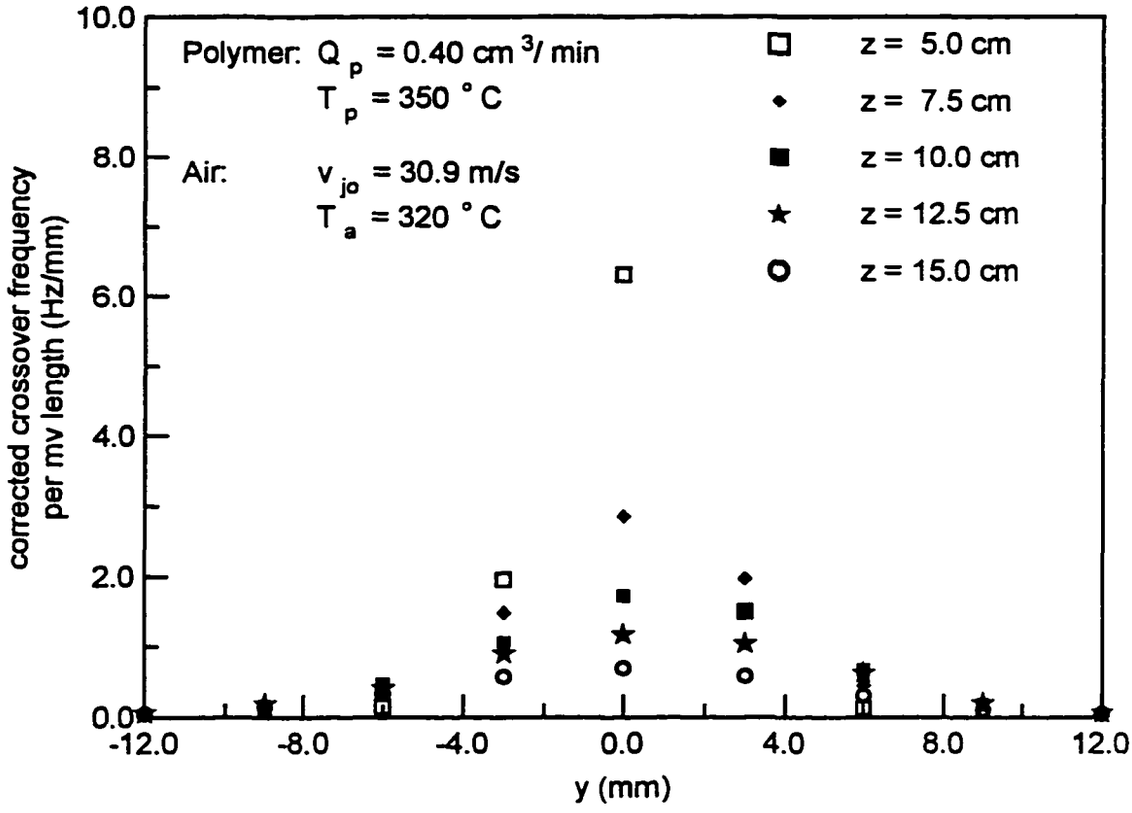

Figure 2.18 The fiber crossover frequency per unit length across the y axis.

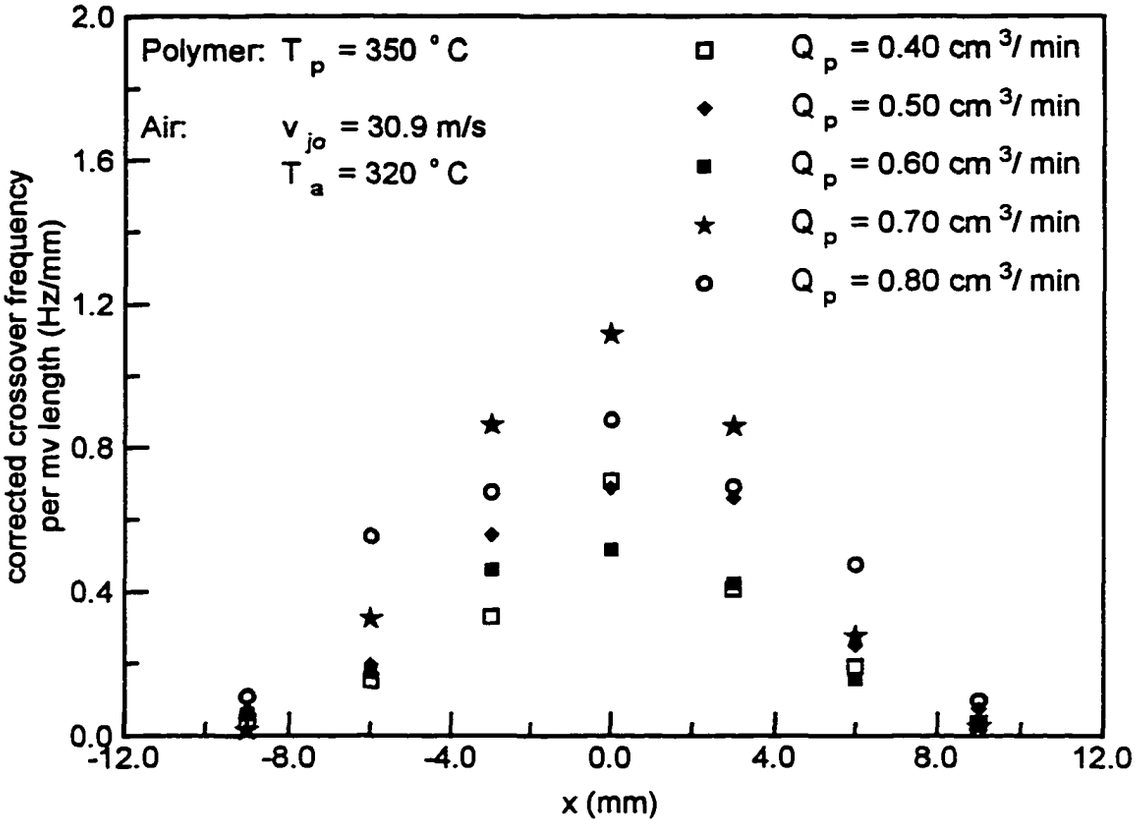

Figure 2.19 Effect of polymer flow rate on crossover frequency per unit length across the x axis at z = 10 cm.

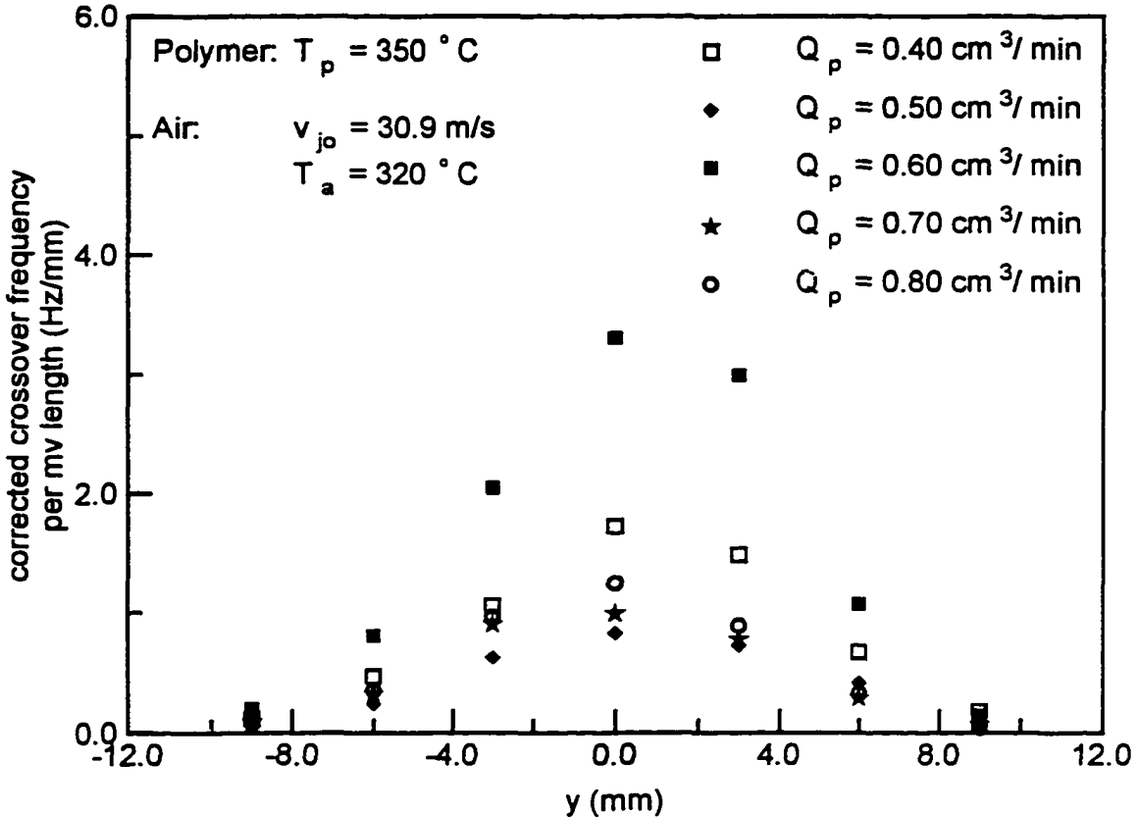

Figure 2.20 Effect of polymer flow rate on crossover frequency per unit length across the y axis at z = 10 cm.

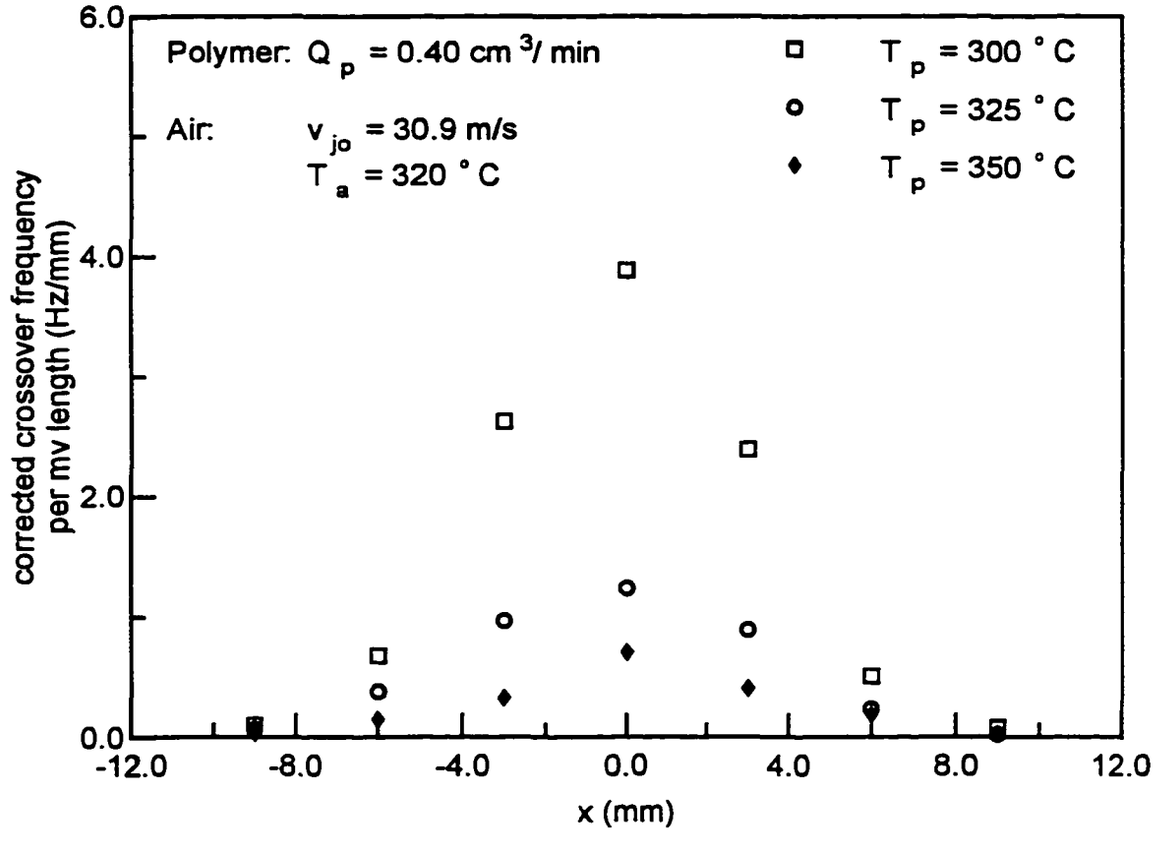

Figure 2.21 Effect of polymer temperature on crossover frequency per unit length across the x axis at z = 10 cm.

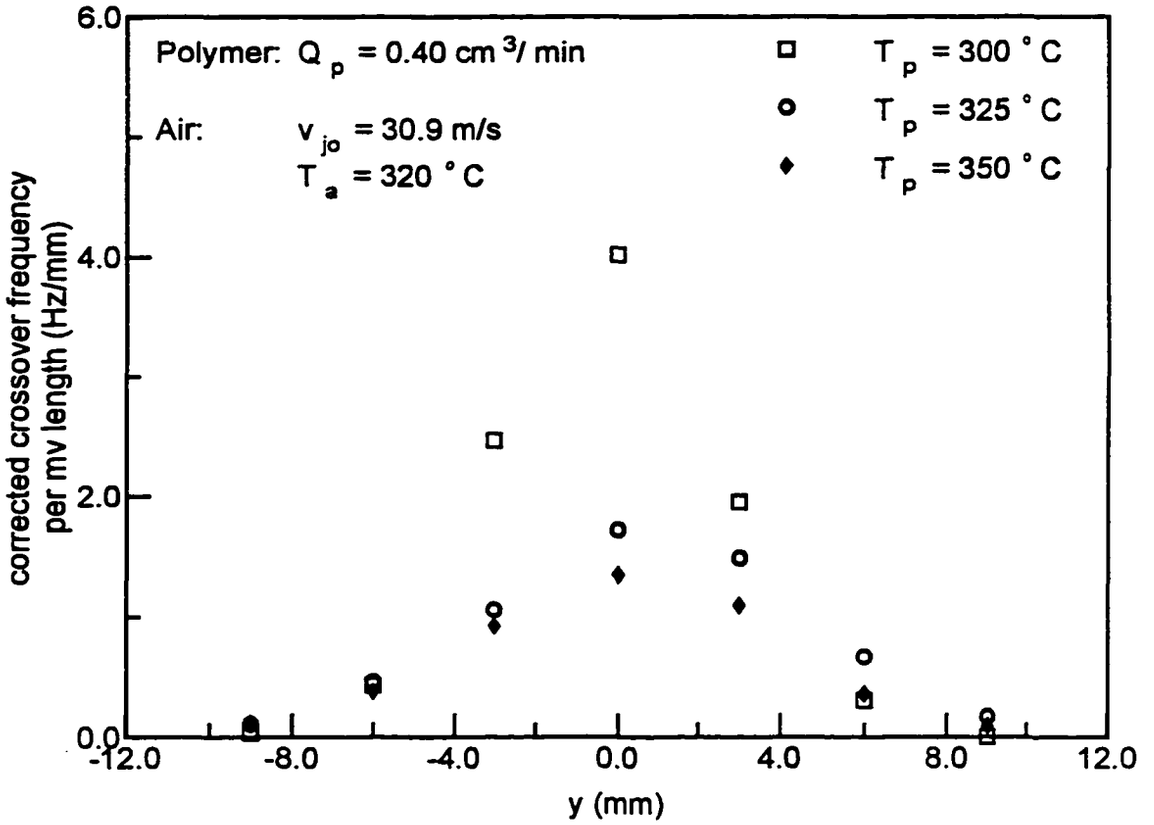

Figure 2.22 Effect of polymer temperature on crossover frequency per unit length across the y axis at z = 10 cm.

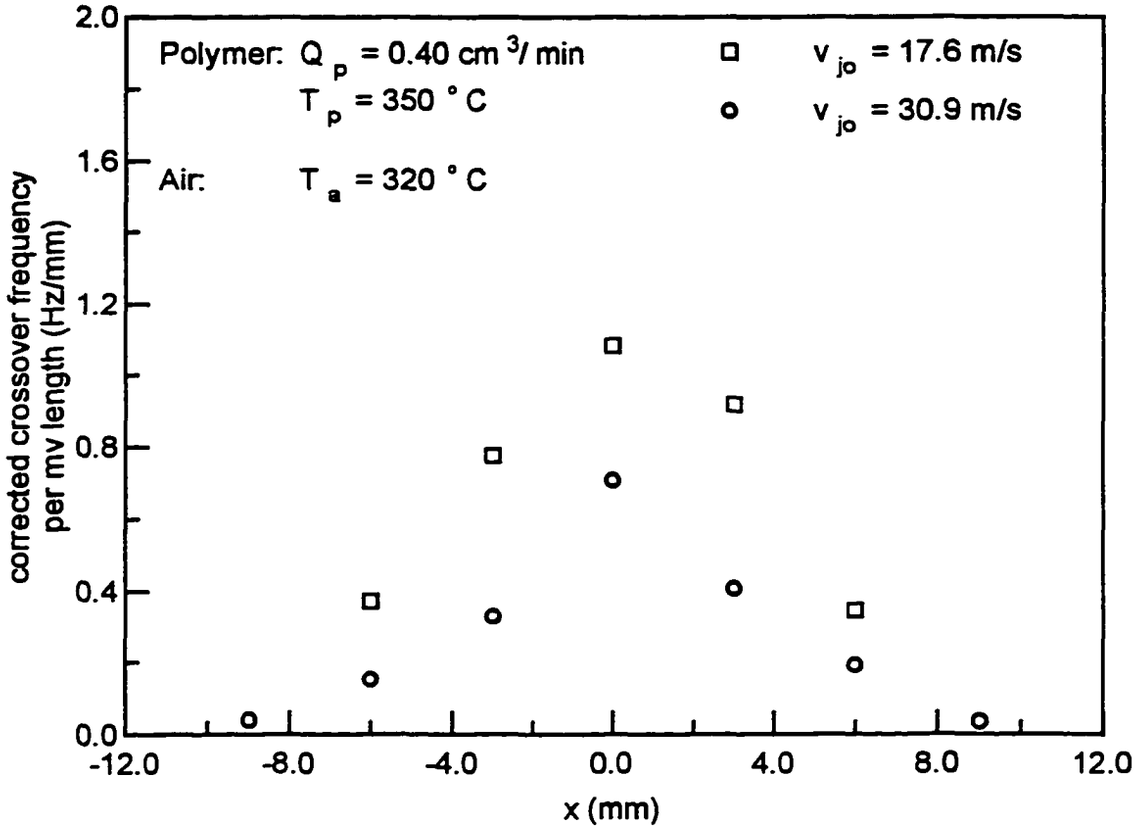

Figure 2.23 Effect of air velocity on crossover frequency per unit length across the x axis at z = 10 cm.

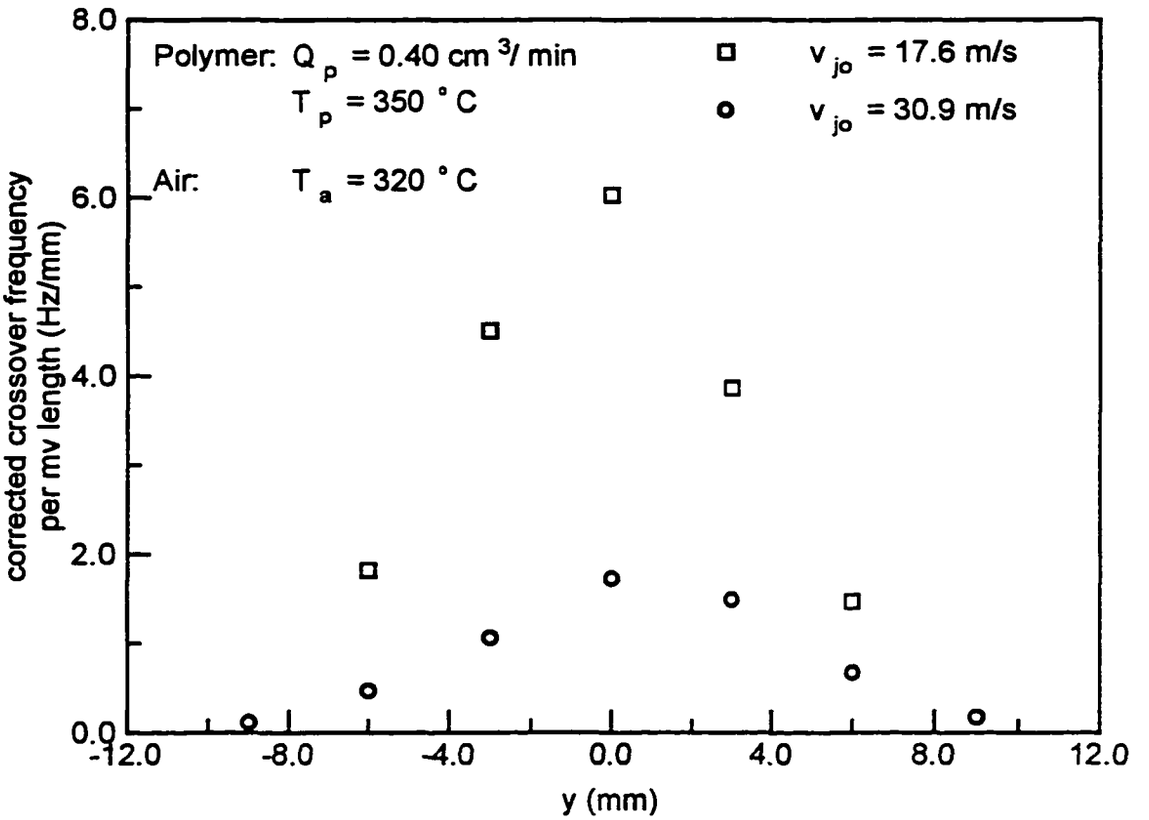

Figure 2.24 Effect of air velocity on crossover frequency per unit length across the y axis at z = 10 cm.

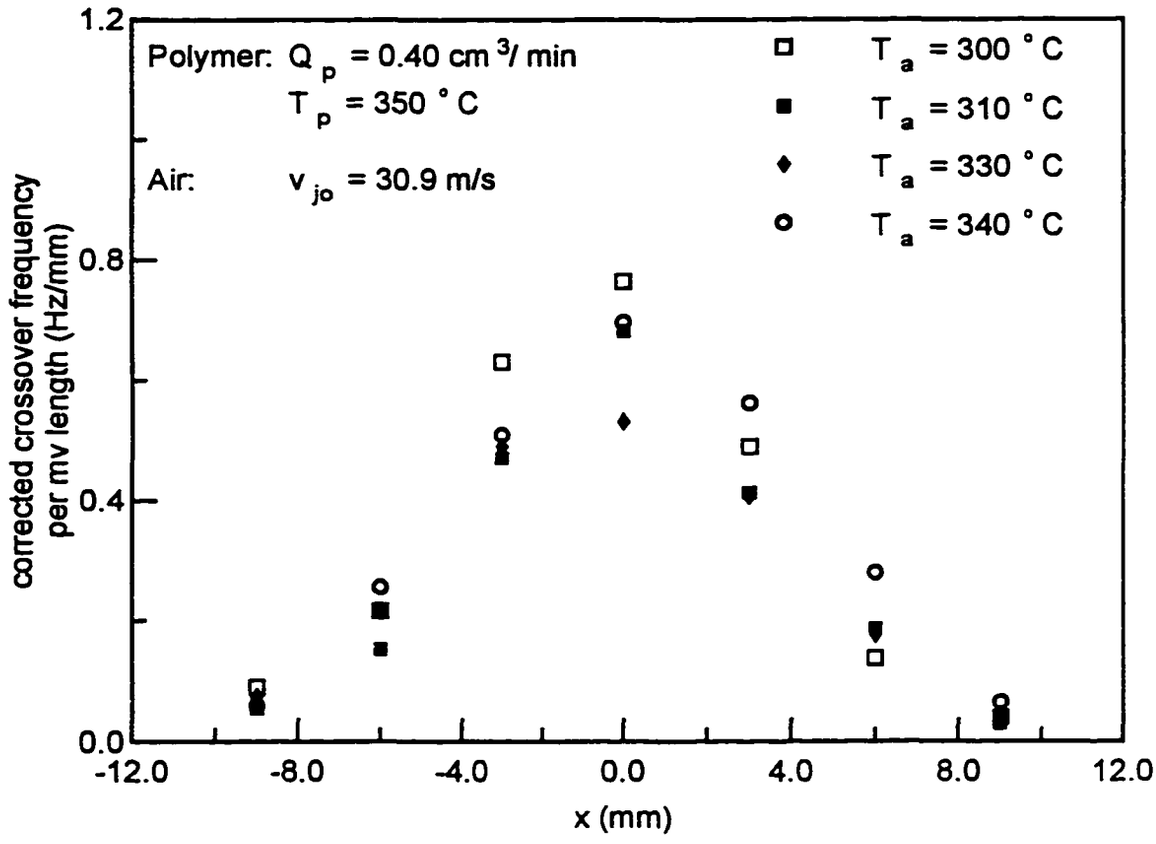

Figure 2.25 Effect of air temperature on crossover frequency per unit length across the x axis at z = 10 cm.

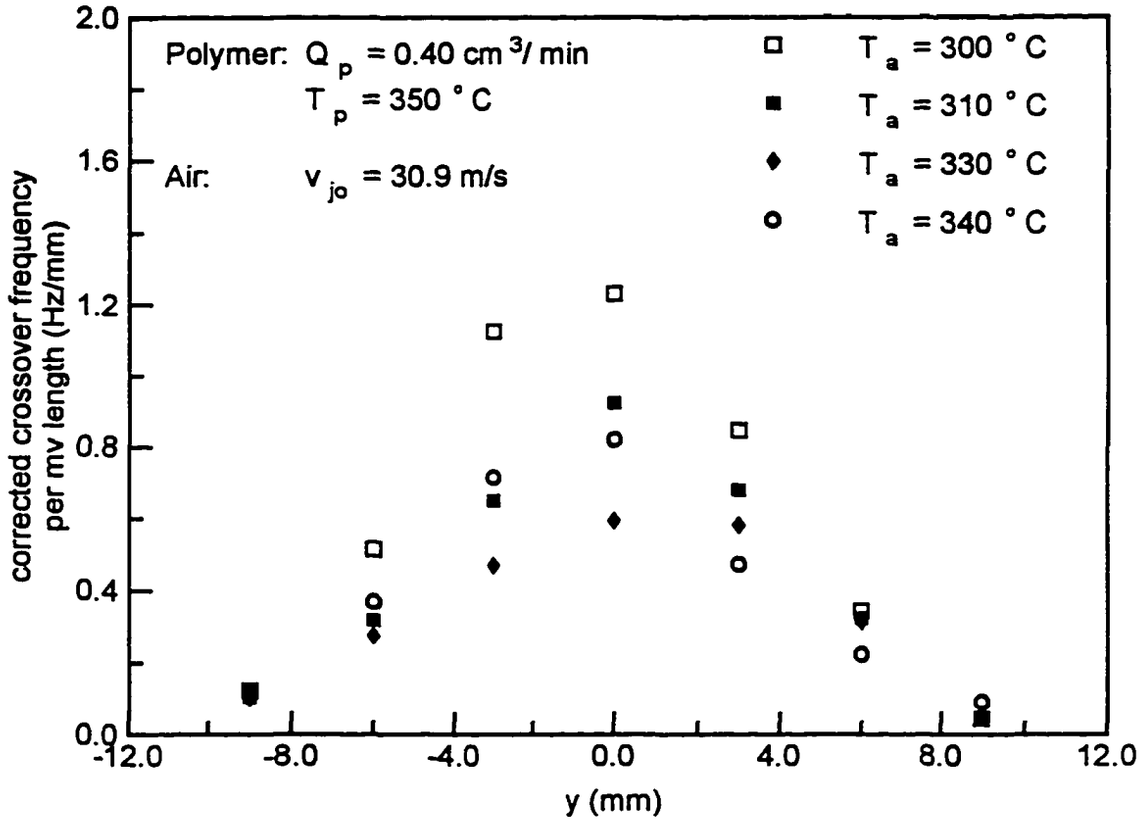

Figure 2.26 Effect of air temperature on crossover frequency per unit length across the y axis at z = 10 cm.

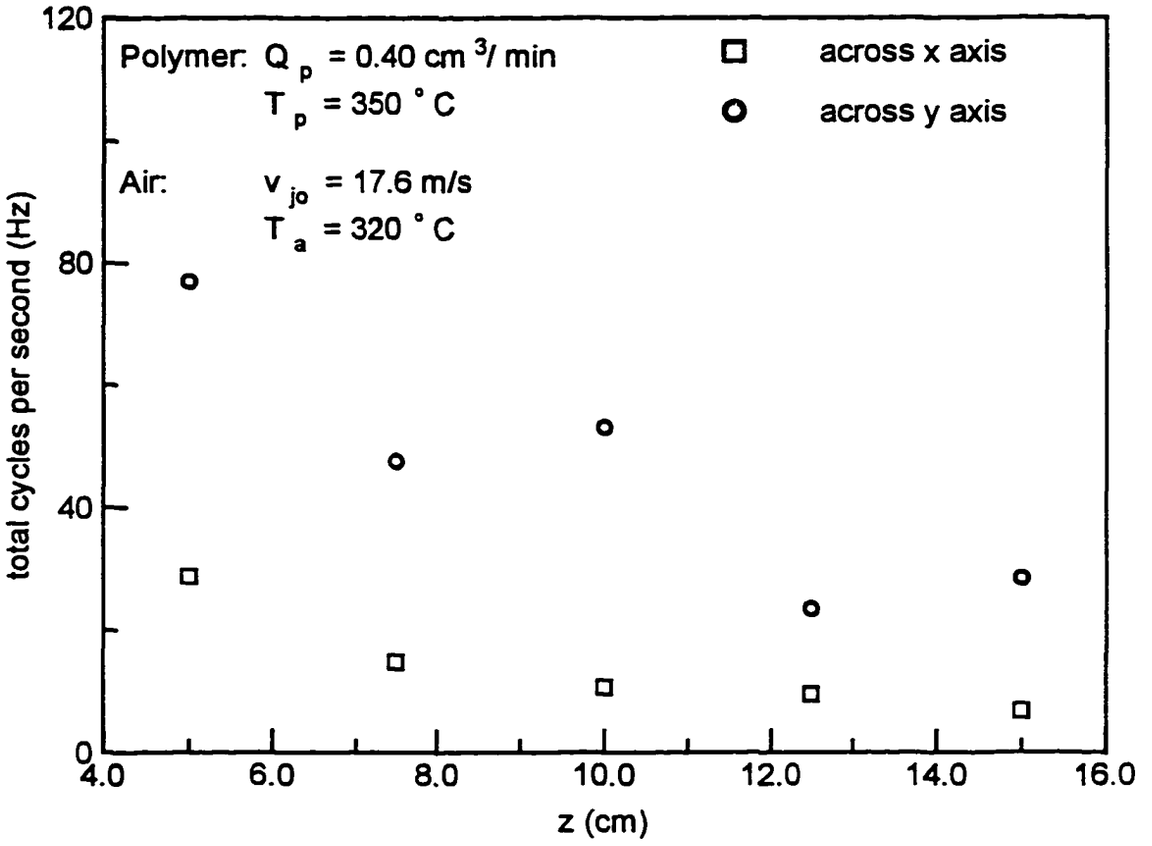

Figure 2.27 The total crossover frequency as a function of z when v_{jo} = 17.6 m/s.

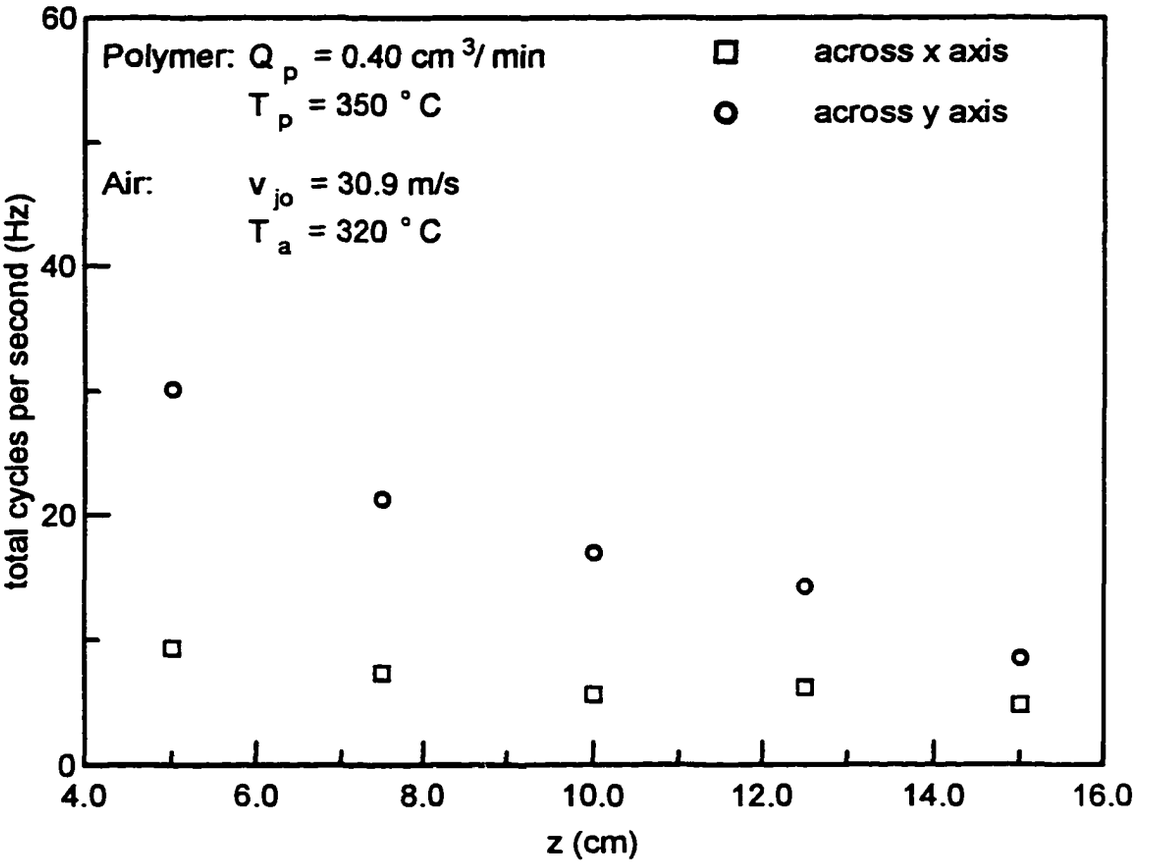

Figure 2.28 The total crossover frequency as a function of z when v_{jo} = 30.9 m/s.

Chapter 3

THE STOCHASTIC NATURE OF FIBER THREADLINE MOTION IN THE MELT BLOWING PROCESS

(The contents of this chapter have been submitted for a publication in the journal *Industrial & Engineering Chemistry Research*)

3.1 Abstract

Fiber threadline motion below a melt blowing slot die was studied as a stochastic process. High speed flash photography was used to obtain the fiber positions in three-dimensional space. For planes transverse to the spinning direction, a good fit of the experimental data to the bivariate normal distribution was obtained. The width of the fiber distribution was found to increase linearly with respect to the

axial distance from the die. There exists a small correlation between the orthogonal position variables in the transverse plane. The orientation angle of the distribution sinusoidally varied as a function of the axial distance from the die; this suggested that the fiber motion was that of an elliptical spiral which sinusoidally rotated in the transverse planes.

3.2 Introduction

In the melt blowing process, a high velocity gas stream or streams attenuate molten polymer strands to form microfibers; see Shambaugh (1988). These microfibers are extensively used in manufacture of nonwoven textiles. Empirical and theoretical studies have shown that the melt blowing process can be controlled to produce fiber webs with desirable characteristics. Shambaugh (1988), Kayser and Shambaugh (1990), and Milligan and Haynes (1995) have empirically modeled the process for different die geometries. The theoretical models of Uyttendaele and Shambaugh (1990) and Rao and Shambaugh (1993) are based on fundamental fluid mechanics and can be used to predict and improve melt blowing performance.

The characteristics of a nonwoven web depend on the fiber orientation and distribution in the web. The fiber orientation and distribution can be controlled by varying the operating conditions during melt blowing. With a fixed die geometry

and a fixed polymer type, the four main operating conditions are gas flowrate, gas temperature, polymer flowrate, and polymer temperature. How these parameters affect the fiber orientation and distribution is of great interest. The models of Uyttendaele and Shambaugh (1990) and Rao and Shambaugh (1993) use these four parameters as inputs. Both models predict final fiber size, while the Rao and Shambaugh model also predicts the presence of characteristic fiber frequencies associated with the melt blowing process. Chhabra and Shambaugh (1996) experimentally measured the fiber threadline amplitudes and frequencies of vibrations. Their work correlates with the predictions of Rao and Shambaugh's model. Their work also suggests that the vibrational pattern of the fiber motion has a well-defined statistical distribution. The present work involves the experimental measurement of the statistical distribution of the fiber threadline motion. This knowledge of fiber motion in melt blowing will help in predicting the resultant fiber laydown in the product sheet.

3.3 Literature Review

Spatial fiber distribution in nonwoven webs plays an important role in defining the physical characteristics of the web. Many analytical and experimental techniques have been developed to study the fiber distribution and orientation. All these techniques have concentrated on characterization of the final product web.

Different methods to evaluate the average angle of orientation of the fibers in a web have been developed by the researchers. Hearle and Stevenson (1963) used a direct fiber counting method to measure the fiber orientation. A small area of the web was viewed under a microscope and the fibers aligned in different directions were counted. Huang and Bresee (1993, Part I) applied image processing techniques to automate and thus speed-up the fiber counting method for measuring the diameter-based fiber orientation distribution. Random samples of a web image were taken, and image analysis techniques were used to evaluate the fiber orientation with respect to the machine direction. Neither Hearle and Stevenson nor Huang and Bresee fit their data to a standard statistical distribution function.

Prud'homme et al. (1975) developed an x-ray diffraction method to convert the crystal angle distribution within the fibers to the fiber orientation distribution in a cellulosic sample. They assumed that the fiber orientation distribution function $N(\epsilon)$ is represented by the following geometrical relation:

$$N(\epsilon) = \frac{C}{C^2 \sin^2\epsilon + \cos^2\epsilon} \tag{3.1}$$

where

ϵ = fiber orientation angle

C = experimentally determined orientation parameter

Kallmes (1969) and Votava (1982) used a zero-span testing method to evaluate the ratio of machine- and cross-directional strengths of paper. Votava used this ratio to determine the fiber orientation with the theory given by Van den Akker, Jentzen and Spiegelberg (1966). Tsai and Bresee (1991) employed electrical measurements to characterize the fiber orientation. Then, with electric field theory, they transformed the electric current distribution into a fiber orientation distribution. Rodrigues et al. (1990) characterized anisotropy of papers in terms of vision entropy. They used Shanon's (1948) famous relation of information entropy to extract the degree of directionality in the spatial fiber distribution. Recently, Pourdeyhimi (1993) applied image processing techniques to assess the fiber orientation in simulated nonwoven webs. These nonwoven webs were simulated with overlapping straight lines generated randomly. He used three methods (the methods were Fourier analysis, pore orientation, and flow-field analysis) to evaluate the dominant direction of alignment of the fibers in a simulated web.

Web uniformity depends on the spatial distribution of fibers. The uniformity of the web structure affects the physical properties and the appearance of the web. For example, in filtration processes, web performance is largely dependent on the uniformity of the web. Any thin spots in the fiber sheet will cause filter failure by allowing large particles to pass through the filter. Typically, nonwoven webs are characterized in terms of basis weight, structure, and visual uniformity. The nonwovens industry uses the coefficient of weight variation as a standard quality index to quantify the web uniformity. Beta rays and electromagnetic radiation (gamma rays and lasers) have been used for online measurement of the web mass and uniformity. See Boeckerman (1992) for details on the application of beta rays for measuring web uniformity. Aggarwal, Kennon and Porat (1992) used a scanned-laser technique to monitor both weight and cover factor of a web. In their method, the scanning laser light was transmitted through the web twice with the aid of a retro-reflector. Then, the intensity of the transmitted light was calibrated to give information about the variations across the web and the web mass. Their technique can be used as a monitoring tool and a feedback signal sending device to control the variations in mass and structure of the web. Huang and Bresee (1993, Part III) correlated an image analysis technique with more conventional methods of measuring the web uniformity. The conventional methods they considered were the measurement of the structural uniformity with a gamma-ray gauge and the cut-and-weigh procedure to measure the coefficient of web mass variation. They correlated the coefficient of web mass variation to the coefficient

of pixel gray level variation of the web image. They also performed a nonuniformity spectral analysis to evaluate the coefficient of variation of the visual uniformity in the machine-direction and the cross-direction. Ericson and Baxter (1973) studied the structural and visual uniformity of spunbonded webs. They correlated the tensile strength of the web with the filament separation and the visual uniformity. They determined the filament separation with a projection microscope. By measuring the intensity of the transmitted light, they evaluated the coefficient of variation of the visual uniformity.

The excellent work of previous researchers concentrated on the characterization of the nonwoven web after its production. However, the present work concerns the measurement and statistical modeling of the presence of a melt blown fiber as a function of its position below the spinneret. Relating this to the laydown pattern is simply a matter of defining the location (z position) of the collection screen below the spinneret. Of course, the implicit assumption here is that the presence of the collection screen does not greatly disturb the fiber distribution. In experimental practice this is not a bad assumption if a proper level of suction is applied to the collection screen.

3.4 The Statistics of Fiber Position

In the melt blowing process, the fiber moves in three orthogonal dimensions. Chhabra and Shambaugh (1996) have described the volume below a melt blowing die in which a fiber travels as a fiber "cone". The apex of the cone is at the spinneret hole. To understand the fiber motion, the fiber position, velocity, and orientation have to be evaluated as a function of time. Wu and Shambaugh (1992) used LDV (laser Doppler velocimetry) to measure the fiber velocities in three-dimensional space during melt blowing. The spatial positions, which the fiber threadline assumes during its motion, can be predicted by rigorous fluid dynamical modeling as was done in the Rao-Shambaugh model (1993). In contrast, the present study considers a statistical approach to understand the fiber motion in melt blowing: a statistical model was fit to experimentally-determined fiber positions.

3.4.1 Mathematical Formulation

Chhabra and Shambaugh (1996) experimentally showed that, for a given transverse plane, the fiber vibrations for a single-hole slot die decreased as the fiber moved away from its mean axial position. This meant that the fiber spent most of its time close to its mean axial position. The tendency of fiber to stay mostly near the center

of the fiber cone was apparent from the multiple exposure photographs. Consequently, it was hypothesized that the fiber threadline positions follow a Gaussian distribution. With this assumed distribution, Chhabra and Shambaugh corrected the frequency of vibrations measured with laser Doppler velocimetry (LDV). The distribution in the x-direction was assumed to be independent of that in the y-direction, and vice versa. This assumption may not be true. Since the fiber is a continuous strand, one would expect motion in one direction to affect the motion in an orthogonal direction. Furthermore, a degree of dependence can also be attributed to the turbulent gas jet which serves as an attenuating force in melt blowing. The momentum of such a turbulent gas jet in the x-direction is correlated to the momentum in the y-direction (Tennekes and Lumley, 1972). As a result of these concerns, the work described herein involved distributions with a dependence parameter (correlation coefficient).

Various bivariate probability distributions could be fitted to the fiber distribution. Examples of commonly used bivariate probability distributions include the normal distribution, binomial distribution, Cauchy distribution, Student's t-distribution, and gamma distribution. A detailed review of bivariate probability distributions is given by Mardia (1970). However, only those distributions that fulfilled the following criteria were considered worth fitting:

(i) Since the fiber motion is continuous, the distribution function should be continuous.

(ii) Experimental observations (Chhabra and Shambaugh, 1996) have shown that most of the fiber threadline positions are close to a central mean position, and the number of positions decrease as distance from the mean position increases. Therefore, the distribution should be unimodal and the probability of occurrences should decrease at distances away from the mean position.

(iii) The random variables should have both positive and negative real values.

Thus, the choice is limited by the above criteria. A bivariate normal distribution is a well-defined distribution which fulfills the above criteria. Examples of other bivariate distributions, which also have above-mentioned properties, include the bivariate Cauchy distribution and the bivariate Student's t-distribution. However, for the bivariate Cauchy distribution and the bivariate Student's t-distribution, the random variables must be from a population that follows a bivariate normal distribution. Therefore, in the present study, only the bivariate normal distribution was considered. Mardia (1970) and Johnson and Kotz (1972) have described the mathematical properties of these bivariate distributions.

The bivariate normal distribution has been applied to many problems in science and engineering. For example, Evans et al. (1993) determined the direction of dominant wave travel, the variance in wave slopes, and the directional spectra of waves in the ocean from the parameters of a fitted bivariate normal distribution. Holst and Schneider (1985) applied the bivariate log-normal distribution to study the stochastic relationship between the diameter and the length of fibers in aerosols. Johnson and Kotz (1972) have presented a detailed review of the mathematical properties of the bivariate normal distribution.

In the present work, the probability $p(x, y)$ was evaluated for the presence of a fiber at a position (x, y) in a plane of constant z below the die. Figure 3.1 shows the die with the appropriate coordinate system. The following assumptions were made concerning the fiber motion:

(a) The fiber threadline is assumed to be made of infinitesimal beads linked to each other along the fiber axis. The link is flexible, but the motion of sequentially connected beads is correlated. The assumption of linked beads is reasonable because, physically, the fiber threadline is not a series of independent beads falling in random directions from the die.

(b) The motion of a bead is assumed to be correlated to the motion of its neighboring beads only. Therefore, the more distant are the two beads, the more independent is their motion. The size of the neighborhood of sequentially connected beads defines the characteristic length of a fiber element. These fiber elements overlap each other as neighborhoods of the beads overlap. Thus, it is assumed that the position vector of a bead is correlated to that of another bead in the same fiber element only. The correlation is called auto-correlation since x and y components of the bead position vector are correlated to the corresponding components of the other bead position vector.

(c) The motion of the fiber threadline is assumed to be a Markov process. As described by Stewart (1994), a Markov process is a stochastic process whose future evolution only depends on its current state and not on its past history. The theory of Markov processes is used to analyze diffusion, Brownian motion, electromagnetic signals, and many other stochastic processes. Gillespie (1992) defines a stochastic process as a random function $X(t)$ whose values up to and including parameter t allow one to probabilistically predict the function's value at an infinitesimally later parameter value $t+dt$. The values of the random function $X(t)$ are called states, and a set of these states is called the state space of the process. The

state space of a stochastic process can be discrete or continuous. A continuous stochastic process has a continuous (real-valued) state space, and its parameter space is also continuous. The fiber threadline motion is considered as a continuous Markov process because the fiber threadline is a continuously moving strand that assumes various positions in a real-valued space at real-valued times. The state of a fiber bead in the fiber threadline is defined by its position and its momentum, which are correlated to the positions and the momentums of the other beads in the same fiber element. Since the motion of a fiber bead is assumed to be a continuous Markov process, the future state of a fiber bead is dependent only on its present state, and is independent of its past states. It is reasonable to consider the motion of the fiber threadline as a continuous Markov process since the momentum from the past state is conserved in the present state and not in the future state. Furthermore, the momentum at the present position of a fiber bead, the momentum transfer from the external forces, and the future states of the other beads in the same fiber element define the future position and the momentum of the fiber bead. Therefore, the future state of a fiber bead is independent of the past states, and only dependent on the present state. This assumption can be used to predict the fiber laydown pattern as described in a later section.

In the present study, the assumptions (a)-(c) are validated using the experimental data. With the above assumptions, the fiber density distribution is the actual probability density distribution of the positions of individual fiber beads. The cumulative distribution function for the fiber bead probability density distribution function is normalized in the xy plane. In the following sections, some relevant mathematical properties for the bivariate normal distribution are presented in relation to the fiber motion.

3.4.1.1 Bivariate Normal Distribution

For a bivariate Gaussian probability distribution, the probability $p(x, y)$ of fiber being present at position (x, y) can be described in the general case as (Johnson and Kotz, 1972)

$$p(x, y) = \frac{1}{2\pi\sigma_x\sigma_y\sqrt{1 - \rho^2}} \exp\left(-\frac{1}{2}g(x, y)\right) \tag{3.2}$$

where

σ_x = standard deviation of positions of fiber in x direction

σ_y = standard deviation of positions of fiber in y direction

ρ = correlation coefficient of fiber positions in x and y directions

The quantity $g(x, y)$ in equation (3.2) is defined as

$$g(x,y) = \frac{1}{(1-\rho^2)}\left[\left(\frac{x-\mu_x}{\sigma_x}\right)^2 - 2\rho\left(\frac{x-\mu_x}{\sigma_x}\right)\left(\frac{y-\mu_y}{\sigma_y}\right) + \left(\frac{y-\mu_y}{\sigma_y}\right)^2\right] \quad (3.3)$$

where

μ_x = mean position of fiber in x direction

μ_y = mean position of fiber in y direction

Fitting the distribution is mathematically simplified if the distribution is standardized. By substituting $\mu_x = \mu_y = 0$ and $\sigma_x = \sigma_y = 1$ in equations (3.2) and (3.3), the following standardized bivariate distribution can be obtained:

$$p(\zeta_x, \zeta_y) = \frac{1}{2\pi\sqrt{1-\rho^2}} \cdot \exp\left(-\frac{1}{2(1-\rho^2)} \cdot \left[\zeta_x^2 - 2\rho\zeta_x\zeta_y + \zeta_y^2 \right] \right) \quad (3.4)$$

The ζ_x and ζ_y are normalized variables given by

$$\zeta_x = \frac{x - \mu_x}{\sigma_x} \quad (3.5a)$$

and

$$\zeta_y = \frac{y - \mu_y}{\sigma_y} \quad (3.5b)$$

Johnson and Kotz (1972) have shown that quadratic term $g(x, y)$ in equation (3.3) follows a χ^2 distribution with 2 degrees of freedom. Therefore, statistic χ^2 with two degrees of freedom ($\nu = 2$) and χ^2 probability distribution $f(\chi^2)$ are represented by

$$\xi = \chi^2_{\nu=2} = g(x, y) \quad (3.6)$$

and

$$f(\xi) = \frac{\xi^{(\nu-2)/2}\exp(-\xi/2)}{\left[2^{\nu/2}\Gamma(\nu/2)\right]} = \frac{1}{2}\cdot\exp\left(-\frac{\xi}{2}\right) \tag{3.7}$$

If α percent of the distribution is contained in the region $0 \le \chi^2 \le K$, then

$$\frac{\alpha}{100} = Pr\left[\chi^2 \le K\right] = 1 - \int_K^{\infty} \frac{\exp\left(-\chi^2/2\right)}{2}\, d\chi^2 \tag{3.8}$$

Integration gives

$$\frac{\alpha}{100} = 1 - \exp\left(-\frac{K}{2}\right) \tag{3.9}$$

Solving for K gives

$$K = -2\ln\left(1 - \frac{\alpha}{100}\right) \tag{3.10}$$

For arbitrary α and K, the ellipse, which contains α percent of the distribution, can be obtained by substituting equations (3.6) and (3.10) into equation (3.3) to obtain

$$\left(\frac{x-\mu_x}{\sigma_x}\right)^2 - 2\rho\left(\frac{x-\mu_x}{\sigma_x}\right)\left(\frac{y-\mu_y}{\sigma_y}\right) + \left(\frac{y-\mu_y}{\sigma_y}\right)^2 = -2(1-\rho^2)\ln\left(1-\frac{\alpha}{100}\right) \qquad (3.11)$$

The equation (3.11) is the most general form of equation for an ellipse. This equation represents an ellipse whose center does not lie at the center of the origin and whose major axis has been rotated about its center. The center of the general ellipse (μ_x, μ_y) can be translated to the origin of the coordinate system. The equation of this translated ellipse is given by

$$\left(\frac{x'}{\sigma_x}\right)^2 - \frac{2\rho x'y'}{\sigma_x\sigma_y} + \left(\frac{y'}{\sigma_y}\right)^2 = -2(1-\rho^2)\ln\left(1-\frac{\alpha}{100}\right) \qquad (3.12)$$

where

$$x' = x - \mu_x$$

and

$$y' = y - \mu_y$$

Then, the translated ellipse, given by equation (3.12), can be rotated by applying the following transformation:

$$\begin{pmatrix} x'' \\ y'' \end{pmatrix} = \begin{pmatrix} \cos\theta & -\sin\theta \\ \sin\theta & \cos\theta \end{pmatrix} \begin{pmatrix} x' \\ y' \end{pmatrix} \tag{3.13}$$

where x'' and y'' are arbitrary coordinates of the ellipse rotated by an angle θ.

Therefore, the equation of the rotated ellipse is

$$\left(\frac{1}{\sigma_x^2} - \frac{\rho \sin 2\theta}{\sigma_x \sigma_y} \right) x'^2 + \left(\frac{1}{\sigma_y^2} + \frac{\rho \sin 2\theta}{\sigma_x \sigma_y} \right) y'^2$$
$$- \left(\frac{\sin 2\theta}{\sigma_x^2} - \frac{\sin 2\theta}{\sigma_y^2} + \frac{2\rho \cos 2\theta}{\sigma_x \sigma_y} \right) x'y' + 2(1 - \rho^2) \ln\left(1 - \frac{\alpha}{100} \right) = 0 \tag{3.14}$$

As described by Palmer and Krathwohl (1921), the major axis of the rotated ellipse coincides with the x axis when the third term (the term containing $x'y'$) in equation (3.14) becomes zero. Mathematically, this condition can be expressed by the following equation:

$$\frac{\sin 2\theta}{\sigma_x^2} - \frac{\sin 2\theta}{\sigma_y^2} + \frac{2\rho \cos 2\theta}{\sigma_x \sigma_y} = 0 \qquad (3.15)$$

Hence, the appropriate angle of rotation of the major axis of the ellipse can be obtained by solving equation (3.15) for θ; the resulting equation is

$$\theta = \frac{1}{2} \arctan \left[\frac{2\rho \sigma_x \sigma_y}{\left(\sigma_x^2 - \sigma_y^2 \right)} \right] \qquad (3.16)$$

Therefore, for a given variance vector, the rotation of the ellipse would depend on the correlation coefficient ρ. Table 3.1 shows the various values θ can have for three different cases. Since the two ends of the major axis of the distribution ellipse are indistinguishable from each other, the orientation angles ranging between 90° and 180° (as in case 3, Table 3.1) can be considered as negative angles lying

between -90° and 0°, respectively. Therefore, the transformed range of the orientation angles would be -90° to 90° instead of 0° to 180°. As described by Johnson and Kotz (1972), a zero correlation (as in case 2, Table 3.1) means that the variables are independent. In our case, it would mean that x coordinate of the fiber position is statistically independent of the y coordinate. However, zero correlation is not expected for the fiber threadline motion as there exists some interdependence between the x dimension momentum and the y dimension momentum of the threadline. Thus, the positions in the two orthogonal directions must depend on each other. This interdependence, however, may not be constant along the fiber threadline and may also vary with time. Varying values of the correlation coefficient along the threadline at a given time would cause the distribution ellipse to be oriented at different angles in the xy planes at different z positions for a given set of variance vectors. In a physical sense, a distribution ellipse is a cross-section of the fiber cone at a z position. A variation in the correlation coefficients along the threadline would mean that the cross-sections of the fiber cone at different z positions are oriented at different angles in the xy planes at a given time. Therefore, at any instant, the fiber cone would be twisted at different angles along the fiber threadline for a given set of variance vectors and correlation coefficients. The variation in the twisting angles could be a regular or irregular function of the z position and/or time. This means that, due to a variation in the twisting angles,

the fiber cone would have an irregular or a regular rotational motion in the xy planes.

A large absolute value of the correlation coefficient is also not expected as it would mean clustering of data points in a highly elliptical manner with the major axis much larger than the minor axis. Since Chhabra and Shambaugh (1996) have shown that fiber amplitude in the x direction is not very much larger than that in the y direction, a small value of the correlation coefficient is expected.

3.4.2 *Fitting the Data to the Distribution Function*

The bivariate normal distribution is a continuous function. However, the experimental data is discrete. The experimental bivariate data were fit by expanding a procedure outlined by Blank (1980) for a univariate normal distribution. For our bivariate case, Blank's procedure was transformed into the following steps:

1. The experimental position data (x and y coordinates for a given value of z) were grouped into cells that form a uniform spatial grid. Figure 3.2 shows the grid with the frequencies of fiber occurrences centered at each grid cell. The number of cells in each direction was calculated as a positive square root of the number

of observed positions. Square root values were rounded to the next higher integer values. The grid size in each direction was calculated by dividing the corresponding range of the measured variable in that direction by the number of cells .

2. The means and the standard deviations of both the variables from the grouped data were found with the following equations:

$$\mu_x = \frac{\sum_{i=1}^{n} fx_i \cdot x_i}{N}; \qquad \mu_y = \frac{\sum_{j=1}^{n} fy_j \cdot y_j}{N}$$

$$\sigma_x = \frac{\sqrt{\left(\sum_{i=1}^{n} fx_i \cdot x_i^2 \right) - \mu_x^2 \cdot N}}{(N-1)}; \qquad \sigma_y = \frac{\sqrt{\left(\sum_{j=1}^{n} fy_j \cdot x_j^2 \right) - \mu_y^2 \cdot N}}{(N-1)} \qquad (3.17)$$

where

$$fx_i = \sum_{j=1}^{n} f_{ij}$$

$$fy_j = \sum_{i=1}^{n} f_{ij}$$

$$N = \sum_{i=1}^{n} \sum_{j=1}^{n} f_{ij} = \text{number of observations}$$

$$n = \text{INTEGER}\left(\sqrt{N}\right) + 1$$

$\left(x_i, y_i\right)$ is the center of the cell C_{ij}

3. The correlation coefficient ρ of the variables was calculated from the raw data with the formula

$$\rho = \frac{\sum_{i=1}^{N}\left(x_i - \bar{x}\right)\cdot\left(y_i - \bar{y}\right)}{\sqrt{\left[\sum_{i=1}^{N}\left(x_i - \bar{x}\right)^2\right]\cdot\left[\sum_{i=1}^{N}\left(y_i - \bar{y}\right)^2\right]}} \tag{3.18}$$

where

$$\bar{x} = \frac{\sum_{i=1}^{N} x_i}{N}$$

$$\bar{y} = \frac{\sum_{i=1}^{N} y_i}{N}$$

4. The variables were normalized using equation set (3.5). The x and y values at the upper boundaries of the cells were used for this calculation.

5. The cumulative probability density function was computed for each grid cell using the normalized probability density function as given by equation (3.4). Since the data obtained from experiments were finite, the cumulative distribution function and the frequency of the grid cell C_{ij} were evaluated with these equations:

$$P\left(\zeta_{x_i}, \zeta_{y_j}\right) = \int_{-\infty}^{\zeta_{x_i}} \int_{-\infty}^{\zeta_{y_j}} p\left(\zeta_x, \zeta_y\right) d\zeta_x \, d\zeta_y - \int_{-\infty}^{\zeta_{x_i}} \int_{-\infty}^{\zeta_{y_{j-1}}} p\left(\zeta_x, \zeta_y\right) d\zeta_x \, d\zeta_y$$
$$- \int_{-\infty}^{\zeta_{x_{i-1}}} \int_{-\infty}^{\zeta_{y_j}} p\left(\zeta_x, \zeta_y\right) d\zeta_x \, d\zeta_y + \int_{-\infty}^{\zeta_{x_{i-1}}} \int_{-\infty}^{\zeta_{y_{j-1}}} p\left(\zeta_x, \zeta_y\right) d\zeta_x \, d\zeta_y \quad (3.19)$$

$$\Phi_{ij} = N \cdot P\left(\zeta_{x_i}, \zeta_{y_j}\right)$$

6. For a 95% confidence level, a χ^2 goodness-of-fit test was performed on the calculated frequencies and the observed frequencies of the cells.

3.4.3 Experimental Equipment

A single hole slot die was used in the experiments. The polymer was melted and pressurized in a Brabender extruder with a 19.0 mm (0.75 in.) diameter barrel and

381 mm (15 in.) long screw. The molten polymer was pumped to the die using a modified Zenith pump. See Tyagi and Shambaugh (1995) for an explanation of the polymer supply details. The polymer capillary of the die was 2.97 mm long and 0.407 mm in diameter, and the air slots were 0.73 mm wide and 74.6 mm long. The polymer used was 88 MFR (melt flow rate) Fina Dypro™ polypropylene with M_w = 160,000 and M_n = 40,000. Figure 3.1 shows the cross-section of the die. The following operating conditions were used in the experiments: discharge (nominal) air velocity = 26.8 m/s, discharge air temperature = 320°C, polymer mass flow rate = 0.3 g/min, and discharge polymer temperature = 330°C.

The fiber exiting the die was photographed with two Canon AE-1 cameras. One camera was equipped with a Tokina AT-X Macro 90 mm lens and the other camera had a Sigma 50 mm macro lens. A Sunpak Auto 622 Pro-system flash provided the illumination.

3.4.4 *Experimental Technique*

Any technique that can measure the fiber positions or the number of times the fiber passes through a position can be used for the stochastic modeling of the fiber motion. Chhabra and Shambaugh (1996) used laser Doppler velocimetry (LDV) to measure the fiber crossover frequency at a position in the *xy* plane below a melt

blowing die. The actual number of fiber crossovers at a position over a period of time was proportional to the crossovers through the measuring volume of the LDV. To evaluate the actual crossover frequency at a position, Chhabra and Shambaugh assumed the fiber distribution to be Gaussian. Since, in our work, the fiber distribution itself was to be evaluated, LDV could not be used. Instead, high speed flash photography was used to measure the fiber position at an instant of time.

The three orthogonal coordinates (x, y, and z) of a Cartesian system were used to define the fiber position. For a fixed value of z, only x and y coordinates need to be measured simultaneously. Two cameras, placed along x and y axes at the same z below the die, were simultaneously fired to capture, respectively, the y and the x coordinates of the fiber. Figure 3.3 shows the top view of the experimental setup. The camera placed along the y axis was called the x-camera since it captured the x coordinate of the fiber position. Similarly, the camera placed along the x axis was called the y-camera. The shutters of the cameras were manually operated in darkened conditions and a flash of about 1/14,000 second duration was fired. Because of the high velocity of light, the reflected light from the fiber essentially reached both cameras simultaneously. The x-camera was fitted with a 50 mm macro lens, while the y-camera had a 90 mm macro lens. To keep the field of view identical for both lenses, the x-camera was placed 9 cm from the fiber, while the y-camera was placed 16 cm from the fiber. With this setup, the field of view of both

the lenses was 6 cm x 4.75 cm. The 50 mm lens was set at an f-stop of 11, while the 90 mm lens was set at an f-stop of 8. A stainless steel ruler with 1 mm graduations was temporarily placed along the z axis. The end of the ruler was placed at the polymer orifice of the die. Thus, a photograph of the ruler both defined the origin of the coordinate system (see Figure 3.1) and allowed us to scale the measurements of fiber positions. The ruler was removed before any polymer was extruded from the die. The film used was Kodak T-Max 400 developed with Kodak T-Max developer. The paper used was Kodak Polymax II RC at 3½ contrast grade.

The cameras were placed at z levels of 2.5 cm and 6.5 cm. At each z level, 100 replicate photographs were taken. A sample size of 100 was assumed to represent the fiber distribution completely. The time taken to obtain a data set at each z position was assumed to be sufficient to make the fiber motion process statistically stationary (i.e., invariant under an arbitrary shift in the time origin). The distance of the fiber from the zero position was measured for both x and y photographs at sixteen z levels between 0.5 cm and 8 cm. Photographic prints were developed with a magnification of four. Measurements had a precision of 0.1 mm in actual distance (not distance on the negative, but distance in the actual melt blowing system).

3.5 Results

A computer program in FORTRAN 77 was developed using the algorithm described previously. The program was run on an IBM RISC 6000 computer using the IMSL subroutine BNRDF to compute the bivariate normal cumulative distribution function (IMSL, 1994). The χ^2 goodness-of-fit test was done with a subroutine developed by Press et al. (1992). Surface and contour plots of the experimental distribution and the fitted bivariate normal distribution were gridded using the Kriging method; see Journel (1989).

It was found that, at a 95% confidence level, the experimental data fitted a bivariate normal distribution at all z positions studied. Figure 3.4 shows the root mean square deviation between the experimental data and the fitted distribution for various values of z. The average root mean square deviation of the probability of occurrence was 0.9%. The fitted distribution was found to normalize in the experimental range of the x and y values. Therefore, the experimental data completely represented the fiber distribution in the xy planes. Figures 3.5 and 3.6 depict the surface plots of the experimental and the fitted bivariate normal distribution at z = 20 mm. Figures 3.7 to 3.12 show both experimental and fitted data surface plots at z levels of 40, 60, and 80 mm (see Appendix II for the experimental and fitted fiber distribution surface plots for z = 10, 30, 50, and 70

mm). From these figures, it can be clearly seen that a bivariate normal distribution fits the experimental data. Figure 3.13 compares the contours of the fitted and the experimental distributions at $z = 20$ mm. Although minor peaks in experimental data are present, the dominant peak(s) is well-fit by the elliptical pattern. The arrow in the figure describes the orientation of the major axis of the (fitted) elliptical pattern with respect to the x axis. Both experimental and fitted data are oriented in the same direction. Similar contour plots for z positions of 40, 60, and 80 mm are shown in Figures 3.14, 3.15, and 3.16, respectively.

As a next step, the variations with z position of the statistical parameters of the fitted data were obtained. Figures 3.17 and 3.18 depict the auto-correlation profiles for the x and y directions, respectively. Both these plots show that a position of the fiber in the z direction is correlated only to those positions of the fiber that are in its close neighborhood along the same direction. The strongest auto-correlation is seen between the fiber z positions that are approximately 5 mm from each other. Therefore, under the studied conditions, a fiber element that forms a neighborhood is contained in a spatial separation of about 5 mm along the z direction (the spatial separation along the z direction is defined as the distance between the two xy planes along the z direction). The results of Figures 3.17 and 3.18 validate our assumptions that (a) the fiber threadline is a linked chain of fiber beads, and (b) the x and the y components of the position vector of a fiber bead are correlated only to

the corresponding components of the position vectors of the fiber beads lying in the same fiber element along fiber axis. However, the direction of the fiber axis may not be the same as the z direction. Shambaugh (1988) described the orientation of the fiber in different zones below a melt blowing die. The Rao and Shambaugh (1993) model emphasizes that the direction of the fiber axis is often different than the vertical direction. Therefore, a spatial separation along the z direction may not necessarily be equal to the length of a section of the fiber contained in it. Consequently, the size of a fiber element (which forms the neighborhood of the fiber beads, and is contained in the characteristic spatial separation of about 5 mm along the z direction) varies with the z position and the orientation of the fiber below the die. However, the characteristic spatial separation along the z direction does not vary with the z position below the die. Furthermore, low values of auto-correlations are seen in Figures 3.17 and 3.18 for the fiber z positions that are separated much further than 5 mm. Since the downstream fiber positions are the past states of the upstream fiber positions and the upstream fiber positions are weakly correlated with the downstream fiber positions further than than 5 mm, the future state (upstream fiber position) of the fiber motion is independent of its past state (downstream fiber position). This result validates our assumption that fiber threadline motion is a Markov process.

Figure 3.19 shows the profile of the correlation coefficient between x and y positions of the fiber. As expected, the correlation coefficient was low for all the z positions studied: an average absolute value of 0.08 was found for the correlation coefficient. This result implies little interdependence between the x and the y positions. As mentioned earlier in the mathematical formulation, a non-zero value of the correlation coefficient means a specific orientation of the major axis of the fiber distribution ellipse with respect to the x axis in the xy plane. Therefore, the physical effect of the variation of the correlation coefficient was studied as a variation of the orientation angle of the distribution ellipse. Figure 3.20 shows the variation of the orientation angle of the major axis of the distribution ellipse with respect to the x axis in the xy planes along the z direction. The graph shows that there is an aperiodic sinusoidal variation in the orientation angle profile. To extract the frequency of variation of the orientation angles, a Fourier transform of the data was taken. Since a fiber element was contained in a characteristic separation length of about 5 mm in the z direction, the data were sampled at a spatial separation (spatial period) of 5 mm. This corresponded to a sampling wave number (spatial frequency) of 1.26 mm^{-1}. Figure 3.21 shows the Fourier orientation angle amplitude spectrum plotted against the z direction spatial separation. The spectrum depicts the spatial separation content of the orientation angles. However, the spectrum does not give any indication where these spatial separations exist in the data set. According to Kramer (1996), a narrow Fourier amplitude spectrum

means that the variation of orientation angles has a dominant frequency or a spatial separation, which can produce almost sinusoidal variation. In contrast, a broad spectrum corresponds to a variety of frequencies that produce an irregular variation. It can be seen from Figure 3.21 that there is a high amplitude, narrow spectrum for the spatial separations of about 5mm, while there is a high amplitude, broad spectrum for the spatial separations larger than 15 mm. The low peaks in the spectrum are present for the spatial separations between 10 and 15 mm. This means that a large number of fiber cone cross-sections, which are spatially separated by 5 mm, have an almost sinusoidal variation in their orientation angles in the xy planes. A small number of fiber cone cross-sections that are spatially separated between 10 and 15 mm also have an almost sinusoidal variation in their orientation angles in the xy planes. However, there are a large number of fiber cone cross-sections that are spatially separated between 20 and 40 mm and have an irregular variation in their orientation angles in the xy planes. These results again show that fiber threadline has a characteristic separation length of about 5 mm in the z direction. Furthermore, the fiber cone is twisted at angles that have a sinusoidal variation with a spatial separation of about 5 mm. A small number of higher harmonics in variation of the fiber cone twisting angles, which have a spatial separation between 10 and 15 mm, is also present. On the other hand, there is no correlation between the fiber cone twisting angles that are spatially separated by more than 15 mm. Thus, the fiber elements follow a Markov property of forgetting their past history. This validates the assumption that the fiber threadline

motion is a Markov process. The varying angles of orientation of the fiber cone cross-sections are seen in the distribution contours in Figures 3.13 through 3.16.

Figures 3.22 and 3.23 show, respectively, the x and the y dimension standard deviation profiles. Higher values of the standard deviation mean a greater spread of the distribution. For the bivariate normal distribution, 46.7% of the distribution is present within one standard deviation of both the variables with an absolute correlation coefficient of 0.08. The spread of the fiber distribution is linear. For the same die, Harpham and Shambaugh (1996; 1997) have shown that the air jets also spread linearly with z position. The air jet half-width describes the jet spread. (The jet half-width is a position, transverse to the axial flow, where the velocity of the jet falls to half its maximum value.) Figure 3.24 compares spreading of the fiber distribution and the air jets. The slope of the fiber spread is different from the slope of the air jet. However, the graph shows that fiber distribution is contained within one jet half-width of the air jet. The best-fit line for the fiber standard deviation profile lies at almost half the distance from the jet half-width line. Furthermore, it has been found that about 96% of the fiber distribution is present within one jet half-width. This means that the energy from the air jet is transferred to the fiber within one jet half-width. Tennekes and Lumley (1972) describe the energy cascade in a turbulent jet. The energy from the mean flow is transferred to the large eddies via shear forces. The large eddies, which are mostly present

between the center and one jet half-width, lose their energy to the small eddies by vortex shedding. These small eddies, which are present toward the center of the jet, lose their energy by viscous dissipation. It is possible that the energy from the eddies is transferred to the fiber in melt blowing. Gutmark and Wygnanski (1976) have shown that most of the energy transactions in a rectangular turbulent jet take place within one jet half-width. A fiber segment might leave the turbulent jet. However, because the segment is linked, the segment tends to be drawn back into the turbulent jet. Therefore, it is reasonable that about 96% the fiber distribution lies within one jet half-width.

The linear spreading and the rotational character of the fiber motion mathematically describe the fiber cone as studied by Chhabra and Shambaugh (1996). Figure 3.25 depicts the profile of the distribution sample mean values in both x and y directions. An expected population mean zero position is shown as the dotted line in the plot. Closeness to mean zero position is seen at all z positions studied.

3.6 Conclusions

The foremost conclusion of this study is that the fiber density distribution follows a unimodal bivariate probability distribution. One such distribution that fits the

experimental data is a bivariate normal distribution. Statistical analysis shows that the fiber motion in the transverse plane (xy plane) is almost independent in the two orthogonal directions (x and y) forming the plane. However, due to the non-zero value of the correlation between the x and y coordinates of the fiber position, the major axis of the distribution ellipse is oriented at a certain angle with respect to the x axis in the xy plane. There is a high degree of sinusoidal variation in the orientation angles of the fiber cone cross-sections along the z direction. This suggests that the fiber motion is that of an elliptical spiral which sinusoidally rotates in the transverse planes.

The fiber distribution spreads linearly with the z direction. This is a corollary to the linear increase in fiber cone amplitude as shown by Chhabra and Shambaugh (1996). From the present study and from the studies on the flow field of the jet by Harpham and Shambaugh (1996; 1997), it can be concluded that most of the transverse motion of the fiber threadline takes place within one jet half-width. The dynamics of the turbulent air jet also suggest the presence of most of the fiber distribution within one jet half-width.

The fiber positions are auto-correlated only to those positions that lie within a length of a fiber element along the fiber axis. This means that a fiber position along the threadline is only affected by the fiber positions that are in the close

neighborhood. This neighborhood of the fiber beads (fiber element) is contained in a characteristic spatial separation of about 5 mm in the z direction. Furthermore, since the motion of the fiber threadline is a continuous Markov process, the future state of a fiber threadline section is only dependent on its present state, and is independent of its past states. Therefore, the downstream fiber positions in the xy plane will not affect the upstream fiber positions, if the positions are further apart than a characteristic spatial separation along the z direction, and vice versa. If an imaginary screen, which allowed only air to pass through, was positioned in the xy plane at an arbitrary z position, the fiber would be captured by that screen. Since the captured fiber sections would not affect the fiber section that is just reaching the screen, the laydown pattern of the fiber would follow a bivariate normal distribution. Therefore, the fiber laydown pattern can be predicted from the obtained fiber distribution. Figure 3.26 shows the top view of the fiber pattern formed on a real (not imaginary) wire-mesh screen placed at z position of 300 mm. The collection time was about one minute. The air flow characteristics of this screen (the screen had 65% open space) approximate the flow character of an imaginary screen. The photograph in Figure 3.27 depicts the side view of the fiber collected for a longer duration (about 10 minutes) on the same screen at the same position. From the bell shape of the fiber distribution in Figure 3.27, we can conclude that the fiber laydown pattern follows a bivariate normal distribution.

Knowledge of the spread and the orientation of a fiber distribution will be used in future work. One future goal will involve predicting fiber-to-fiber entanglements below a multiple hole die. This knowledge of entanglements should be useful for tasks such as (a) designing the spatial separation of the spinneret holes in the melt blowing dies, and (b) predicting the structural properties of the melt-blown webs.

3.7 Nomenclature

c = camera to filament distance defined in Figure 3.3, cm

C = experimentally determined orientation parameter [see eq (3.1)]

C_{ij} = grid cell in Figure 3.2

fx_i = sum of frequencies of cells in the x direction [see eq (3.17)]

fy_i = sum of frequencies of cells in the y direction [see eq (3.17)]

f_{ij} = frequency of occurrence of fiber in grid cell C_{ij}

$f(\xi) = \chi^2$ probability distribution [see eq (3.6)]

K = upper limit of χ^2 probability distribution region [see eq (3.10)]

m_p = polymer mass flow rate, g/min

N = number of observations

$N(\epsilon)$ = fiber orientation distribution function [see eq (3.1)]

$p(x, y)$ = probability density distribution function

$P(\zeta_x, \zeta_y)$ = cumulative probability density distribution function of a cell [see eq (3.19)]

s = flash to filament distance defined in Figure 3.3, cm

T_a = air temperature at die discharge, °C

T_p = polymer temperature at die discharge, °C

v_{jo} = nominal air discharge velocity, m/s

x = Cartesian coordinate defined in Figure 3.1, mm

$\bar{x}$ = abscissa of the center of the grid cell C_{ij} [see eq (3.17)]

x' = arbitrary x coordinate of the translated ellipse [see eq (3.12)]

x'' = arbitrary x coordinate of the rotated ellipse [see eq (3.13)]

y = Cartesian coordinate defined in Figure 3.1, mm

$\bar{y}$ = ordinate of the center of the grid cell C_{ij} [see eq (3.17)]

y' = arbitrary y coordinate of the translated ellipse [see eq (3.12)]

y'' = arbitrary y coordinate of the rotated ellipse [see eq (3.13)]

z = Cartesian coordinate defined in Figure 3.1, mm

Greek Symbols

α = percentage distribution contained in the ellipse [see eq (3.10)]

ϵ = fiber orientation angle [see eq (3.1)]

μ = mean position of the fiber [see eq (3.17)], mm

Φ_{ij} = calculated frequency of the grid cell C_{ij}

ν = degrees of freedom

θ = angle between major axis of the distribution ellipse and the x axis [see eq (3.16)], deg

ρ = correlation coefficient of the fiber positions in x and y directions [see eq (3.18)]

σ = standard deviation of the fiber positions [see eq (3.17)], mm

ω = angle between the flash and the y-camera defined in Figure 3.3, deg

$\xi = \chi^2$ statistic defined in eq (3.6)

ζ = normalized random variable [see eq (3.5)]

3.8 References

Aggarwal, R. K.; Kennon, W. R.; Porat, I. A Scanned-laser Technique for Monitoring Fibrous Webs and Nonwoven Fabrics. *J. Textile Inst.* **1992,** *83* (3), 386-398.

Blank, L. T. *Statistical Procedures for Engineering, Management, and Science*; McGraw-Hill: New York, NY, 1980, 229-231.

Boeckerman, P. A. Meeting the Special Requirements for On-line Basis Weight Measurement of Lightweight Nonwoven Fabrics. *Tappi J.* **1992,** *75* (12), 166-172.

Chhabra, R.; Shambaugh, R. L. Experimental Measurements of Fiber Threadline Vibrations in the Melt-Blowing Process. *Ind. Eng. Chem. Res.* **1996,** *35* (11), 4366-4374.

Ericson, C. W.; Baxter, J. F. Spunbonded Nonwoven Fabric Studies I: Characterization of Filament Arrangement in the Web. *Textile Res. J.* **1973,** *43*, 371-378.

Evans, C.; Haimov, S.; Moore, R. K.; Hesany, V. Determination of Ocean Environmental Parameters from a Ka-band Scatterometer. *Proc. Conference Oceans '93*, British Columbia, Canada, Oct 18-21. **1993,** 1-4.

Gillespie, D. T. *Markov Processes: An Introduction for Physical Scientists*; Academic Press: San Diego, CA, 1992, 59-61.

Gutmark, E.; Wygnanski, I. The Planar Turbulent Jet. *J. Fluid Mech.* **1976,** *73* (3), 465-495.

Harpham, A. S.; Shambaugh, R. L. Flow Field of Practical Dual Rectangular Jets. *Ind. Eng. Chem. Res.* **1996,** *35* (10), 3776-3781.

Harpham, A. S.; Shambaugh, R. L. Velocity and Temperature Fields of Dual Rectangular Jets. *Ind. Eng. Chem. Res.* **1997**, *36* (9), 3937-3943.

Hearle, J. W. S.; Stevenson, P. J. Nonwoven Fabric Studies, Part III: The Anisotropy of Nonwoven Fabrics. *Textile Res. J.* **1963**, *33*, 877-888.

Holst, E.; Schneider, T. Fiber Size Characterization and Size Analysis using General and Bivariate Log-normal Distributions. *J. Aerosol Sci.* **1985**, *16* (5), 407-413.

Huang, X. C.; Bresee, R. R. Characterizing Nonwoven Web Structure using Image Analysis Techniques. Part I: Pore Analysis in Thin Webs. *INDA J. Nonwovens Res.* **1993**, *5* (1), 13-21.

Huang, X. C.; Bresee, R. R. Characterizing Nonwoven Web Structure using Image Analysis Techniques. Part III: Web Uniformity Analysis. *INDA J. Nonwovens Res.* **1993**, *5* (3), 28-38.

IMSL Integrated Mathematical and Statistical Libraries Stat/Library. *FORTRAN Subroutines for Statistical Applications*, Vol. 2; Visual Numerics: Houston, TX, 1994, 1128-1129.

Johnson, N. L.; Kotz, S. *Distributions in Statistics: Continuous Multivariate Distributions*; John Wiley and Sons: New York, NY, 1972.

Journel, A. G. *Fundamentals of Geostatistics in Five Lessons. A Short Course on Geology*, Vol. 8; American Geophysical Union: Washington D.C. 1989, 15-21.

Kallmes, O. J. Technique for Determining the Fiber Orientation Distribution Throughout the Thickness of a Sheet. *Tappi J.* **1969**, *52* (3), 482-485.

Kayser, J. C.; Shambaugh, R. L. The Manufacture of Continuous Polymeric Filaments by the Melt Blowing Process. *Polym. Eng. Sci.* **1990**, *30* (19), 1237-1251.

Kramer, S. L. *Geotechnical Earthquake Engineering*; Prentice Hall: NJ, 1996, 71-72.

Mardia, K. V. *Families of Bivariate Distributions*; Hafner Publishing Co.: Darien, Conn. 1970.

Milligan, M. W.; Haynes, B. D. Empirical Models for Melt Blowing. *J. Appl. Polym. Sci.* **1995**, *58*, 159-163.

Palmer, C. L; Krathwohl, W. C. *Analytic Geometry*, 1st ed.; McGraw Hill Book Company: New York, NY, 1921, 127-128.

Pourdeyhimi, B. Assessing Fiber Orientation in Nonwoven Fabrics. *INDA J. Nonwovens Res.* **1993**, *5* (4), 29-36.

Press, W. H.; Teukolsky, S. A.; Vetterling, W. T.; Flannery, B. P. *Numerical Recipes in FORTRAN: The Art of Scientific Computing*, 2nd ed.; Cambridge University Press: New York, NY, 1992, 615-617.

Prud'homme, R. E.; Hien, N. V.; Noah, J.; Marchessault, R. H. Determination of Fiber Orientation of Cellulosic Samples by X-ray Diffraction. *J. Appl. Polym. Sci.* **1975**, *19*, 2609-2620.

Rao, R. S.; Shambaugh, R. L. Vibration and Stability in the Melt Blowing Process. *Ind. Eng. Chem. Res.* **1993**, *32* (12), 3100-3111.

Rodrigues, F. C.; Carvalho, F. D.; Silva, M. S.; Peixoto, J. P. Measurement of Randomness in Fiber Distribution in Paper using Computer Vision. *Tappi J.* **1990**, *73* (12), 209-212.

Shambaugh, R. L. A Macroscopic View of the Melt Blowing Process for Producing Microfibers. *Ind. Eng. Chem. Res.* **1988**, *27* (12), 2363-2372.

Shanon, C. E. A Mathematical Theory of Communication. *Bell Sys. Tech. J.* **1948**, *27*, 379-423, 623-656.

Stewart, W. J. *Introduction to Numerical Solution of Markov Chains;* Princeton University Press: Princeton, NJ, 1994, 3-5.

Tennekes H.; Lumley, J. L. *A First Course in Turbulence;* The MIT Press: Cambridge, MA, 1972.

Tsai, P. P.; Bresee, R. R. Fiber Orientation Distribution from Electrical Measurements, Part II: Instrument and Experimental Measurements. *INDA J. Nonwovens Res.* **1991,** *3* (4), 1-6.

Tyagi, M. K.; Shambaugh, R. L. Use of Oscillating Gas Jets in Fiber Processing. *Ind. Eng. Chem. Res.* **1995,** *34* (2), 656-660.

Uyttendaele, M. A. J.; Shambaugh, R. L. Melt Blowing: General Equation Development and Experimental Verification. *AICHE J.* **1990,** *36* (2), 175-186.

Van den Akker, J. A.; Jentzen, C. A.; Spiegelberg. Effects on Individual Fibers of Drying under Tension. *Consolidation of the Paper Web,* 1st ed.; British Paper and Board Makers' Assn., 1966, 500-506.

Votava, R. J. A Practical Method - Measuring Paper Asymmetry Regarding Fiber Orientation. *Tappi J.* **1982,** *65* (4), 67-70.

Wu, T. T.; Shambaugh, R. L. Characterization of the Melt Blowing Process with Laser Doppler Velocimetry. *Ind. Eng. Chem. Res.* **1992,** *31* (1), 379-389.

ρ	σ	θ
case 1: $\rho > 0$	$\sigma_x > \sigma_y$	$0° < \theta < 45°$
	$\sigma_x = \sigma_y$	$\theta = 45°$
	$\sigma_x < \sigma_y$	$45° < \theta < 90°$
case 2: $\rho = 0$	$\sigma_x > \sigma_y$	$\theta = 0°$
	$\sigma_x = \sigma_y$	$\theta = 0°$
	$\sigma_x < \sigma_y$	$\theta = 0°$
case 3: $\rho < 0$	$\sigma_x > \sigma_y$	$135° < \theta < 180°$
	$\sigma_x = \sigma_y$	$\theta = 135°$
	$\sigma_x < \sigma_y$	$90° < \theta < 135°$

Table 3.1 Various values of θ for different values of ρ, σ_x, and σ_y

ρ	σ	θ
$\rho < 0$	$\sigma_x > \sigma_y$	$-45° < \theta < 0°$
	$\sigma_x = \sigma_y$	$\theta = -45°$
	$\sigma_x < \sigma_y$	$-90° < \theta < -45°$

Table 3.2 Modified values of θ for case 3, Table 3.1

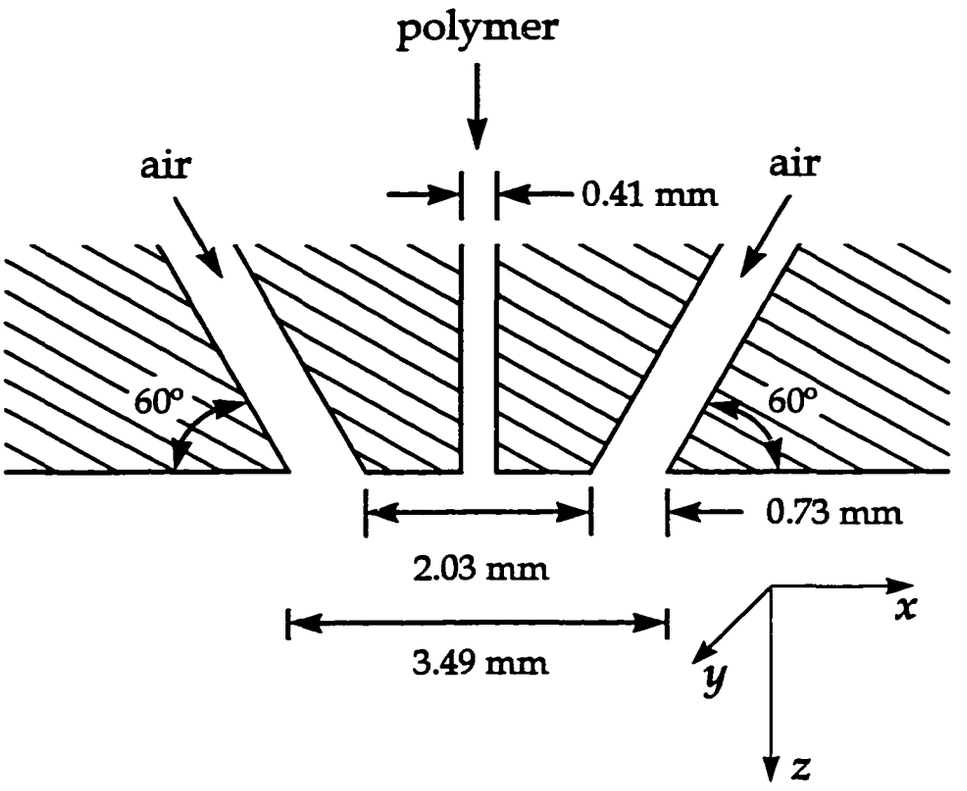

Figure 3.1 Cross section of the melt blowing die used in the experiments. The origin of the coordinate system, which is shown separately, lies at the polymer orifice of the die.

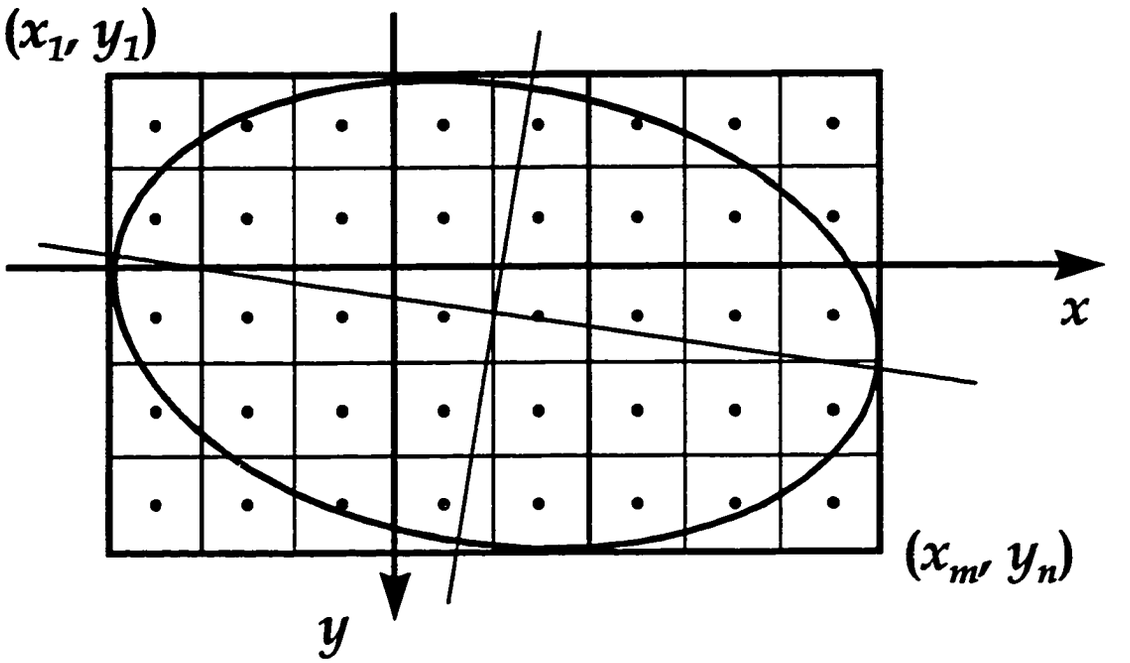

Figure 3.2 Gridding used to group the fiber position (x, y) data. Frequencies are shown to lie at the center of each grid cell. The fiber distribution is contained in the shown ellipse.

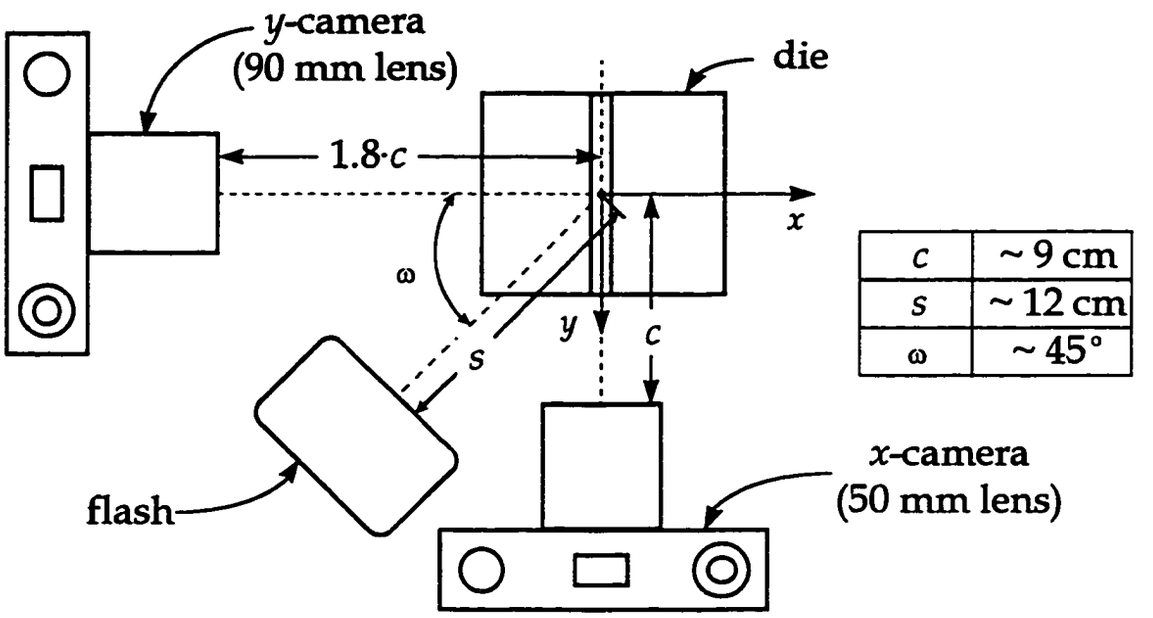

Figure 3.3 Top view of the experimental setup used to measure the fiber position data.

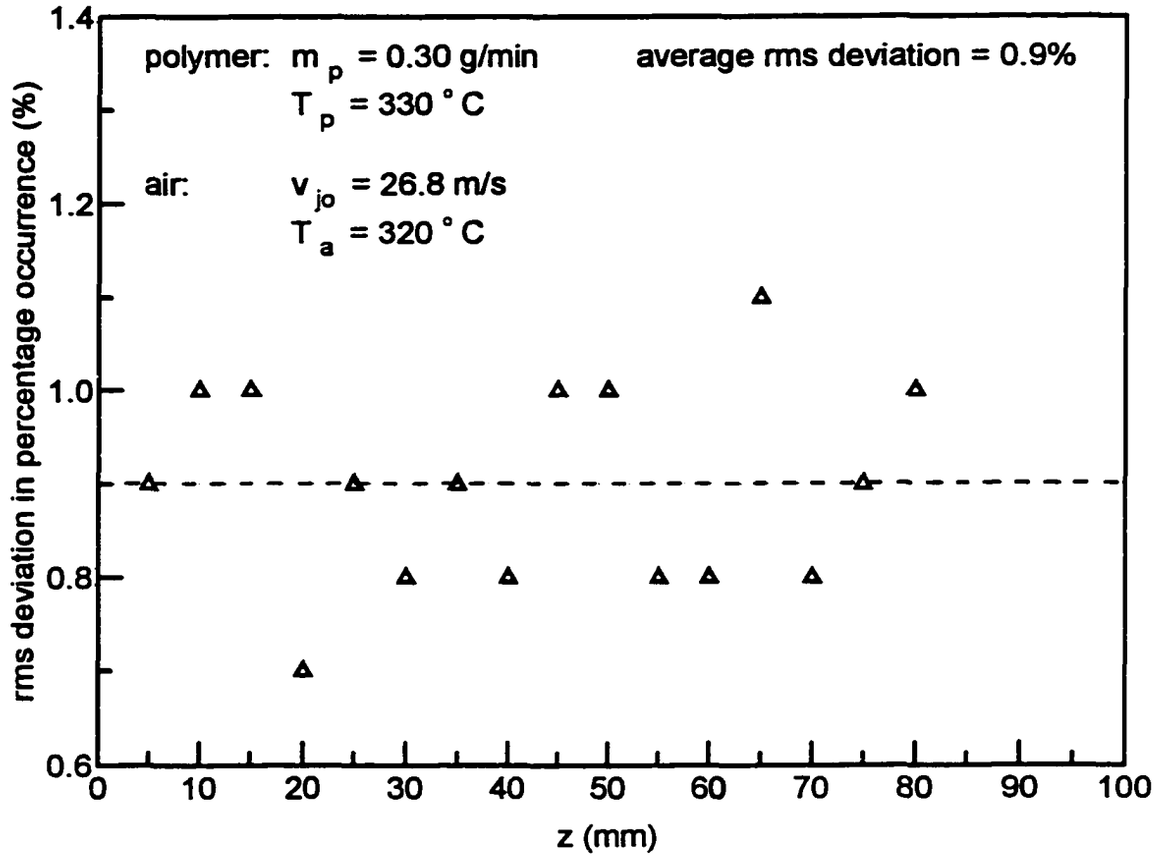

Figure 3.4 Root mean square deviation between the experimental data and the fitted distribution for various values of z below the die.

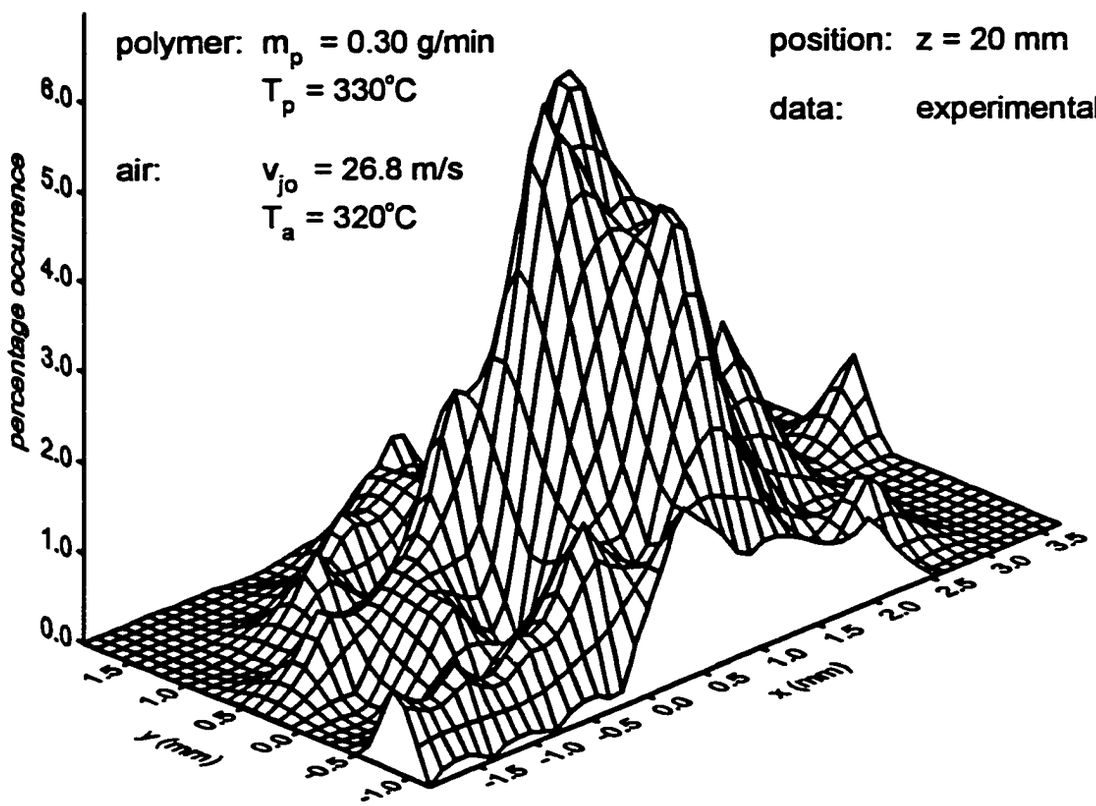

Figure 3.5 Surface plot of experimental fiber density distribution at z = 20 mm.

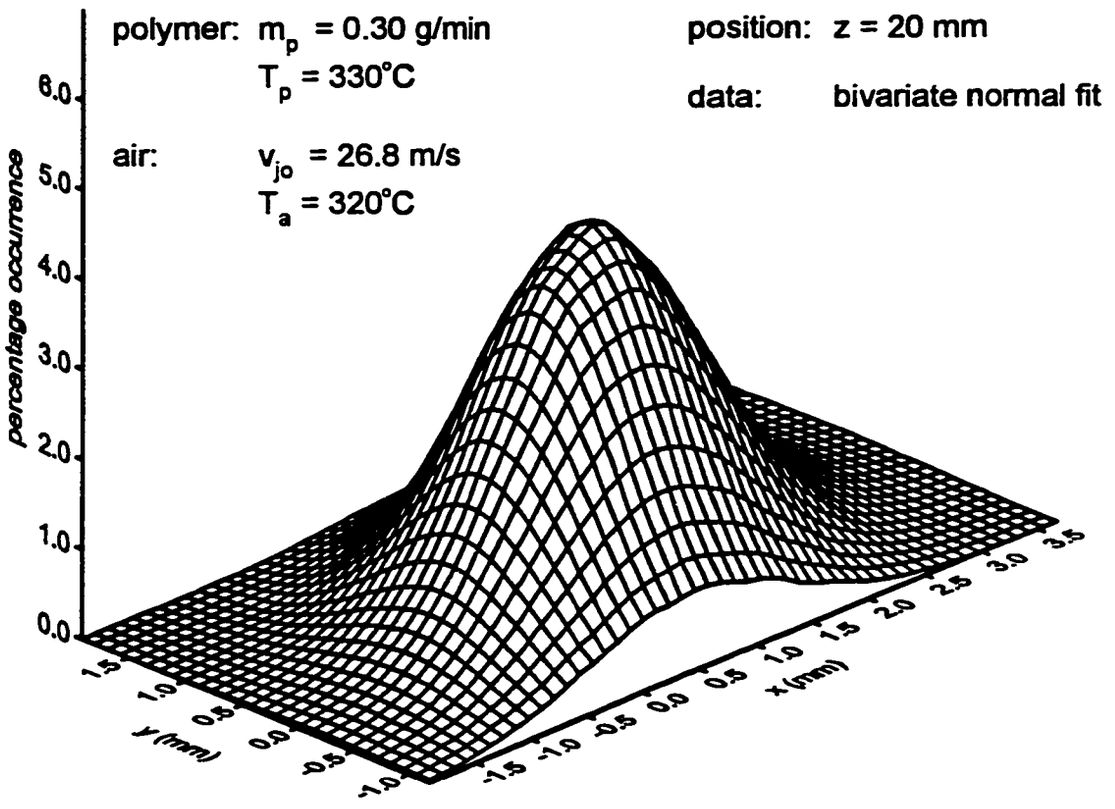

Figure 3.6 Surface plot of fitted bivariate normal distribution at z = 20 mm.

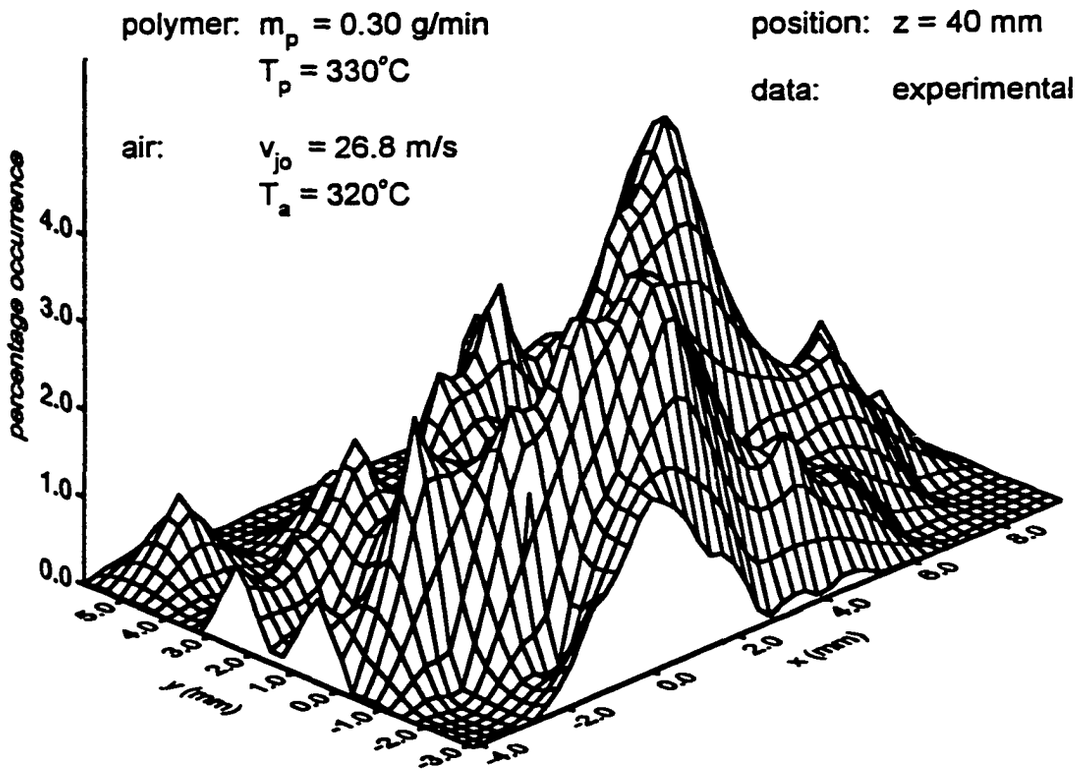

Figure 3.7 Surface plot of experimental fiber density distribution at z = 40 mm.

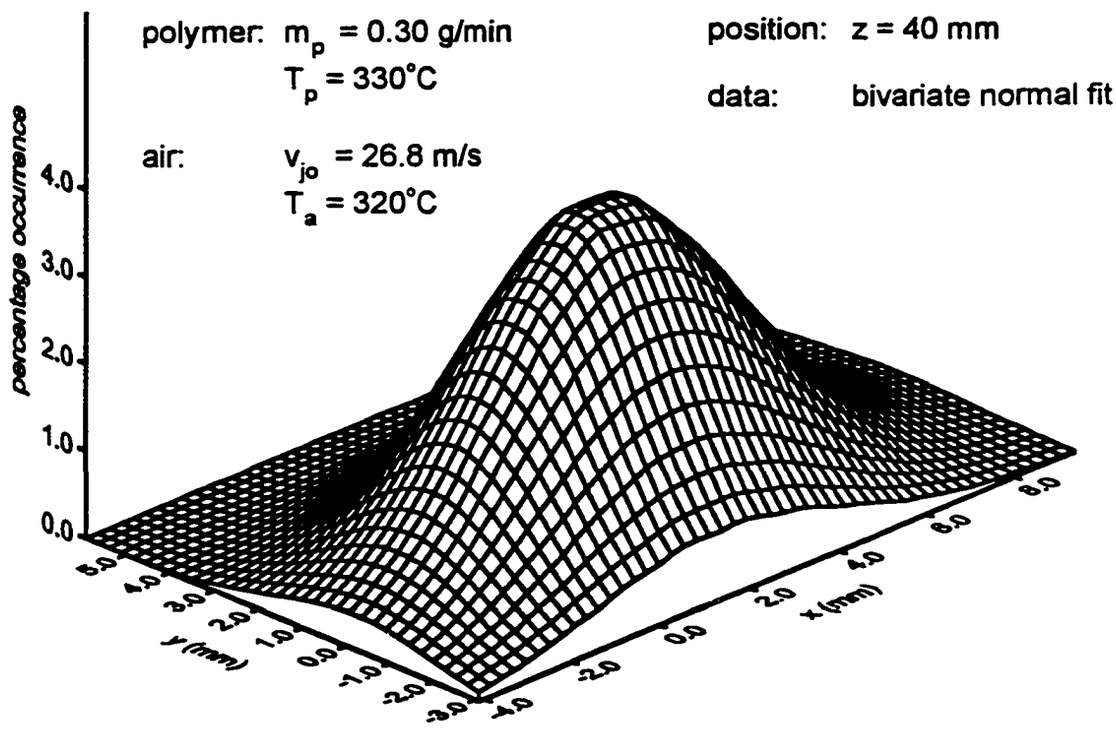

Figure 3.8 Surface plot of fitted bivariate normal distribution at z = 40 mm.

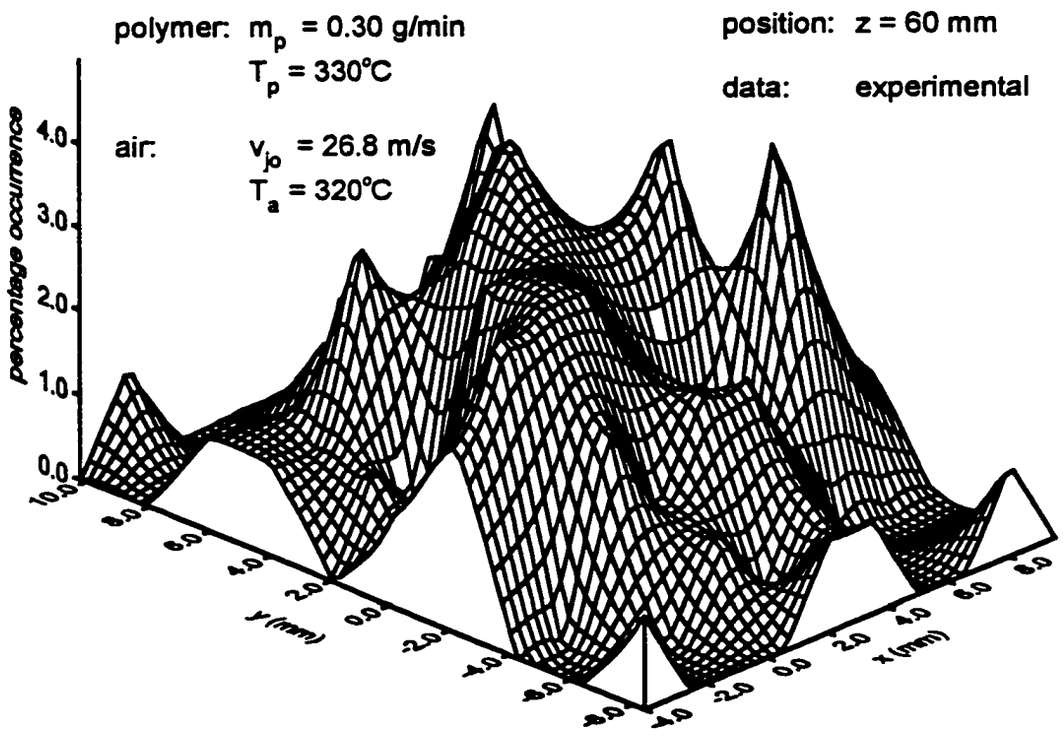

Figure 3.9 Surface plot of experimental fiber density distribution at z = 60 mm.

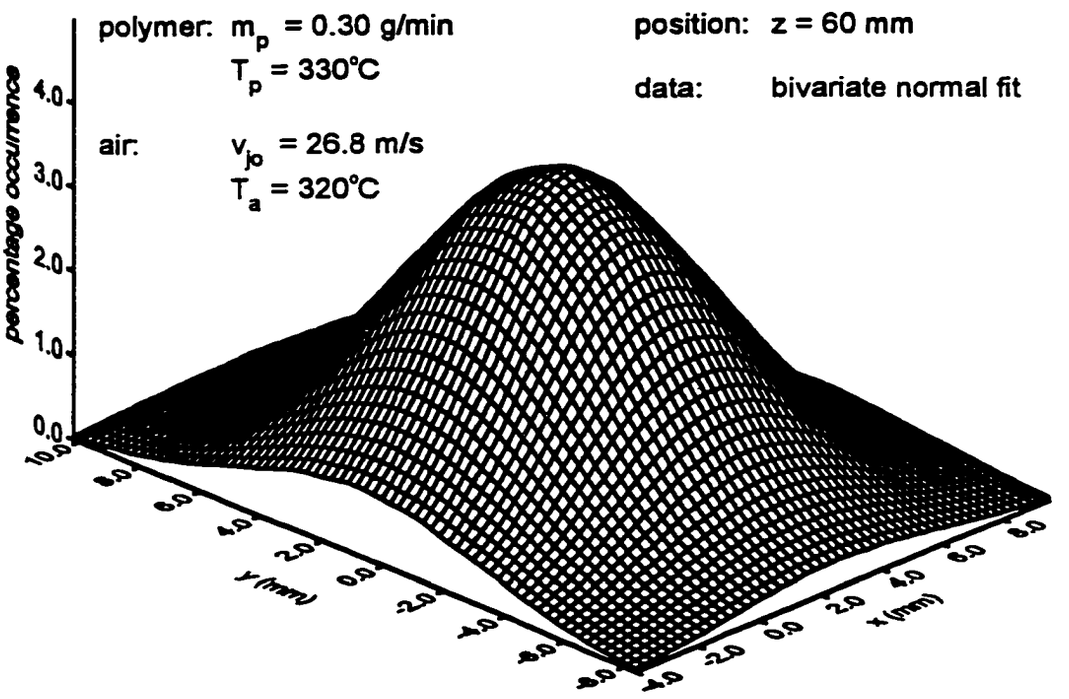

Figure 3.10 Surface plot of fitted bivariate normal distribution at z = 60 mm.

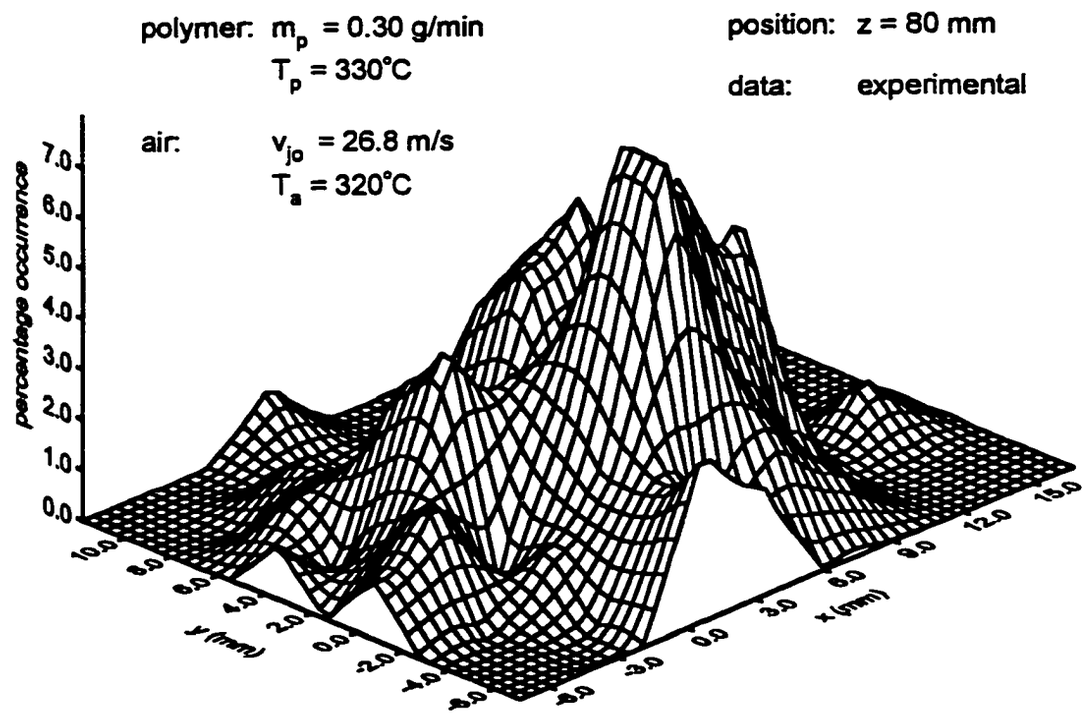

Figure 3.11 Surface plot of experimental fiber density distribution at z = 80 mm.

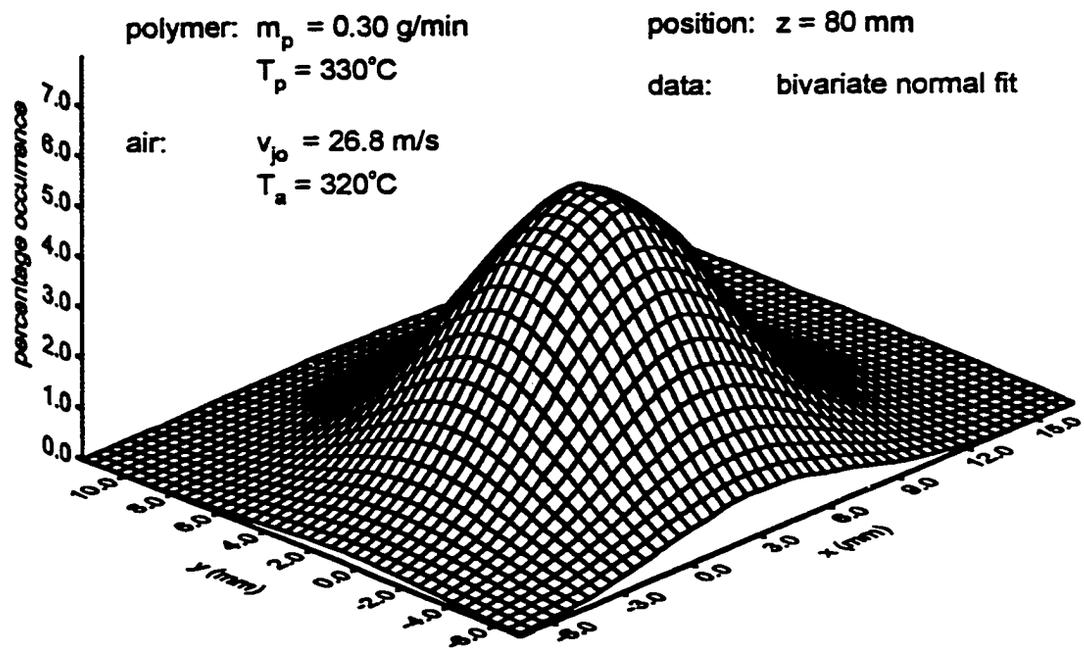

Figure 3.12 Surface plot of fitted bivariate normal distribution at z = 80 mm.

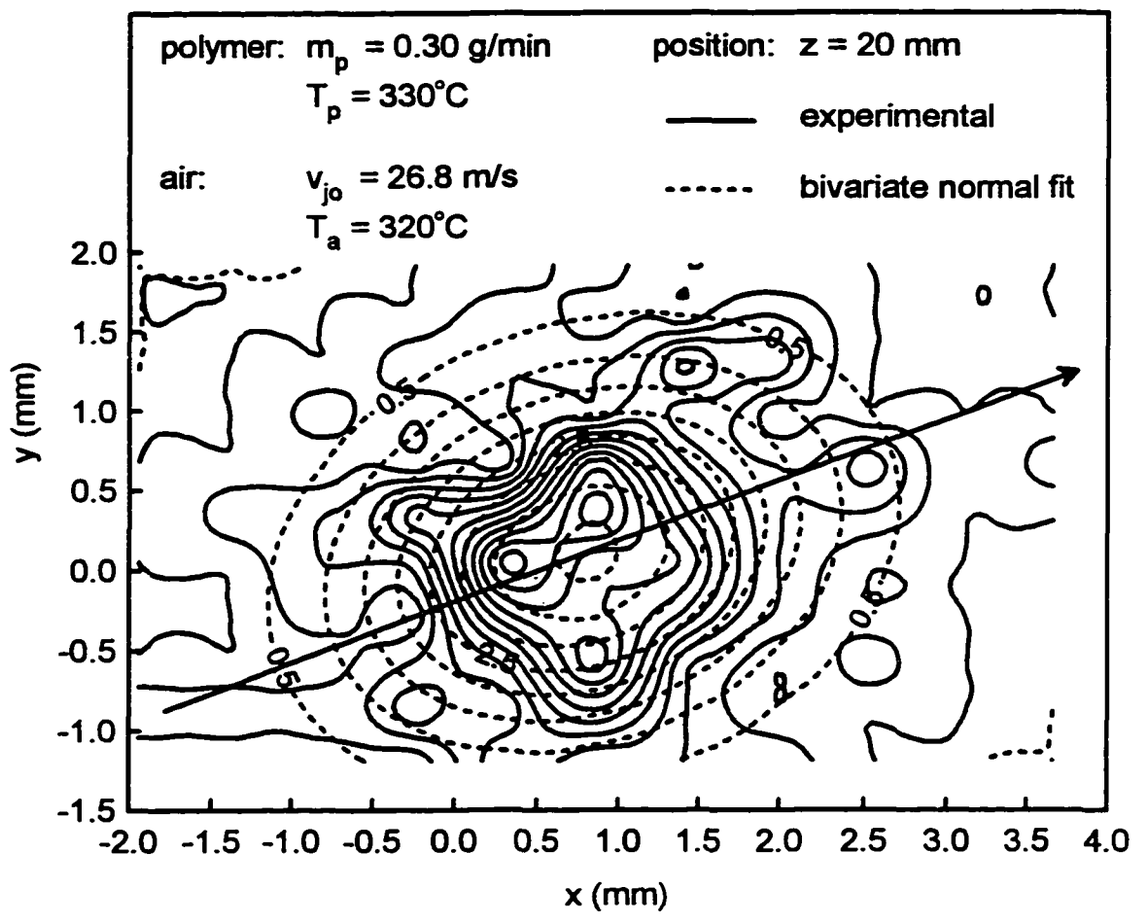

Figure 3.13 Contour plots showing the experimental and fitted bivariate normal distribution at $z = 20$ mm. The direction of the arrow shows that the major axis of the elliptical pattern is oriented at 20.8° with respect to the x axis.

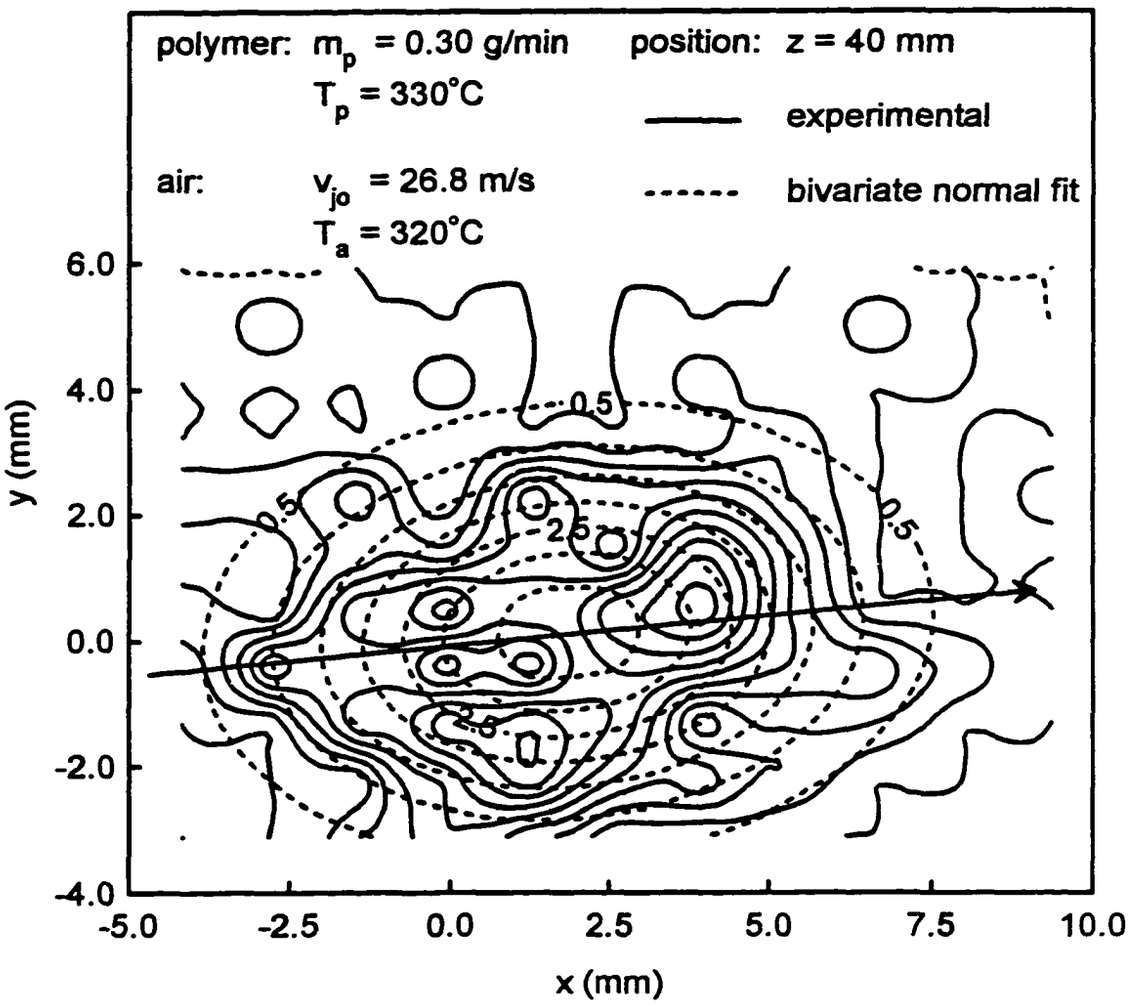

Figure 3.14 Contour plots showing the experimental and fitted bivariate normal distribution at $z = 40$ mm. The direction of the arrow shows that the major axis of the elliptical pattern is oriented at 5.5° with respect to the x axis.

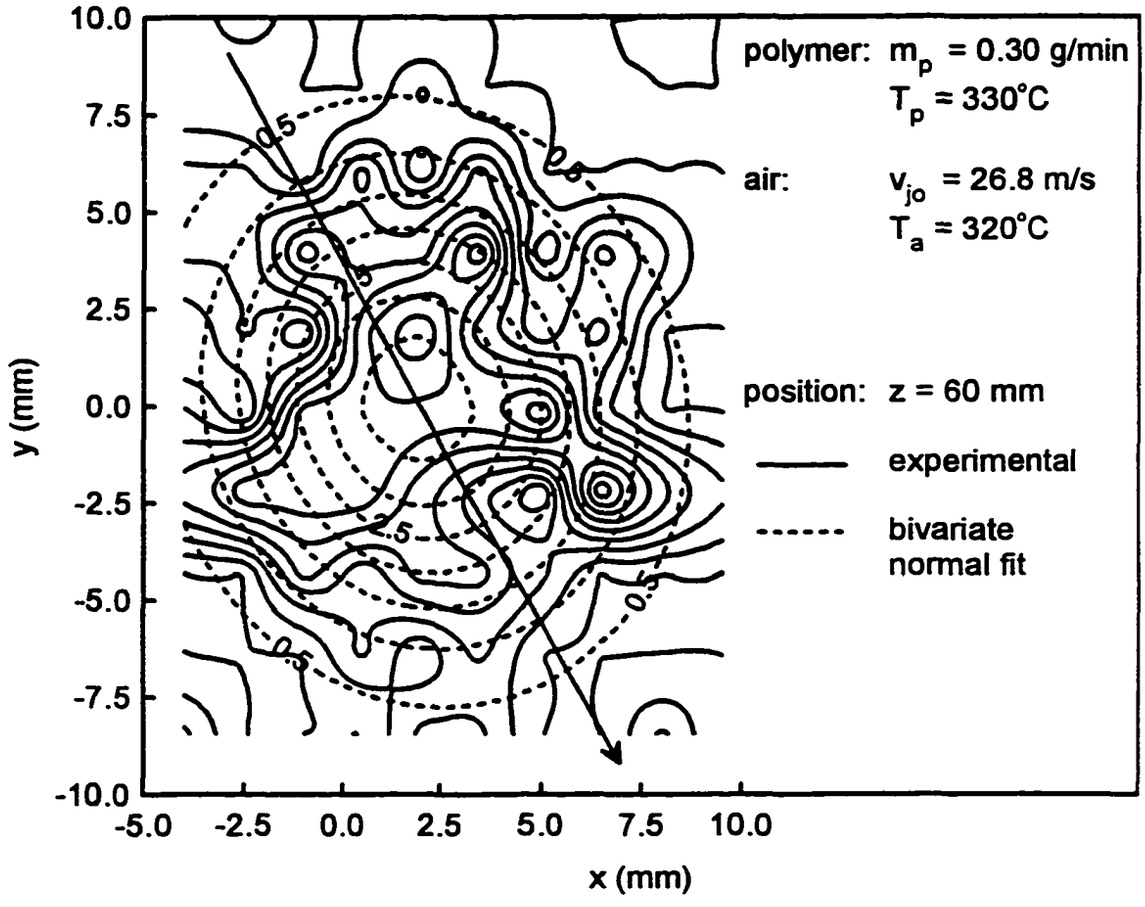

Figure 3.15 Contour plots showing the experimental and fitted bivariate normal distribution at $z = 60$ mm. The direction of the arrow shows that the major axis of the elliptical pattern is oriented at -73.4° with respect to the x axis.

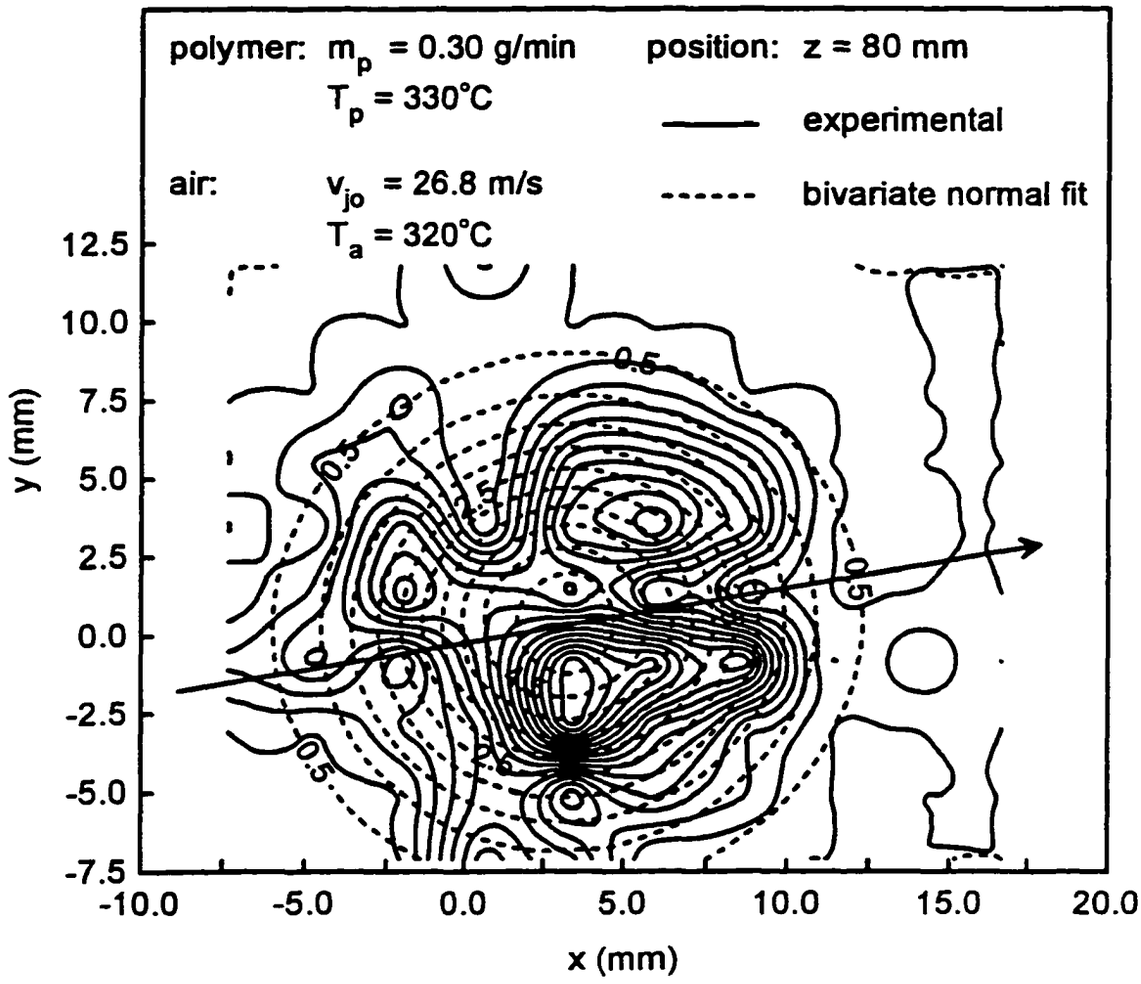

Figure 3.16 Contour plots showing the experimental and fitted bivariate normal distribution at $z = 80$ mm. The direction of the arrow shows that the major axis of the elliptical pattern is oriented at 9.9° with respect to the x axis.

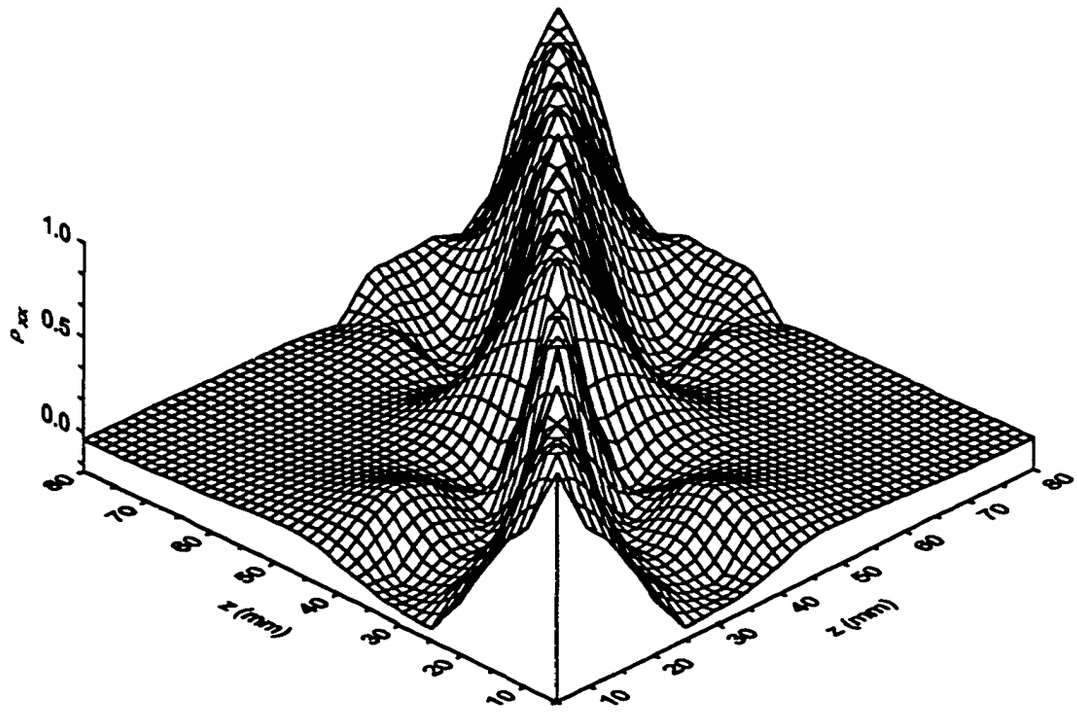

Figure 3.17 Surface plot showing the auto-correlation ρ_{xx} between the x components of the fiber positions in the xy planes at different z levels below the die.

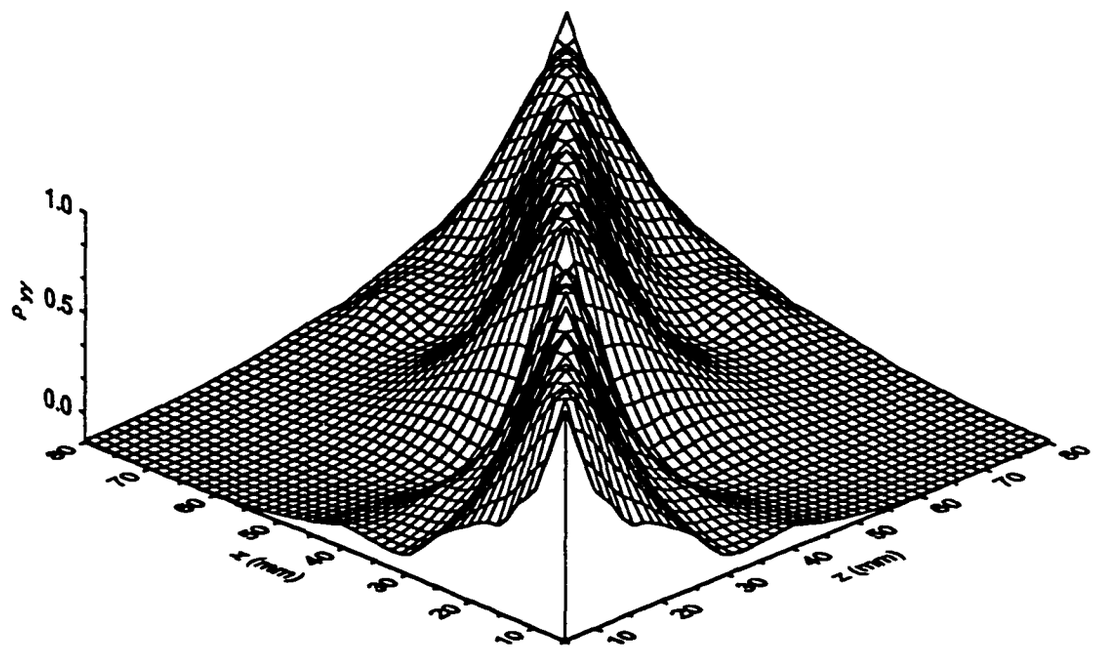

Figure 3.18 Surface plot showing the auto-correlation ρ_{yy} between the y components of the fiber positions in the xy planes at different z levels below the die.

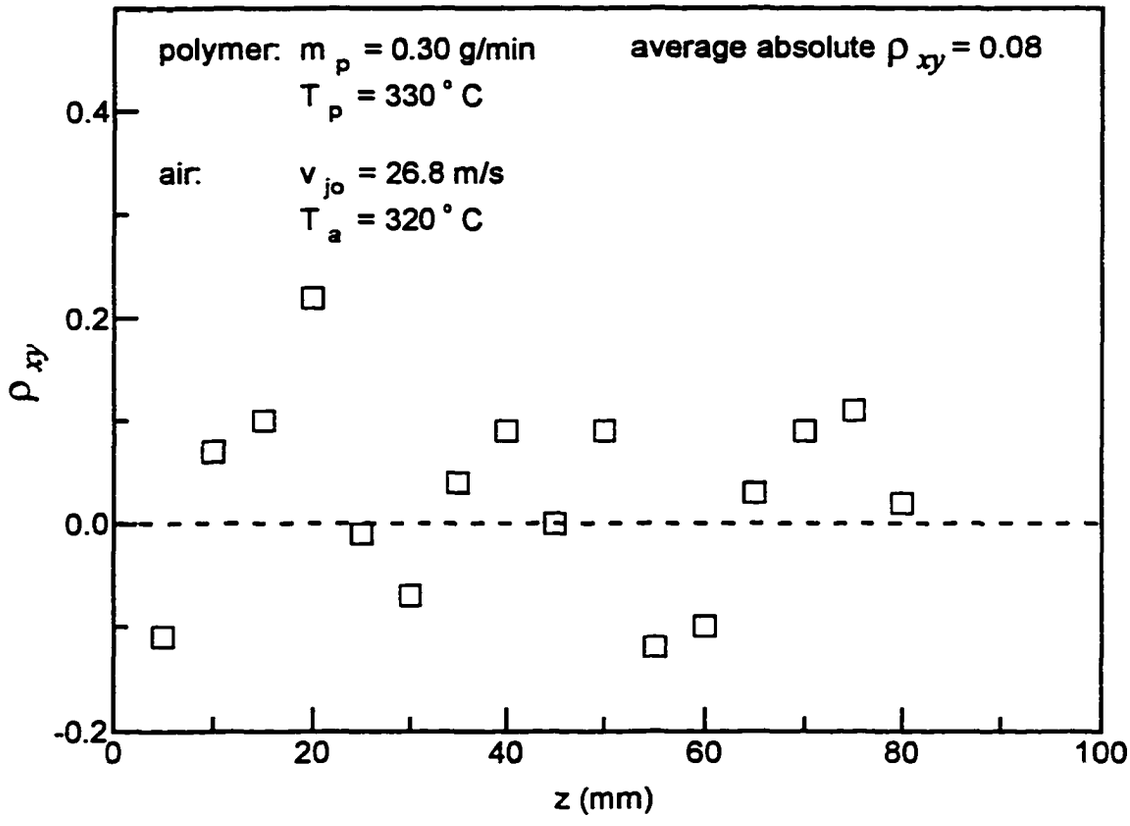

Figure 3.19 Correlation coefficient between the x and y components of fiber positions at different z levels below the die.

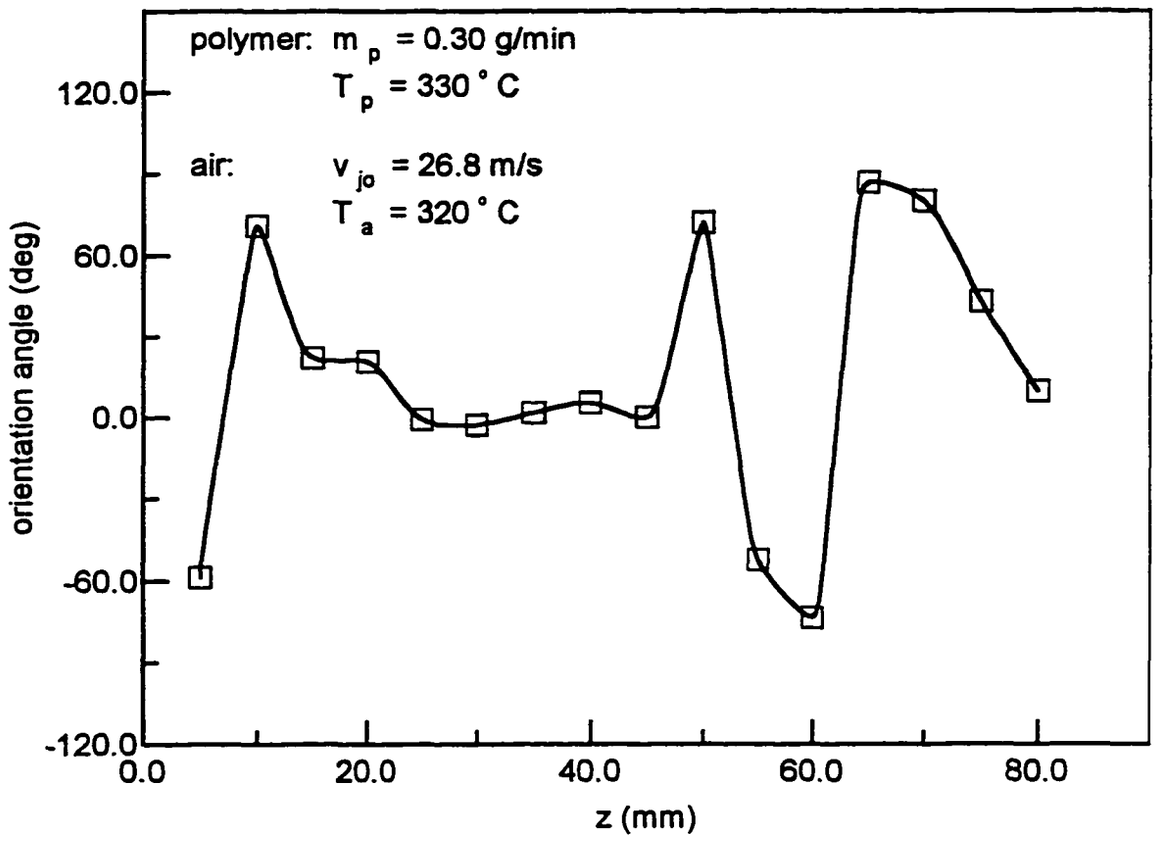

Figure 3.20 Orientation angle of the fiber distribution ellipse at different z levels below the die.

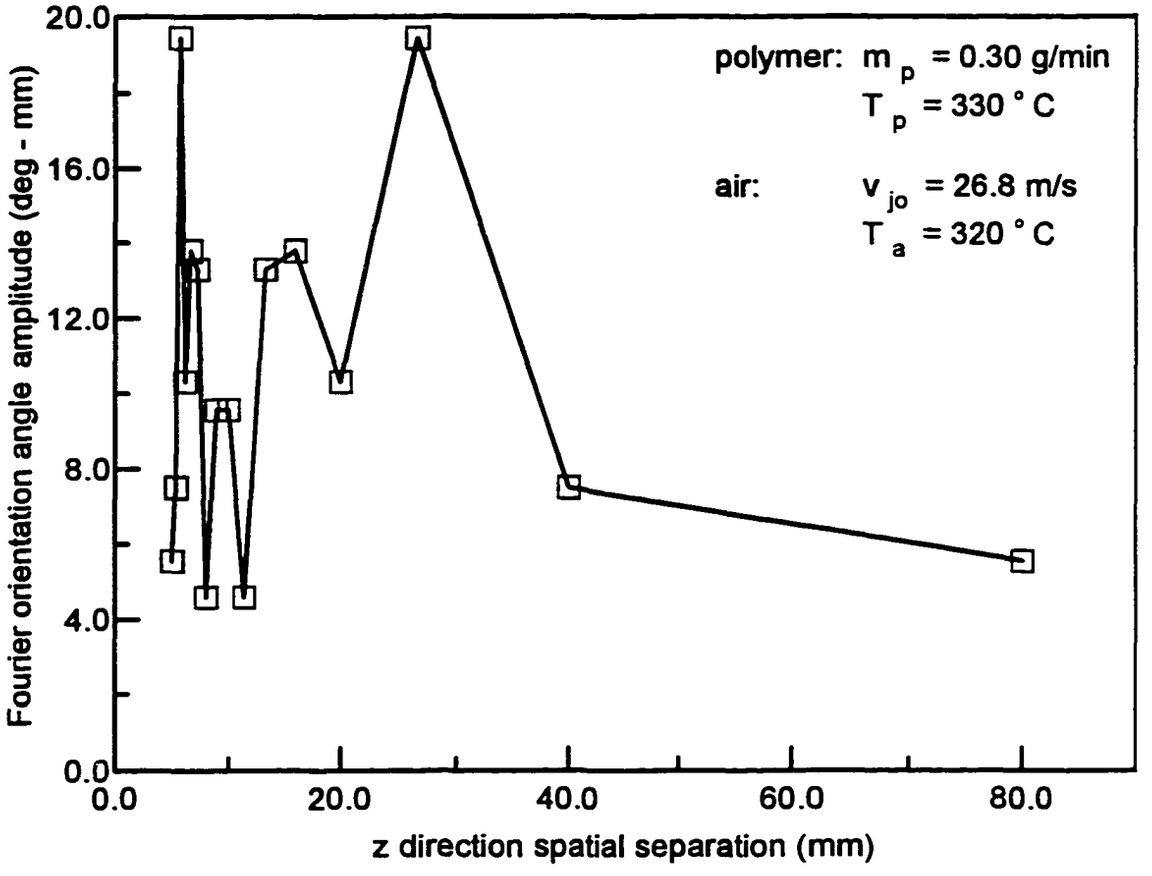

Figure 3.21 Fourier orientation angle amplitude spectra as a function of spatial separation (spatial period) along the *z* direction.

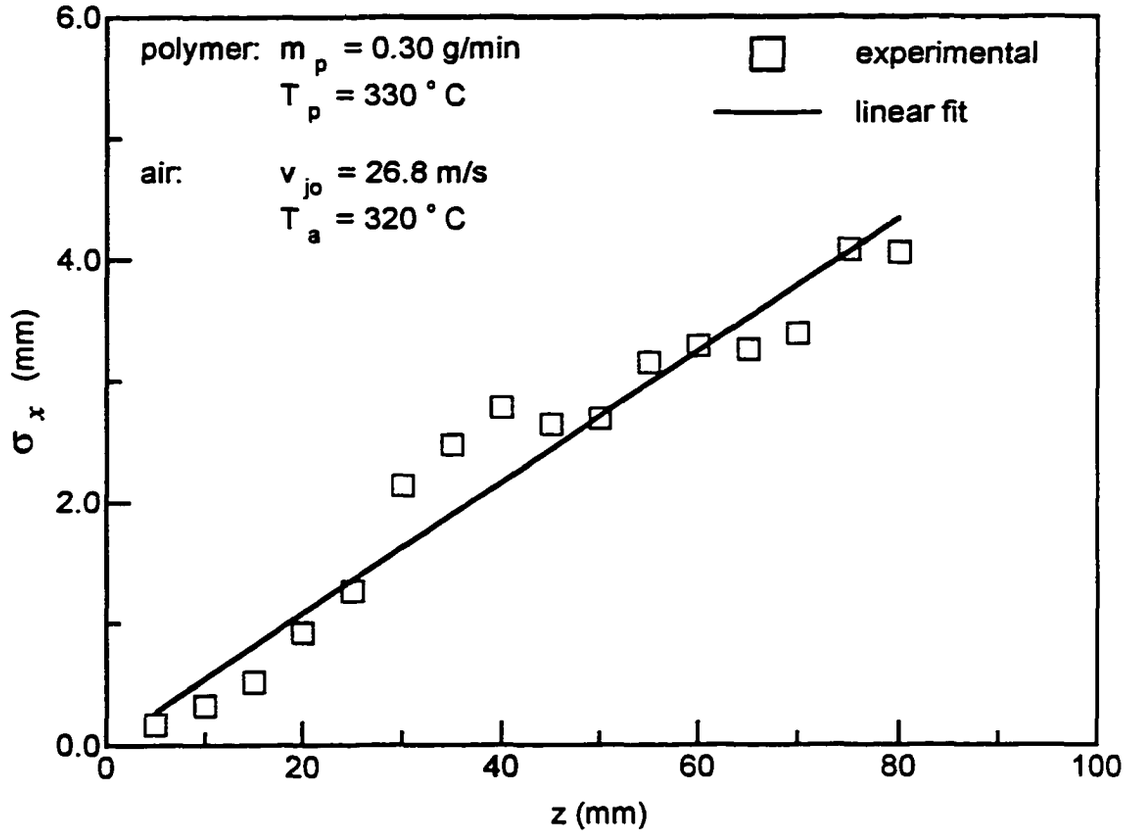

Figure 3.22 Variation in the x direction standard deviation of the fiber distribution with z position.

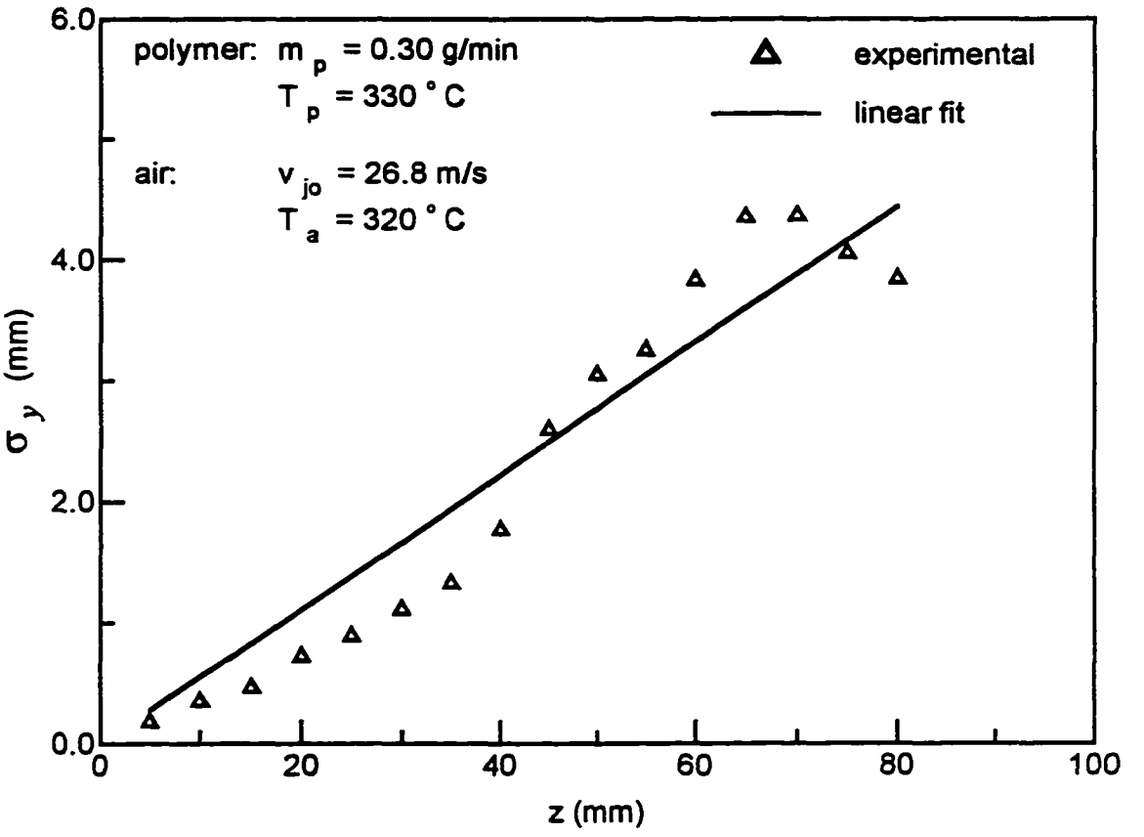

Figure 3.23 Variation in the *y* direction standard deviation of the fiber distribution with *z* position.

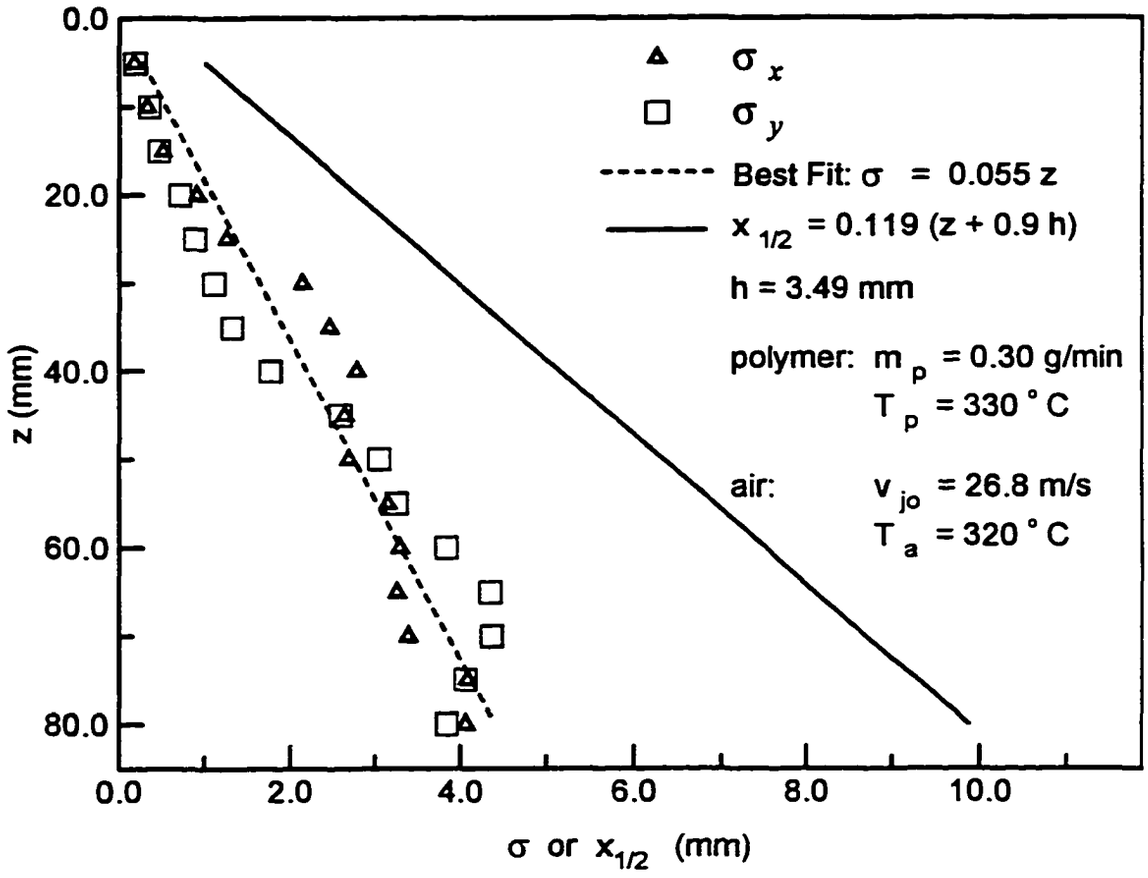

Figure 3.24 Comparison of spreading characteristics of the fiber distribution and the air jets in the z direction.

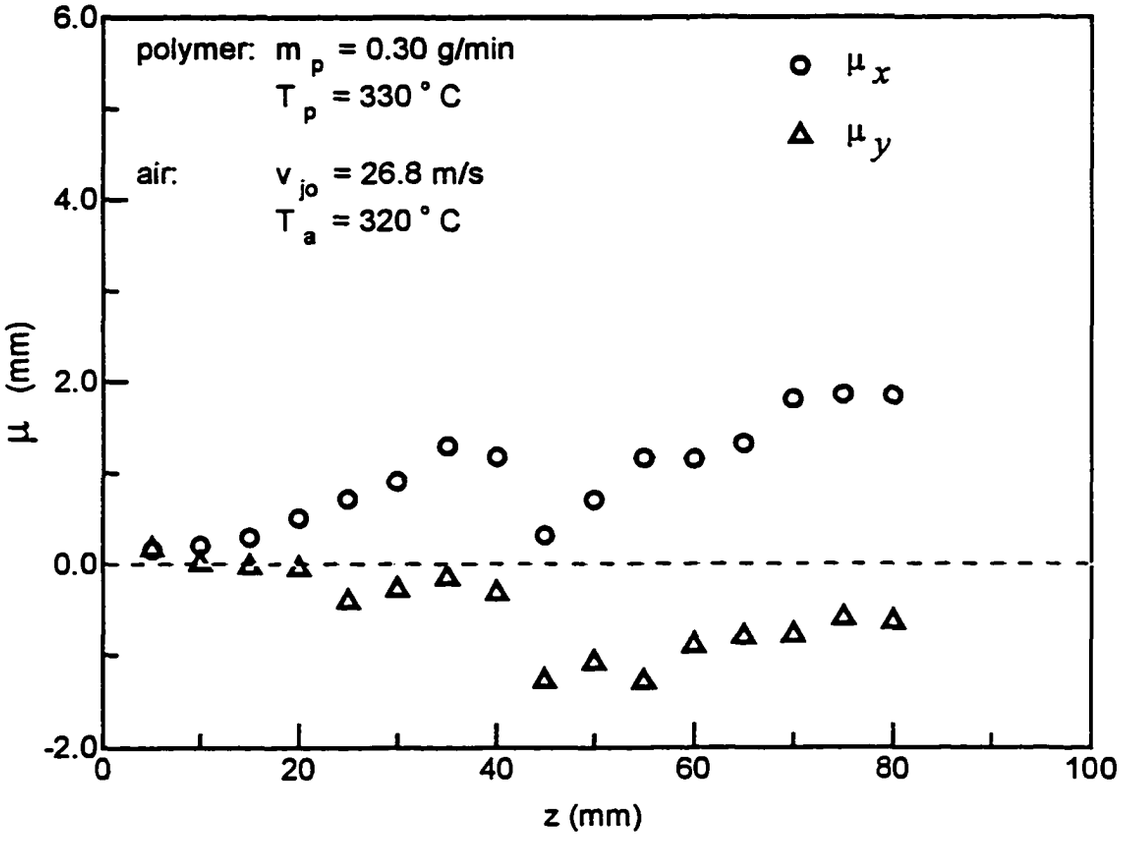

Figure 3.25 Variation in the x and y direction mean positions of the fiber threadline with z position below the die.

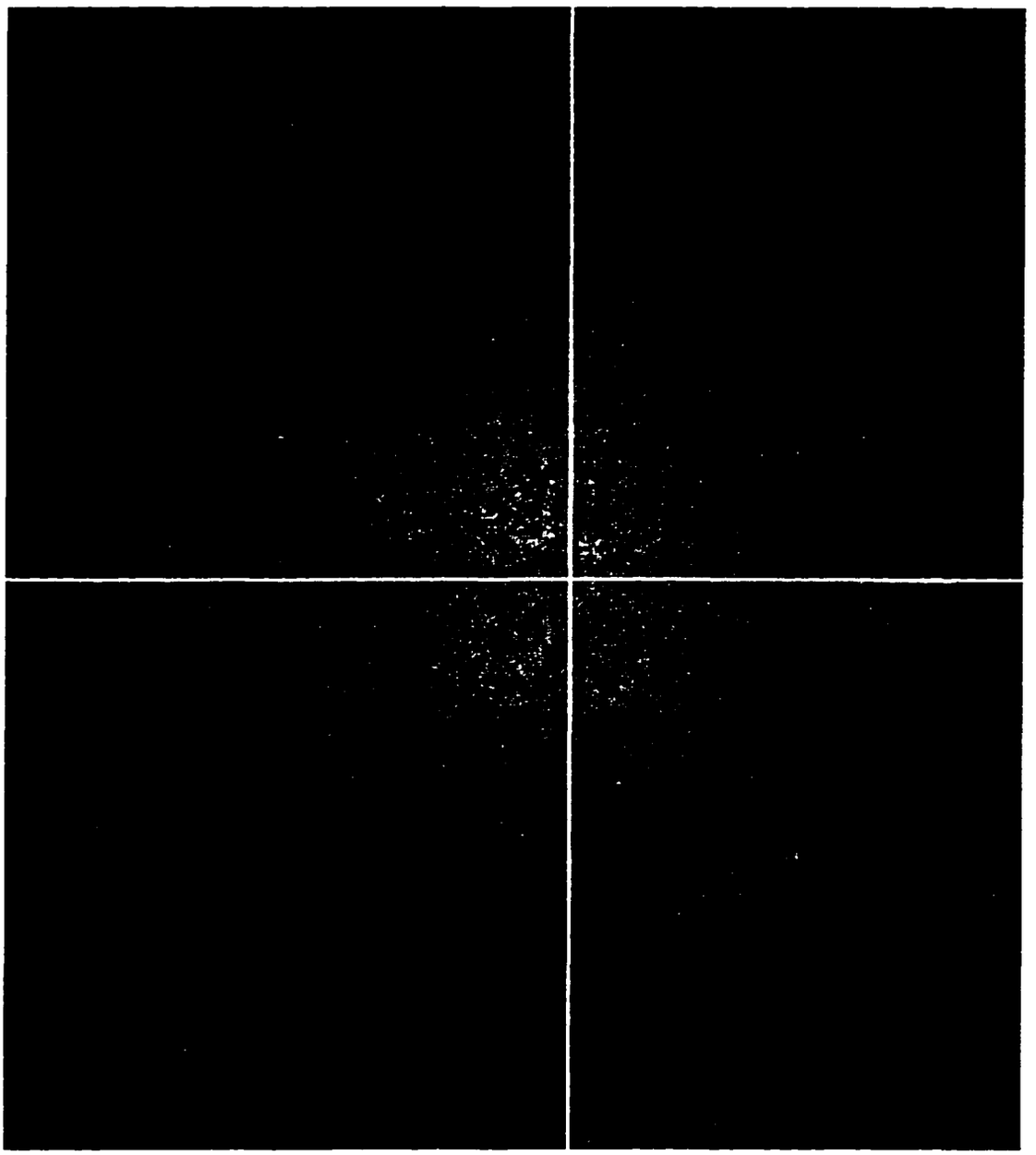

Figure 3.26 Top view image of the fiber pattern formed on a black wire-mesh screen placed at z = 300 mm. The white lines shown in the image correspond to the digitally overlaid coordinate axes.

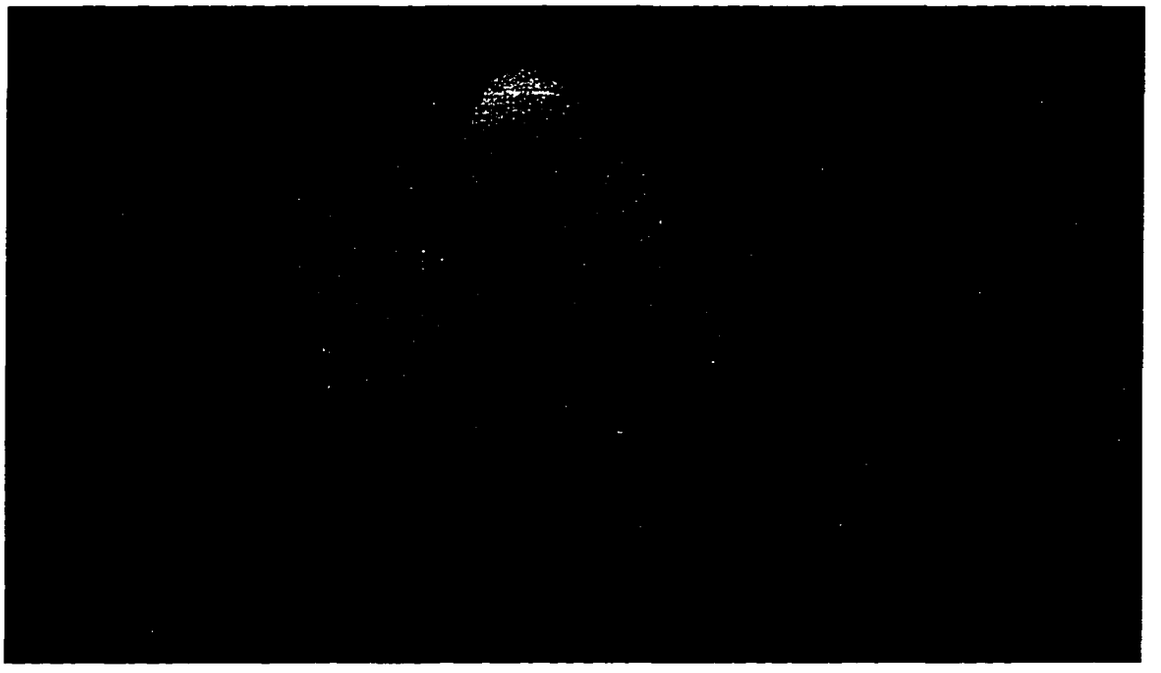

Figure 3.27 Side view image of the fiber collected on a black wire-mesh screen placed at z = 300 mm. The white lines in the image correspond to the coordinate axes which were set on the screen before fiber collection.

Chapter 4

AN ENTROPIC MEASURE OF SPATIAL FIBER DISTRIBUTION IN A MELT-BLOWN WEB

(The contents of this chapter will be submitted for a publication in the journal *Industrial & Engineering Chemistry Research*)

4.1 Abstract

A method based on spatial entropy of a web image was developed to evaluate the fiber distribution in a melt-blown web. The spread of the web distribution was found to be a function of the axial position below the die and the process variables (nominal air jet velocity, discharge air temperature, polymer mass flow rate, and polymer temperature). The width of the web distribution increased (a) linearly with the axial distance from the die, and (b) for a value of a process variable that

reduced the fiber diameter. The orientation of the web distribution varied irregularly for all conditions. The large standard deviation of the web orientation angle suggested that the web orientation angle is a function of time. A method, similar to the one used in the present study, has been proposed for multiple filament melt-blown webs.

4.2 Introduction

Melt blowing and spunbonding are two of the most important processes for producing nonwovens. Melt blowing produces nonwovens made of low strength microfibers, while spunbonded nonwoven fabrics have larger fiber diameters and strong mechanical properties. The kind of web to be used depends on the application. Therefore, it becomes very important to understand the properties of these webs. Morphological and mechanical properties of the webs are related to the web structure that in turn greatly depends on the process mechanics and conditions. Shambaugh (1988), Kayser and Shambaugh (1990), and Milligan and Haynes (1995) empirically modeled melt blowing for various conditions to understand the process mechanics. The theoretical fluid mechanics models of Uyttendaele and Shambaugh (1990) and Rao and Shambaugh (1993) can be used to predict the fiber diameter and various aspects of fiber motion in melt blowing. Both empirical and theoretical models of melt blowing can be used to predict the

properties of melt-blown web. Many researchers have independently studied different techniques to determine the web structure and the effect of process variables on the web properties. Lee and Wadsworth (1992) have studied the effect of process conditions on the physical and mechanical properties of the melt-blown webs. A similar detailed study on the spunbonded webs has been done by Malkan, Wadsworth, and Davey (1994). However, the correlations between the process variables and the web structure parameters have not been quantified.

In the present study, a method has been developed for evaluating the distribution of fibers in a melt-blown web. The method used is based on the conclusions of the fiber distribution studies described in Chapter 3 that, in the melt blowing process, the fiber positions in a transverse plane follow a bivariate normal distribution. Furthermore, it was concluded that the fiber laydown pattern should also follow a bivariate normal distribution. Therefore, for a given set of process variables, the probability of the fiber being present at a position in a given transverse plane can be predicted using the distribution function. As discussed by Tyagi and Shambaugh (1995), there are four main process variables in melt blowing: air flow rate (or gas velocity), air temperature, polymer flow rate, and polymer temperature. The effects of each of these variables on the statistical parameters of the web distribution have been examined in this study. Though this study has been done for a web produced from a single hole melt blowing die, the fiber

distribution in any nonwoven web can be evaluated on a similar basis. In the following sections, a method based on the spatial entropic analysis of the web image to evaluate the fiber web distribution has been developed.

4.3 Literature Review

The properties of the nonwoven webs are dependent on the positional and the directional pattern of the fibers in web. Many researchers have studied this vectorial nature of the fiber presence in nonwoven webs. A review of the literature on the web characterization has been given in Chapter 3. Heretofore, most researchers have quantified nonwoven webs in terms of fiber orientation and web uniformity.

Web uniformity is characterized in terms of basis weight, structure, and visual uniformity. The nonwovens industry uses the coefficient of weight variation as a standard quality index to quantify the web uniformity. Boeckerman (1992) and Aggarwal, Kennon, and Porat (1992) have calibrated the intensity of the transmitted radiation through the web to evaluate the weight uniformity. Huang and Bresee (1993, Part III) analyzed the web images to correlate the coefficient of web mass variation to the coefficient of pixel gray level variation. Ericson and Baxter (1973) used a projection microscope to find the filament separation, which

was correlated to the tensile strength of the web. They determined the coefficient of visual uniformity by measuring the intensity of transmitted light.

In most methods for the measurement of the fiber orientation, the directionality is evaluated by measuring the fiber position vectors directly. Hearle and Stevenson (1963), Huang and Bresee (1993, Part I) and Pourdeyhimi (1993) have described the methods to measure the fiber orientation with respect to the machine direction directly. Prud'homme et al. (1975), Kallmes (1969), Votava (1982), and Tsai and Bresee (1991) indirectly measured the fiber orientation by correlating physical properties of a web to the fiber orientation.

Conventional methods for the characterization of nonwoven webs do not quantify the correlation between web structure parameters and the process variables. It was shown in Chapter 3 that, during the fiber motion, the transverse positions of a single filament in melt blowing follow a bivariate normal distribution. A high speed photographic method was developed to determine the statistical pattern of the fiber positions. The variance vector of the distribution defined the spread of the distribution, and the correlation coefficient described the orientation of the cross-sections of the fiber cone in the transverse planes; Chhabra and Shambaugh (1996) define the fiber "cone" as the volume below a melt blowing die in which a fiber travels. By varying the process variables, the variance vector and the

correlation coefficient of the distribution could be changed. Therefore, the nature of the fiber motion could be transformed by changing the process variables. Since it was concluded in the fiber motion study (see Chapter 3) that the fiber web structure was dependent on the fiber threadline motion, the fiber web could be transformed by varying the process variables (air velocity, air temperature, polymer flow rate, and polymer temperature). However, they did not correlate the statistical parameters of the fiber position distribution to the process variables. In the present work, the effect of the process variables on the variance vector and the correlation coefficient of the fiber web distribution has been quantified.

4.4 Technique Development

As discussed in Chapter 3, a direct method was developed to stochastically explain the fiber threadline motion. In this method, fiber threadline was photographed simultaneously from two orthogonal angles. The position data was fitted to a known probability distribution. It was found that the fiber threadline followed a bivariate normal distribution. However, this direct method could only be applied to positions that are close (up to 80 mm) to the single hole melt blowing die because further away from the die, the fiber amplitudes become large, and many positions of the fiber lie out of depth-of-field of the cameras; see Chhabra and Shambaugh (1996) for fiber amplitude measurements. For the positions further

away from the die, and for multiple hole die system, another method had to be developed.

4.4.1 Origin

The technique discussed in this chapter has its origin in the fiber position distribution study described in Chapter 3. They found that the fiber positions were auto-correlated only to those positions that lie within a length of a fiber element along the fiber axis. Furthermore, it was found that the fiber motion was a continuous Markov process so that the future state of a fiber threadline element was only dependent on its present state, and was independent of its past states. Therefore, it was concluded that the downstream fiber positions in the xy plane would not affect the upstream fiber positions, if the positions were further apart than a characteristic spatial separation along the z direction, and vice versa. Consequently, if an imaginary screen, which allowed only air to pass through, was kept in the xy plane at an arbitrary z position, the fiber elements captured on the screen would not affect the fiber elements just reaching the screen. Thus, the laydown pattern of the captured fiber would also follow a bivariate normal distribution. From an experiment, they found that the side-view of the fiber collected on a real wire-mesh screen had a bell shape. The air flow characteristics of this screen approximated the flow character of the imaginary screen mentioned

earlier. This experiment further confirmed that the laydown pattern followed a bivariate normal distribution. Hence, the fiber motion and the web structure could be characterized by a bivariate normal distribution function. From the conclusions obtained in the fiber distribution study described in Chapter 3, it can be inferred that, by measuring the distribution of fibers in the web, the distribution of the fiber positions while the fiber is in motion can be obtained. Therefore, in this study, an image processing method has been developed for evaluating the probability distribution function of the laydown pattern from an image of a melt-blown web.

In principle, a photograph of the fiber web can store all the information about the fiber distribution in a web. The fibers reflect light when illuminated. The reflectance of the fibers at different positions can be recorded as different intensity levels of gray present in the black and white photograph of the web sample. As the number of fibers at a position will increase, reflectance at that position will increase because the fibers are translucent (not opaque). Evidently, the fiber distribution can be estimated from the spatial gray level intensity distribution of the web image. However, after a number of the fiber presences (not maximum), the reflectance will reach its maximum. The image gray level will reach a maximum value for a lesser number of the fiber presences than the true maximum. Consequently, the computed spatial gray level distribution of the web image will be the apparent fiber distribution. Since the data will be lost due to the limited

bandwidth of the imaging method (photography), the model fiber distribution function cannot be directly estimated from the apparent fiber distribution. In other words, the gray level distribution of the image will give "insufficient" information about the true fiber distribution, especially in the regions where a larger number of fibers will be present. Figure 4.1 shows a typical image of the top view of a melt-blown web. The completely white areas corresponding to the flat regions of the image intensity distribution. The information is lost in these flat regions of the web image intensity distribution. Nevertheless, it is expected that the spatial order of fibers in the varying (non-maximum) gray levels of the web image will be identical to the spatial order of fibers in the actual web. Therefore, the spatial order information from the image can be used to estimate the true fiber distribution.

Rodrigues et al. (1990) used information entropy of the image intensity distribution to extract the degree of directionality of the fibers in printing papers. They characterized anisotropy of the printing paper in terms of the information entropy. However, they did not use the entropy relation to predict the fiber distribution function. In the following sections, a mathematical formulation has been described for evaluating the spatial distribution of fibers in a nonwoven web using the concepts of the information entropy.

4.4.2 *Mathematical Formulation*

The estimation of the fiber distribution has been subdivided into two main sections. In the first section, the formulation for calculating the fiber presence probability density function of the sample web image has been described. The mathematical relationships to predict the fiber web distribution from the web image distribution using the principles of information entropy are given in the second section.

4.4.2.1 Evaluation of the Fiber Presence Probability Density Function of the Sample Web Image

The photographic image of the collected web sample can be digitized and stored as an 8-bit (256 gray levels) image. According to Frieden (1972), the statistical model of an image can be derived by dividing the image into n resolution cells, or n events. The normalized frequency of occurrence of the ith event in the image is given by

$$\Gamma_i = \frac{\gamma_i}{\sum_{i=1}^{n} \gamma_i} \tag{4.1}$$

where γ_i is the gray level intensity of the ith cell. Similarly, a statistical model for the web image can be developed. The web image is divided into W windows such that

$$W = \left[\sqrt{N}\right]_{int} \times \left[\sqrt{M}\right]_{int} \tag{4.2}$$

where

N = number of rows of pixels or height of the image in pixels

M = number of columns of pixels or width of the image in pixels

$[A]_{int}$ = next higher integer value of real A

If n be the number of pixels in each window, then

$$n = \frac{N \times M}{W} \tag{4.3}$$

The gray levels of the pixels in the image are assigned such that g_o is the lowest, and g_{max} is the highest gray level for the image. The gray level g_o corresponds to the intensity of the light reflected from an area of the collection screen where no fiber

is present.

The fiber presence probability density function of the sample web image is evaluated as the normalized frequency of the fiber presences of each window. Using Frieden's statistical model (1972), the apparent frequency of the fiber presences in the *k*th window of the web image can be defined as a sum of the gray level intensities of all the pixels in the window; the resulting equation is

$$\bar{f}_k = \sum_{i=0}^{i_{max}} \bar{m}_{ki} \, \Delta r_i \qquad (4.4)$$

where

i_{max} = index of the highest gray level in the web image

$\bar{m}_{ki}$ = number of pixels with *i*th gray level in the *k*th window of the web image

Δr_i = *i*th relative gray level of a pixel

The relative gray level Δr_i is defined as

$$\Delta r_i = g_i - g_o \tag{4.5}$$

where

g_i = ith gray level in the image

g_o = lowest gray level in the image

The relative gray level Δr_i represents the amount of light reflected from the number of fibers present at a pixel with ith gray level in the web image. However, it has to be shown that the relative gray level Δr_{max} does not necessarily correspond to the maximum number of the fiber presences in the web. Huang and Bresee (1993, Part III) have shown that the intensity of light transmitted through the fiber web is reduced by reflection and scattering. They viewed the reduction in the intensity of the transmitted light as a reduction in the "effective" incident light. Furthermore, they have shown that the amount of reduction is proportional to the intensity of incident light. Since the reduction is due to reflection and scattering, the combined intensity of the reflected and the scattered light can be represented by

$$I_{rs} = \lambda I_o \tag{4.6}$$

where

I_{rs} = combined intensity of the reflected and the scattered light from the fibers

I_o = intensity of the light incident on the fibers

λ = proportionality constant such that $0 \leq \lambda \leq 1$

According to Huang and Bresee (1993, Part III), the proportionality constant λ is a function of web thickness, fiber spatial arrangement, and other web structural features. Therefore, the proportionality constant λ can be represented by

$$\lambda = \lambda(t, \Omega) \tag{4.7}$$

where

t = web thickness

Ω = factor representing fiber spatial arrangement and other structural features of web

The web thickness t is given by

$$t = \nu d \tag{4.8}$$

where

d = mean fiber diameter in the web

ν = number of fibers at a position in the web

Since the mean diameter of the fibers is the same throughout the whole web (variation in the fiber diameter can be assumed to be the same throughout the web), equation (4.7) is reduced to

$$\lambda = \lambda(\nu, \Omega) \tag{4.9}$$

Furthermore, for a given spatial arrangement of the fibers in the web, the factor Ω is constant. Therefore, λ should be a function of the number of fiber presences

at a position only. Consequently, equation (4.9) reduces to

$$\lambda = \lambda(v) \tag{4.10}$$

As the number of fibers at a position will increase, the intensity of reflected light will increase. The intensity of reflected light will reach a maximum value, i.e., almost equal to the intensity of incident light [$\lambda \approx 1$; see equation (4.6)], and will not increase any more with the increasing number of fibers. Therefore, the domain of λ, for which the intensity of the reflected light increases almost linearly with the number of fibers, will represent a true measure of the actual number of fibers present at a position.

For a pixel position with the relative gray level Δr_i corresponding to the presence of v_i number of fibers, substituting equation (4.10) in equation (4.6) gives

$$\left(\frac{I_{rs}}{I_o} \right)_i = \lambda(v_i) \tag{4.11}$$

For a pixel position with the relative gray level Δr_{max} due to the presence of v_{max} number of fibers, equation (4.11) becomes

$$\left(\frac{I_{rs}}{I_o}\right)_{max} = \lambda(v_{max}) \tag{4.12}$$

Dividing the equation (4.11) by the equation (4.12) gives

$$\frac{[I_{rs}]_i}{[I_{rs}]_{max}} = \frac{\lambda(v_i)}{\lambda(v_{max})} \tag{4.13}$$

However, the intensity of the reflected light I_{rs} is proportional to the relative gray level Δr. Therefore, equation (4.13) is transformed to the following equation:

$$\frac{\Delta r_i}{\Delta r_{max}} = \frac{\lambda(v_i)}{\lambda(v_{max})} \tag{4.14}$$

Now, the specific apparent frequency of the kth window can be defined from equation (4.4) as

$$\tilde{f}_{sp_k} = \frac{\tilde{f}_k}{\Delta r_{max}} = \sum_{i=0}^{i_{max}} \tilde{m}_{ki} \frac{\Delta r_i}{\Delta r_{max}} \tag{4.15}$$

Substituting equation (4.14) in equation (4.15) gives

$$\tilde{f}_{sp_k} = \sum_{i=0}^{i_{max}} \tilde{m}_{ki} \frac{\lambda(\nu_i)}{\lambda(\nu_{max})} \tag{4.16}$$

The specific apparent frequency can be normalized as

$$\tilde{F}_k = \frac{\tilde{f}_{sp_k}}{\sum_{k=1}^{W} \tilde{f}_{sp_k}} \tag{4.17}$$

Substituting equation (4.16) in equation (4.17) gives

$$\tilde{F}_k = \frac{\sum_{i=0}^{i_{max}} \tilde{m}_{ki} \frac{\lambda(\nu_i)}{\lambda(\nu_{max})}}{\sum_{k=1}^{W} \sum_{i=0}^{i_{max}} m \frac{\lambda(\nu_i)}{\lambda(\nu_{max})}} \tag{4.18}$$

Since $\lambda(\nu_{max})$ is constant for an image, the equation (4.18) reduces to

$$\tilde{F}_k = \frac{\sum_{i=0}^{i_{max}} \tilde{m}_{ki}\, \lambda(v_i)}{\sum_{k=1}^{W} \sum_{i=0}^{i_{max}} \tilde{m}_{ki}\, \lambda(v_i)} \tag{4.19}$$

Equation (4.19) represents the normalized apparent frequency of the fiber presences in terms of number of fibers present in the *k*th window. Since v_i represents relative gray level Δr_i, equation (4.19) can be written as

$$\tilde{F}_k = \frac{\sum_{i=0}^{i_{max}} \tilde{m}_{ki}\, \Delta r_i}{\sum_{k=1}^{W} \sum_{i=0}^{i_{max}} \tilde{m}_{ki}\, \Delta r_i} \tag{4.20}$$

From equations (4.19) and (4.20), it can be seen that knowledge of v_{max} and Δr_{max}, respectively, is not required to evaluate the normalized apparent frequency of the windows in the web image. However, the normalized frequency has to be compared with the normalized actual frequency to know the deviation between the apparent (web image) and the actual web distribution functions. The actual frequency of the fiber presences in the *k*th window is

$$f_k = \sum_{j=0}^{j_{max}} m_{kj}\, j \tag{4.21}$$

where

m_{kj} = number of coordinate positions of pixel-area size with j number of the fiber presences in the kth window

j_{max} = maximum number of fibers present at any coordinate position of pixel-area size in the web sample

Therefore, the actual normalized frequency of the fiber presences in the kth window is given by

$$F_k = \frac{\sum_{j=0}^{j_{max}} m_{kj}\, j}{\sum_{k=1}^{W} \sum_{j=0}^{j_{max}} m_{kj}\, j} \tag{4.22}$$

From the equations (4.19) and (4.22), it can be seen that, since v_{max} is less than or equal to the actual maximum number of the fiber presences j_{max} at any position in the web sample, the probability density function evaluated from the image analysis is not the true probability density function. Consequently, the data is lost because of the image saturation. Nevertheless, as stated earlier, it is possible to estimate the data loss with the spatial entropy analysis. Hence, the true fiber probability

density function of web can be estimated from the apparent (web image) probability density function given by equation (4.20).

4.4.2.2 Evaluation of Fiber Presence Probability Density Function using Information Entropy

In the preceding section, it has been shown that the web image spatial intensity distribution is not a true estimate of the fiber presence distribution because of the loss of information. However, the lost information, as mentioned earlier, can be estimated using information entropy. The fiber presence information can be evaluated in terms of entropy of the fiber presence in the web. According to Shannon (1948), the information entropy of the fiber presence in the web can be defined by

$$H_n(\psi) = -\sum_{i=1}^{n} \psi_i \ln \psi_i \qquad (4.23)$$

where

ψ = fiber presence probability density function

$H_n(\psi)$ = information entropy of n fiber presence positions

If the true fiber presence distribution is considered to be the message distribution and the web image fiber presence distribution is considered to be the signal distribution, then by Shanon's information theory, the entropies of these distributions are related by the following equation:

$$H(S) - H_R(S) = H(R) - H_S(R) \tag{4.24}$$

where

$H(S)$ = entropy of the source of messages (actual web distribution)

$H(R)$ = entropy of the received signals (web image distribution)

$H_R(S)$ = equivocation or uncertainty in the message source (actual web distribution) if signal (web image distribution) be known

$H_S(R)$ = uncertainty in the received signals (web image distribution) if the message (actual web distribution) sent be known

Rearrangement of equation (4.24) gives

$$H(S) = H(R) - H_S(R) + H_R(S) \qquad (4.25)$$

Consequently, the true fiber presence distribution can be estimated from the equations (4.23) and (4.25) if the uncertainty terms are known. Equivocation or uncertainty in the true fiber distribution is related to the variance of the distribution. Uncertainty in web image fiber presence distribution is due to the noisy or the bandwidth limited image capture of the web sample. However, both these uncertainty terms cannot be directly estimated. Therefore, instead of extracting the information directly from the fiber presence coordinates in the web image, another method to obtain the spatial information of the web was developed.

As stated earlier, it is expected that the spatial order of the fibers in a web is the same as that in the web image. Therefore, a method based on the directed divergence between the observed spatial distribution F and the model spatial distribution G can be used to estimate the true distribution. Spatial distribution includes the information about the spatial order of the fiber positions in the web.

It is assumed that the observed spatial distribution F describes a web such that minimum spatial order information is lost in imaging the actual web. The directed divergence between the two distributions is given by Kullback-Leibler (KL) information (Kullback and Leibler, 1951). Mathematically, the KL information function can be written as

$$I(f:g) = \int_{-\infty}^{+\infty} f(\vec{p}) \ln \frac{f(\vec{p})}{g(\vec{p})} \, d\vec{p} \tag{4.26}$$

where

$I(f:g) \geq 0$ and the equality exists when $f(\vec{p}) = g(\vec{p})$

$f(\vec{p})$ = observed (spatial, in our case) probability density function

$g(\vec{p})$ = model (spatial, in our case) probability density function

$\vec{p}$ = random variable vector

The smaller the KL information function $I(f:g)$ is, the closer the observed spatial distribution F is to the model spatial distribution (Arizono and Ohta, 1989). Therefore, the problem is reduced to bringing the observed spatial distribution F

close to the model spatial distribution G as much as possible. As described by Kapur and Kesavan (1992), this problem can be solved by minimizing the KL information function. The minimization can be achieved by iteratively varying the parameters of the model spatial distribution G, and is subject to the following set of constraints:

$$\int_{-\infty}^{+\infty} f(\vec{p})\, d\vec{p} = 1 \qquad (4.27a)$$

and

$$\int_{-\infty}^{+\infty} g(\vec{p})\, d\vec{p} = 1 \qquad (4.27b)$$

The spatial order can be measured in terms of interrelationships between the values of the random variable at various positions in the web sample. The fiber presence probability density function $P(x, y)$ of a window is taken as the random variable function for the sample web. The interrelationships between the fiber presence probability density function of different pairs of windows in the web image have to be evaluated to calculate the spatial distribution function. Only the non-flat regions of the web image distribution are considered for the evaluation of the spatial distribution since no information is assumed to be lost in these regions. The interrelationship between the fiber presence probability density function $P(x,$

y) of the two pairs of windows in the image can be computed as a bivariate probability density function. As described by Rossi and Posa (1992), the spatial bivariate cumulative distribution function for the interrelationship between two pairs of windows is given by

$$\Phi_h(p, p'; \vec{h}) = \text{Prob}\left(P(\vec{x}) \leq p, P(\vec{x} + \vec{h}) \leq p' \right) \tag{4.28}$$

where

$\vec{h}$ = lag vector, measuring the displacement between the two position vectors of the center of the windows

p = maximum fiber presence probability value for the first window

p' = maximum fiber presence probability value for the second window

$P(\vec{x})$ = fiber presence probability of the first window

$P(\vec{x} + \vec{h})$ = fiber presence probability of the second window

$\vec{x}$ = position vector of the center of the first window

The maximum fiber presence probability values p and p' for the two windows can take K outcome values of the fiber presence probabilities. Rossi and Posa described that the bivariate spatial probability density function $\phi_h(p, p'; \vec{h})$ can be estimated from the cumulative distribution function $\Phi_h(p, p'; \vec{h})$ with the following equation:

$$\phi_h(p, p'; \vec{h}) = \left[\Phi_h(p + \Delta p, p' + \Delta p'; \vec{h}) - \Phi_h(p, p' + \Delta p'; \vec{h}) - \Phi_h(p + \Delta p, p'; \vec{h}) + \Phi_h(p, p'; \vec{h}) \right] / (\Delta p \cdot \Delta p') \quad (4.29)$$

where Δp and $\Delta p'$, respectively, are the discrete increments in the maximum fiber presence probability values for the two windows. The spatial probability density function $\phi_h(p, p'; \vec{h})$ is highly dependent on the values of Δp and $\Delta p'$. The values of Δp and $\Delta p'$ can be optimized by reducing the absolute deviation in values of ϕ_h in the consecutive iterations of the evaluation procedure. The cumulative distribution function $\Phi_h(p, p'; \vec{h})$ is dependent on the representability of the sample pairs $[P(\vec{x}), P(\vec{x}+\vec{h})]$. According to Journel and Deutsch (1993), if the sample pairs $[P(\vec{x}), P(\vec{x}+\vec{h})]$ are spatially positioned very far from each other, i.e., $\vec{h} = \pm\infty$, then the sample pairs can be considered statistically independent: $\Phi_h(p, p'; \vec{h}) = 0$. This case of independence is not very useful as the information about the spatial interrelationship has to be evaluated. Therefore, a lag vector $\vec{h}$ has to be

chosen such that the information about the spatial order is retained. For this purpose, Brink (1995) has shown the sample can be considered as a type of Markov random field with each position dependent only on the positions in its immediate 3×3 or 5×5 neighborhood. This means that the lag vector $\vec{h}$ is (h_i, h_j) with $-1 \le h_i \le +1$ and $-1 \le h_j \le +1$ for the 3×3 neighborhood, or $-2 \le h_i \le +2$ and $-2 \le h_j \le +2$ for the 5×5 neighborhood. In fact, Brink (1995) has shown that redundancy in calculations in the 3×3 or 5×5 neighborhood can be reduced by modifying the neighborhood to include only the origin, its immediate neighbors to the right and below, and its diagonal neighbors below the 3×3 or 5×5 neighborhood. Table 4.1 shows the modified asymmetrical 5×5 neighborhood of coordinate (i, j) as the non-shaded cells.

Thus, the cumulative distribution function and probability density function can be calculated over all the values (12, if considering asymmetrical 5×5 neighborhood) of the lag vector $\vec{h}$ considered over the whole image. Then, the *KL* information can be computed as an average over the asymmetrical neighborhood to include the spatial information completely.

The observed and model spatial probability density functions are normalized to calculate the *KL* information. The normalization is with respect to the maximum observed fiber presences in the non-flat region of the web image distribution. This

"maximum" is calculated as the maximum value of the observed fiber presence probability of a window $P_o(\vec{x})$ after which the absolute value of the partial derivative $\partial P_o/\partial x_i$ starts decreasing. Furthermore, *KL* information function described by equation (4.26) is only valid for the continuous distribution functions. For the normalized values of P_o and P_m, the integral in equation (4.26) is transformed to summations in the discrete case as shown in the following equation:

$$I_h(f:g;\vec{h}) = \frac{1}{n} \sum_{k_{i-1}}^{k_{i-n}} \sum_{p=0}^{1} \sum_{p'=0}^{1} f(p, p';\vec{h}) \ln \frac{f(p, p';\vec{h})}{g(p, p';\vec{h})} \qquad (4.30)$$

From equation (4.28), the observed and the model spatial cumulative distribution function can derived as

$$F_h(p, p';\vec{h}) = \text{Prob}\left(\hat{P}_o(\vec{x}) \le p, \hat{P}_o(\vec{x} + \vec{h}) \le p' \right) \qquad (4.31a)$$

$$G_h(p, p';\vec{h}) = \text{Prob}\left(\hat{P}_m(\vec{x}) \le p, \hat{P}_m(\vec{x} + \vec{h}) \le p' \right) \qquad (4.31b)$$

where $\hat{P}_o$ is the normalized observed fiber presence probability density function, and $\hat{P}_m$ is the normalized model fiber presence probability density function of the web image.

For a single hole die, the model fiber presence probability density function is taken

as bivariate normal distribution following the conclusions of fiber motion study described in Chapter 3. Therefore, the model fiber presence probability density function is given by

$$p_m(x, y) = \frac{1}{2\pi\sigma_x\sigma_y\sqrt{1 - \rho^2}} \exp\left[- \frac{1}{2}\omega(x, y)\right] \tag{4.32}$$

where

σ_x = the x direction standard deviation of the fiber positions

σ_y = the y direction standard deviation of the fiber positions

ρ = correlation coefficient of the fiber positions in the x and y directions

The quantity $\omega(x, y)$ in equation (4.32) is defined by

$$\omega(x,y) = \frac{1}{(1-\rho^2)}\left[\left(\frac{x-\mu_x}{\sigma_x}\right)^2 - 2\rho\left(\frac{x-\mu_x}{\sigma_x}\right)\left(\frac{y-\mu_y}{\sigma_y}\right) + \left(\frac{y-\mu_y}{\sigma_y}\right)^2\right] \tag{4.33}$$

where

μ_x = the x direction mean position of the fibers

μ_y = the y direction mean position of the fibers

The spatial probability density functions for both cumulative distribution functions given by equation set (4.31) can be calculated with the equations (4.29), (4.32), and (4.33). The discretized *KL* information $I_h(f{:}g;\ \vec{h})$ given by the equation (4.30) is minimized by varying the parameters of the model spatial density distribution $g(p, p';\ \vec{h})$. Since the model fiber presence probability density function P_m is a function of the statistical parameters $\vec{\mu}$, $\vec{\sigma}$, and ρ, the model spatial density distribution $g(p, p';\ \vec{h})$ can be varied by varying the parameters of P_m. However, all the statistical parameters, i.e., $\vec{\mu}$, $\vec{\sigma}$, and ρ, do not have to be varied. As shown in Chapter 3, the mean vector $\vec{\mu}$ of the fiber distribution, which is a bivariate normal distribution, forms the coordinates of the center of the distribution ellipse. Johnson and Kotz (1972) have shown that if α percent of the distribution is contained in the ellipse, then the equation of the ellipse is given by (also see Chapter 3)

$$\left(\frac{x-\mu_x}{\sigma_x}\right)^2 - 2\rho\left(\frac{x-\mu_x}{\sigma_x}\right)\left(\frac{y-\mu_y}{\sigma_y}\right) + \left(\frac{y-\mu_y}{\sigma_y}\right)^2 = -2(1-\rho^2)\ln\left(1-\frac{\alpha}{100}\right) \quad (4.34)$$

Since the variance vector $\vec{\sigma}^2$ describes the axes of the distribution ellipse, it is a measure of the spread of the distribution. A non-zero correlation coefficient ρ of the distribution explains the angular orientation of the distribution with respect to the x direction. As shown in Chapter 3, the angular displacement θ between the major axis of the bivariate normal distribution ellipse and the x direction can be evaluated by

$$\theta = \frac{1}{2}\arctan\left[\frac{2\rho\sigma_x\sigma_y}{\left(\sigma_x^2 - \sigma_y^2\right)}\right] \quad (4.35)$$

Therefore, the fiber web orientation angle can be evaluated in terms of the correlation coefficient and the variance vector. From Figure 4.1, it can be seen that the information about the mean position of the actual web is not lost in the web image. Consequently, the means in both the x and the y dimensions of the model distribution can be assumed to be equal to the means observed in the web image intensity distribution. In fact, the mean or the center of the distribution ellipse should theoretically coincide with the origin in the xy plane. Since the web image

distribution is expected to be flat where most fibers are present, the variance vector $\bar{\sigma}^2$ should differ from that of the observed web image probability density function. However, the orientation of the web image distribution and the model distribution should be identical because the only difference between the two distributions is the flatness of the web image distribution. The invariance of the orientation of the web distribution can be used as a constraint for minimizing *KL* function. The correlation coefficient of the two distributions should be identical because it is only related to the orientation of the distribution. Thus, the value of the variance vector $\bar{\sigma}^2$ that minimizes the *KL* function should be the best estimated value for the model distribution as predicted by the information entropy.

4.4.3 Web Distribution in Multiple Filament Melt Blowing

The image analysis described in the preceding section can also be applied to evaluate the apparent distribution of fibers in multiple filament melt blowing. Equation (4.20) used for evaluating the apparent or observed fiber presence density distribution P_o from the web image intensity distribution is independent of the fiber motion and the number of fiber filaments coming out of the die. Since only spatial information considered in the entropic analysis is the information about the arrangement of fibers in a web, the entropic analysis used for a single filament melt-blown web can be applied to a multiple filament melt-blown web. Both

observed spatial density distribution $f(p, p'; \vec{h})$ and model spatial density distribution $g(p, p'; \vec{h})$ can be evaluated from the observed and the model fiber presence density distributions P_o and P_m, respectively, in the same way as in a single filament system. However, the model fiber presence distribution P_m in multiple filament melt blowing will not be the same as in the case of single filament process. As an approximation to the actual web distribution, the model fiber presence distribution can be a superposition of the bivariate normal distributions of the fiber filaments. Therefore, the model fiber presence distribution $\tilde{P}_m$ in n filament melt blowing can be described by

$$\tilde{P}_m = \sum_{i=1}^{n} a_i P_{m_i} \tag{4.36}$$

where

a_i = coefficient describing the contribution of ith fiber filament to the overall model fiber presence distribution $\tilde{P}_m$

P_{m_i} = bivariate normal distribution of ith fiber filament

The coefficient a_i can be a function of the fiber-to-fiber interaction parameter. Consequently, in multiple filament melt blowing, the fiber-to-fiber interaction parameter will have to be determined to evaluate the model fiber presence distribution P_m. Once the model fiber presence distribution is obtained, the *KL* information function given by equation (4.30) can be minimized by varying the statistical parameters (more than two) of the model fiber presence distribution. However, the web orientation angle constraint used in the case of single filament process cannot be used. A new constraint based on the geometrical information of the multiple filament web will have to be developed. Nevertheless, the method developed in the preceding section can be applied to evaluate the distribution of fibers in a multiple filament melt-blown web.

4.5 Technique Implementation

4.5.1 Experimental Details

A single hole slot die was used in the experiments. The polymer was melted and pressurized with a Brabender extruder with a 19.0 mm (0.75 in) diameter barrel and 381 mm (15 in) long screw. The molten polymer was pumped in the die with a modified Zenith pump. Tyagi and Shambaugh (1995) have further explained the polymer supply details. The polymer capillary of the die had an inside diameter

of 0.407 mm and a length of 2.97 mm. The two rectangular air slots in the die were 74 mm long and 0.74 mm wide. The die was the same as that used by Chhabra and Shambaugh (1996) and in Chapter 3. Figure 4.2 shows the cross-section of the die. The polymer used was 88 MFR (melt flow rate) Fina Dypro™ polypropylene with M_w = 160,000 and M_n = 40,000. The ranges of basic operating conditions used for experiments are given in Table 4.2.

The fiber coming out of the spinneret was collected on a metal wire-mesh screen (65% open space) painted with non-reflecting Krylon® 1613 Semi Flat Black paint. The wire-mesh screen allowed only air to pass through it. The fiber was collected for a sufficient amount of time to make the fiber collection process statistically stationary (i.e., invariant under an arbitrary shift in the time origin). The characteristic time to make the process statistically stationary was empirically determined to vary from 30 seconds to 1 minute. Any longer than this period of time started blocking the collection screen, and led to a nonuniform web.

After the web was collected on the screen, the top view of the web was photographed using a Canon AE-1 Program camera at an automatic exposure. The camera was equipped with a Sigma 50 mm macro lens. Three 100 Watts General Electric Soft White tungsten bulbs provided the illumination. The film used was Kodak T-Max 400 and the prints were made on Ilford Multigrade IV RC paper.

The prints were digitized with a Hewlett-Packard ScanJet 3C scanner at a resolution of 300 dots per inch. The web images were digitally overlaid with 3 pixel wide coordinate axes lines corresponding to the actual geometrical coordinate axes in the xy plane. Adobe Photoshop® 4.0 software was used for digitally overlaying the coordinate axes lines. These web images were stored as 8-bit grayscale images in the Portable Gray Map (PGM) format. Figure 4.1 shows a typical web image with digitally overlaid coordinate axes.

4.5.2 *Data Analysis*

The mathematical formulation described earlier was used to develop a FORTRAN 77 computer program to analyze the web images. The analysis procedure used in developing the computer program is summarized as follows:

1. The web image was divided into W windows as described by equation (4.2). The number of pixels in each window was calculated with equation (4.3). The web image fiber presence probability density function was evaluated as the normalized frequency of fiber presences in a window P_o with equation (4.20). The normalized frequency of each window (group) was assumed to lie at the center of each window. The means, the standard deviations, and the correlation coefficient of the grouped data were computed with the procedure

outlined in Chapter 3. The angular orientation of the web image was calculated with equation (4.35). It was assumed that the web image distribution ellipse had the same orientation as a bivariate normal distribution ellipse with the same statistical parameters as that of the web image distribution. By making this assumption, the variances of the model distribution were constrained to have a specific relationship between them, while keeping the orientation of the web image distribution identical to the orientation of the model probability distribution. The orientation constraint was mathematically defined as the difference between the orientations of the web image distribution ellipse and the model probability distribution ellipse. This constraint was used to keep the variance variables in a reasonable range.

2. The means and the correlation coefficient of the web image distribution were taken as the best estimates for the model fiber presence distribution. The standard deviations of the web image distribution were taken as the guess values in the first iteration loop of optimization. In the subsequent iterations, the minimization routine provided the estimates of the standard deviations. Using these estimated statistical parameters, the model fiber presence probability density function was evaluated as a bivariate normal probability distribution. An IMSL subroutine BNRDF was used to evaluate the bivariate normal cumulative distribution function of each window (IMSL, 1994). The

bivariate normal cumulative distribution function of a window was considered as the model fiber presence distribution P_m of the window.

3. For normalizing the fiber presence probabilities, the partial derivatives of the observed fiber presence probability distribution P_o with respect to each direction (x and y) were computed. The maximum value of the observed fiber presence probability after which the absolute value of the partial derivative $\partial P_o / \partial x_i$ started decreasing was selected for normalizing both observed and model fiber presence probabilities. The four vector positions of the windows (two positions for positive and negative directions of each dimension) after which the partial derivatives started decreasing were considered as the positions which enclosed the flat region of the observed fiber presence distribution. The flat region of the observed fiber presence distribution was not considered for evaluating the spatial distribution functions.

4. The observed and model spatial cumulative distribution functions were calculated with the equation set (4.31). From the observed and the model cumulative distribution function, the spatial probability density functions were computed with the equation (4.29).

5. The discretized *KL* information function was evaluated with the equation (4.30).

The objective function $f_{objective}$ for the minimization was constructed by adding the squared *KL* function to the squared orientation constraint function. The *KL* function and the orientation constraint function were squared to make the objective function a convex function of the standard deviations. The objective function $f_{objective}$ can be mathematically described by the following equation:

$$f_{objective} = I_h^2\left(f:g;\vec{h}\right) + \left(\theta_m - \theta_o\right)^2 \tag{4.37}$$

where

θ_m = angle of orientation of the major axis of the model distribution ellipse

θ_o = angle of orientation of the major axis of the observe distribution ellipse

6. The objective function $f_{objective}$ was minimized with the *Simulated Annealing* algorithm developed by Goffe, Ferrier, and Rogers (1994). This minimization algorithm repeated the steps 2 through 4 with different values of the variance vector of the estimator bivariate normal fiber presence probability density function to minimize the objective function $f_{objective}$.

7. The best estimate of the fiber presence probability density function was calculated with the best estimate of the variance vector $\vec{\sigma}^2$ that minimized the objective function.

4.6 Results

A computer program in FORTRAN 77 (see Appendix III for program code) was developed to analyze the web image data. The program was run on an IBM RISC 6000 42T computer workstation. The average CPU time to run the program was about 40 hours. The bivariate normal probability distribution of the fiber presences in the melt-blown web was successfully estimated from the flat web image intensity distribution with the entropic analysis for all the conditions listed in Table 4.2.

Figures 4.3 and 4.4, respectively, depict the typical surface plots of the observed and the model spatial probability density functions. The spatial probability density functions in the plots represent the typical spatial interrelationship between the two adjacent windows ($h_x = 0$ and $h_y = +1$) in the y direction of the web. The closeness in the surface plots shows that the observed and the model spatial distributions are almost equal. Therefore, the Kullback-Liebler information function describing the directed divergence between the two spatial distributions has been minimized. The best estimates of the standard deviations obtained by minimizing the KL information function were used to compute the bivariate normal fiber presence distribution of the web. Figures 4.5 and 4.6, respectively, show the typical surface plots of the observed (web image) fiber presence

distribution and the model (bivariate normal) fiber presence distribution. On comparing Figures 4.5 and 4.6, it can be seen that the web image intensity distribution underpredicts the bivariate normal distribution of the web. However, the underprediction is corrected by the spatial information entropy analysis. The corrected bivariate normal distribution in Figure 4.6 represents the best estimate of the true fiber distribution in a typical single filament melt-blown web.

4.6.1 Effect of z Position on the Spread of the Web Distribution

Figure 4.7 shows the spread of web distribution along the z direction. The standard deviations of the model fiber distribution increase linearly with the z direction. The linear increase in the standard deviations of web distribution with the z direction is similar to the one shown in Chapter 3 for the case of fiber position distribution. For the same die, Harpham and Shambaugh (1996; 1997) have shown that the air jets also spread linearly with the z position. The air jet half-width describes the jet spread. One jet half-width is a position, transverse to the axial flow, where the velocity of the jet falls to half its maximum value. Figure 4.8 compares spreading of the web distribution and the air jets. The slope of the web distribution spread is different from the slope of the air jet spread. However, it can be seen that most of the web distribution is contained within one jet half width. The standard deviation profiles lie at about half the distance from the jet half-width

line (shown as a solid line on the graph). About 94% of the web distribution is contained in one jet half-width for the range of z positions investigated. In Chapter 3, the containment of fiber distribution within one jet half-width is explained using turbulent air jet dynamics. In Figure 4.7, it can also be seen that the x direction standard deviation is larger than the y direction standard deviation at all the z positions. Therefore, the web distribution is elliptical for all the z positions studied.

4.6.2 Effect of Process Variables on the Spread of the Web Distribution

The effect of each of the four main process variables - nominal air jet velocity, discharge air temperature, polymer mass flow rate, and discharge polymer temperature - on the standard deviations of the web distribution was examined. Before discussing the effects of these variables, a brief description of dynamics of fiber motion in melt blowing is presented to help in understanding the effect of the process variables.

In melt blowing, the fiber attenuates under the action of the aerodynamic force. The greater the aerodynamic force (higher nominal air jet velocity), the greater the fiber attenuates (Shambaugh, 1988). Uyttendaele and Shambaugh (1990) determined that the final diameter of the fiber is reached by $z = 50$ mm. A similar

result was also observed in the present study. Figure 4.9 shows the fiber diameter remains almost constant for all the z positions studied (z = 200 to 400 mm). After the fiber attains its final diameter, the aerodynamic force only affects the fiber motion. As described by Rao and Shambaugh (1993), this aerodynamic force can be resolved into lift and drag forces. The drag force is responsible for the downward motion of the fiber, while the lift force is responsible for the transverse motion of the fiber. The fiber elements of different masses per unit length should respond differently to these forces. At a distance greater than 50 mm from the die, for the same amount of aerodynamic lift stress, a fiber element with a lesser mass per unit length (thinner fiber element) should move a larger distance in a transverse plane than a fiber element with a larger mass per unit length (thicker fiber element). Since the spread of the web distribution is the spread of the fiber position distribution while the fiber is in motion (see Chapter 3), this effect of aerodynamic lift stresses on the fiber motion can be used in explaining the variation in spread of the web distribution.

Figure 4.10 shows the variation of the model standard deviations with the nominal air jet velocity. It is seen that the standard deviations increase gradually with the increase in nominal air jet velocity at z = 300 mm. The increase in spread of the web distribution with the increase in nominal air jet velocities is expected since the fiber attenuates more at the higher nominal jet velocities and, as explained earlier,

a thinner fiber element (lesser mass per unit length) moves a larger distance in the transverse plane than a thicker fiber element (larger mass per unit length) for the same amount of lift stress. Figure 4.11 shows the decrease in the fiber diameter with the increase in the nominal air jet velocity. However, the fiber diameter does not decrease sharply with the nominal air jet velocity. Consequently, the gradual increase in spread of the web distribution is reasonable. The amount of lift stress acting on the fiber at the various nominal air jet velocities can be judged from the air jet flow characteristics of the die. At the studied conditions, the air velocity and temperature correlations developed by Harpham and Shambaugh (1997) for the same die can be used to obtain the air velocity profiles. Figure 4.12 shows the decay in the centerline velocity of the jet for the various nominal air jet velocities at a discharge temperature of 330°C. From the graph, it can be seen that, at z = 300 mm, the centerline velocities for all the nominal air jet velocities have decayed to about 2 m/s. Therefore, there should not be a large difference in the amount of aerodynamic lift stresses acting on the fiber. Consequently, almost the same amount of lift stress should be acting on the fibers of different diameters (different masses per unit length) obtained at different nominal air jet velocities. Hence, larger spreads of the web distribution are obtained for the nominal air jet velocities that produce finer fiber diameters. Furthermore, in Figure 4.10, the x direction standard deviation is larger than the y direction standard deviation for all nominal air jet velocities studied. Therefore, the web distribution remains elliptical with changing nominal air jet velocities.

Figure 4.13 illustrates that the fiber diameter does not change with discharge air temperature (at least for the range of temperatures investigated). Therefore, the spread of the web distribution should not vary with discharge air temperature. As expected, Figure 4.14 shows that the standard deviations of the web distribution do not vary appreciably with discharge air temperature. Furthermore, it can be seen from the graph that the web distribution spreads more in the x direction than in the y direction.

The effect of polymer mass flow rate on the fiber diameter is shown in Figure 4.15. From the graph, it can be seen that, with the increase in polymer throughput, the fiber diameter increases. The increase in fiber diameter with the increase in polymer throughput is expected since a fiber element with a higher mass per unit length will require a greater amount of aerodynamic stress than a fiber element with a lower mass per unit length to attenuate by the same amount. An increase in the fiber diameter with polymer throughput suggests that the standard deviations of the web distribution should decrease with an increase in polymer throughput. This effect can be observed in Figure 4.16 which shows the variation of standard deviations with polymer mass flow rate. Furthermore, it is evident from Figure 4.16 that the web distribution is elliptical with the x direction standard deviation larger than the y direction standard deviation for all polymer mass flow rates investigated.

Figure 4.17 shows the effect of discharge polymer temperature on the fiber diameter. An increase in discharge polymer temperature gave finer diameter fibers. This effect was expected since, at higher polymer temperatures, the viscosity of the polymer reduces. Consequently, for the same amount of aerodynamic stress, the less viscous polymeric fiber attenuates more than the fiber with a higher polymer viscosity. A decrease in the fiber diameter implies a greater spread in the web distribution. Figure 4.18 illustrates the increase in the standard deviations of the web distribution with discharge polymer temperature. Once again, the x direction standard deviation is larger than the y direction standard deviation for all polymer temperatures studied.

4.6.3 *Effect on the Orientation Angle of the Web*

Figure 4.19 shows the variation in the orientation angle of the web distribution with the z position. As shown in Chapter 3, in the xy plane, the orientation angle of the fiber position distribution varies almost sinusoidally with a spatial separation (spatial period) of about 5 mm in the z direction. For the spatial separations of more than 15 mm in the z direction, they have shown that there is an irregular variation of the distribution orientation angle. Furthermore, in Chapter 3, it was suggested that the fiber moved in an elliptical spiral following a bivariate normal distribution in the transverse plane, and the ellipse rotated

sinusoidally in the same transverse plane (at the same z position). The sinusoidal rotation of the ellipse in a transverse plane means that the orientation angle of the ellipse should have a large variation. As expected, both these effects - an irregular variation of the "average" web orientation angle with the z position, and a large variation of the web orientation angle at a z position - are observed in Figure 4.19.

Figures 4.20 through 4.23 show the effect of four main process variables on the orientation angle of the web distribution. From these figures, it is evident that the "average" web orientation angle varies irregularly with the process variables investigated. However, there is some degree of sinusoidal variation, but it is not definitive. Furthermore, the web orientation angles have large standard deviations for all the values of the process variables examined. The large values of the standard deviation of the web orientation angle suggest that, for any value of a process variable, the web orientation angle distribution has a large spread. Since only five web samples were collected at a process condition, the web orientation angle distribution could not be estimated. Furthermore, the large variation of the orientation angle suggests that the web orientation angle may be a function of time. However, the variation of the web orientation angle with time was not studied.

4.7 Conclusions

The foremost conclusion of this study is that the fiber presence distribution in a melt-blown web can be estimated from the spatial information of the pixel intensity in the web image. The distribution of fibers in a single filament melt-blown web is a bivariate normal distribution. This distribution is the same as the fiber position distribution described in Chapter 3 for the fiber motion in melt blowing. Therefore, the fiber position distribution while the fiber is in motion can be evaluated from the web distribution, and vice versa.

For all the z positions and the process conditions studied, the web distribution is elliptical. The web spreads more in the x direction than in the y direction. The spreads in both x and y directions are linear functions of the z position below the die. The linear spreading of the web distribution is similar to that of the fiber position distribution as observed in Chapter 3, and to the increase in fiber cone amplitude as shown by Chhabra and Shambaugh (1996). From the present study and the studies on the velocity and temperature fields of the air jets by Harpham and Shambaugh (1997), it can be concluded that most of the web distribution is contained in one jet half-width.

The spread of the web distribution is a strong function of the fiber diameter. The

values of the process variables that reduced the fiber diameter increase the spread of the web distribution. Figure 4.24 shows the increase in the standard deviations with the decrease in the fiber diameter for various ranges of the process variables. Since nominal air jet velocity, polymer mass flow rate, and discharge polymer temperature affect the fiber diameter to a large extent, the spread in the web distribution depends largely on these variables. The discharge air temperature does not appear to affect the spread of the web distribution because the range of discharge air temperature studied did not affect the fiber diameter. In conclusion, any process variable that would reduce the fiber diameter should increase the spread of the web distribution. This conclusion should be very helpful in controlling the basis weight (mass per unit area) of a nonwoven web.

The web orientation angle varies irregularly with the z position and the process variables studied. However, the variation in the average web orientation angle appears to have a sinusoidal character. For the z direction spatial separation studied (50 mm), the variation of the web orientation angle is similar to the variation of the orientation angle of the fiber position distribution observed in Chapter 3. At a z position and for a value of a process variable, the web orientation angle has a large variance which suggests that the web orientation angle is a function of time. Furthermore, there may be a correlation between the orientation of fibers in web and the web orientation angle because it appears that most fibers

should lie in a specific orientation for a web to have an orientation in a preferred direction. Therefore, the orientation of fibers in a web may be evaluated in terms of the web orientation angle. Knowledge of variation of spread and orientation angle of the web distribution with the z position and process variables should be useful in predicting fiber-to-fiber contact and entanglement since the web distribution is the same as the fiber position distribution while the fiber is in motion.

Another important future goal will be studying the web distribution in multiple filament melt blowing. An information entropic analysis similar to the one used for single filament web has been suggested to evaluate the web distribution in a multiple filament system. The fiber-to-fiber interaction parameter for multiple filament melt blowing will be obtained to evaluate the web distribution.

4.8 Nomenclature

a_i = coefficient describing the contribution of *i*th fiber filament to overall distribution [see eq (4.36)]

$[A]_{int}$ = next higher integer value of real A

d = web average fiber diameter

$\tilde{f}_k$ = apparent frequency of fiber presences in the *k*th window

$f_{objective}$ = objective function for minimization

$\tilde{f}_{sp_k}$ = specific apparent frequency of fiber presences in the *k*th window

$f(\vec{p})$ = observed spatial probability density function

F_h = observed spatial cumulative distribution function

$\tilde{F}_k$ = normalized apparent frequency of fiber presences in the *k*th window

F_k = normalized frequency of the fibers presences in the *k*th window

g_o = lowest gray level in the image

g_{max} = highest gray level in the image

$g(\vec{p})$ = model spatial probability density function

G_h = model spatial cumulative distribution function

h_i = x component of the lag vector $\vec{h}$

h_j = y component of the lag vector $\vec{h}$

$\vec{h}$ = lag vector

$H(S)$ = entropy of the source of messages (actual web distribution)

$H(R)$ = entropy of the received signals (web image distribution)

$H_R(S)$ = equivocation or uncertainty in the message source (actual web distribution) if signal (web image distribution) be known

$H_S(R)$ = uncertainty in the received signals (web image distribution) if the message (actual web distribution) sent be known

$H_n(\psi)$ = information entropy of n fiber presence positions

i = image pixel index

i_{max} = index of the highest gray level in the web image

$I(f:g)$ = Kullback-Leibler information function

$I_h(f:g;\ \vec{h})$ = Kullback-Leibler information function for the discrete case [see eq (4.30)]

I_o = intensity of the light incident on the fibers

I_{rs} = combined intensity of the reflected and the scattered light from the fibers

j = actual number of fibers present at a position

j_{max} = maximum number of fibers present at a coordinate position of pixel-area size

k = index of the windows in the web image

m_{kj} = number of coordinate positions of pixel-area size with j number of fiber presences in the kth window of actual web

$\tilde{m}_{ki}$ = number of pixels with *i*th gray level in the *k*th window of the web image

M = number of rows of pixels in the image or height of the image in pixels

n = number of pixels in each window of the image

N = number of columns of pixels in the image or width of the image in pixels

p = maximum fiber presence probability for first window [see eq (4.28)]

p' = maximum fiber presence probability for second window [see eq (4.28)]

$p_m(x, y)$ = fiber presence probability density function

Δp = discrete increment in maximum fiber presence probability for first window

$\Delta p'$ = discrete increment in maximum fiber presence probability for second window

$\vec{p}$ = random variable vector [see eq (4.26)]

$P(\vec{x})$ = fiber presence probability of a window with position vector $\vec{x}$

$P_o(\vec{x})$ = observed fiber presence probability of a window with position vector $\vec{x}$

$P_m(\vec{x})$ = model fiber presence probability of a window with position vector $\vec{x}$

$\hat{P}_o(\vec{x})$ = normalized observed fiber presence probability of a window with position vector $\vec{x}$

$\hat{P}_m(\vec{x})$ = normalized model fiber presence probability of a window with position vector $\vec{x}$

P_{m_i} = bivariate normal distribution of *i*th fiber filament in multiple filament melt

blowing

P_m = model fiber presence distribution in multiple filament melt blowing

Δr_i = relative gray level of ith pixel in the image

t = web thickness

W = number of windows in the image

x = abscissa of the fiber position in a web

$\vec{x}$ = position vector of the center of a window

y = ordinate of the fiber position in a web

Greek Symbols

α = percentage of the distribution contained in the ellipse [see eq (4.34)]

η = proportionality constant in eq (4.10)

$\phi_h(p, p'; \vec{h})$ = spatial bivariate probability density function

$\Phi_h(p, p'; \vec{h})$ = spatial bivariate cumulative distribution function

γ_i = gray level intensity of ith cell [see eq (4.1)]

Γ_i = normalized frequency of occurrence of ith event [see eq (4.1)]

λ = proportionality constant in eq (4.6)

μ_x = x direction mean position of the fibers

μ_y = y direction mean position of the fibers

$\vec{\mu}$ = mean vector of the fiber positions

ν = number of fibers present at a position in web

ν_i = number of fibers present at a pixel of gray level g_i in the web image

ν_{max} = number of fibers present at a pixel of gray level g_{max} in the web image

θ = orientation angle of the major axis of the web distribution ellipse [see eq (4.35)]

θ_m = orientation angle of the major axis of the model web distribution ellipse

θ_o = orientation angle of the major axis of the observed web distribution ellipse

ρ = correlation coefficient of the fiber positions in the x and y directions

σ_x = x direction standard deviation of the fiber positions

σ_y = y direction standard deviation of the fiber positions

$\vec{\sigma}$ = standard deviation vector of the fiber positions

$\vec{\sigma}^2$ = variance vector of the fiber positions

Ω = factor representing fiber spatial arrangement and other structural properties of web in eq (4.7)

ψ = fiber presence probability density function [see eq (4.23)]

4.9 References

Aggarwal, R. K.; Kennon, W. R.; Porat, I. A Scanned-laser Technique for Monitoring Fibrous Webs and Nonwoven Fabrics. *J. Textile Inst.* **1992,** *83* (3), 386-398.

Arizono, I.; Ohta, H. A. Test for Normality Based on Kullback-Leibler Information, *The American Statistician* **1989,** *43* (1), 20-22.

Brink, A. D. Minimum Spatial Entropy Threshold Selection. *IEE Proc.-Vis. Image Signal Process.* **1995,** *142* (3), 128-132.

Boeckerman, P. Meeting the Special Requirements for On-line Basis Weight Measurement of Light Weight Nonwoven Fabrics. *Tappi J.*, **1992,** *75* (12), 166-172.

Chhabra, R.; Shambaugh, R. L. Experimental Measurements of Fiber Threadline Vibrations in the Melt-Blowing Process. *Ind. Eng. Chem. Res.* **1996,** *35* (11), 4366-4374.

Ericson, C. W.; Baxter, J. F. Spunbonded Nonwoven Fabric Studies, I: Characterization of Filament Arrangement in the Web. *Textile Res. J.* **1973,** *43*, 371-378.

Frieden, B. R. Restoring with Maximum Likelihood and Maximum Entropy. *J. Opt. Soc. Amer.* **1972,** *62* (4), 511-518.

Goffe, W. L.; Ferrier, G. D.; Rogers, J. Global Optimization of Statistical Functions With Simulated Annealing. *J. Econometrics* **1994,** *60*, 65-99.

Harpham, A. S.; Shambaugh, R. L. Flow Field of Practical Dual Rectangular Jets. *Ind. Eng. Chem. Res.* **1996,** *35* (10), 3776-3781.

Harpham, A. S.; Shambaugh, R. L. Velocity and Temperature Fields of Dual Rectangular Jets. *Ind. Eng. Chem. Res.* **1997,** *36* (9), 3937-3943.

Hearle, J. W. S.; Stevenson, P. J. Nonwoven Fabric Studies, Part III: The Anisotropy of Nonwoven Fabrics. *Textile Res. J.* **1963**, *33*, 877-888.

Huang, X. C.; Bresee, R. R. Characterizing Nonwoven Web Structure using Image Analysis Techniques. Part I: Pore Analysis in Thin Webs. *INDA J. Nonwovens Res.* **1993**, *5* (1), 13-21.

Huang, X. C.; Bresee, R. R. Characterizing Nonwoven Web Structure using Image Analysis Techniques. Part III: Web Uniformity Analysis. *INDA J. Nonwovens Res.* **1993**, *5* (3), 28-38.

IMSL Integrated Mathematical and Statistical Libraries Stat/Library. *FORTRAN Subroutines for Statistical Applications*, Vol. 2; Visual Numerics, Inc.: Houston, TX, 1994, 1128-1129.

Johnson, N. L.; Kotz, S. *Distributions in Statistics: Continuous Multivariate Distributions*; John Wiley and Sons: New York, NY, 1972.

Journel, A. G.; Deutsch, C. V. Entropy and Spatial Order. *Mathematical Geology* **1993**, *25* (3), 329-355.

Kallmes, O. J. Technique for Determining the Fiber Orientation Distribution Throughout the Thickness of a Sheet. *Tappi J.* **1969**, *52* (3), 482-485.

Kapur, J. N.; Kesavan, H. K. *Entropy Optimization Principles with Applications*; Academic Press: San Diego, CA, 1992, 151-170.

Kayser, J. C.; Shambaugh, R. L. The Manufacture of Continuous Polymeric Filaments by the Melt Blowing Process. *Polym. Eng. Sci.* **1990**, *30* (19), 1237-1251.

Kullback, S.; Leibler, R. A. On Information and Sufficiency. *Annals of Mathematical Statistics* **1951**, *22*, 79-86.

Lee, Y.; Wadsworth, L. Effects of Melt-blowing Process Conditions on Morphological and Mechanical Properties of Polypropylene Webs. *Polymer* **1992**, *33* (6), 1200-1209.

Malkan, S.; Wadsworth, L.; Davey, C. Parametric Studies of the 'Reicofil' Spunbonding Process. *Int. Nonwovens J.* **1994**, *6* (2), 42-70.

Milligan, M. W.; Haynes, B. D. Empirical Models for Melt Blowing. *J. Appl. Polym. Sci.* **1995**, *58*, 159-163.

Pourdeyhimi, B. Assessing Fiber Orientation in Nonwoven Fabrics. *INDA J. Nonwovens Res.* **1993**, *5* (4), 29-36.

Prud'homme, R. E.; Hien, N. V.; Noah, J.; Marchessault, R. H. Determination of Fiber Orientation of Cellulosic Samples by X-ray Diffraction. *J. Appl. Polym. Sci.* **1975**, *19*, 2609-2620.

Rao, R. S.; Shambaugh, R. L. Vibration and Stability in the Melt Blowing Process. *Ind. Eng. Chem. Res.* **1993**, *32* (12), 3100-3111.

Rodrigues, F. C.; Carvalho, F. D.; Silva, M. S.; Peixoto, J. P. Measurement of Randomness in Fiber Distribution in Paper using Computer Vision. *Tappi J.* **1990**, *73* (12), 209-212.

Rossi, M.; Posa, D. A Non-Parametric Bivariate Entropy Estimator for Spatial Processes. *Mathematical Geology* **1992**, *24* (5), 539-553.

Shambaugh, R. L. A Macroscopic View of the Melt Blowing Process for Producing Microfibres. *Ind. Eng. Chem. Res.* **1988**, *27* (12), 2363.

Shanon, C. E. A Mathematical Theory of Communication. *Bell Sys. Tech. J.* **1948**, *27*, 379-423, 623-656.

Tsai, P. P.; Bresee, R. R. Fiber Orientation Distribution from Electrical Measurements, Part II: Instrument and Experimental Measurements. *INDA J. Nonwovens Res.* **1991**, *3* (4), 1-6.

Tyagi, M. K.; Shambaugh, R. L. Use of Oscillating Gas Jets in Fiber Processing. *Ind. Eng. Chem. Res.* **1995**, *34* (2), 656-660.

Uyttendaele, M. A. J.; Shambaugh, R. L. Melt Blowing: General Equation Development and Experimental Verification. *AICHE J.* **1990**, *36* (2), 175-186.

Votava, R. J. A Practical Method - Measuring Paper Asymmetry Regarding Fiber Orientation. *Tappi J.* **1982**, *65* (4), 67-70.

				$(i+2, j-1)$
		(i, j)	$(i+1, j)$	$(i+2, j)$
	$(i-1, j-1)$	$(i, j+1)$	$(i+1, j+1)$	$(i+2, j+1)$
$(i-2, j+2)$	$(i-1, j+2)$	$(i, j+2)$	$(i+1, j+2)$	$(i+2, j+2)$

Table 4.1 Asymmetrical 5×5 neighborhood, shown as non-shaded cells, of window (i, j) in a web image.

(1) z-positions below the die:	200, 250, 300, 350, and 400 mm
(2) discharge (nominal) air velocities:	17.6, 22.2, 26.8, and 30.9 m/s
(3) discharge air temperature:	270, 300, 330°C
(4) polymer mass flow rate:	0.3, 0.4, 0.5, 0.6, 0.7 g/min
(5) discharge polymer temperature:	290, 305, 320, 335°C

Table 4.2 The operating conditions used in the experiments

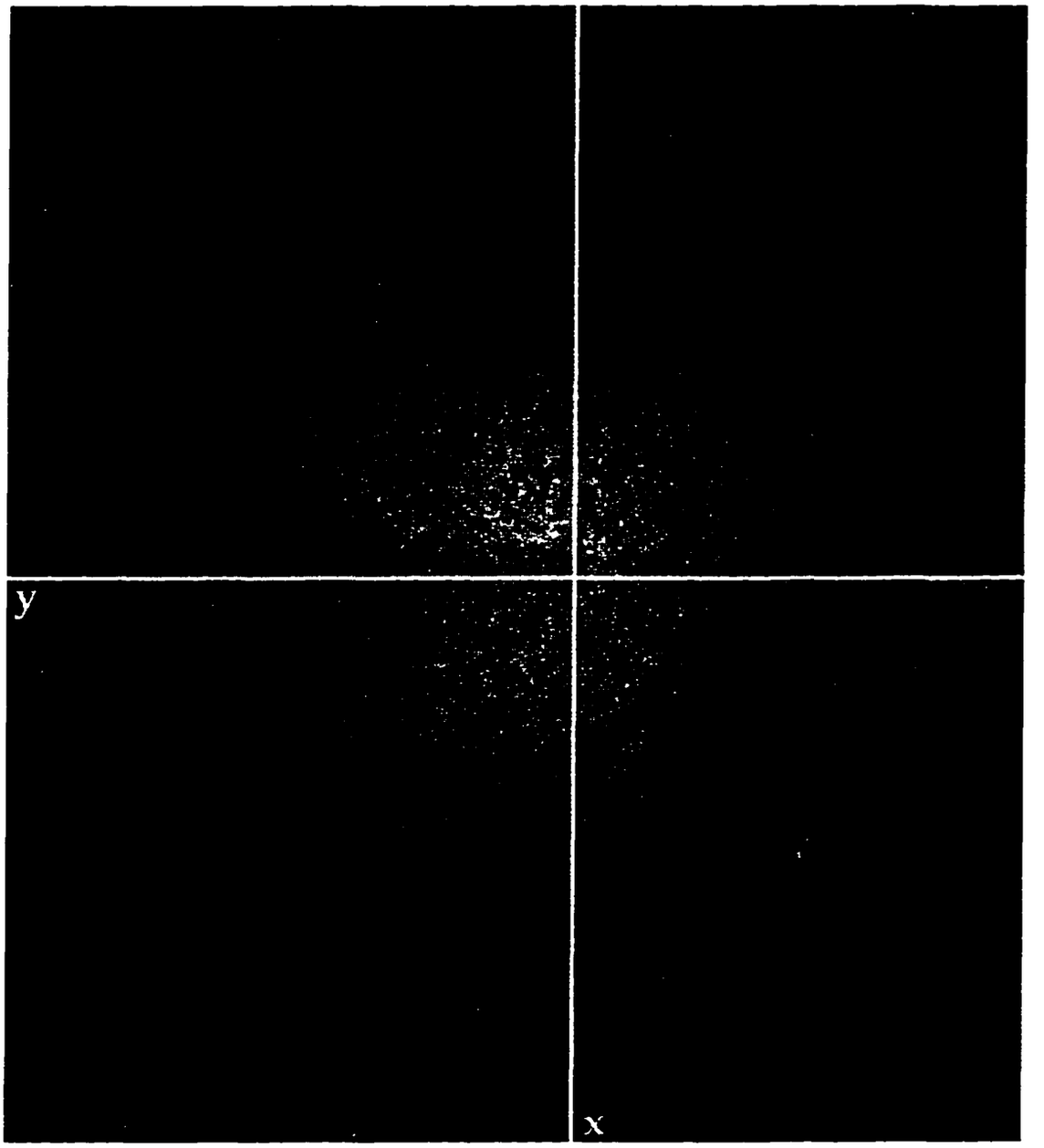

Figure 4.1 Typical top-view image of a single filament melt-blown web. The two orthogonal white lines, corresponding to the coordinate axes, were digitally overlaid on the image.

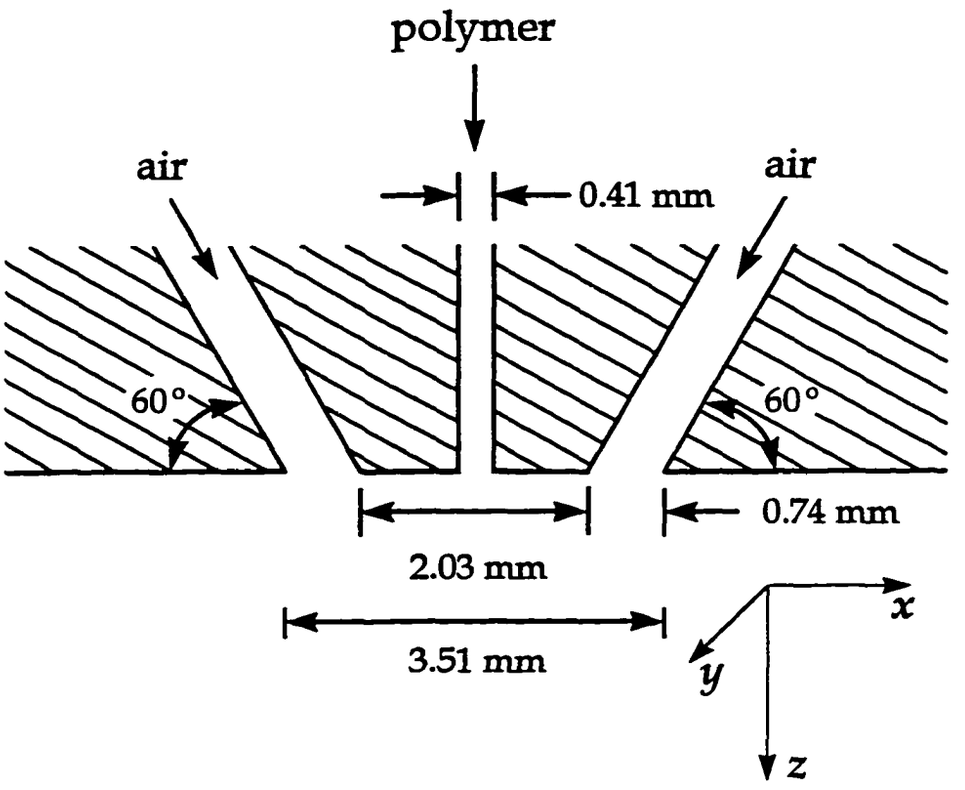

Figure 4.2 Cross-section of the melt blowing die used in the experiments. The origin of the coordinate system, which is shown separately, lies at the polymer orifice of the die.

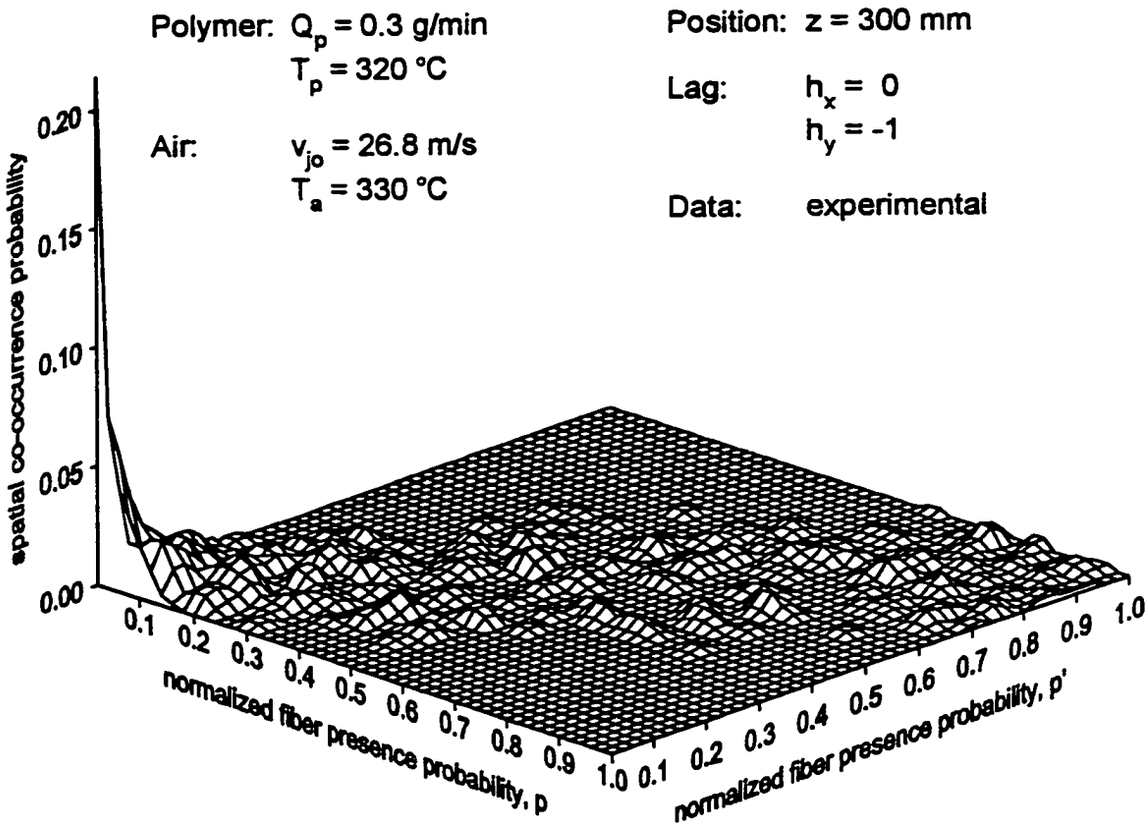

Figure 4.3 Typical surface plot of the observed (web image) spatial order distribution.

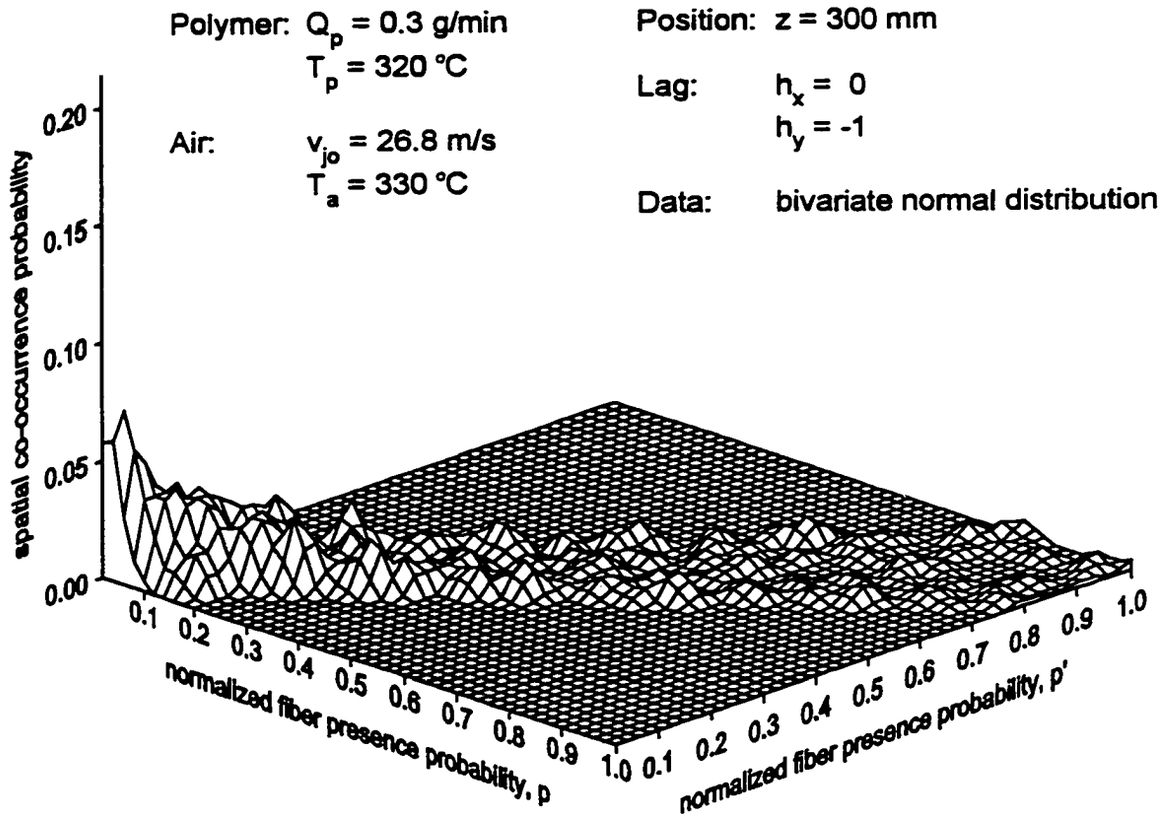

Figure 4.4 Typical surface plot of the model spatial order distribution.

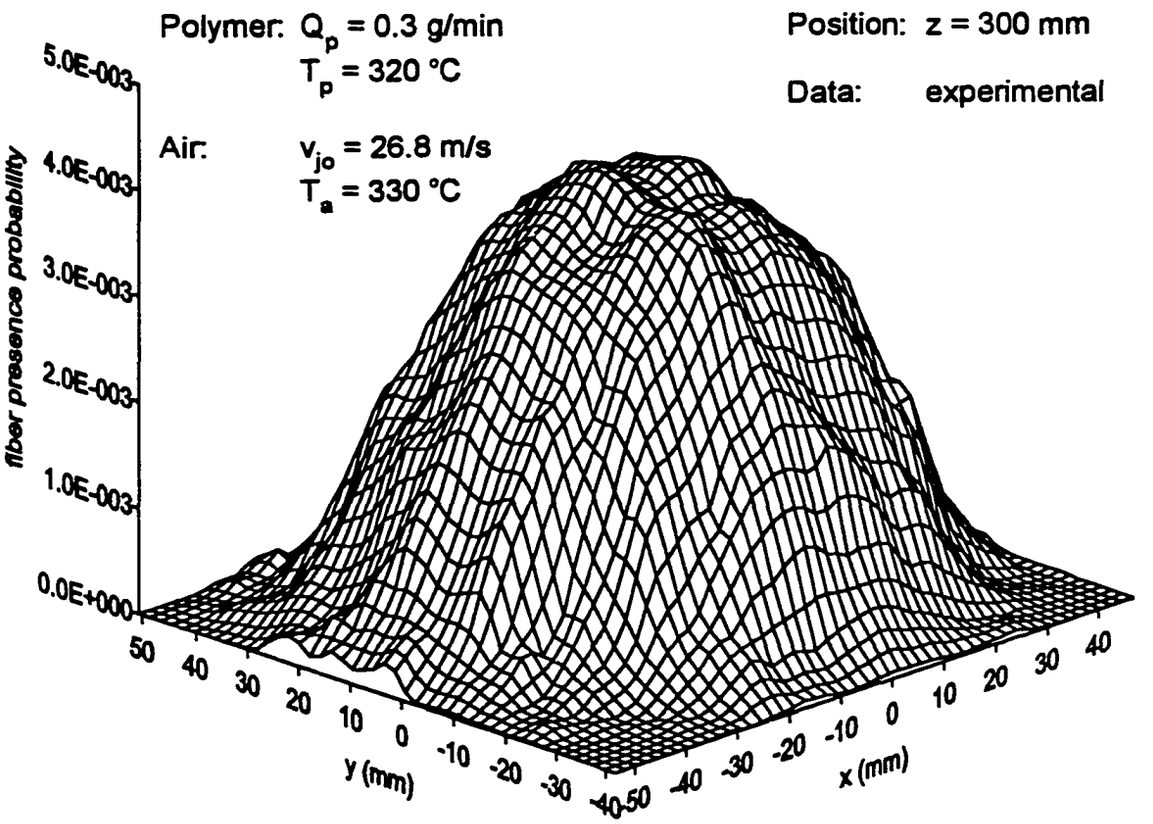

Figure 4.5 Typical surface plot of the observed (web image) distribution of fibers in a single filament melt-blown web.

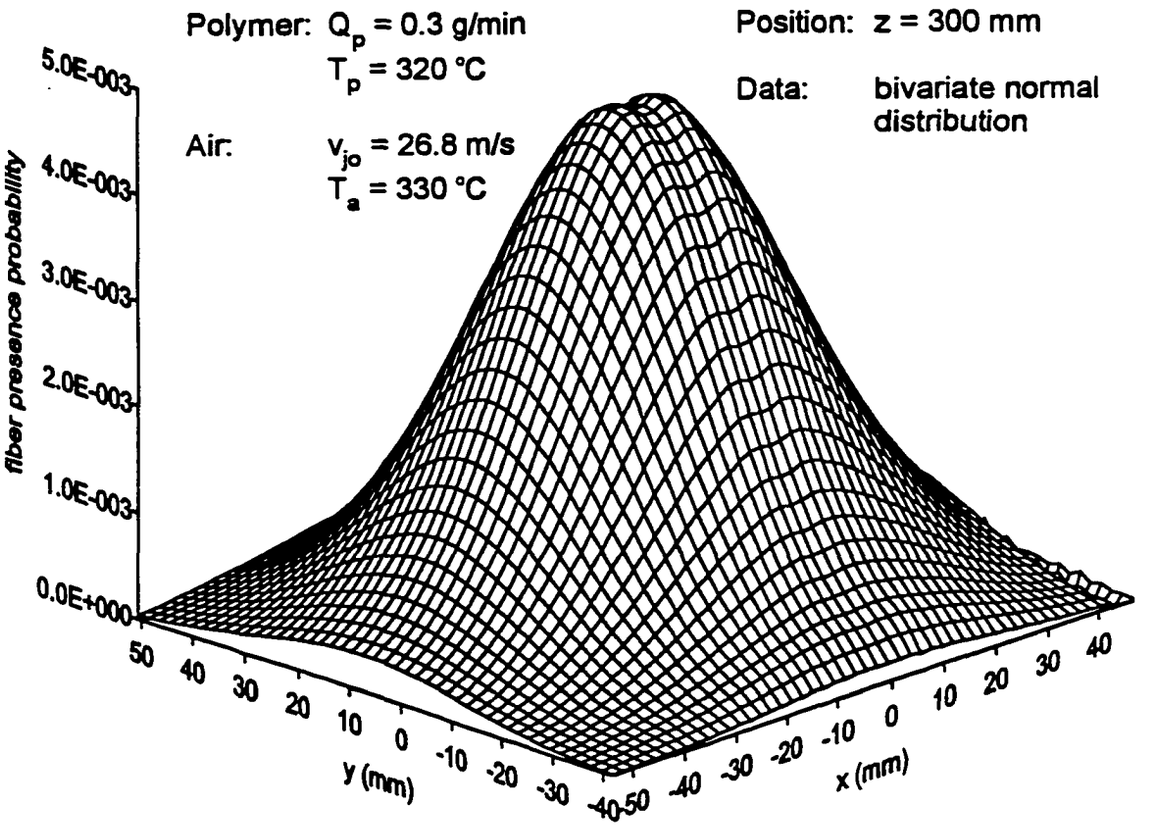

Figure 4.6 Typical surface plot of the model fiber presence distribution in a single filament melt-blown web.

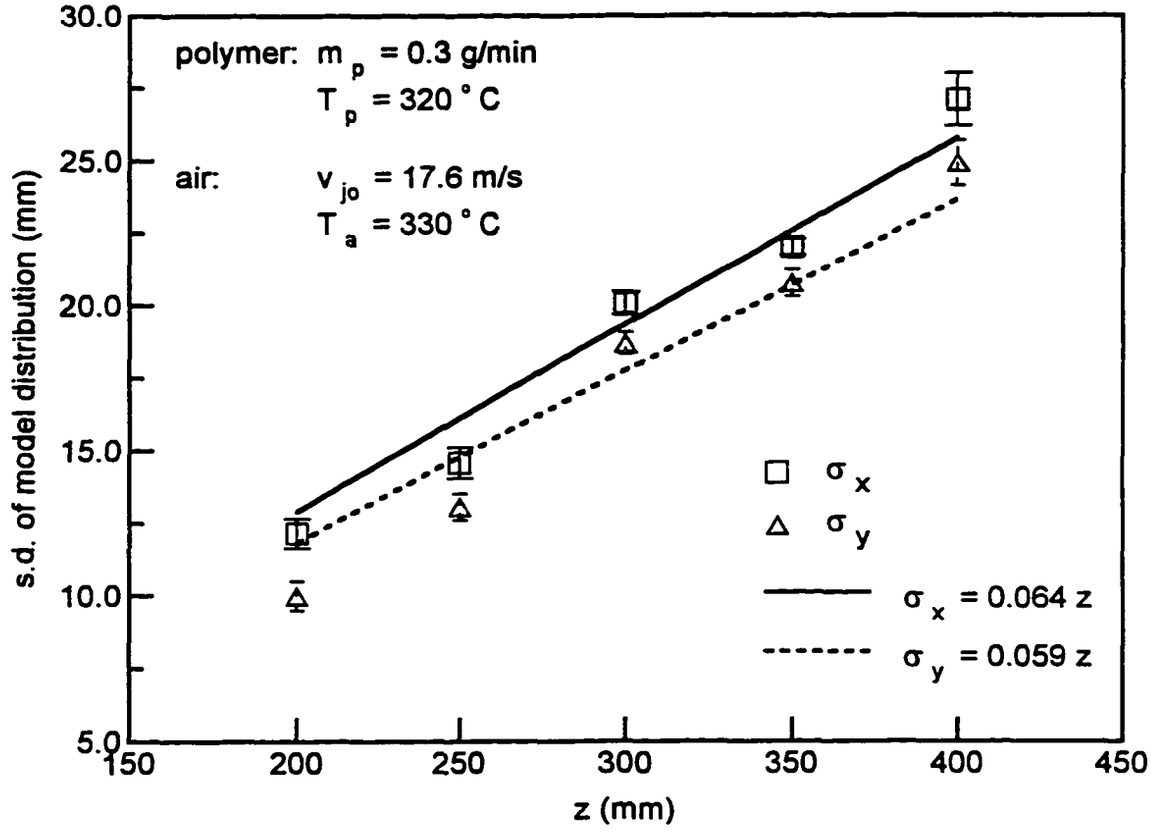

Figure 4.7 Variation in the standard deviations of the web distribution with the z position.

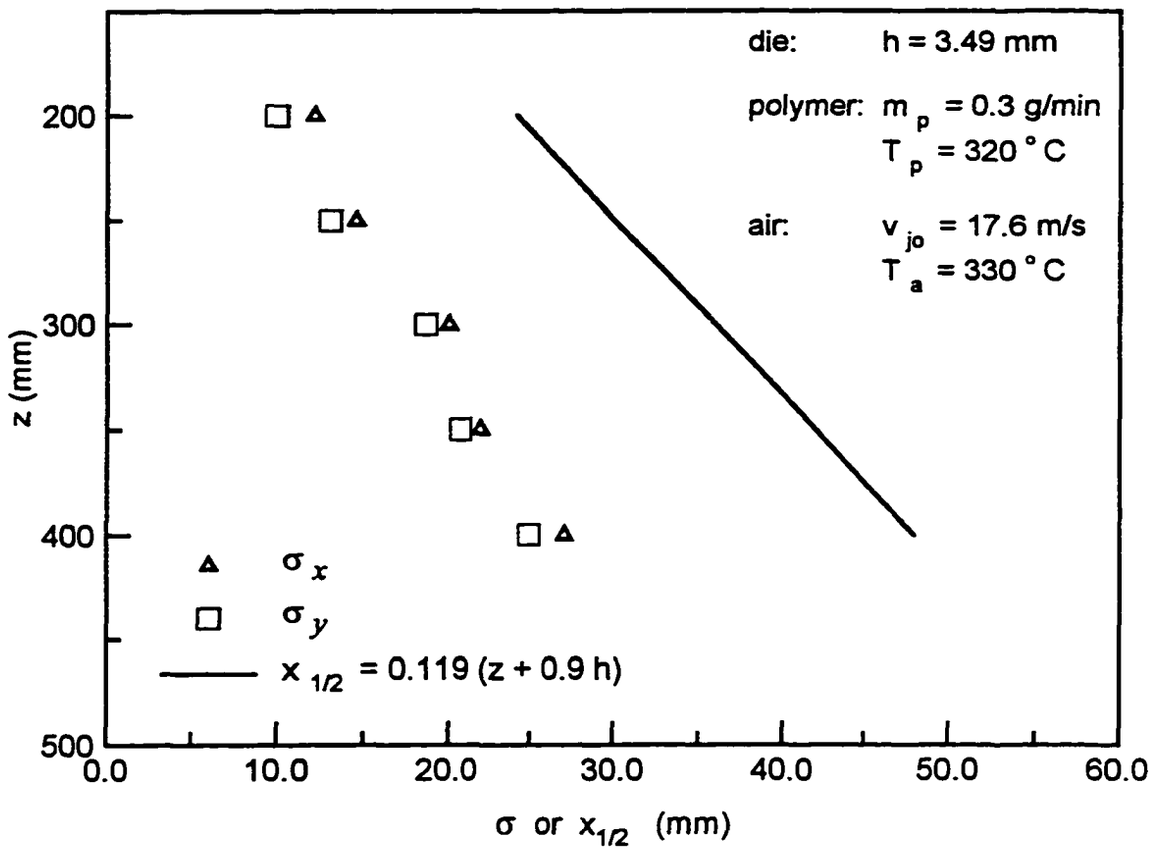

Figure 4.8 Comaprison of spreading characteristics of the web distribution and the air jets in the z direction.

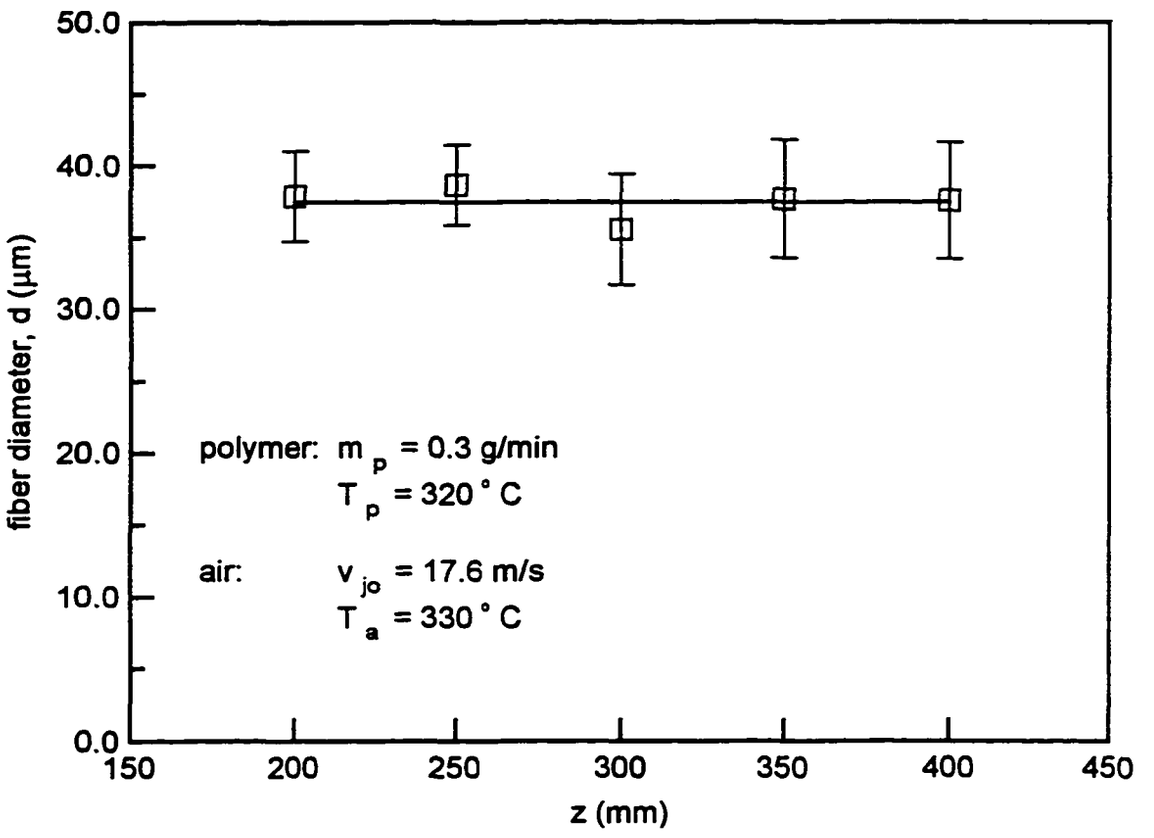

Figure 4.9 Fiber diameter at different z positions below the melt blowing die.

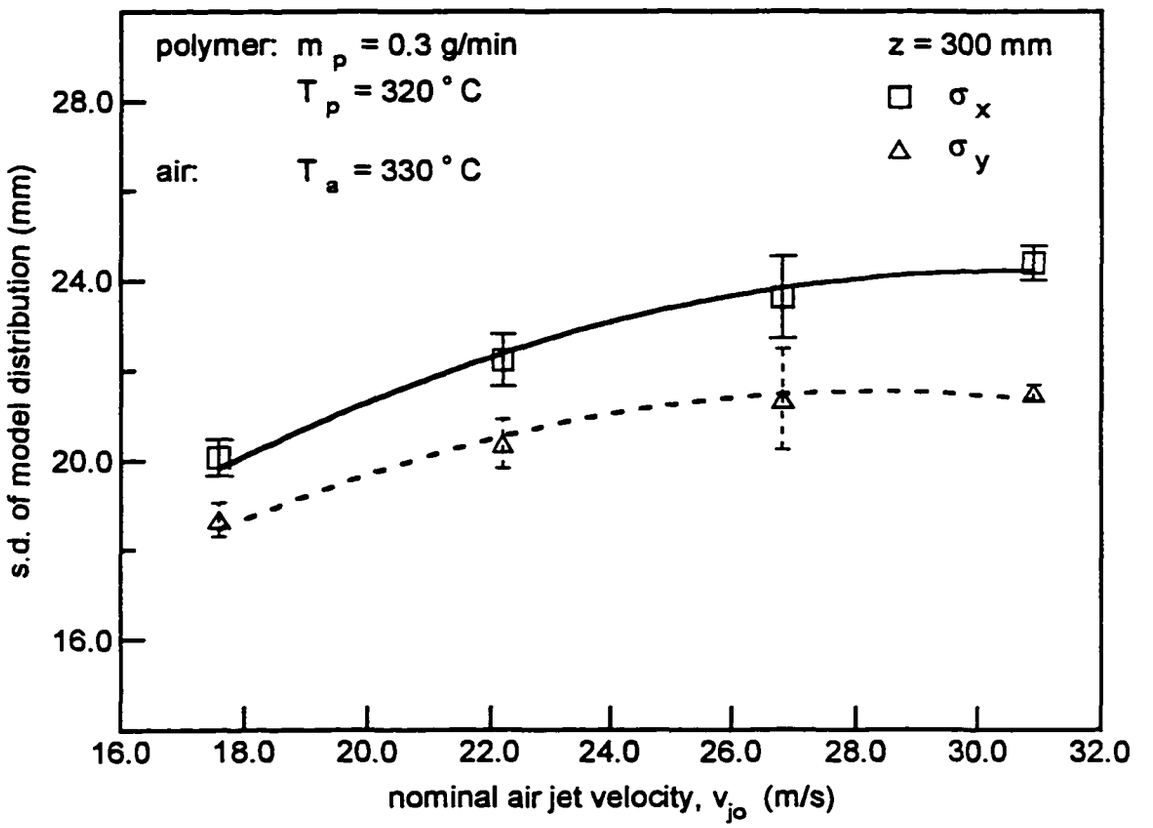

Figure 4.10 Variation in the standard deviations of the web distribution with nominal air jet velocity at z = 300 mm.

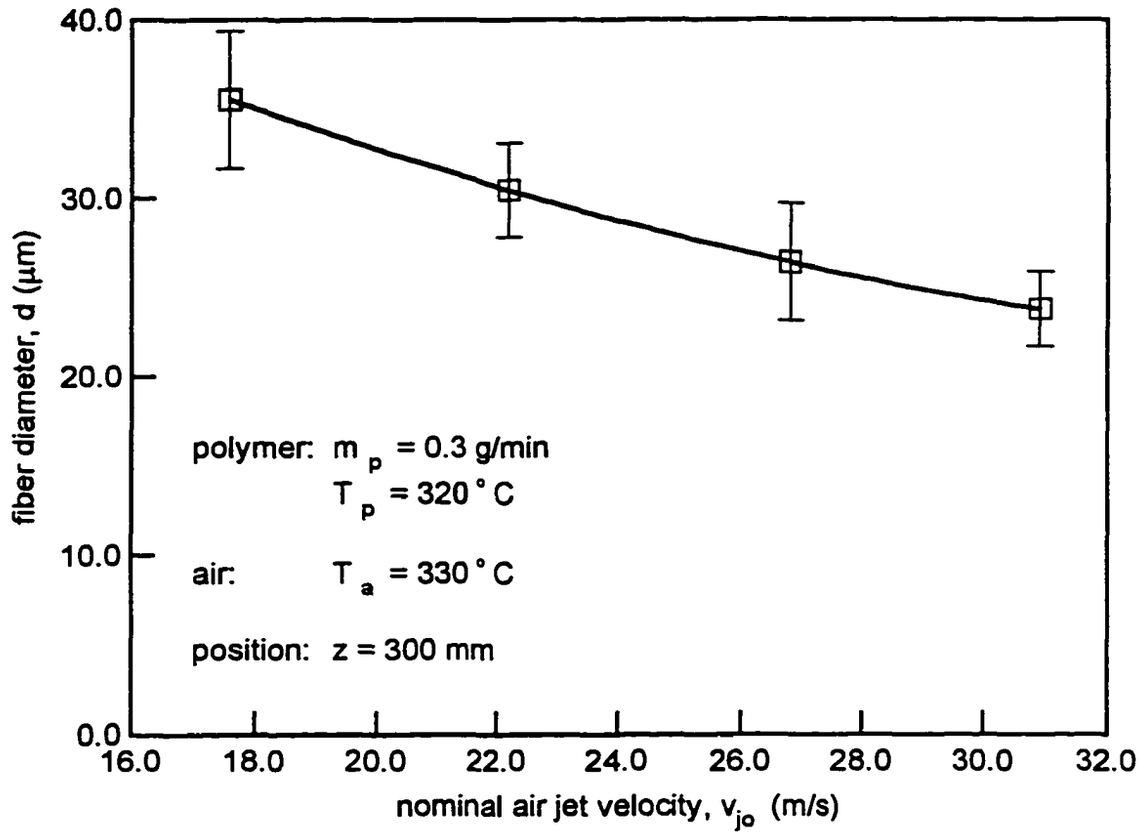

Figure 4.11 Effect of nominal air jet velocity on the fiber diameter at $z = 300$ mm.

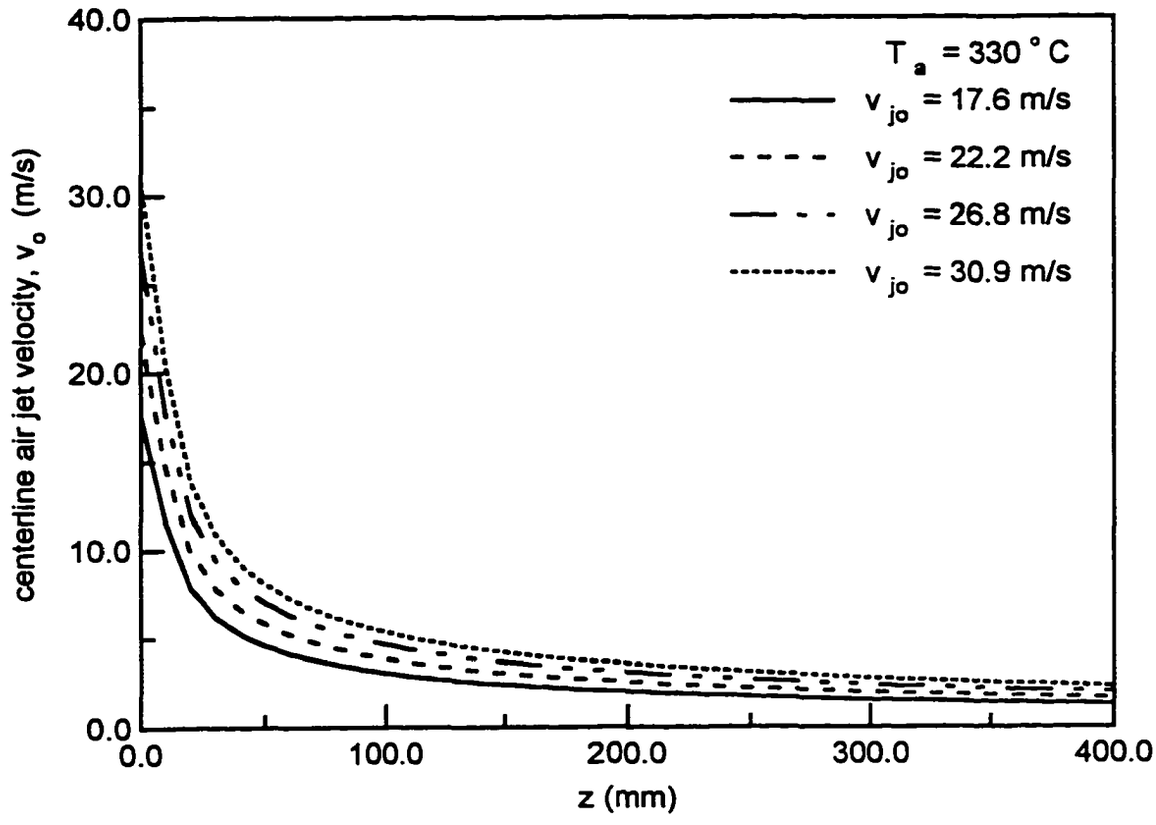

Figure 4.12 Centerline air velocity profile below the die.

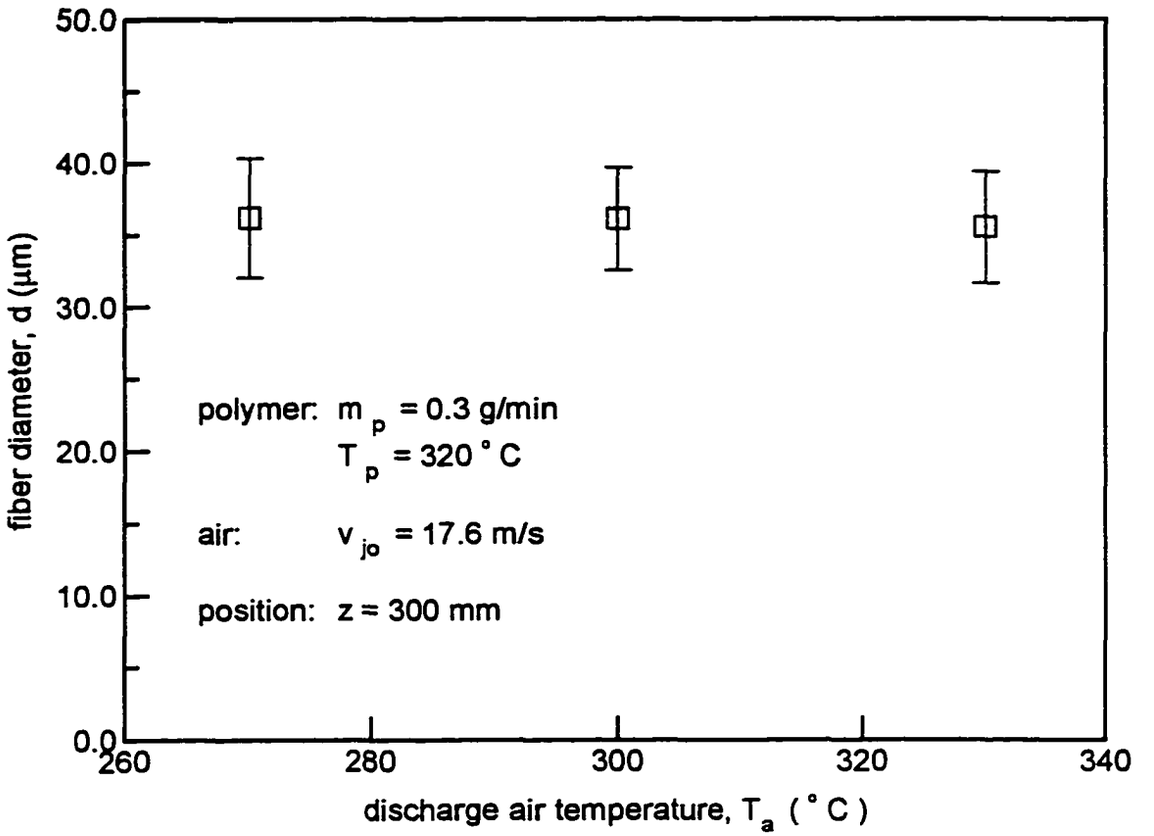

Figure 4.13 Effect of discharge air temperature on the fiber diameter at z = 300 mm.

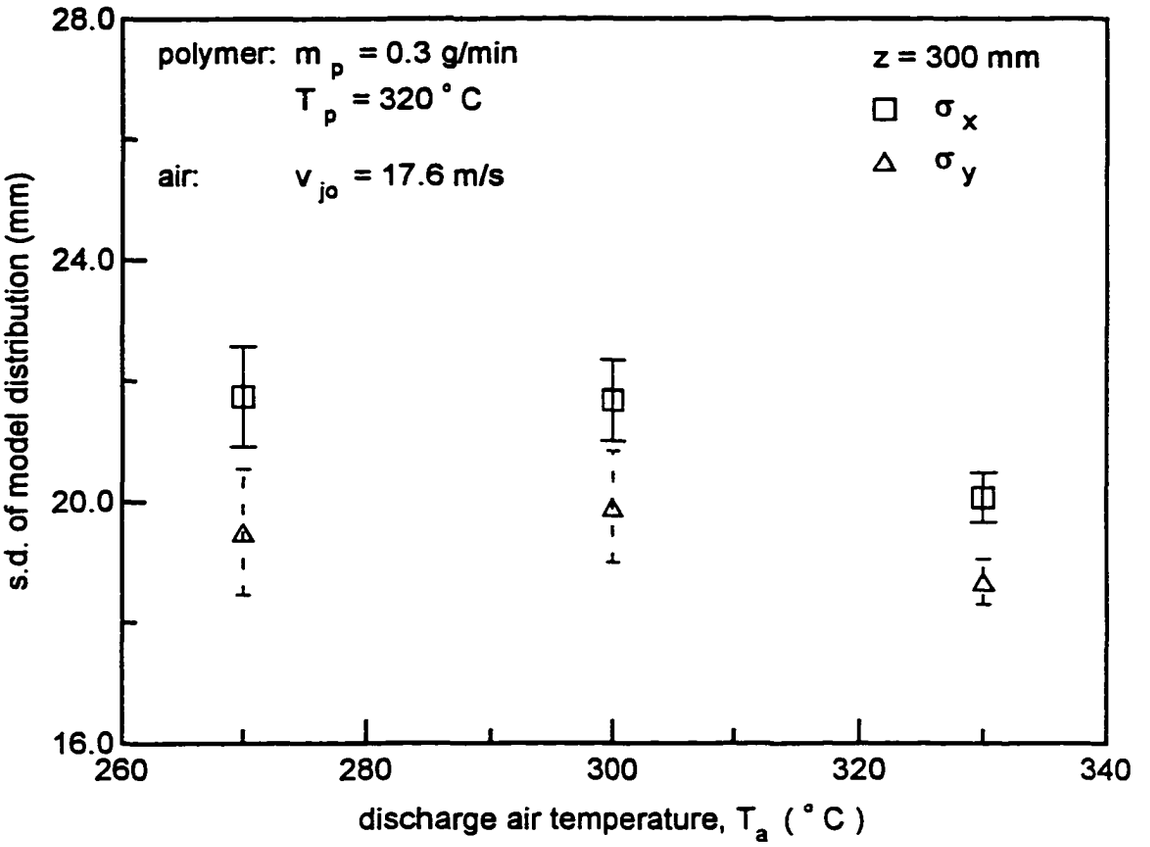

Figure 4.14 Variation in the standard deviations of the web distribution with discharge air temperature at z = 300 mm.

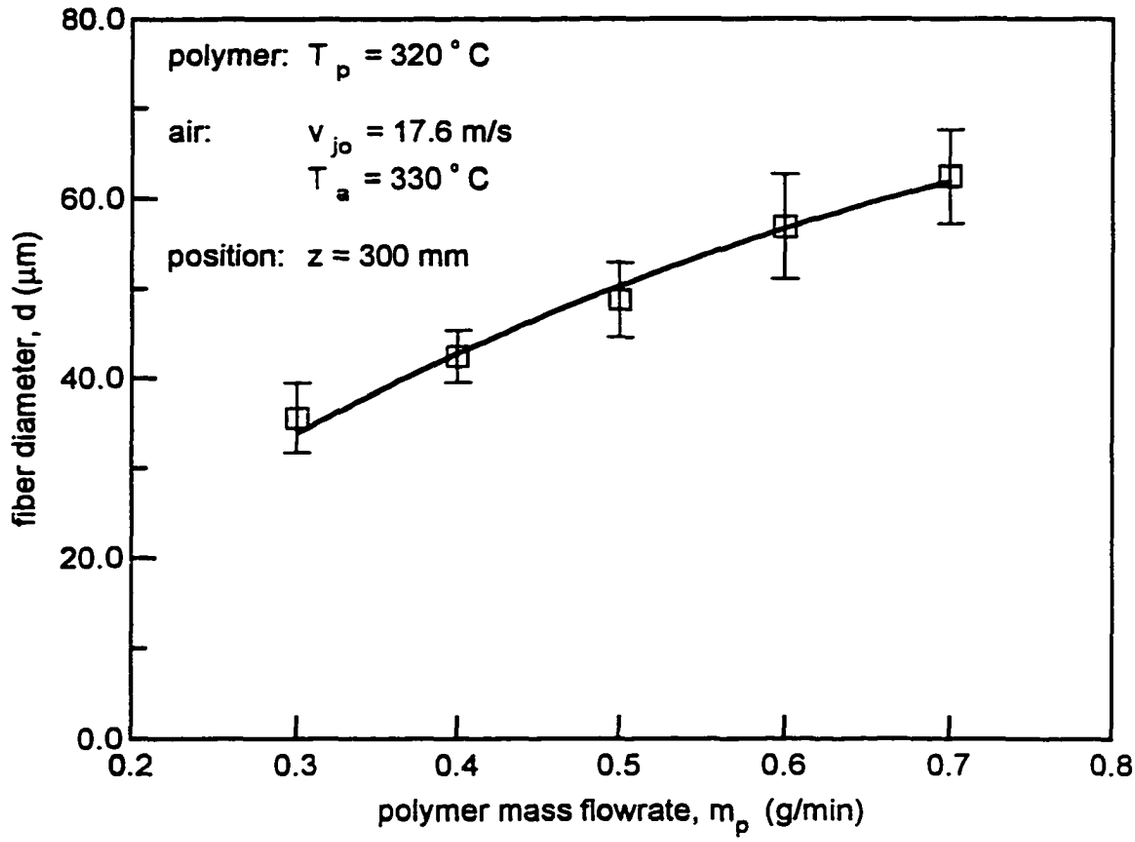

Figure 4.15 Effect of polymer mass flow rate on the fiber diameter at z = 300 mm.

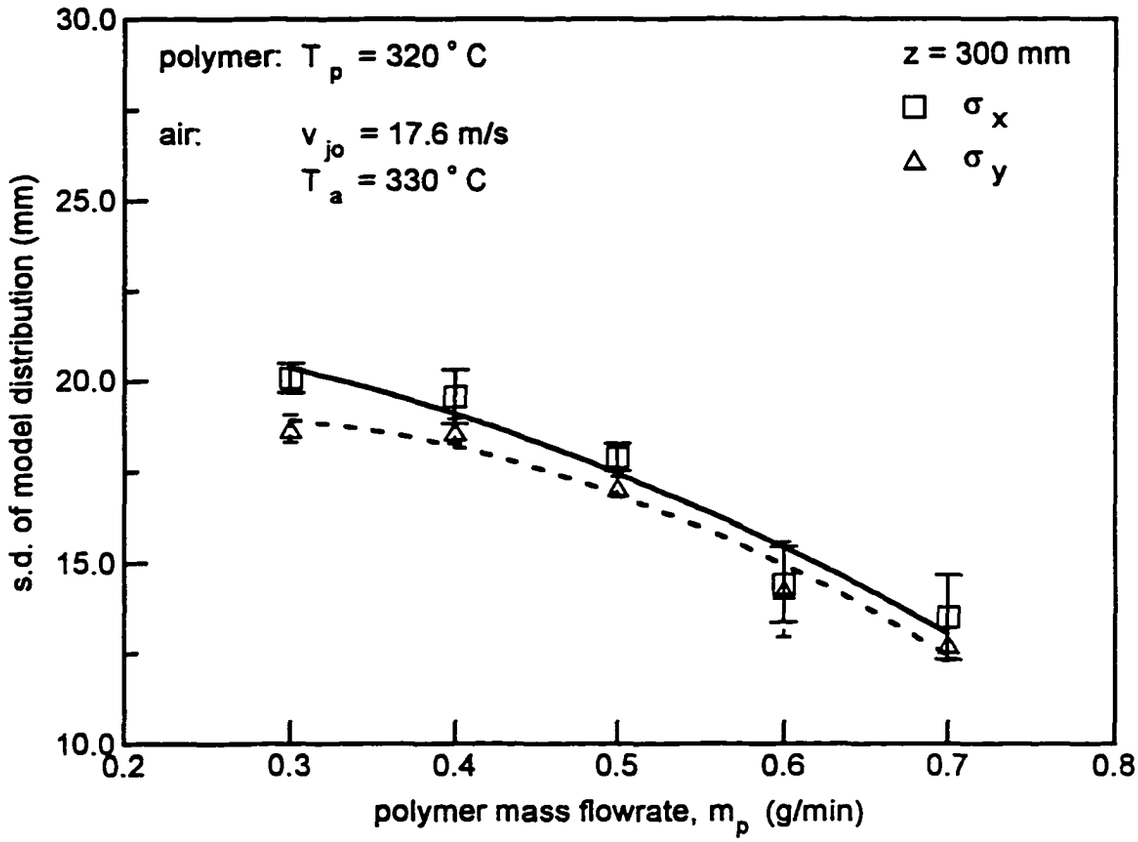

Figure 4.16 Variation in the standard deviations of the web distribution with polymer mass flow rate at $z = 300$ mm.

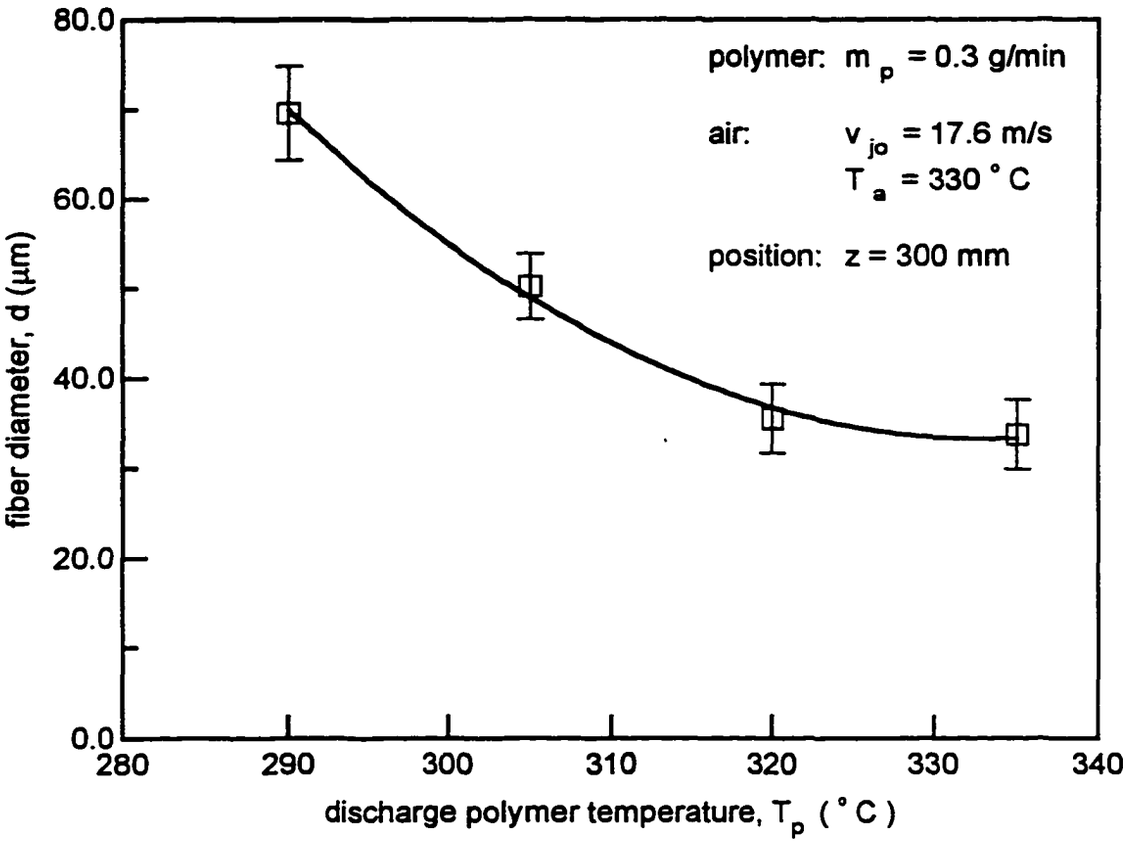

Figure 4.17 Effect of discharge polymer temperature on the fiber diameter at z = 300 mm.

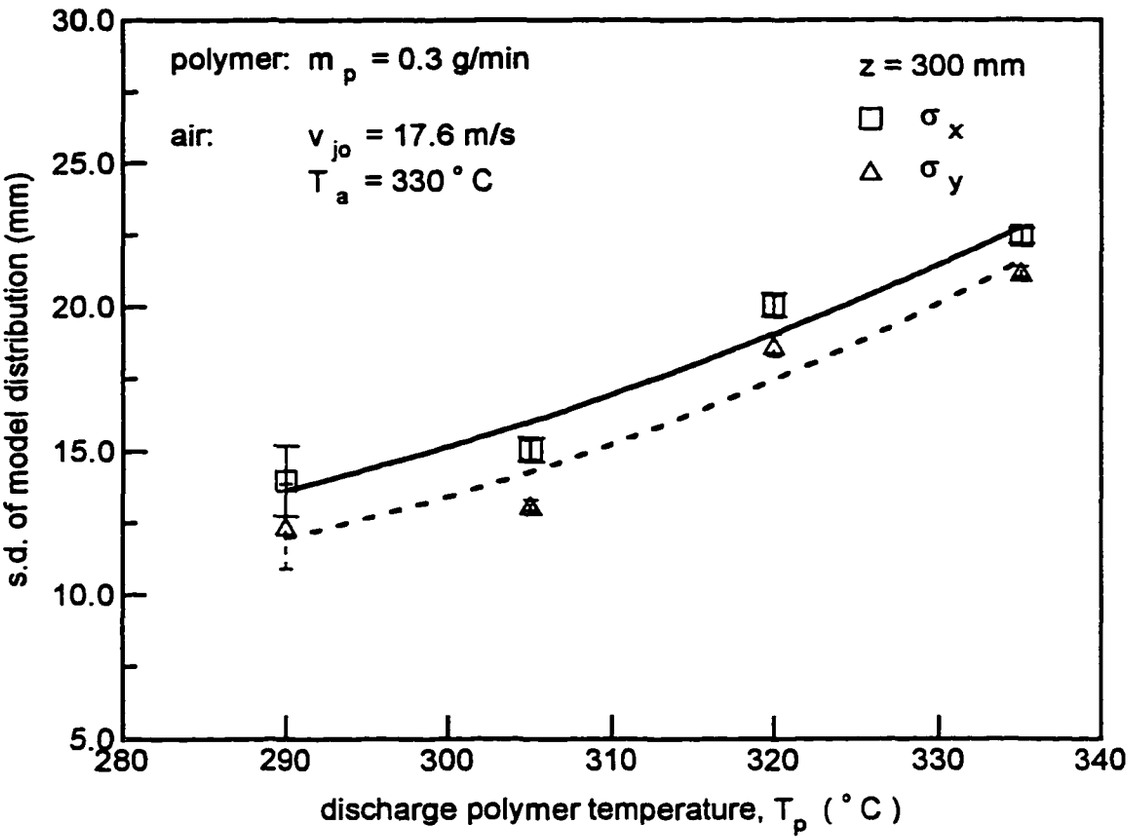

Figure 4.18 Variation in the standard deviations of the web distribution with discharge polymer temperature at z = 300 mm.

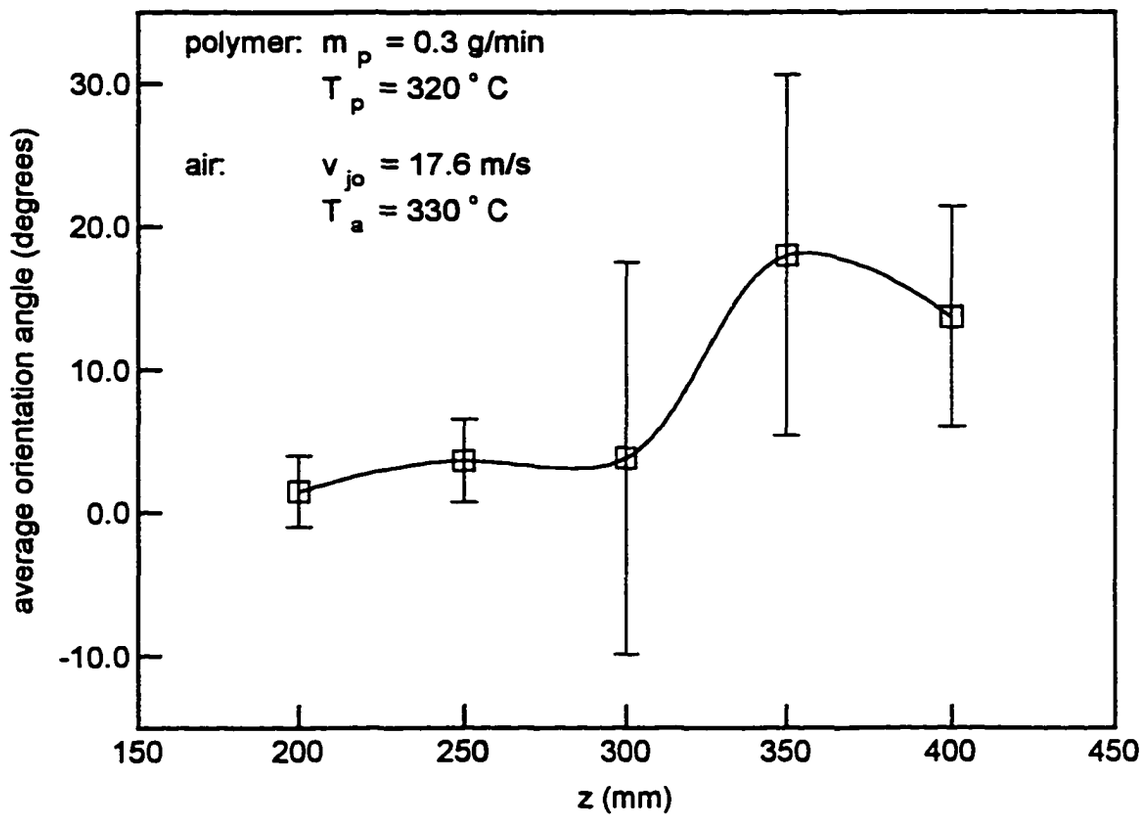

Figure 4.19 Variation in the web orientation angle with the z position. The solid line shown on the graph is a smooth line joining the average web orientation angles.

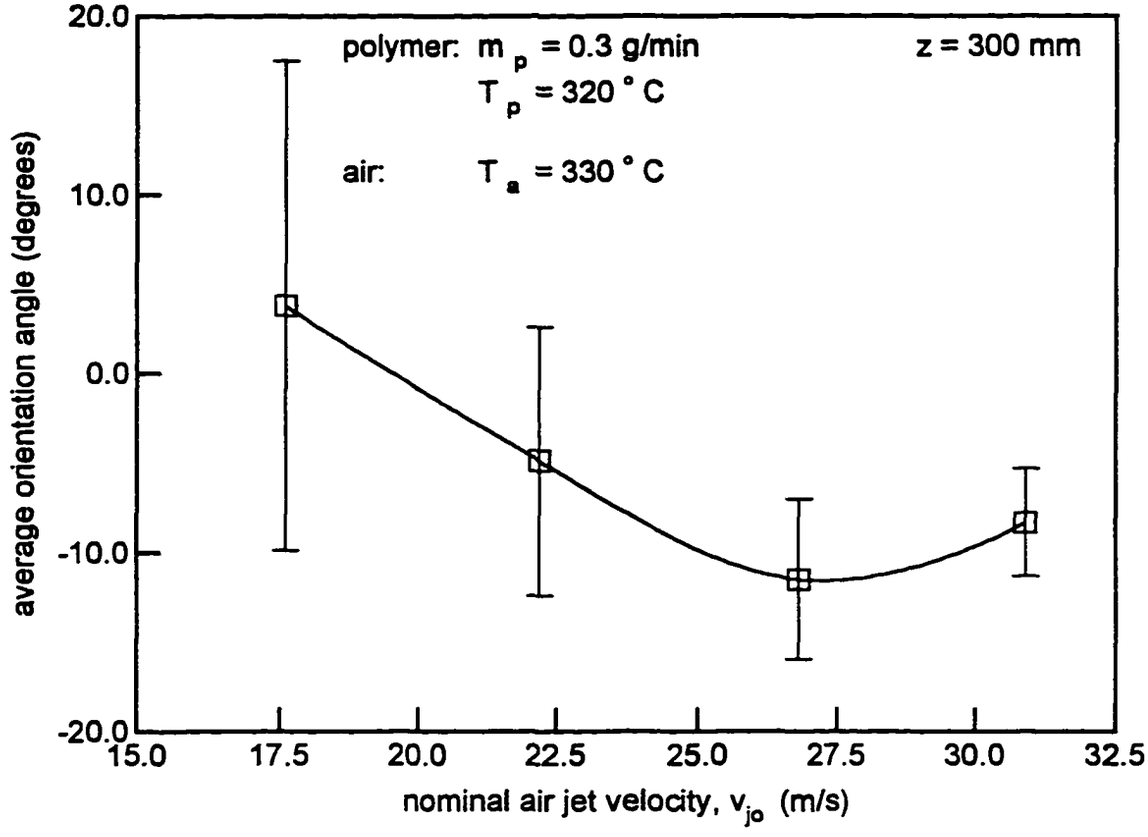

Figure 4.20 Effect of nominal air jet velocity on the web orientation angle at z = 300 mm. The solid line shown on the graph is a smooth line joining the average web orientation angles.

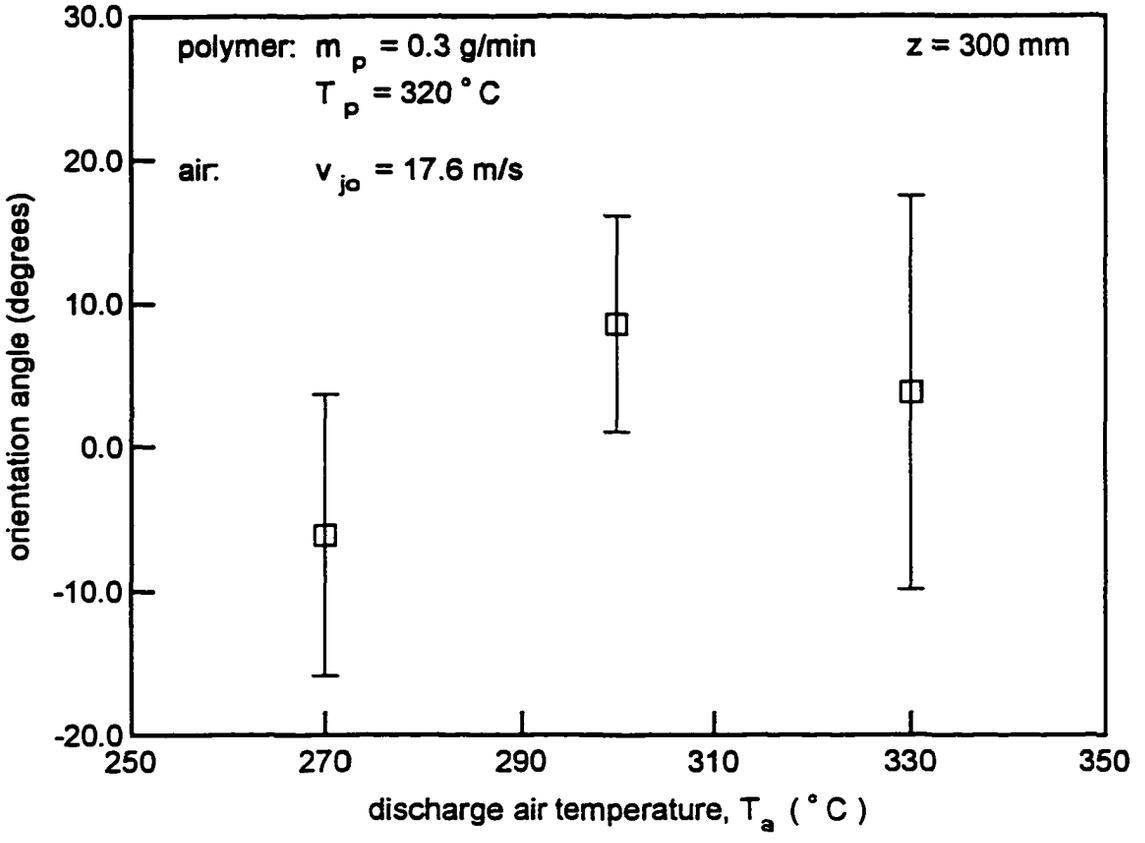

Figure 4.21 Effect of discharge air temperature on the web orientation angle at z = 300 mm. The solid line shown on the graph is a smooth line joining the average web orientation angles.

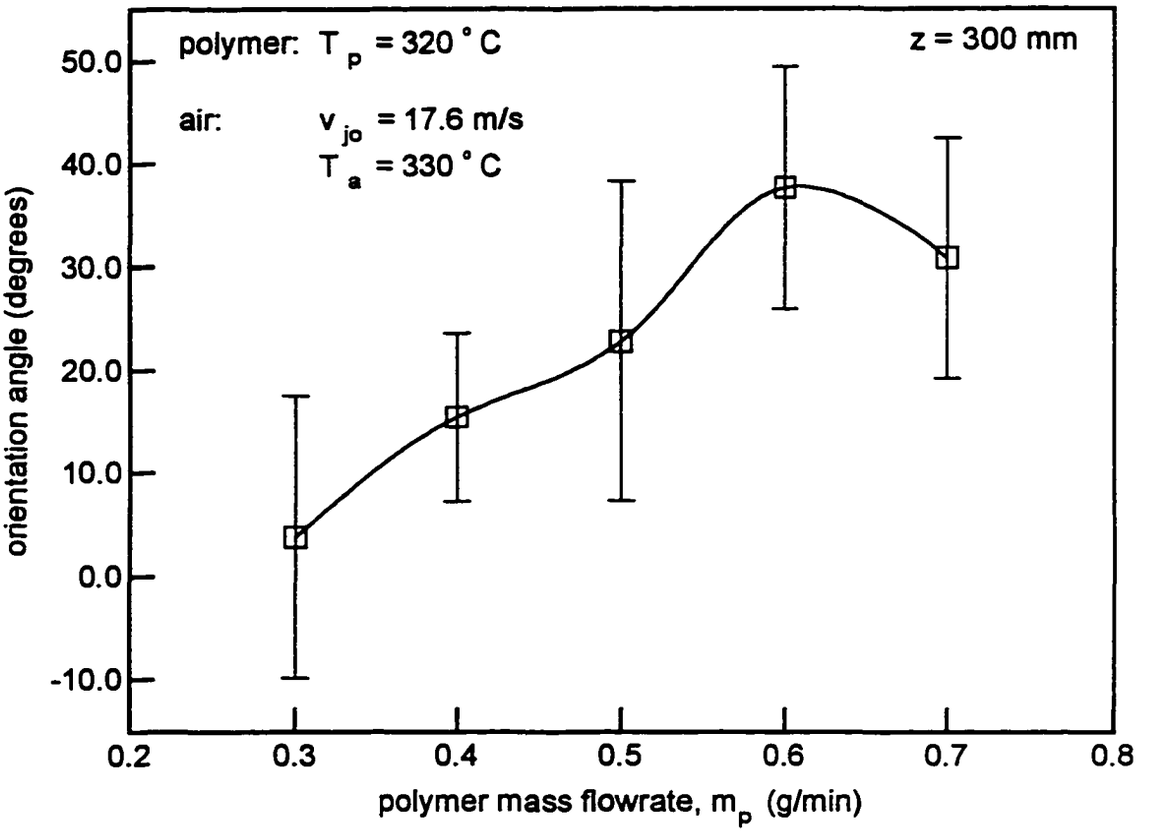

Figure 4.22 Effect of polymer mass flow rate on the web orientation angle at z = 300 mm. The solid line shown on the graph is a smooth line joining the average web orientation angles.

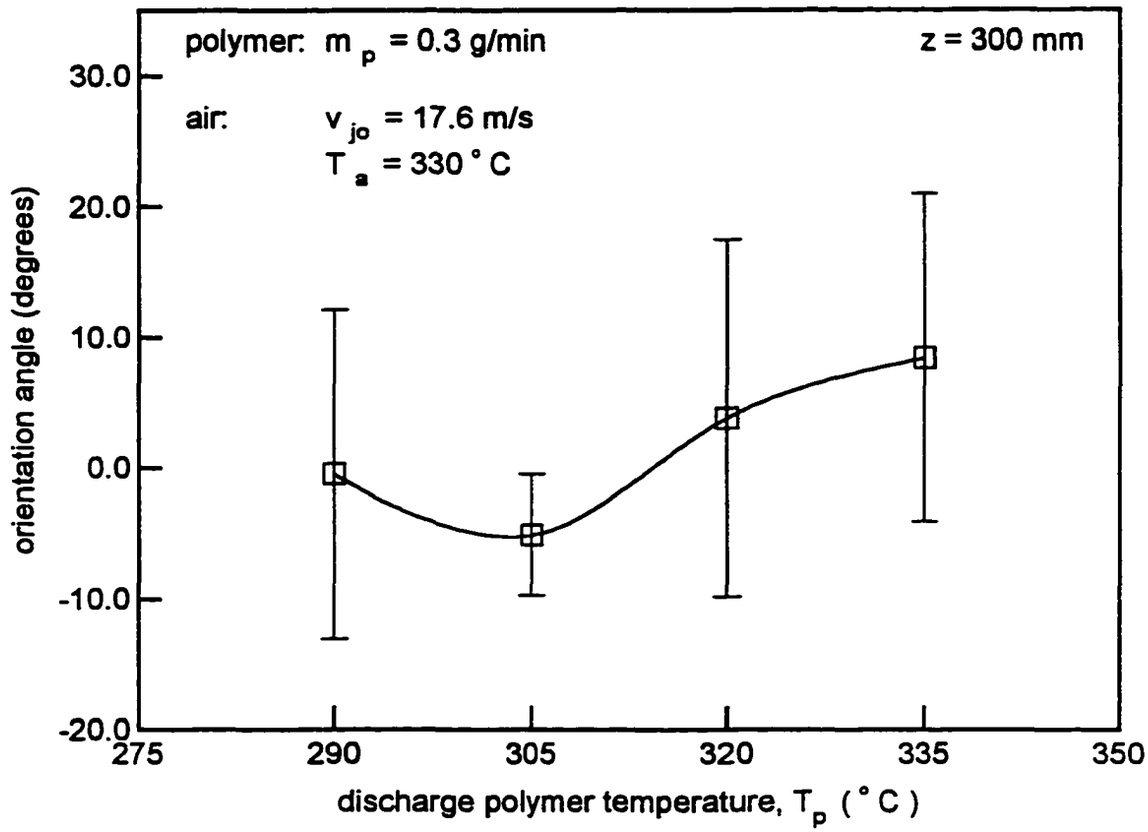

Figure 4.23 Effect of discharge polymer temperature on the web orientation angle at z = 300 mm. The solid line shown on the graph is a smooth line joining the average web orientation angles.

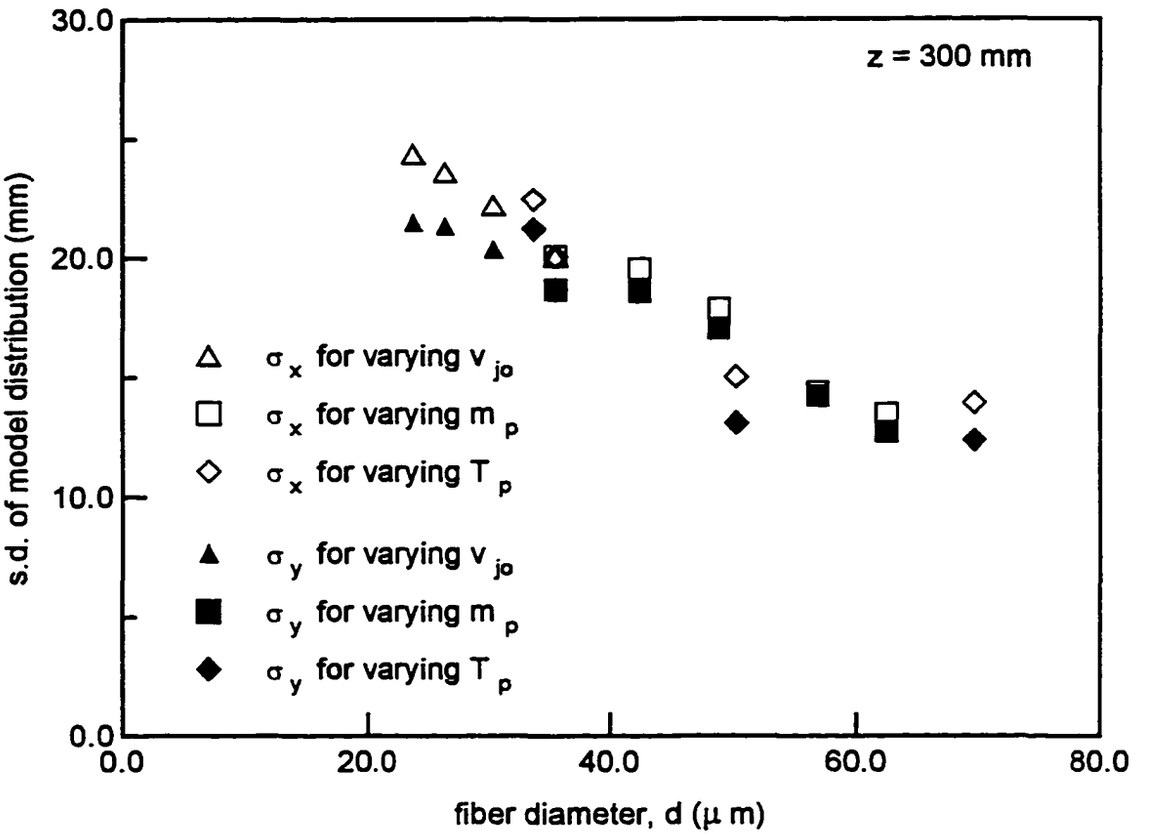

Figure 4.24 Effect of the fiber diameter on the spread of the web distribution. Different fiber diameters were obtained by varying the melt blowing process conditions.

Chapter 5

AIR TURBULENCE STRUCTURE IN MELT BLOWING

5.1 Overview

In melt blowing, the aerodynamic drag force of a high velocity hot air (gas) jet rapidly attenuates the fiber. The higher the air velocity, the larger the aerodynamic drag force on the fiber; the greater the fiber attenuates. Shambaugh (1988) has shown that the melt blowing process has three main regions of air velocity in the order of increasing velocity. Air jet turbulence increases as higher air velocity regions are reached. Therefore, it is possible to explain the nature of aerodynamic drag force in three air velocity regions if jet turbulence characteristics are known.

Air jet turbulence also varies as the distance from the die increases. Wu and Shambaugh (1992) defined three spatial *zones* of fiber motion at the exit of melt blowing die. Fiber has different orientations in three spatial zones. Once again, it is possible to explain the spatial orientation of fiber by understanding the air jet turbulence below the die.

Besides the qualitative explanation for the observed fiber diameter and motion at different air velocities, knowledge of air jet turbulence is needed to quantitatively predict the fiber parameters in melt blowing. Mathematical models of Uyttendaele and Shambaugh (1990), Rao and Shambaugh (1993), and Bansal (1997) can be used to predict the diameter, rheological stress, velocity, and temperature of the fiber. The mathematical models of Rao and Shambaugh (two-dimensional) and Bansal (three-dimensional) can also predict the vibrations of the fiber threadline. These models use extensions of Matsui's (1976) correlation to evaluate the drag and skin friction coefficients required for calculating aerodynamic drag and lift forces acting the fiber. Matsui developed the correlation for drag coefficient for the fiber threadline in melt spinning up to the spinning speed of 6000 m/min. Using Prandtl's mixing length model [Tennekes and Lumley (1972, p. 49)] to approximate the Reynolds stress in the boundary layer parallel to the fiber filament, he derived the following relation for the drag coefficient:

$$C_f = \beta \cdot Re^{-0.61} \tag{5.1}$$

where

C_f = drag coefficient of the filament

Re = Reynolds number of the air flow based on the diameter of the filament

β = empirically determined constant

Narsimahan and Shambaugh (1986) extended Matsui's correlation up to 30,000 m/min in melt blowing. Their correlation was used in the Uyttendaele-Shambaugh model. Later, Majumdar and Shambaugh (1990) experimentally measured the drag force on the fiber filament in an annular, turbulent air stream to determine the drag coefficient in a flow parallel to the filament. Their correlation for the drag coefficient was also proportional to $Re^{-0.61}$. In melt blowing, since the fiber axis is mostly oriented at an angle with respect to the air flow, the assumption of parallel air flow is incorrect. Therefore, Ju and Shambaugh (1994) developed correlations for the air drag on the fiber filament at oblique and normal angles to the flow. In their work, the oblique fiber filaments were exposed to the air flow field near the end of a pipe. For a given Reynolds number, the

aerodynamic force acting on the fiber in this flow field was expected to be identical to that in the flow field below an annular melt blowing die; see Kayser and Shambaugh (1990) for details of the annular die, and Uyttendaele and Shambaugh (1989) and Majumdar and Shambaugh (1991) for the velocity and temperature flow fields of the same die. Rao and Shambaugh's model uses the drag coefficient correlation developed by Ju and Shambaugh to predict the diameter, velocity, and amplitude and frequency of vibration of the fiber. However, their model underpredicts the amplitude of fiber vibrations. One possible reason for the underprediction could be that the turbulent air flow field used by Ju and Shambaugh was not the same as the annular air flow field used by Rao and Shambaugh. Another reason could be that Rao and Shambaugh's model uses only the axial direction mean velocity flow field studied by Majumdar and Shambaugh (1991). Though, Ju and Shambaugh give correlation to evaluate the lift forces in the transverse direction using axial direction mean air velocity, there must be some types of aerodynamic forces acting in the transverse directions due to turbulent air velocity flow field in the transverse directions.

Recently, Harpham and Shambaugh (1996; 1997) studied the axial mean velocity and temperature flow fields of a slot ("Exxon" type) die. Figure 5.1 shows the cross-section of the slot die used by Harpham and Shambaugh (the same die was used in the present work). For the same slot die, Bansal (1997) extended two-

dimensional Rao-Shambaugh model to three dimensions. However, Bansal's model also underpredicts the fiber amplitude for the slot die. One of the reasons for the underprediction of the fiber amplitude for the slot die could be that Bansal's model uses only axial flow field of the slot die to evaluate the aerodynamic drag and lift forces, and does not take into account the effect of transverse components of velocity on the aerodynamic drag and lift forces. Furthermore, the slot die has two inclined jets crossing close to the die face. The crossing of the jets affects the turbulent air flow field of a slot die. Owing to the "history" effect of the jet crossing, the turbulent air flow field of such a die is expected to be different than that studied by Ju and Shambaugh for evaluating the drag coefficient. The difference in the two air flow fields may affect the aerodynamic force acting on the fiber filament; hence, the fiber amplitude is underpredicted.

Milligan (1991) experimentally related the "form" drag or pressure drag to the "flapping" or changing shape of the fiber threadline for a melt blowing slot die. The aerodynamic flapping of the fibers can be attributed to the air turbulence in melt blowing.

The melt blowing model of Rao and Shambaugh (1993) predicted that the fiber vibrates with a characteristic natural frequency under the action of aerodynamic forces. Tyagi and Shambaugh (1995) found that the fiber diameter could be

reduced by oscillating the primary air jets of a slot die with a frequency that matches the natural frequency of the fiber. They found that the most significant reduction in the fiber diameter was achieved by oscillating the jets with frequencies in the range of 28 Hz to 46 Hz for three different air flow rates: 54, 100, 144 standard liters per minute. Furthermore, they observed the air-to-polymer mass loading was significantly reduced by oscillating the jets. Therefore, Tyagi and Shambaugh concluded that, to produce a fiber of given desired diameter, less air is needed if oscillation is used. From their results, it can be conjectured that, by oscillating the air jets of a slot die, the same or higher degree of air turbulence is achieved as in a continuous flow; hence a reduction in the fiber diameter is observed. Consequently, in order to understand the effects of oscillating jets in melt blowing, it becomes important to study the air turbulence structure of flow field formed by these turbulent jets.

In an effort to explain the above mentioned effects, a study was done to understand air turbulence in melt blowing. A one-dimensional hot-wire anemometer probe was used to measure air turbulence characteristics. However, a three-dimensional probe was needed to completely understand the air turbulence structure below the die. Due to the lack of equipment, the study could not be extended to higher dimensions. Nevertheless, some characteristics of air turbulence below the die were obtained with one-dimensional probe. In the following sections, a review of

literature on the turbulent air jets in melt blowing, an experimental procedure for measuring the air turbulence structure for a slot die, and a discussion of results of the study are presented.

5.2 Literature Review

The axial mean velocity and temperature fields of annular melt blowing dies have been studied by Uyttendaele and Shambaugh (1989) and Majumdar and Shambaugh (1991). Mohammed and Shambaugh (1993; 1994) studied the axial mean velocity and temperature fields of a Schwarz die. Recently, Harpham and Shambaugh (1996; 1997) did a similar study for a slot die. All these studies were done with a Pitot (impact) tube, and air turbulence characteristics were not measured.

As mentioned earlier, a slot die has two inclined, rectangular jets crossing close to the die face. Figure 5.2 shows the crossing of the two inclined slot jets. The cross-point of the two jets affects the development of the combined jet flow field. Heretofore, no work has been done to study the turbulent flow characteristics of inclined, rectangular free cross-jets. However, a lot of work has been reported on mean and turbulent flow characteristics of single and multiple jets in a cross-flow. Examples include the works of Abramovich (1963), Kamotani and Greber (1972),

Rudinger and Moon (1976), Andreopoulos and Rodi (1984), Andreopoulos (1985), Issac and Jakubowski (1985), Ahmed and So (1987), Barata et al. (1991; 1992), and Savory and Toy (1991). Extensive experimental studies on turbulent flow of circular, free cross-jets have been done by Rho and Choi (1989), Rho et al. (1990; 1995). They have analyzed the turbulent mixing characteristics such as mean and fluctuating velocities, probability density distributions, intermittency factors, turbulence intensities, and Reynolds stresses. They found that the inclined, circular jets after crossing formed an elliptical jet which transformed to a circular jet further downstream. Their work has been correlated to the present work on turbulence characteristics of rectangular, free cross-jets of melt blowing slot die.

5.3 Experimental Details

5.3.1 Experimental Equipment

The turbulent air flow field below a slot die was measured at isothermal conditions. Figure 5.1 shows the cross-section of the slot die used. Figure 5.35.3 shows the top view of the same die. Each slot of the die had a width b = 0.64 mm and a length l = 74.6 mm. The outer edges of the slots were separated by a distance h = 5.03 mm. Harpham and Shambaugh (1996) have further explained the air supply details.

A single channel hot-wire anemometer was used. Goldstein (1983) and Hinze (1975) have detailed the theory and working principle of the hot-wire anemometer. A constant current Dantec hot-wire anemometer set - model 55-M-10 CTA bridge amplifier with model 55-M-01 main unit - was used. A Keithley Metrabyte DAC/ASYST terminal accessory board STA-16 DAS-16 was used to convert analog signals from bridge amplifier to digital signals. An IBM-compatible 386 computer equipped with a math co-processor was used to analyze the digital data with AcqWire® (version 1.05) software. A single wire Dantec probe (model 55P11) was used to collect the data. The probe sensor wire was Platinum-plated tungsten wire with a diameter of 5 μm and a length of 1.25 mm. The sensor wire had a resistance of 3.9 ohm at 20°C and a temperature coefficient of resistance of 0.0036 /°C. The probe was mounted on a Velmex 3-D traverse system that permitted x, y, and z motions in 0.01 mm increments.

Figure 5.3 shows the coordinate system used in the experiments. The origin of the system lies at the center of the face of the die. The y direction is parallel to the slots, the x direction is perpendicular to the slots, and the z direction perpendicular to the plane of the drawing with the positive z axis directed into the plane of the drawing.

All the runs were done at an air temperature of 21°C. The air flow rate, at standard conditions of 21°C and 1 atm pressure, was set at 1.67×10^{-3} m^3/s (100 L/min). For a slot width of b = 0.64 mm, the two air flows through the two slots corresponded to average nominal discharge velocities of V_{jo} = 17.5 m/s and Reynolds number (based on h = 5.03 mm) of about 5800. There was no polymer flowing through the die during the experiments, and the temperature of the die was 21°C.

5.3.2 *Hot-wire System Calibration Procedure*

The hot-wire system needs to be calibrated both before and after each experimental run. If the calibration changes during the experimental run, the collected data are meaningless. In such case, the experiment has to be redone. The calibration is done after the experiment to ensure that calibration had not change during the experiment. Thus, calibration is one of the most important steps which has to be performed very carefully.

For calibrating the hot-wire system, a low turbulence flat velocity field is required (Goldstein, 1983). In such a field, all velocities, at least up to the maximum velocity to be measured, should be possible and reproducible. This kind of velocity field was obtained using 180-cm-long plastic pipe with a flat and low turbulence

velocity profile. The pipe was long enough to give fully developed flow. The pipe was the same as used by Ju and Shambaugh (1994) for air drag measurements. The pipe had an inside diameter of 12.6 mm. The air was supplied at the top end of the pipe at flow rates ranging from 0.03 to 0.14 m^3 (STP)/min (30 to 140 standard L/min). The temperature of the air was 21°C. To characterize the air velocities at different air flow rates through the pipe, a Pitot (impact) tube was placed vertically at the end of the pipe. The Pitot (impact) tube was the same as used by Harpham and Shambaugh (1996; 1997) in their study of air flow fields below a melt blowing slot die. The Pitot tube was mounted on the Velmex 3-D traverse system, and was traversed across the diameter of the pipe to measure the air velocity profiles. The Pitot tube had an outer diameter of 0.71 mm, an inner diameter of 0.45 mm, and a conical nose shape with a cone angle of 25 deg. The tube was 22.9 mm long and was connected with 1.19 mm inner diameter tubing to an oil-filled manometer. Uyttendaele and Shambaugh (1989) have discussed the formula to convert pressure to velocity. The Pitot tube pressure was referenced to ambient static pressure. It is possible that the hot-wire probe may not be placed at the exact same spatial position for calibrations before and after an experimental run. Furthermore, as discussed by Goldstein (1983), a nonuniform velocity profile along the sensor increases the error in calibration. Therefore, to minimize the error in calibration, a flat velocity profile of the pipe was needed. Since the flow was the least turbulent at the center of the cross-section at the end of the pipe, the hot-wire probe was placed there. To avoid mixing of flow with the ambient flow, the tips of both

the Pitot tube and the hot-wire probe were placed vertically about 1 mm from the end of the pipe. The flow rates were chosen such that there was more data for the lower range of velocities since the relation between the velocity and voltage was nonlinear.

Step-wise Pipe Flow Characterization

1. The pipe was set vertical with a plumb line. The Pitot tube was placed normal (vertical) to the flow. To check whether the Pitot tube was in a normal position or not, it was rotated sideways and the position, where the maximum pressure indicated, was selected as the vertical position. The vertical traverse position corresponding to the end of the pipe was then found out.

2. The Pitot tube was traversed along a chord close to the end of the pipe to find the two diametrically opposite ends. The positions, where the velocities were about zero (velocities become zero near the wall) and maximum, were noted. The length of the chord was equal to the difference between the two positions with zero velocity. This value was compared with the diameter of the pipe (12.6 mm). If the relative difference between the two values was less than 1%, the above procedure was performed for the transverse direction. Otherwise, the Pitot tube was moved to a new position closer to the center of the cross-

section of the pipe, and the above procedure was repeated until the center of the pipe cross-section was found. After the center of the pipe was obtained, the Pitot tube was traversed along one of the diameters of the pipe to measure the velocity profiles.

3. The air flow rate was set corresponding to the lowest velocity required to be measured in the actual flow. A rough estimate of the air velocity at the end of the pipe was obtained with the continuity equation. The data at 25 different air flow rates (ranging from 0.03 to 0.14 m^3 (STP)/min) was taken. Figure 5.4 shows the flat velocity profiles of the calibration pipe at three different air flow rates.

After the pipe flow was characterized, the above steps were not repeated during each calibration. The data were stored as pressure differences and not as velocities because the velocity depended on the ambient pressure and flow temperature that change with time [see Uyttendaele and Shambaugh (1989) for the formula to convert pressure to velocity]. The ambient pressure and air temperature were noted each time the calibration was performed. The air velocities were then calculated using the existing values of ambient pressure and air temperature.

The sensor of the hot-wire probe was positioned horizontally at the center of cross-section of end of the pipe. The vertical position of the sensor was about 1 mm from the end of the pipe. The center of cross-section was found using the procedure described in step 2 of the characterization of the pipe flow. However, for the hot-wire probe, instead of finding zero velocity, minimum voltage was found. A Tektronix oscilloscope (Model 2445B) was used to find the minimum voltage. For each known air flow rate or velocity, the value of voltage was measured on the bridge-amplifier of the hot-wire system. A low turbulence profile becomes important since it lessens the uncertainty in the measurement of both air velocity (measured with the Pitot tube) and voltage (measured with bridge-amplifier). Therefore, the mean value of the voltage corresponding to each velocity was measured. This mean value was not an ensemble average, but a time average. Thus, the time-averaged voltage was measured with on-line signal analysis module of the AcqWire® software. In order to find out the optimum time for averaging, the mean values of the voltages were measured for 2.5 minutes and 5 minutes. Since the relative difference between the two mean voltage values was less than 1%, the values corresponding to a period of 2.5 minutes were selected as optimum. The air velocities corresponding to the air flow rates were found from the pressure data obtained from the pipe characterization experiment performed earlier. The formula for converting pressure to velocity has been discussed by Uyttendaele and Shambaugh (1989). Then, each of the mean voltage values along with the corresponding air velocities were entered in the calibration module, and

the best-fit curve of the voltage versus velocity was obtained with the AcqWire® software.

5.3.3 *Experimental Conditions*

At a fixed z position below the die, the sensor wire of the probe was aligned parallel to the y axis or the slots, and the probe traversed along the x axis (transverse to the slot direction). The length-to-width ratio (l/b) of the die was about 117 while the l/h ratio was about 15. Since these ratios were large, the cross-jets were assumed to be infinite for the positions near the center plane of the die and not very far from the die face. Therefore, all the experiments were done at positions in the bisecting plane ($y = 0$) of the die.

From the schematic of the flow geometry in Figure 5.2, it can be seen that the two inclined slot jets combine to form a single jet. The geometrical cross-point of the two inclined slot jets was found to be $z_c = 3.8$ mm. In their study of circular cross-jets, Rho et al. (1990) considered the distance of geometrical crossing of the jets as the characteristic length for non-dimensional analysis. This length was characteristic since it combines the effect of the distance of separation between the jets and their angle of inclination. Rho et al. (1990) observed that the turbulence intensities reached their maximum after the cross-point. Consequently, it was

concluded that the position of crossing of the jets plays an important role in defining the turbulence characteristics of the combined jet. Therefore, in the present study, the distance of geometrical crossing of two slot jets was considered as the characteristic length for non-dimensionalizing the z distance below the die. The mean air velocity, turbulence intensity, skewness, and flatness profiles were studied at seven z positions corresponding to z/z_c of 1.0 to 2.5 with the increments of 0.25. Since the air velocities are time-averaged, the averaging time should be much larger than the integral (characteristic) time scale of the flow (Tennekes and Lumley, 1972, pp. 211-212). However, the integral time scale of the flow was not known. Therefore, the "averaging time" was found by comparing various data collection time periods. Thus, the velocity data was collected for 1 min at a position, and was compared with data collected for 2 min at the same position. Since the percentage difference between the data collected for two time periods was greater than 1%, a period of 1 min was not the correct "averaging time". The procedure was repeated for time periods of 2 min and 3 min. It was found that a time period of 2 min was an optimum "averaging time". Though for time-averaging the effect of sampling frequency is insignificant, a large number of samples have to be taken for averaging. A sampling frequency of 136.5 Hz (corresponding to 16384 samples in a 2 min time interval) was selected as the highest possible sampling frequency with the available hardware. The sampling frequency only affects the energy spectra of the flow. Since the energy spectra of

the flow was not measured, the sampling frequency did not affect the air velocity results.

5.4 Results

5.4.1 Definitions of Terms Used

1. Mean Velocity and Fluctuating Velocity: As described by Tennekes and Lumley (1972), the Reynolds decomposition of the instantaneous velocity $\tilde{v}$ in a turbulent flow field is given by

$$\tilde{v} = V + v \tag{5.2}$$

where V is the mean (time averaged) velocity component of the instantaneous velocity $\tilde{v}$, and v is the fluctuating component of the instantaneous velocity $\tilde{v}$.

2. Root Mean Square of Velocity Fluctuations: The root mean square of velocity fluctuations v_{rms} is defined as

$$v_{rms} = \sqrt{\overline{v^2}} \tag{5.3}$$

3. Turbulence Intensity: The turbulence intensity $T(v)$ is defined as the ratio of the root mean square of velocity fluctuations v_{rms} and the mean velocity of that component. Mathematically,

$$T(v) = \frac{v_{rms}}{V} \tag{5.4}$$

4. Skewness Factor: It is a dimensionless measure of asymmetry of the fluctuating velocity probability distribution. The skewness factor $S(v)$ is defined as

$$S(v) = \frac{\overline{v^3}}{v_{rms}^3} \tag{5.5}$$

For example, for a normal distribution, the skewness factor is zero since a normal distribution is symmetrical about the mean position.

5. Flatness Factor or *Kurtosis*: It is a dimensionless measure of the flatness of the probability tails, or the peakedness of the fluctuating velocity distribution. The flatness factor or kurtosis $K(v)$ is defined as

$$K(v) = \frac{\overline{v^4}}{v_{rms}^4} \tag{5.6}$$

As described by Hinze (1975, pp. 242), for a normal distribution, the flatness factor is equal to 3. A velocity fluctuation distribution with zero mean and a value of flatness factor higher than 3 has a more peaked distribution around zero mean than a normal distribution. Therefore, the probability for zero values is higher than the probability for nonzero values, indicating an intermittent character of the velocity fluctuations. Consequently, he suggested that, if the flow is known to be intermittent in a separate way, the flatness factor might be considered as a measure of degree of intermittency. The intermittency factor γ is defined as a fraction of time for which turbulence occurs at a point in the flow. A low value of the intermittency factor γ would mean that the flow is mostly laminar and intermittently turbulent, while a high value of γ means that the flow is mostly turbulent.

5.4.2 *Mean Velocity Field*

Figure 5.5 shows the development of axial mean velocity profile for all the z positions studied. Since all the positions studied were beyond the cross-point of

the jets, only one peak was seen. The mean velocity profile becomes flatter as the axial distance from the die increases. Figure 5.6 shows the nondimensional axial mean velocity profile below the die. The velocity (ordinate) has been nondimensionalized by dividing by maximum velocity at the respective z level. The position (abscissa) has been nondimensionalized with the jet half-width: the width at which the mean jet velocity drops to half its maximum value. It is seen from the graph that, for all the z positions studied, the nondimensional mean velocity profiles are the same. This self-similar behavior of the jet in the studied region shows that the combined jet flow is self-preserving with respect to the axial mean velocity downstream from the jet cross-point. The semi-empirical correlations developed for simple jet flows are not available for such complex flows as in the present study. However, the correlations developed for simple jet flows can be used for comparison with the data from the flow of the cross-jets. Figure 5.6 shows three correlations applied to the experimental data. The solid line on the graph is the correlation developed using Tollmien (1926) and Reichardt (1942) analysis for a circular turbulent jet. The details of the Tollmien-Reichardt analysis have been shown by Uyttendaele and Shambaugh (1989). The dotted line on the graph is the predicted velocity profile based on the correlation developed by Görtler (1942) for a plane turbulent jet; see Rajaratnam (1976) for details. The third line (dotted and dashed line) corresponds to Bradbury's (1965) correlation for a rectangular turbulent jet. These semi-empirical correlations are shown in the following equation set:

Tollmien-Reichardt: $$\frac{V}{V_o} = \left(1 + (\sqrt{2} - 1)\left(\frac{x}{x_{1/2}}\right)^2\right)^{-2} \quad (5.7a)$$

Görtler: $$\frac{V}{V_o} = 1 - \tanh^2\left(0.881\frac{x}{x_{1/2}}\right) \quad (5.7b)$$

Bradbury: $$\frac{V}{V_o} = \exp\left[-0.6749\left(\frac{x}{x_{1/2}}\right)^2 \cdot \left(1 + 0.027\left(\frac{x}{x_{1/2}}\right)^4\right)\right] \quad (5.7c)$$

where

$\frac{x}{x_{1/2}}$ = transverse nondimensional position

$\frac{V}{V_o}$ = nondimensional axial mean velocity

From Figure 5.6, it is seen that Tollmien-Reichardt and Görtler correlations fit the data very well with coefficient of determination R^2 values of 0.996 and 0.995 respectively. The R^2 values for each of seven data sets fit separately to Tollmien-Reichardt correlation range from 0.990 to 0.998, while the R^2 values range from 0.993 to 0.997 for the data sets fit separately to Görtler's equation. Furthermore, Bradbury's equation for rectangular jets fits the data with an R^2 of 0.984. It is seen from the graph that Bradbury's equation fits the data well up to 1.5 jet half-widths, but beyond that it does not represent the data as good. Harpham and Shambaugh (1996; 1997) also found that, for the same flow geometry, Bradbury's equation fits

the nondimensional axial mean velocity data very well up to 1.5 jet half-widths. However, in the present study, both Tollmien-Reichardt's and Görtler's equations represent the data very well at all the x-positions (up to three jet half-widths). Rho et al. found that, for the two circular jets crossing at 45° angle, the experimental nondimensional axial mean velocity data fits well with the correlations of Görtler within one jet half-width.

Figure 5.7 shows the decay of the centerline axial mean velocity. For a self-preserving plane turbulent jet, Bradbury (1965) described that the centerline axial mean velocity V_o should be proportional to $z^{-1/2}$; in particular

$$\frac{V_o}{V_{jo}} = C_1\left(\frac{z}{z_c} - C_2\right)^{-1/2}$$

where

V_o = centerline axial mean velocity

V_{jo} = nominal jet exit velocity

c_1, c_2 = empirical constants

The solid line on Figure 5.7 is a least-squares fit of equation (5.8). It can be seen that the data fits the equation well ($R^2 = 0.950$) with $c_1 = 0.874$ and $c_2 = 0.526$.

Gutmark and Wygnanski (1976) showed that a plane turbulent jet spreads linearly with the z direction. Kotsovinos (1976) described the spread of a rectangular jet by the following equation:

$$\frac{x_{1/2}}{w} = k_1\left(\frac{z}{w} + k_2\right)$$

where k_1 is the measure of spreading rate of the jet. The constant k_2 is related to the virtual origin z_o of the jet by the following equation:

$$k_2 = -\frac{z_o}{w}$$

where w is the width of the jet. Figure 5.8 shows spreading of the jet in terms of the jet half-width. The position x (abscissa) has been nondimensionalized by dividing by h which is assumed to replace w in equations (5.9) and (5.10). The solid line on Figure 5.8 is a least-squares fit of equation (5.9) to the data. The fitted values of k_1 and k_2 are 0.11 and 0.116, respectively, and the R^2 of the fit is 0.960. For a plane turbulent jet, Gutmark and Wygnanski (1976) found the values of k_1 and k_2 to be 0.1 and 2, respectively. Kotsovinos found that the value of k_1 ranges from 0.087 to 0.128 with a typical value of 0.11, while the value of k_2 ranges from -4.5 to +6.5. Therefore, the values of k_1 and k_2 obtained in the present study are in the range of those obtained for a single plane turbulent jet. The dotted line on Figure 5.8 is spread of the jet obtained by Harpham and Shambaugh (1996) for the same flow geometry. The jet spread obtained by Harpham and Shambaugh is larger than that obtained in the present study. The difference between the two jet spreads is explained later in the next section.

5.4.3 *Turbulence Structure of the Jet Flow*

Figure 5.9 shows the variation of turbulence intensity along the centerline of the combined jet flow. From the graph, it is seen that the centerline turbulence intensity increases with the dimensionless distance z/z_c at least up to $z/z_c = 2.5$. The increasing turbulence intensities in the center plane of the jet suggest the

generation of turbulence after the crossing of two inclined slot jets. Rho et al. (1990) found that the centerline turbulence intensity in a circular cross-jet flow (two circular jets inclined at 45°) had a peak near z/z_c of two. Beyond the peak position, the turbulence intensity values decreased and became constant. In the present study, Figure 5.9 shows that a similar "maximum" in centerline turbulence intensity is not present. However, there is a possibility that the centerline turbulence intensity might reach a peak value and/or become constant after z/z_c = 2.5 ($z/h \simeq 2$). Bradbury (1965) and Gutmark and Wygnanski (1976) observed that the centerline turbulence intensity of a plane turbulent jet increased initially, and then became constant (self-preserving) about 40 slot-widths downstream from the nozzle. Furthermore, they found that, in the initial region ($z/h \leq 10$) of a plane turbulent jet, the magnitude of the centerline turbulence intensity was less that 10%. However, in the present study, the magnitude of turbulence intensity at z/z_c = 2.5 ($z/h \simeq 2$) is about 22%. Consequently, in the initial region of the jet flow, a turbulent cross-jet has a higher level of turbulence than a plane turbulent jet.

Figure 5.10 shows the variation of turbulence intensity profile along the z direction. The turbulence intensity of the axial component of the air velocity sharply increases on moving away from the center of the jet. The turbulence intensity reaches a maximum at a distance of about 1.75 jet half-widths for all the z positions studied. Furthermore, Figure 5.10 shows that the turbulence intensities across the

jet increase with the z position. The increase in turbulence intensities with the z position signifies (a) a strong generation of turbulence after the crossing of the two inclined jets, and (b) a lack of self-preservation of the jet flow, at least in the initial region of the jet flow. The maximum value of turbulence intensity across the jet varies from about 50% at z/z_c = 1.0 to about 62% at z/z_c = 2.5. Gutmark and Wygnanski (1976) observed that, for the axial positions further than 40 slot-widths, the turbulence intensity profiles became the same, indicating the self-preserving region of the jet. Furthermore, they found that the axial-component turbulence intensity increases slowly across the jet, and reaches a peak value around one jet half-width. However, they observed that the peak value of the turbulence intensity was about 30% as compared to the peak value of about 62% observed in the present study. Consequently, in the present study, the cross-jet flow has a different turbulent structure than the plane jet at least in the initial region of the flow. Rho et al. (1990) found similar results on comparing the axial component turbulence intensity of circular cross-jets with that of a round jet.

The asymmetry of the velocity fluctuation distribution is illustrated as skewness factor profile in Figure 5.11. From the graph, it is seen that, close to the center of the jet, the distribution of velocity fluctuations is symmetrical: the large velocity fluctuations in both the positive and negative z directions are equally probable. However, the distribution starts becoming positively skewed on moving about one

jet half-width across the jet: the large velocity fluctuations are mostly in the positive z direction. The skewness factor reaches a positive peak value about two jet half-widths further from the center of the jet. Similar profiles of skewness factor are observed for all the z positions studied. Close to the center of the jet, the skewness factor of the velocity fluctuation distribution is almost zero for all the z positions. However, on moving away from the center of the jet, the skewness factor becomes more positive for the higher values of z/z_c. The variation in skewness factor with the z position indicates the absence of self-preserving nature of the jet.

Figure 5.12 shows the flatness factor profile across the jet. From the graph, it is seen that the flatness factor is almost Gaussian (with value equal to 3) up to one jet half-width, and large values are observed as jet boundary approaches. Rho et al. (1990) and Gutmark and Wygnanski (1976), respectively, observed a similar behavior for the circular turbulent cross-jets and a plane turbulent jet. The large positive values of the skewness factor and the flatness factor about two jet half-widths (close to the jet boundary) from the center of the jet suggest that the intermittency factor is low, i.e., the flow is less turbulent, and is mixing with the irrotational flow outside of the jet boundary: entrainment of the external irrotational flow.

5.4.3.1 A Comment on the Jet Spread

Figure 5.8 illustrates that the jet half-widths obtained in the present study are smaller than that obtained by Harpham and Shambaugh (1996) for the same flow geometry. This difference is attributed to the different instruments used for measuring the flow field. Harpham and Shambaugh used a Pitot (impact) tube for measuring the mean velocities, while a hot-wire anemometer was used in the present study. As discussed by Goldstein (1983, pp. 14-16 and 64-66), with a Pitot (impact) tube, the error in measuring the mean velocity in a turbulent flow is proporional to $\overline{v^2}$, mean square of velocity fluctuations. Mathematically,

$$V_{pitot} = V\left(1 + \frac{\overline{v^2}}{V^2}\right)^{1/2} \tag{5.11}$$

where V_{pitot} is the mean velocity measured by the Pitot (impact) tube. Therefore, for the flows with large turbulent intensity, the mean velocity measured by a Pitot (impact) tube will be much larger than the actual mean velocity V. For example, in the present flow, for the highest turbulence intensity of 0.62 (see Figure 5.10), the mean velocity measured with a Pitot (impact) tube will be about 20% more than the actual mean velocity at that position. Furthermore, with a Pitot tube, the mean

velocity measured is the spatial root mean square of the instantaneous velocity over the circumferential plane of the Pitot probe [Goldstein (1983, pp. 14-16)]. Therefore, the size of the probe (diameter of the Pitot probe) becomes very important. Goldstein has discussed that the shear flow displaces the effective center of the probe (measured value of the average pressure is assumed to lie at the center of the probe) is shifted toward the high velocity region by 15% of the inside diameter of the Pitot probe. Therefore, the velocity measured at a position is higher than the actual the velocity at that position. Because of (a) the turbulence and (b) a shift in the effective center of the probe, the velocities measured with a Pitot tube will be higher than the actual velocities. Since a jet half-width is a position where the mean velocity falls to half its maximum value, the jet half-width measured by a Pitot tube is expected to be larger than the jet half-width measured by a hot-wire anemometer. Table 5.1 shows a comparison of jet half-widths measured in the present study (with a hot-wire anemometer) and those obtained with Harpham and Shambaugh (1996) correlation for jet half-width. The probe sizes used in two studies are also shown in Table 5.1.

Figure 5.13 shows the turbulence intensity profile across the jet. The x position is nondimensionalized with jet half-width calculated using the correlation developed by Harpham and Shambaugh for the same flow geometry. A comparison of Figures 5.10 and 5.13 shows that the peak in turbulence intensity (maximum

velocity fluctuations), which is observed at about 1.75 jet half-widths in Figure 5.10, has moved to about one jet half-width in Figure 5.13. Since, for their work, Harpham and Shambaugh used a Pitot (impact) tube, they measured a higher value for the mean velocity V at the positions corresponding to high levels of turbulence intensity. Moreover, from Table 5.1, it can be seen that spatial size of the Pitot probe is of the same order of magnitude as the jet half-width. Therefore, the possibility of error increases in averaging the pressure of the highly turbulent flow (as in the present case) over the circumferential plane of the Pitot probe. Consequently, for the same flow geometry, the jet half-width calculated with the Harpham and Shambaugh correlation is larger than the jet half-width measured in the present study.

5.4.4 Mean Velocity in Oscillating Jets

In oscillating flow, the air emits from one slot at a time, while in continuous flow, the air emits from both slots at the same time. The two inclined slot jets of the die were pulsed using the experimental procedure described by Tyagi and Shambaugh (1995) for the same melt blowing arrangement. There was no polymer flowing through the die during the experiments. The temperature of the air was 21°C. For the same nominal jet exit velocity (V_{jo} = 17.5 m/s) through each of the oscillating jets, Tyagi and Shambaugh found that a peak in the fiber diameter profile (fiber

diameters greater than that obtained for a continuous flow) was observed at an oscillation frequency of 9 Hz, and a plateau in the diameter profile (fiber diameters smaller than that obtained for a continuous flow) was observed between the oscillation frequencies of 28 and 46 Hz. Therefore, the flow field of the oscillating jets was studied for pulsation frequencies of 9, 28, and 46 Hz at the dimensionless position $z/z_c = 1.0$. The sampling time and frequency of the hot-wire anemometer system for the case of pulsating flow were the same as used for the continuous flow: a sampling frequency of 136.5 Hz and a sampling time of 2 minutes.

Figure 5.14 compares the axial mean velocity profile of the continuous flow and the flow of oscillating jets. At an oscillation frequency of 9 Hz, the velocity profile is flatter as compared to the velocity profile of the continuous flow, and the centerline mean velocity of oscillating flow is lower than that of the continuous flow. However, at oscillation frequencies of 28 and 46 Hz, the mean velocity profiles become almost identical to the mean velocity profile of the continuous flow. Since the same sampling time was used for all the flow conditions and the flow at 9 Hz oscillates slower than the flows at 28 and 46 Hz, it is possible that the sampling time for the case of 9 Hz was not sufficient to evaluate the actual mean velocity V by time-averaging the instantaneous velocity $\bar{v}$. Therefore, a flatter velocity profile was obtained for the flow at 9 Hz. Figure 5.15 shows the nondimensional mean velocity profile for all the four flow conditions. The velocity (ordinate) has been

nondimensionalized by dividing by the maximum axial mean velocity for the respective flow condition. The position (abscissa) has been nondimensionalized with the jet half-width. It is seen from the graph that, for all the flow conditions, the nondimensional profiles are the same. This self-similar behavior of the jet shows that, despite the oscillations, the flow is self-preserving with respect to the axial mean velocity. The three semi-empirical correlations described by the equation set (5.7) were applied to the experimental data. The solid line on the Figure 5.15 is the correlation developed using Tollmien (1926) and Reichardt (1942) analysis for a circular turbulent jet. The dotted line on the graph is the predicted axial mean velocity profile based on the correlation developed by Görtler (1942) for a plane turbulent jet. The third line (dotted and dashed line) corresponds to Bradbury's (1965) correlation for a rectangular turbulent jet. From the figure, it can be seen that all three correlations fit well with the data. The R^2 values for the least-squares fit of the correlations of Tollmien-Reichardt, Görtler, and Bradbury were found to be 0.987, 0.991, and 0.990, respectively.

5.4.5 Turbulence Structure in Oscillating Jets

The turbulence intensity profile at all four flow conditions is illustrated in Figure 5.16. The turbulence intensity profiles of 28 Hz and 46 Hz oscillating flow are the same as observed for the continuous flow. A peak in turbulence intensities is

observed around 1.5-1.75 jet half-widths. However, for the flow at 9 Hz, the turbulence intensities are much higher than that for other flow conditions. At an oscillation frequency of 9 Hz, the turbulence intensity rises sharply on moving away from the center of the jet, reaches a peak value around 1.5 jet half-widths, and starts decreasing sharply. At the same oscillation frequency (9 Hz), the peak value of the root mean square of the fluctuations matches the mean velocity at that position. This suggests that there is a strong generation of turbulence.

Figure 5.17 shows the skewness factor profile at all the flow conditions. From the graph, it can be seen that, for all flow conditions, the velocity fluctuation distribution is symmetrical within one jet half-width: both positive and negative velocity fluctuations are equally probable. Beyond one jet half-width, the profiles show that the distributions start becoming positively skewed, and reach a peak value about two jet half-widths from the center of the jet. The flows oscillating at 28 Hz and 46 Hz have almost the same skewness factors as the continuous flow at all the positions across the jet. At 9 Hz, the skewness profile is the same as continuous flow up to one jet half-width. However, beyond one jet half-width, the flow at 9 Hz starts having higher positive values of the skewness factor that for the continuous flow. Furthermore, for the flow at 9 Hz, the peak value of the skewness factor is much larger than the peak value for other flow conditions studied.

Figure 5.18 illustrates the flatness factor profile for both the oscillating and continuous flows. Once again, the jets oscillating at 28 and 46 Hz have the same flatness factor profile as the continuous flow: the flatness factor has a Gaussian value of 3 up to one jet half-width, and then starts increasing for the intermittent flow near the jet boundary. However, for the flow at 9 Hz, the flatness factor has a lower value than Gaussian value of 3 up to one jet half-width. Beyond one jet half-width, for the flow at 9 Hz, the flatness factor starts increasing sharply to the values much greater than Gaussian value of 3.

From the turbulence intensity, skewness factor, and flatness factor profiles across the jet (Figures 5.16, 5.17, and 5.18, respectively), it is evident that, by oscillating the jets at the frequencies of 28 and 46 Hz, a turbulence structure identical to the continuous flow is generated. The trends in Figures 5.16 through 5.18 suggest that, by oscillating the flow at 9 Hz, a much stronger turbulence structure is generated. However, it is possible that, for the flow at 9 Hz, the obtained turbulence intensity, skewness factor, and flatness factor distributions could be due to either a measurement error (because of the small sampling time) or the resonance of jets.

5.5 Conclusions and Recommendations

Following conclusions can drawn from one-dimensional experimental studies on isothermal, turbulent cross-jets in melt blowing:

1. The dimensionless axial mean velocity profiles can be predicted from (a) Görtler's or Tollmien-Reichardt's correlations, (b) a power law equation for the centerline mean velocity (see Figure 5.7), and (c) the linear equation for jet half-width (see Figure 5.8). The axial mean velocity profile was narrower than that measured by Harpham and Shambaugh (1996) for the same flow geometry. The turbulence structure of the jet flow field explains the difference in two mean velocity profiles.

2. The turbulence structure of the inclined, rectangular cross-jets is different from the turbulence structure of a plane jet or a round jet, but matches the turbulence structure of inclined, circular cross-jets (see Rho et al., 1990). Higher levels of turbulence are observed in the initial region of the cross-jet flow than that in a plane jet or a round jet. As described by Rho et al., due to the crossing of the jets, a very strong history effect in the turbulence structure is present in the cross-jet flow. Therefore, the jet cross-point region is the key to the downstream development of the flow. Consequently, the modeling of the cross-jet flow requires

a complete understanding of this region of the flow. Therefore, for the mathematical modeling of melt blowing below a slot die, the drag force and lift force correlations developed by Majumdar and Shambaugh (1990) and Ju and Shambaugh (1994) have to be corrected to include the turbulence effects due to the crossing of the jets. Furthermore, studies need to be done to understand the turbulence structure due to the transverse components of the air velocity. In melt blowing, the turbulence effects due to all three components of the air velocity must be included in the drag and lift force correlations to predict the fiber diameter and the amplitude of fiber vibrations accurately.

3. Since the jet cross-point plays an important role in defining the turbulence structure of the cross-jet flow field, the distance of geometric cross-point of air jets z_c can be used as a characteristic length for the melt blowing process. Consequently, the characteristic z direction spatial separation of 5 mm, which contains a fiber element formed with the neighborhood of correlated fiber beads (see Chapter 3), can be nondimensionalized by dividing by the corresponding value of z_c used. For the die settings used in the study described in Chapter 3, z_c = 2.39 mm; see Figure 3.1. Therefore, the nondimensionalized characteristic z direction spatial separation will be 2.1 corresponding to the melt blowing conditions used in the study.

4. The dimensionless axial mean velocity profiles of the oscillating jets follow the semi-empirical correlations of Görtler and Bradbury. Since Görtler's correlation can also be used to predict the axial mean velocity profile for the continuous flow, the use of Görtler's equation for predicting the axial mean velocity profiles of both continuous and oscillating flows is suggested. The dimensional axial mean velocity profiles of the flows oscillating at 28 and 46 Hz are similar to that of the continuous flow. However, the dimensional axial mean velocity profile of the flow at 9 Hz is flatter than the velocity profile of the continuous flow. Therefore, it is expected that the axial mean velocity flow field of jet oscillating with the frequencies in the range of 28 Hz to 46 Hz (corresponding to the plateau region of the fiber diameter profile; see Tyagi and Shambaugh, 1995) is similar to the velocity profile of the continuous flow.

5. For the jets oscillating at 28 and 46 Hz, the turbulence structure of the flow field is similar to the turbulence structure of the continuous flow. The flow field of the jets oscillating at 9 Hz is much more turbulent than the flow field of continuous flow or the flow at 28 or 46 Hz. Therefore, it can be concluded that, by oscillating the jets with the frequencies in the range of 28 to 46 Hz (corresponding to the plateau region of the fiber diameter profile), a "constructive" turbulence structure similar to that of the continuous flow is generated at a lesser air flow rate. However, by oscillating the jets with a frequency of 9 Hz (corresponding to the

peak of the fiber diameter profile), a turbulence structure, "destructive" for the fiber diameter, is generated. Further studies need to be done to understand the turbulence structure of the air velocity flow field in oscillating jets. Such studies would help in understanding the reduction in the fiber diameter due to oscillating jets in melt blowing.

6. The present study of one-dimensional turbulent flow field of continuous and oscillating flow should be a good starting point for two and three-dimensional studies. These studies would help to improve the understanding of spatial orientation and vibrations of the fiber threadline in melt blowing.

5.6 Nomenclature

b = width of an individual slot of the die as defined on Figure 5.3, mm

c_1 = dimensionless empirical constant in eq (5.8)

c_2 = dimensionless empirical constant in eq (5.8)

C_f = drag coefficient of the filament

h = distance between edges of two slots (see Figure 5.3), mm

k_1 = dimensionless constant in eq (5.9)

k_2 = dimensionless constant in eq (5.9)

$K(v)$ = dimensionless flatness factor or kurtosis of axial component of air velocity defined in eq (5.4)

l = total length of an individual slot as defined on Figure 5.3, mm

Re = Reynolds number of the air flow based on the diameter of the filament

$S(v)$ = dimensionless skewness factor of axial component of air velocity defined in eq (5.5)

$T(v)$ = dimensionless turbulence intensity of axial component of air velocity defined in eq (5.4)

v = axial component of velocity fluctuations [see eq (5.2)], m/s

v_{rms} = root mean square of axial velocity fluctuations defined in eq (5.3), m/s

$\bar{v}$ = instantaneous axial air velocity defined in eq (5.2), m/s

$\overline{v^2}$ = mean of the square of axial velocity fluctuations [see eq (5.4)], m^2/s^2

$\overline{v^3}$ = mean of the cube of axial velocity fluctuations [see eq (5.5)], m^3/s^3

$\overline{v^4}$ = mean of the fourth power of axial velocity fluctuations [see eq (5.6)], m^4/s^4

V = axial mean velocity [see eq (5.2)], m/s

V_o = centerline axial mean velocity [see eq (5.2)], m/s

V_{jo} = nominal air jet exit velocity, m/s

V_{pitot} = mean air velocity measured by a Pitot tube [see eq (5.11)], m/s

w = width of single rectangular jet [see eq (5.10)], mm

x = Cartesian coordinate defined on Figure 5.1, mm

$x_{1/2}$ = jet half-width in the x direction, mm

y = Cartesian coordinate defined on Figure 5.1, mm

z = distance below the die (see Figure 5.1), mm

z_c = geometrical cross-point of two inclined, slot jets of the die (see Figure 5.2), mm

z_o = position of the virtual origin of a rectangular jet [see eq (5.10)], mm

Greek Symbols

β = dimensionless empirical constant in eq (5.1)

5.7 References

Abramovich, G. N. *The Theory of Turbulent Jets;* MIT Press; Cambridge, MA, 1963; pp 551-553.

Ahmed, S. A.; So, M. C. Characteristics of Air Jets Discharging Normally into a Swirling Crossflow. *AIAA J.* **1987**, *23* (3), 429-435.

Andreopoulos, J.; Rodi, W. Experimental Investigation of Jets in a Crossflow. *J. Fluid Mech.* **1984**, *138*, 93-127.

Andreopoulos, J. Measurement in a Jet-Pipe Flow Issuing Perpendicularly into Cross Stream. *ASME J. Fluid Eng.* **1985**, *104*, 493-499.

Bansal, V.; Shambaugh, R. L. Online Measurement and Mathematical Modeling of Fiber Properties During the Melt Blowing and Melt Spinning Processes. Ph.D. Dissertation, University of Oklahoma, Norman, OK, 1997.

Barata, J. M. M.; Durao, D. F. G.; Heiter, N. V. Impingement of Single and Twin Turbulent Jets Through a Crossflow. *AIAA J.* **1991**, *29* (4), 595-602.

Barata, J. M. M.; Durao, D. F. G.; Heiter, N. V. Velocity Characteristics of Multiple Impinging Jets Through a Crossflow. *ASME J. Fluid Eng.* **1992**, *114*, 231-239.

Bradbury, L. J. S. The Structure of a Self-Preserving Turbulent Plane Jet. *J. Fluid Mech.* **1965**, *23*, 31-64.

Goldstein, R. J. *Fluid Mechanics Measurements;* Hemisphere Publishing: Washington, DC, 1983; pp 72-73.

Görtler, H. Berechnung von Aufgaben der freien Turbulenz auf Grund eines neuen Näherungsansatzes. *Zeitschrift für angewandte Mathematik und Mechanik* **1942**, *22*, 244-254.

Gutmark, E.; Wygnanski, I. The Planar Turbulent Jet. *J. Fluid Mech.* **1976**, *73* (3), 465-495.

Harpham, A. S.; Shambaugh, R. L. Flow Field of Practical Dual Rectangular Jets. *Ind. Eng. Chem. Res.* **1996**, *35* (10), 3776-3781.

Harpham, A. S.; Shambaugh, R. L. Velocity and Temperature Fields of Dual Rectangular Jets. *Ind. Eng. Chem. Res.* **1997**, *36* (9), 3937-3943.

Hinze, J. O. *Turbulence*, 2nd ed.; McGraw-Hill: New York, NY, 1975.

Issac, K. M.; Jakubowski, A. K. Experimental Study of the Interaction of Multiple Jets with a Crossflow. *AIAA J.* **1985**, *23* (11), 1679-1683.

Ju, Y. D.; Shambaugh, R. L. Air Drag on Fine Filaments at Oblique and Normal Angles to the Air Stream. *Polym. Eng. Sci.* **1994**, *34* (12), 958-964.

Kamotani, Y.; Greber, I. Experiments on a Turbulent Jet in a Crossflow. *AIAA J.* **1972**, *10* (11), 1425-1429.

Kayser, J. C.; Shambaugh, R. L. The Manufacture of Continuous Polymeric Filaments by the Melt Blowing Process. *Polym. Eng. Sci.* **1990**, *30* (19), 1237-1251.

Kotsovinos, N. E. A Note on the Spreading rate and Virtual Origin of a Plane Turbulent Jet. *J. Fluid Mech.* **1976**, *77*, 305-311.

Majumdar, B.; Shambaugh, R. L. Air Drag on Filaments in the Melt Blowing Process. *J. Rheol.* **1990**, *34* (4), 591-601.

Majumdar, B.; Shambaugh, R. L. Velocity and Temperature Fields in Annular Jets. *Ind. Eng. Chem. Res.* **1991**, *30* (6), 1300-1306.

Matsui, M. Air Drag on a Continuous Filament in Melt Spinning. *Trans. Soc. Rheol.* **1976**, *20* (3), 466-473.

Milligan, M. W. Aerodynamic Flapping Characteristics of Meltblown Fibers. *ASME Ind. Appl. Fluid. Mech.* **1991**, *FED. 132*, 1-5.

Mohammed, A.; Shambaugh, R. L. Three-Dimensional Flow Field of a Rectangular Array of Practical Air Jets. *Ind. Eng. Chem. Res.* **1993**, *32* (5), 976-980.

Mohammed, A.; Shambaugh, R. L. Three-Dimensional Temperature Field of a Rectangular Array of Practical Air Jets. *Ind. Eng. Chem. Res.* **1994**, *33* (3), 730-735.

Narasimhan, K. M.; Shambaugh, R. L. Fiber/Gas Interaction During Melt Blowing. Society of Rheology Meeting, Tulsa, OK, 1986.

Rajaratnam, N. *Turbulent Jets*; Elsevier: New York, NY, 1976, pp 18-21.

Rao, R. S.; Shambaugh, R. L. Vibration and Stability in the Melt Blowing Process. *Ind. Eng. Chem. Res.* **1993**, *32* (12), 3100-3111.

Reichardt, H. Gesetzmässigkeiten der freien Turbulenz. *VDI-For-schungsh.* **1942**, *414*, 1951.

Rho, B. J.; Choi, J. C. On the Structure of a Turbulent Cross Jet Corresponding to Cross Angle Variation. *Fluids Eng. Seminar: Korea-U.S. Progress*, Taejon, Korea, September 3-8, 1989; sponsored by Korea Science and Engineering Foundation and U. S. National Science Foundation, 259-270.

Rho, B. J.; Kim, J. K.; Dwyer, H. A. Experimental Study of a Turbulent Cross Jet. *AIAA J.* **1990**, *28* (5), 784-789.

Rho, B. J.; Oh, J. H.; Lee, D. O. On the Mixing Flow Structure of a Turbulent Cross Jet. *KSME J.* **1995**, *9* (1), 68-79.

Rudinger, Y.; Moon, L. F. Laser Doppler Measurement in a Subsonic Jet Injected into a Subsonic Crossflow. *ASME J. Fluids Eng.* **1976**, *98* (3), 515-520.

Savory, E.; Toy, N. Real-Time Video Analysis of Twin Jets in a Crossflow. *ASME J. Fluids Eng.* **1991**, *113*, 68-72.

Shambaugh, R. L. A Macroscopic View of the Melt Blowing Process for Producing Microfibers. *Ind. Eng. Chem. Res.* **1988**, *27* (12), 2363-2372.

Tennekes, H.; Lumley, J. L. *A First Course in Turbulence*; MIT Press: Cambridge, MA, 1972.

Tollmien, W. Berechnung Turbulenter Ausbreitungsvorgänge. *Z. Angew. Math. Mech.* **1926**, *6*, 468.

Tyagi, M. K.; Shambaugh, R. L. Use of Oscillating Gas Jets in Fiber Processing. *Ind. Eng. Chem. Res.* **1995**, *34* (2), 656-660.

Uyttendaele, M. A. J.; Shambaugh, R. L. The Flow Field of Annular Jets at Moderate Reynolds Numbers. *Ind. Eng. Chem. Res.* **1989**, *28* (11), 1735-1740.

Uyttendaele, M. A. J.; Shambaugh, R. L. Melt Blowing: General Equation Development and Experimental Verification. *AICHE J.* **1990**, *36* (2), 175-186.

Wu, T. T.; Shambaugh, R. L. Characterization of the Melt Blowing Process with Laser Doppler Velocimetry. *Ind. Eng. Chem. Res.* **1992**, *31* (1), 379-389.

z (mm)	$x_{1/2}$ [Harpham and Shambaugh (1996)] (mm)	inner diameter of Pitot probe (mm)	$x_{1/2}$ [present study] (mm)	hot-wire sensor wire diameter (mm)
3.80	1.08	0.45	0.48	0.005
4.75	1.19	0.45	0.59	0.005
5.70	1.30	0.45	0.69	0.005
6.65	1.41	0.45	0.80	0.005
7.60	1.52	0.45	0.90	0.005
8.55	1.64	0.45	1.01	0.005
9.50	1.75	0.45	1.11	0.005

Table 5.1 Comparison of jet half-widths and the probe sizes used in the present study and by Harpham and Shambaugh (1996)

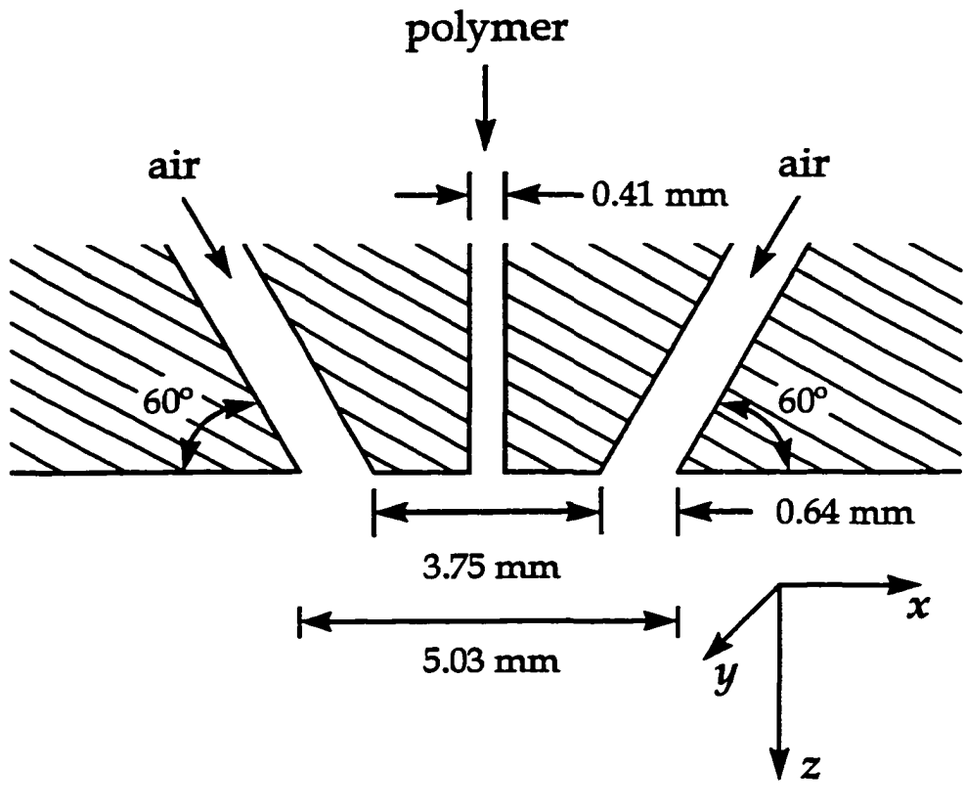

Figure 5.1 Cross-section of the melt blowing slot die used in the experiments. The origin of the coordinate system, which is shown separately, lies at the polymer orifice of the die.

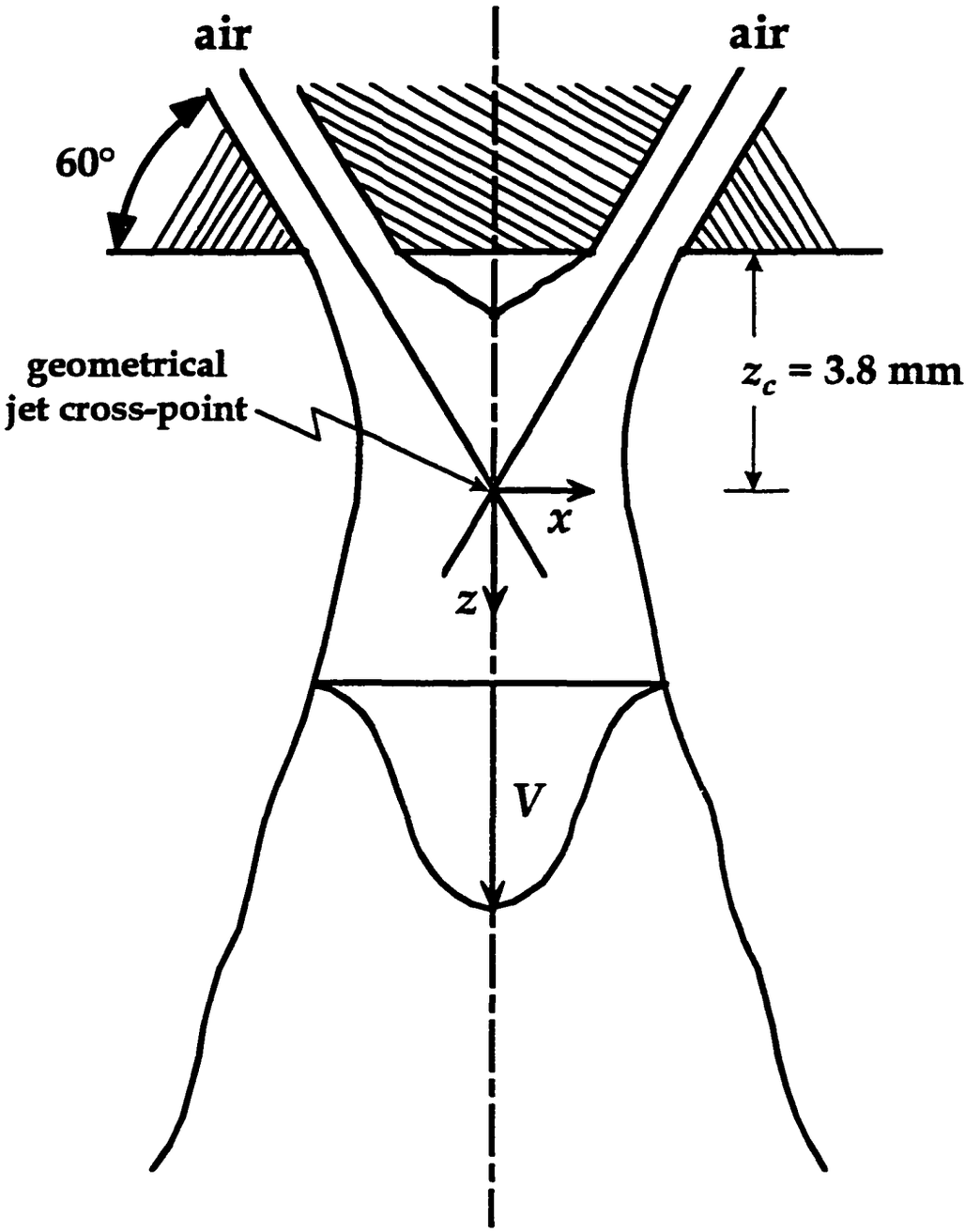

Figure 5.2 Structure of cross-jet mixing flow below a melt blowing slot die.

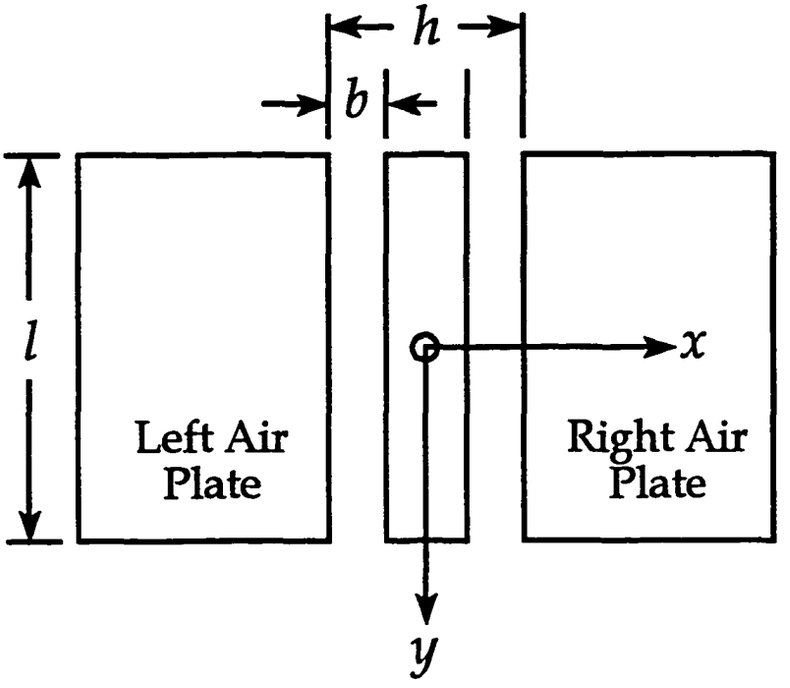

Figure 5.3 Top view of the die face. The z axis (not shown) is perpendicular to the plane of the drawing with positive z axis direction into the plane of the drawing.

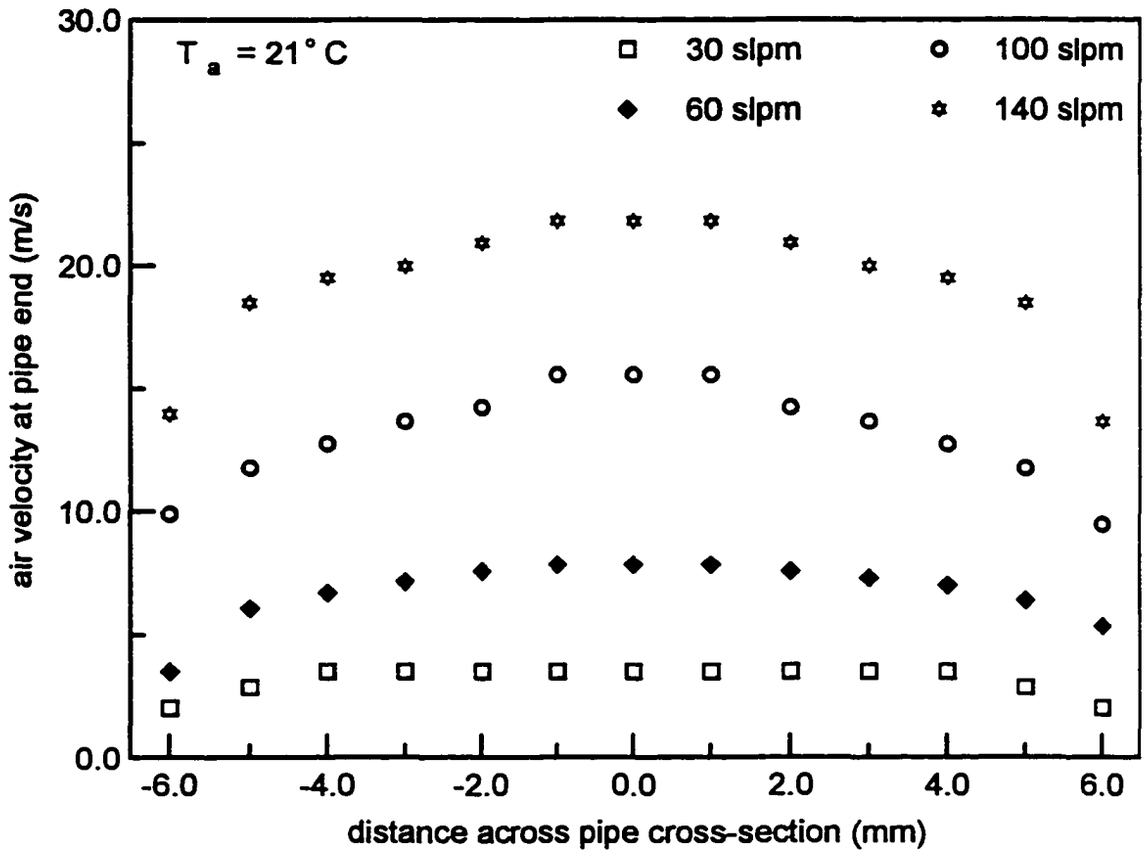

Figure 5.4 Development of flat velocity profiles at the end of the calibration pipe for four different air flow rates. The measurements done at other air flow rates are not shown on the figure.

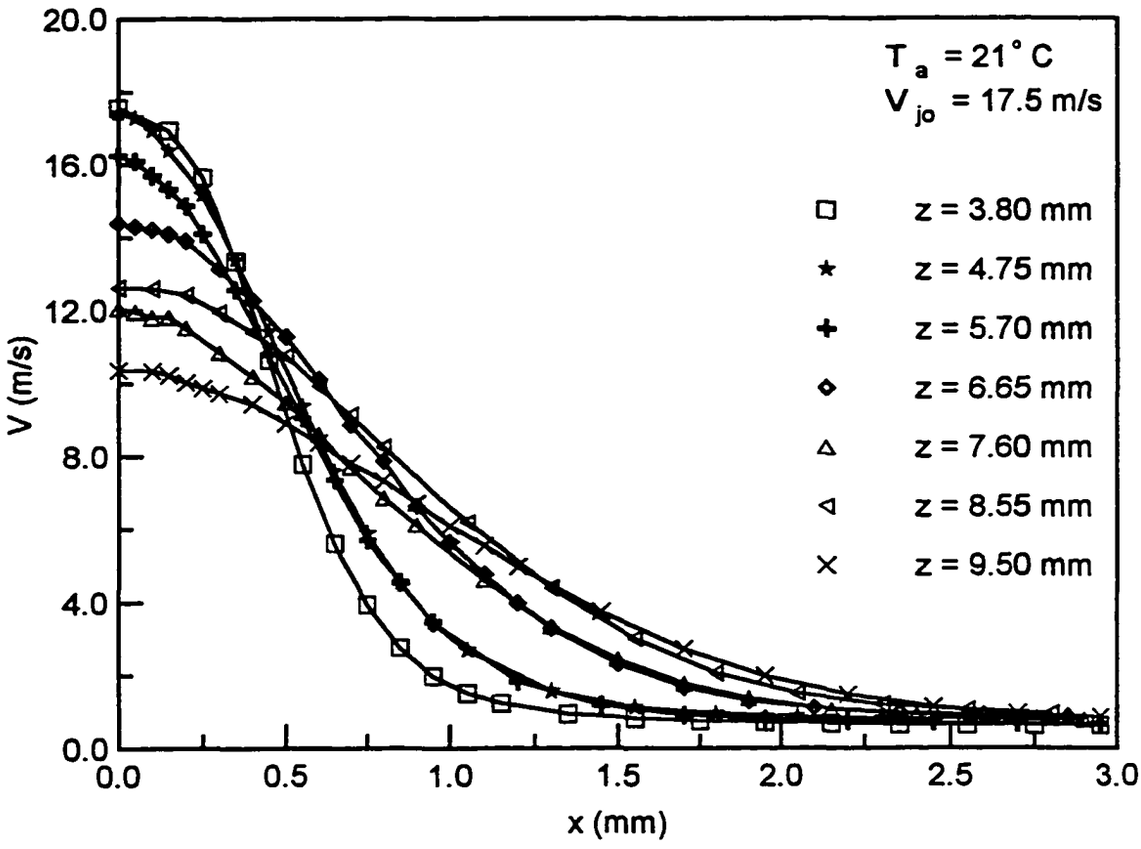

Figure 5.5 Development of the axial mean velocity profile for seven z positions below the die. All measurements were done at $y = 0$ with a hot-wire anemometer.

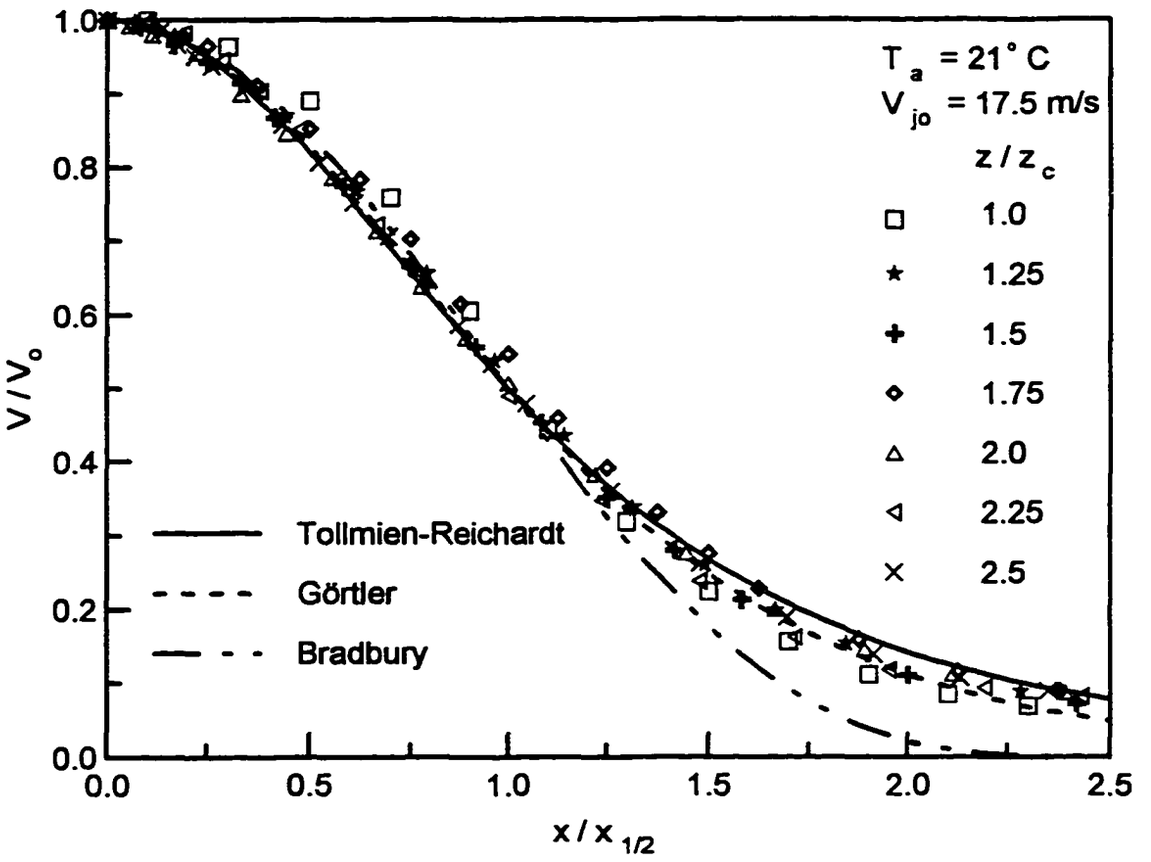

Figure 5.6 Nondimensional axial mean velocity profiles for different z positions studied.

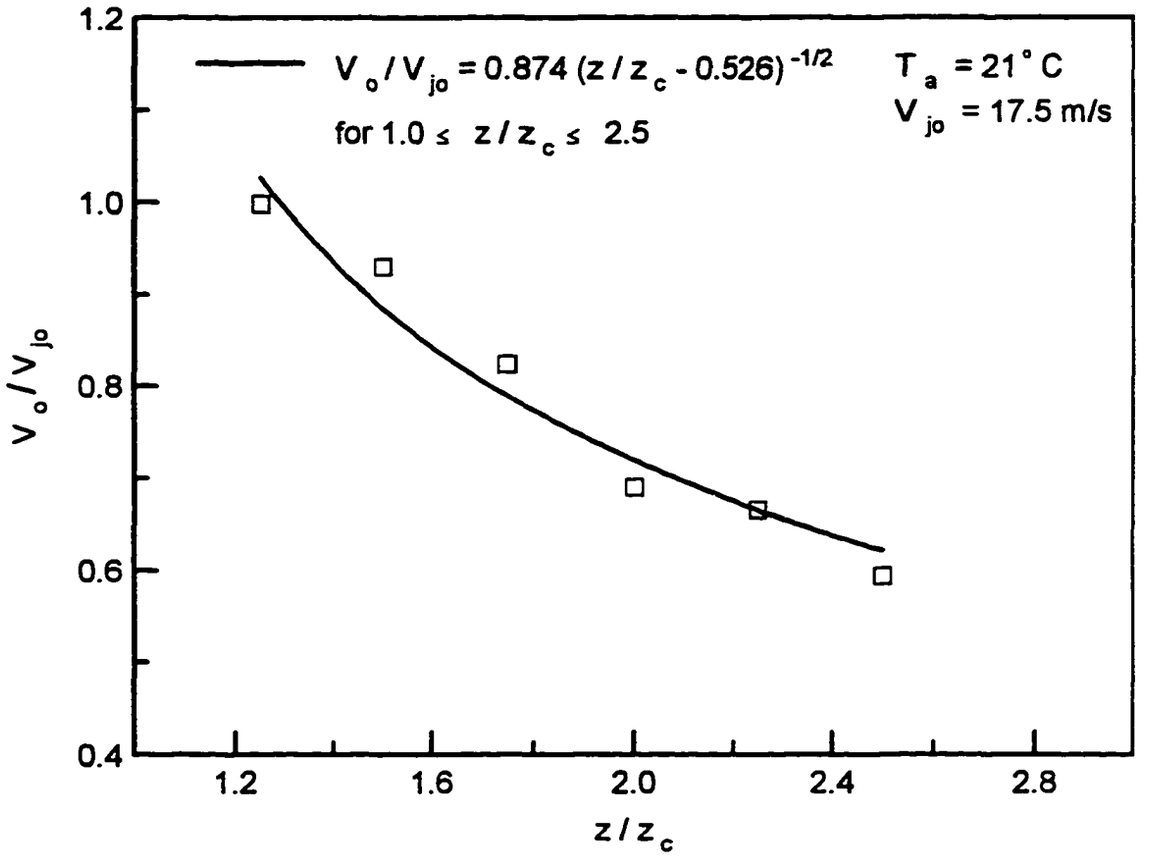

Figure 5.7 Dimensionless centerline axial mean velocity distribution at different z positions below the die.

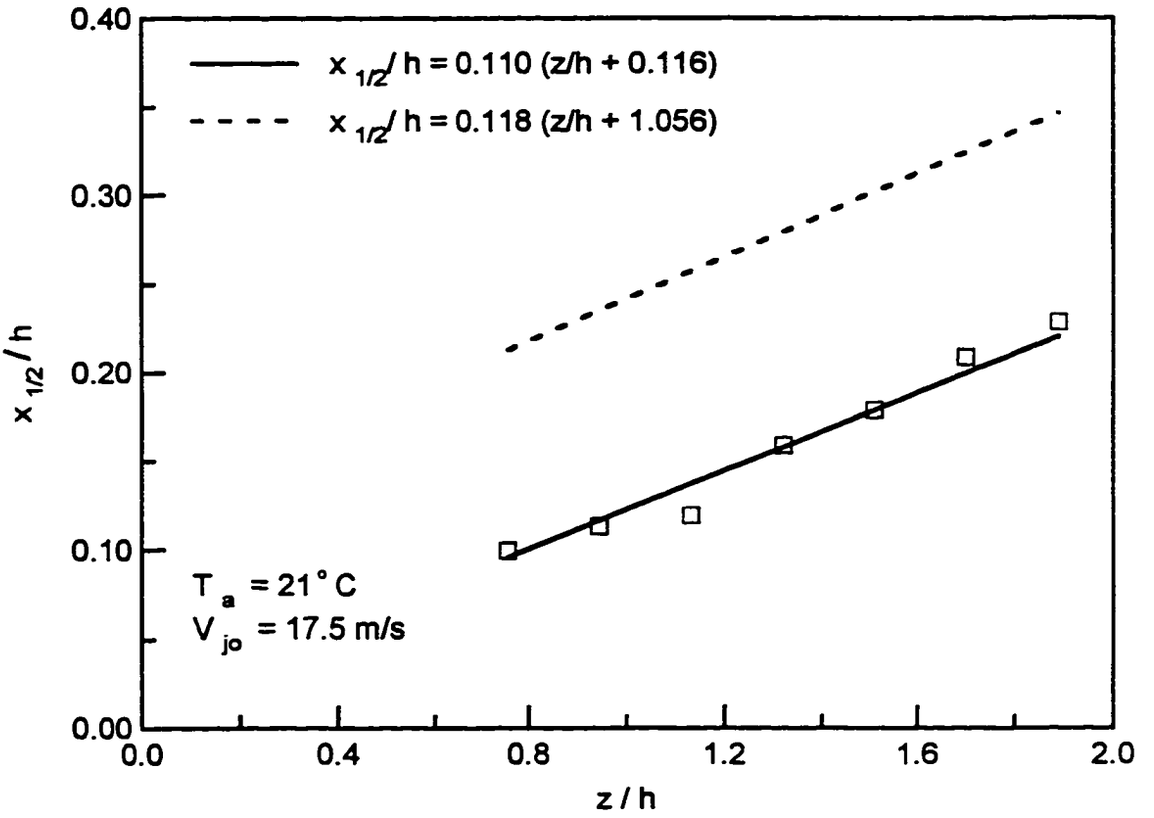

Figure 5.8 Growth of jet half-width with increasing distance from the die.

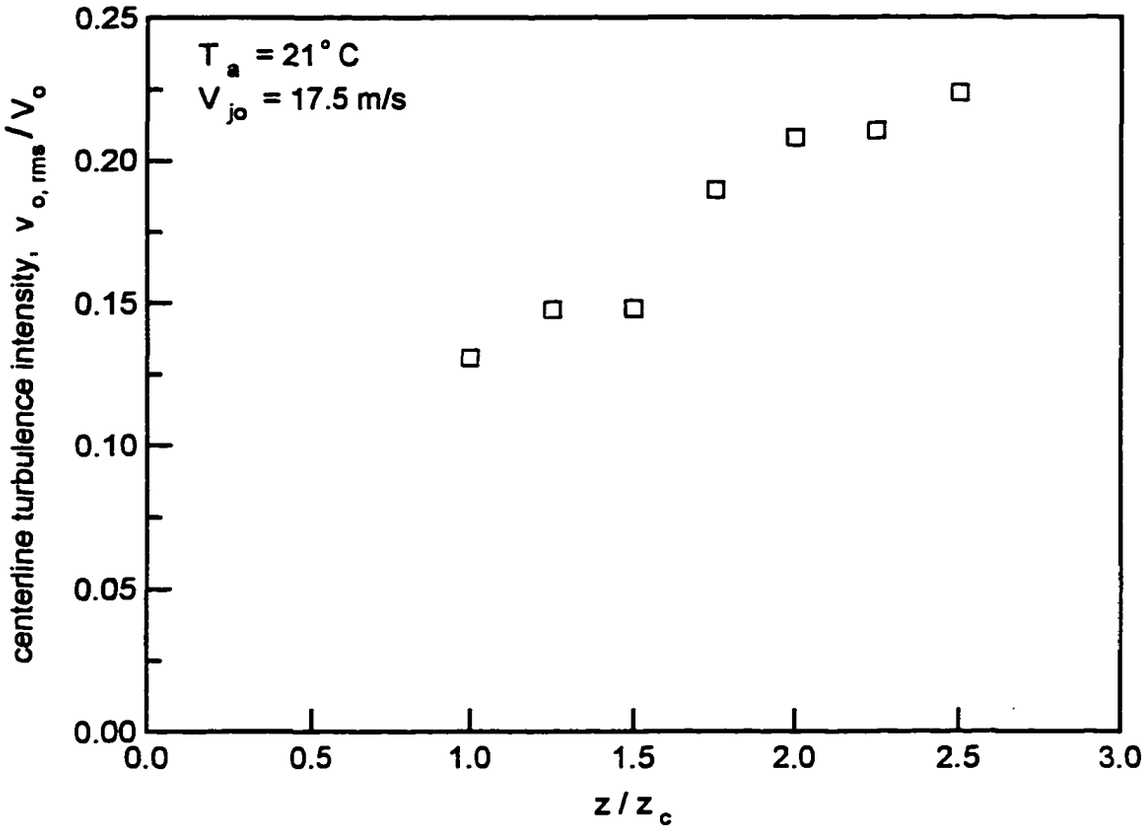

Figure 5.9 Centerline axial component turbulence intensity distribution at different z positions below the die.

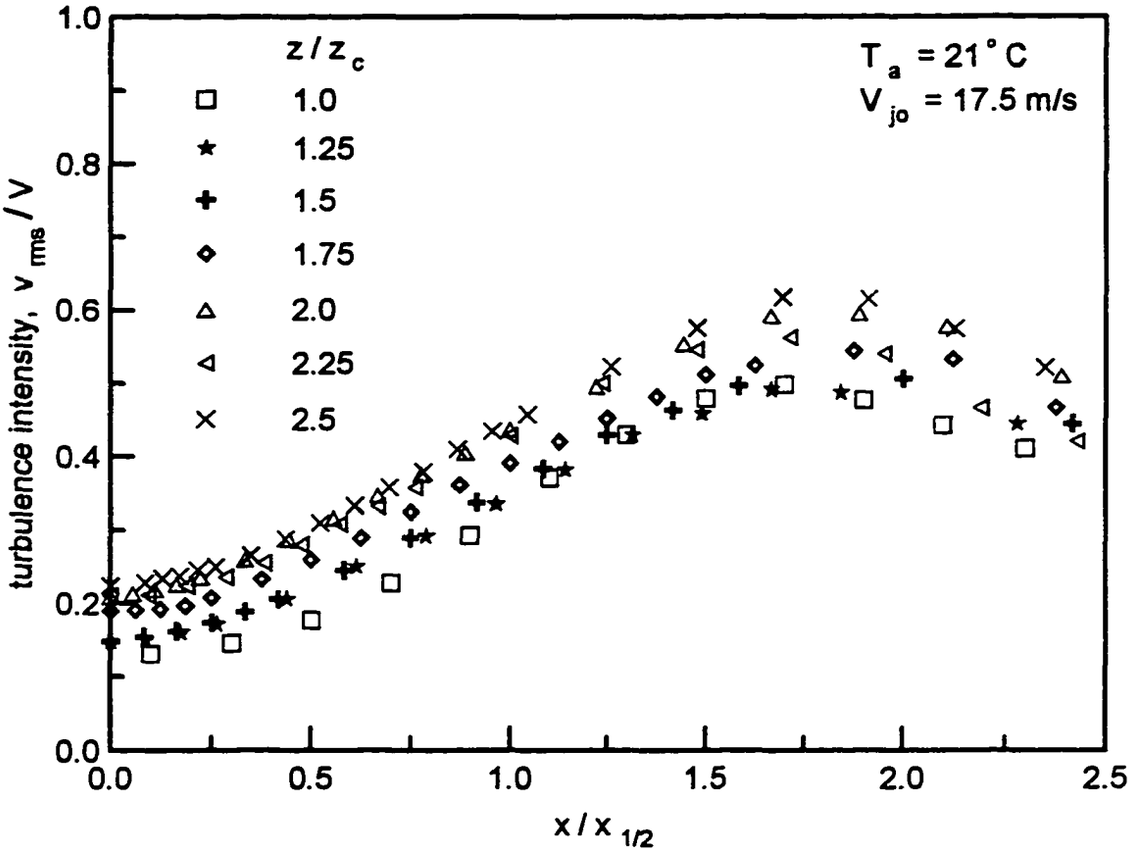

Figure 5.10 Dimensionless axial component turbulence intensity distribution across the cross-jet flow.

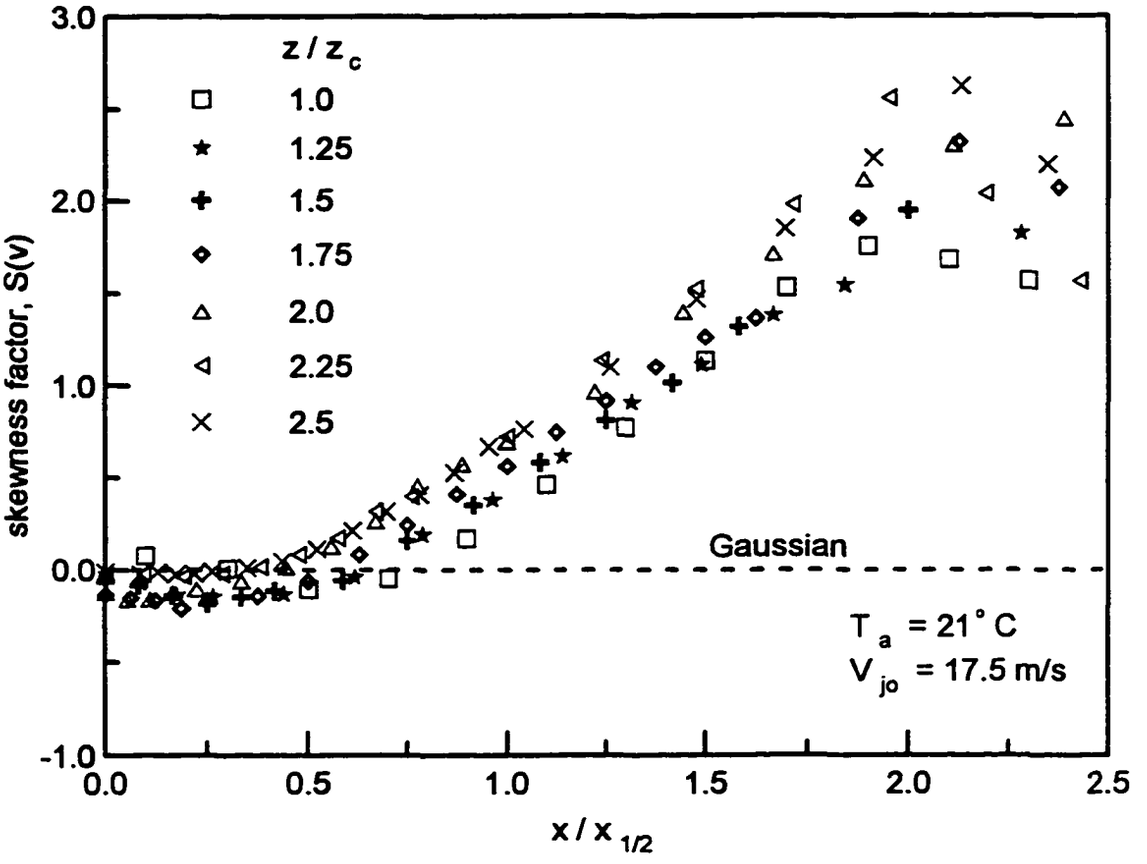

Figure 5.11 Dimensionless axial component skewness factor profile. Gaussian value of zero is shown as the dotted line on the figure.

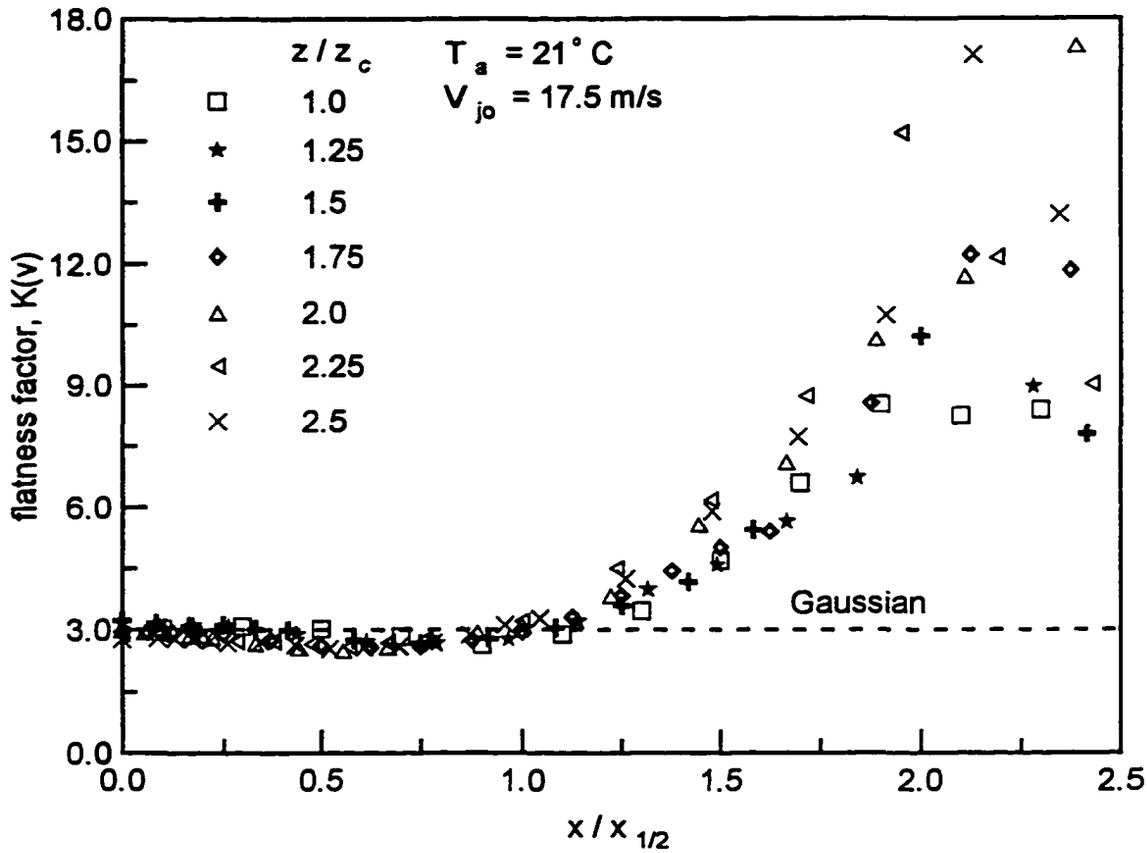

Figure 5.12 Dimensionless axial component flatness factor profile. Gaussian value of 3 is shown as the dotted line on the figure.

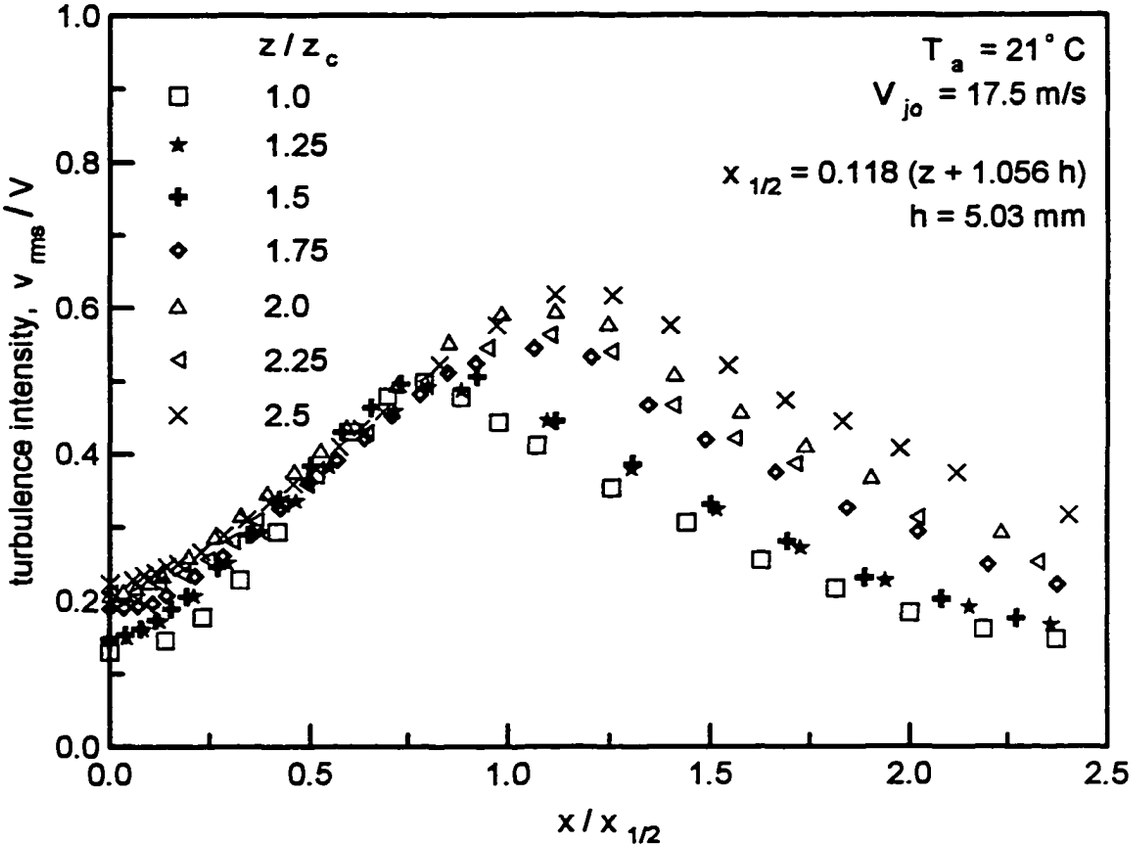

Figure 5.13 Dimensionless axial component turbulent intensity distribution across the jet. For nondimensionalizing the transverse position x, Harpham and Shambaugh's (1996) equation was used to calculate the jet half-width $x_{1/2}$.

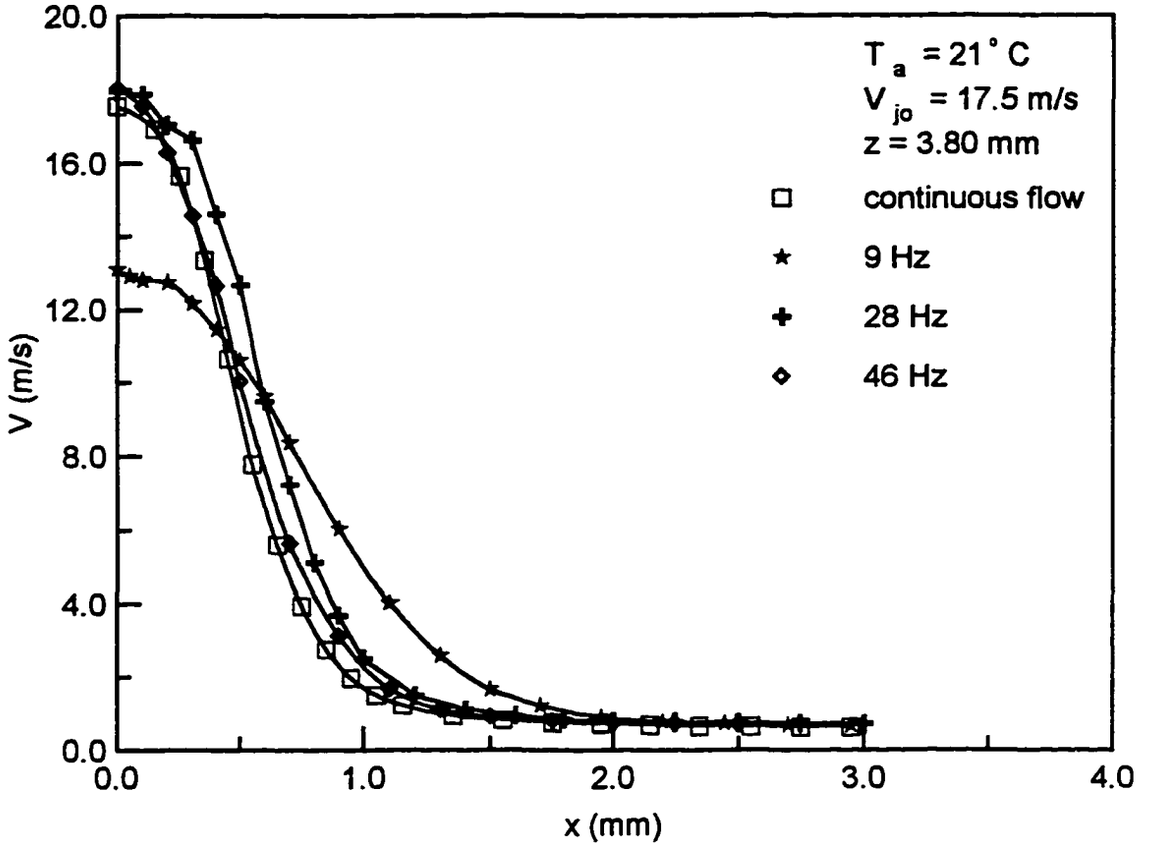

Figure 5.14 Comparison of axial mean velocity profiles of oscillating flow and continuous flow through the die slots.

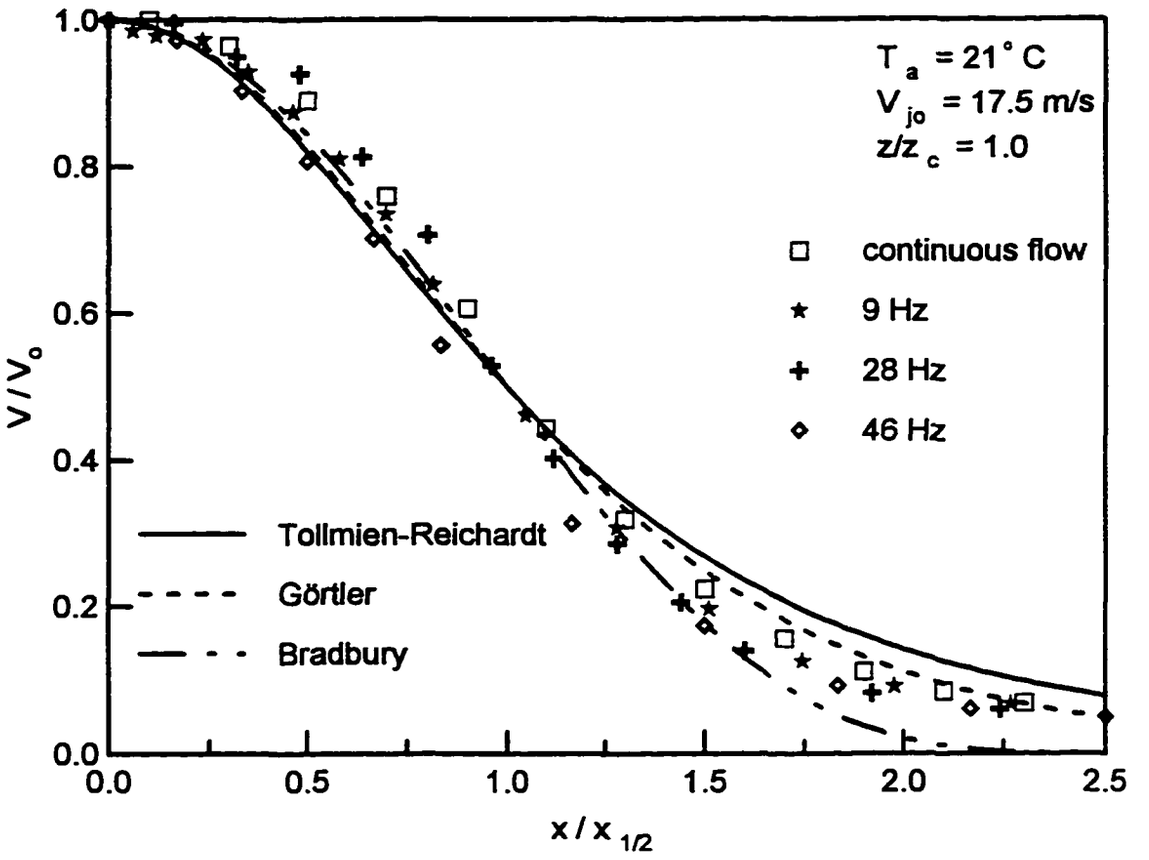

Figure 5.15 Comparison of dimensionless axial mean velocity profiles of oscillating flow and continuous flow through the die slots.

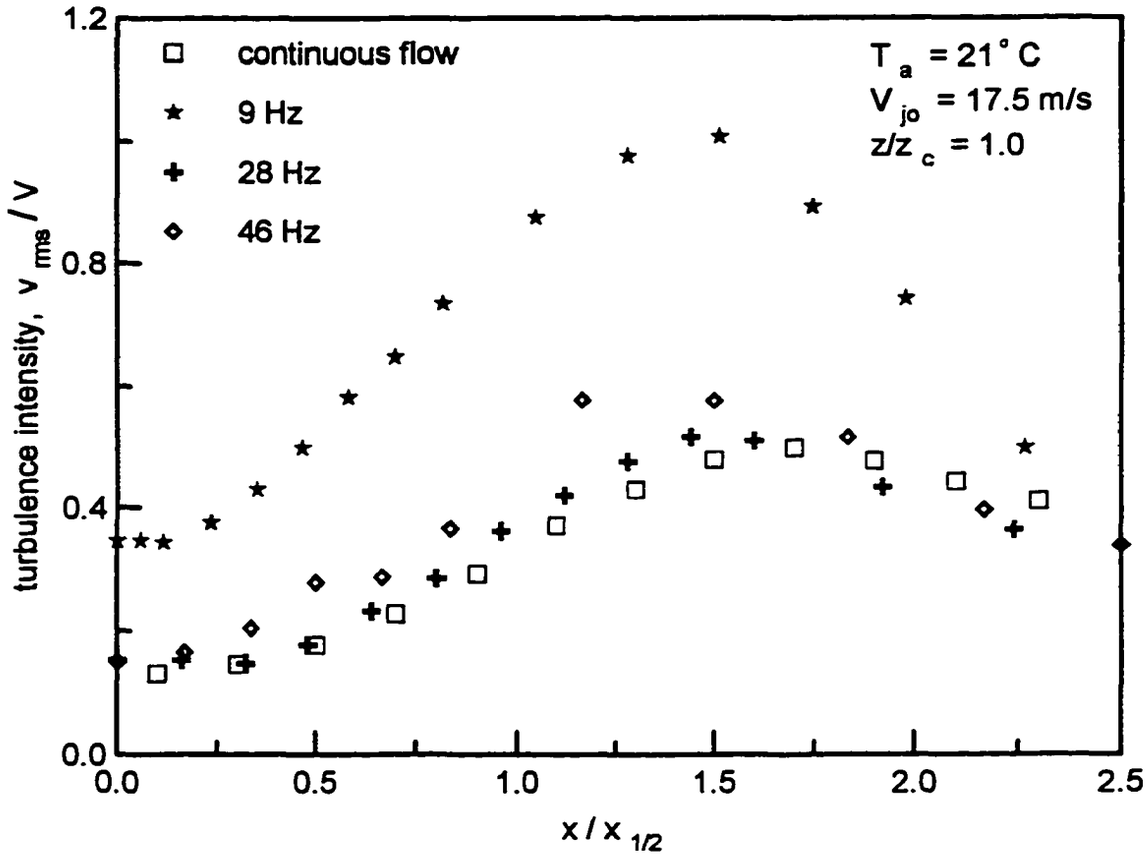

Figure 5.16 Comparison of dimensionless axial component turbulence intensity profiles of oscillating flow and continuous flow through the die slots.

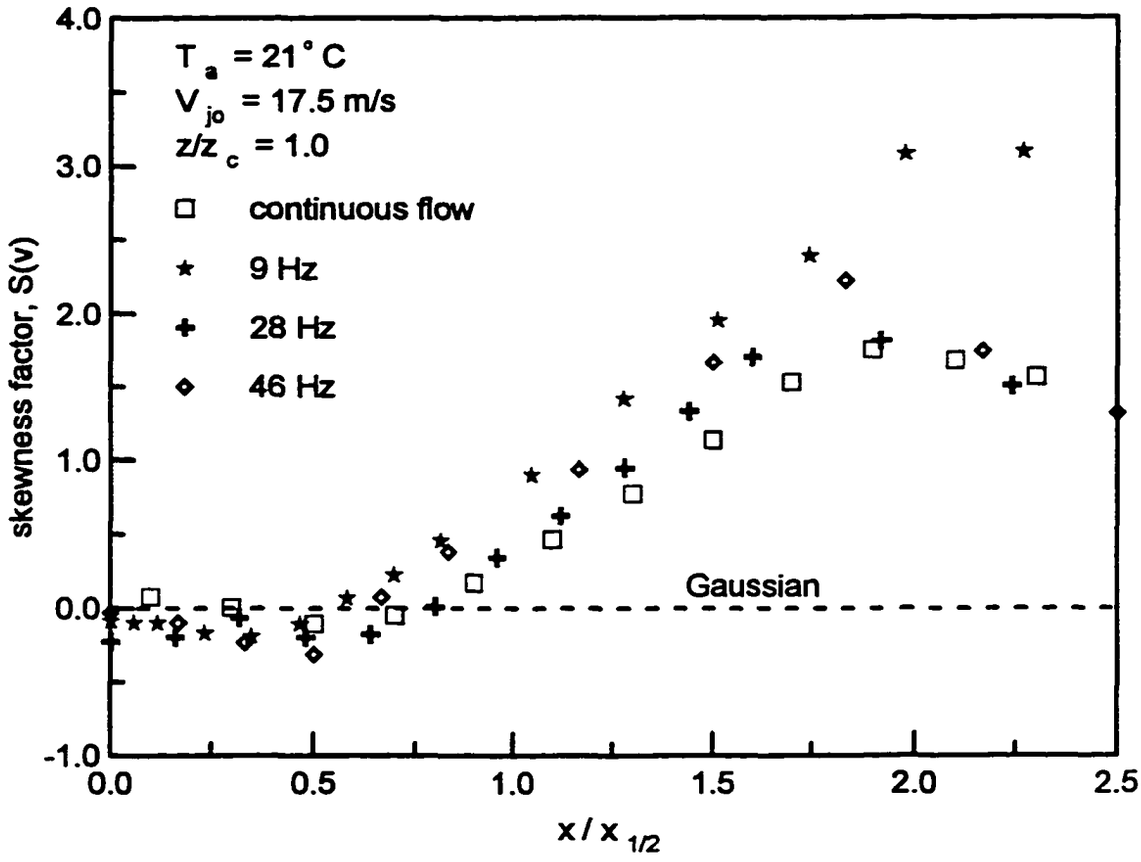

Figure 5.17 Comparison of dimensionless axial component skewness factor profiles of oscillating and continuous flows through the die slots.

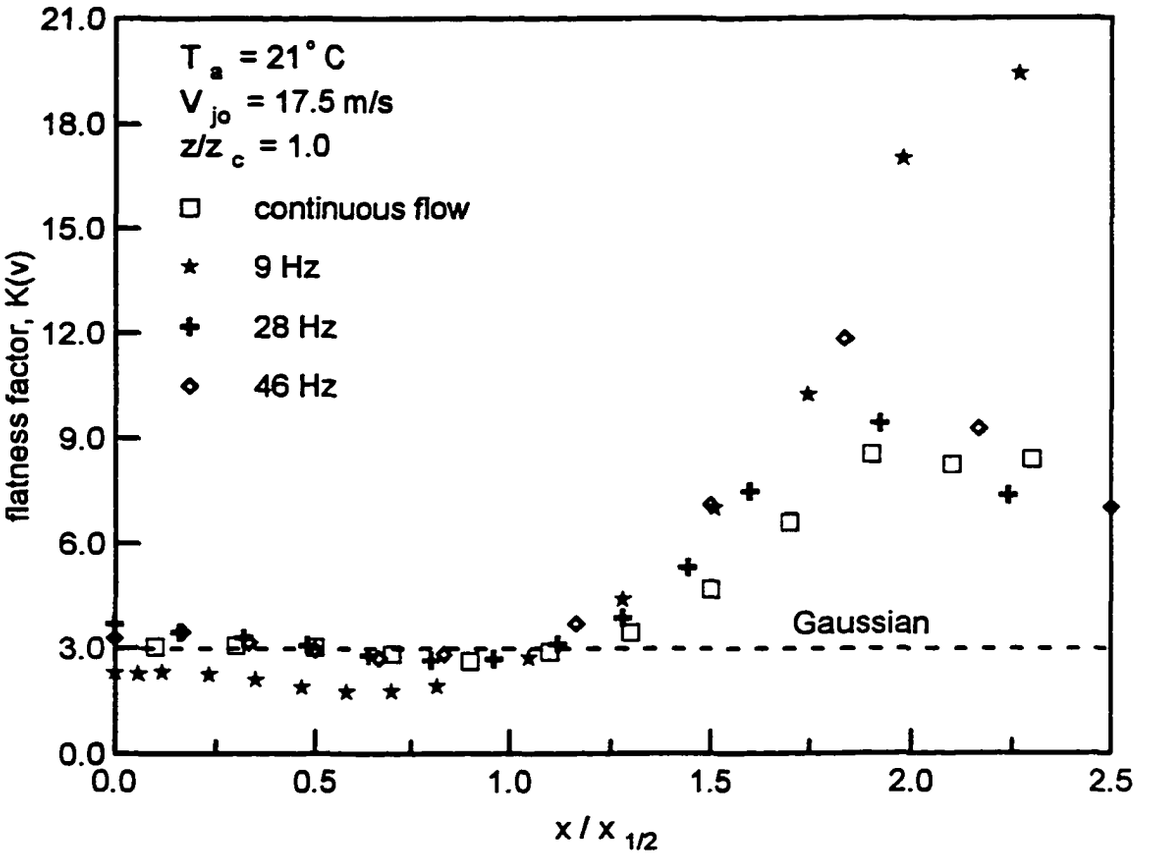

Figure 5.18 Comparison of dimensionless axial component flatness factor profiles of oscillating and continuous flows through the die slots.

Chapter 6

CONCLUSIONS AND RECOMMENDATIONS

6.1 Summary of Conclusions

The nature of fiber motion, nonwoven webs, and air turbulence structure in single-filament melt blowing has been experimentally studied. Fiber motion has been studied in terms of both fiber vibrations and fiber position distribution. The statistical parameters of a single-filament melt-blown web have been correlated to the fiber motion that in turn has been related to the air turbulence structure in melt blowing. Numerous conclusions have been drawn from the various results obtained in this study.

The results of fiber vibrations study (see Chapter 2) show that the fiber cone is elliptical with the direction across the slots of the die forming the major axis of the ellipse. Furthermore, it was found that, across the axis in the direction of slots, the frequency of fiber oscillations was more than the frequency of oscillations across the direction perpendicular to the slots. Therefore, the fiber motion is predominantly in the direction across the slots. The elliptical behavior of the fiber motion is further illustrated in the fiber position distribution that follows a unimodal bivariate probability distribution. One such distribution that was fit to the experimental data was a bivariate normal distribution (see Chapter 3). The fiber distribution spreads linearly with the increase in distance from the spinneret. Furthermore, it was found that the fiber motion in the two transverse directions was correlated. Hence, the elliptical cross-section of the fiber cone has a preferred orientation in the plane transverse to the spinning direction. The angle of orientation was found to vary sinusoidally for the fiber positions that were within a characteristic spatial separation along the spinning direction. Therefore, it is suggested that the fiber motion be that of an elliptical spiral that sinusoidally rotates in the transverse planes. Furthermore, it was observed that the fiber positions were auto-correlated only to those positions that were within a length of a fiber element along the fiber axis. Consequently, the fiber laydown pattern or the distribution of fibers in the web will follow the same distribution as the fiber positions of a moving threadline follow in a transverse plane. To evaluate the web distribution and the effect of melt blowing process variables on the statistical

parameters of the distribution, an analysis of web images was done (see Chapter 4). The image analysis technique was based on Kullback-Leibler principle of information entropy. The web distribution was found to spread linearly with the distance from the die. In addition, it was observed that process conditions, which reduced the fiber diameter, increased the spread of the web distribution. This result should be very helpful in controlling the basis weight (mass per unit area) of a melt-blown web. Furthermore, for a fixed z position below the die and for a given set of process variables, a large variance in the web orientation angle suggests that the web orientation angle is a function of time. This variation of the web orientation angle with time is a corollary to an earlier suggestion that the fiber moves spirally in a transverse plane, and the spiral rotates sinusoidally.

The study of the turbulent cross-jets shows that the position, at which the two slot jets cross below a melt blowing die, plays an important role in defining the turbulence structure of the flow field. Therefore, the distance of geometric cross-point of the cross-jets can be used as a characteristic length in melt blowing. The flow field of rectangular cross-jets is different from that of a single rectangular/two-dimensional jet. Since the fiber motion is dependent on the aerodynamic forces acting on the fiber, the existing correlations for the drag coefficient in melt blowing have to be corrected to include the turbulence effects due to crossing of the jets. The turbulence structure of oscillating cross-jets shows

that, by oscillating the jets between 28 - 46 Hz, an air turbulence structure similar to that of a continuous flow is generated at a lower air flow. However, a strong generation of turbulence is observed for the flow oscillating at frequencies (close to 9 Hz) for which a peak in the fiber diameter profile is seen. Therefore, it is suggested that an optimum amount of turbulence is required to produce finer fibers.

6.2 Applications and Recommendations

The foremost implication of the present work is that, for a given set of process variables and z position below the die, the structure of a melt-blown web can be predicted before the production of an actual web. Though the method implemented to predict the web distribution is mathematically and computationally intensive, the experimental equipment and number of experiments required for the prediction make the method very economical. Therefore, the method employed in the present study can be used for future studies of the web structure.

Fiber motion and web distribution studies suggest that knowledge of spread and orientation of the distribution of fiber positions would be useful in (a) predicting fiber-to-fiber entanglements in multiple filament melt blowing, (b) designing

spatial separation of the spinneret holes in the melt blowing dies, and (c) predicting the structural properties of melt-blown webs.

Another important goal achieved in the present study was the understanding of one-dimensional turbulence structure of the air flow field in melt blowing. This work can be used as a starting point for two- and three-dimensional turbulence studies, and eventually turbulence modeling of the melt blowing process. The turbulence study of the flow field of oscillating jets can be applied to control and improve the laydown pattern and structure of melt-blown webs.

APPENDICES

Appendix I

A SUPPLEMENT TO CHAPTER 2

AI.1 LDV Settings for Amplitude and Frequency Measurements

From the calibration wheel experiments, the following settings for LDV equipment were found optimum for the measurement of amplitude and frequency of fiber vibrations:

Counter mode:	Total Burst Count (TBC)
Frequncy shift:	0.5 MHz
Number of samples:	up to 1024
Number of cycles:	8
Timer comparison:	10%
Gain:	10
Low filter limit:	0.3 MHz
High filter limit:	1.0 MHz
Probe rotation:	90°
Sampling time:	30 - 150 seconds

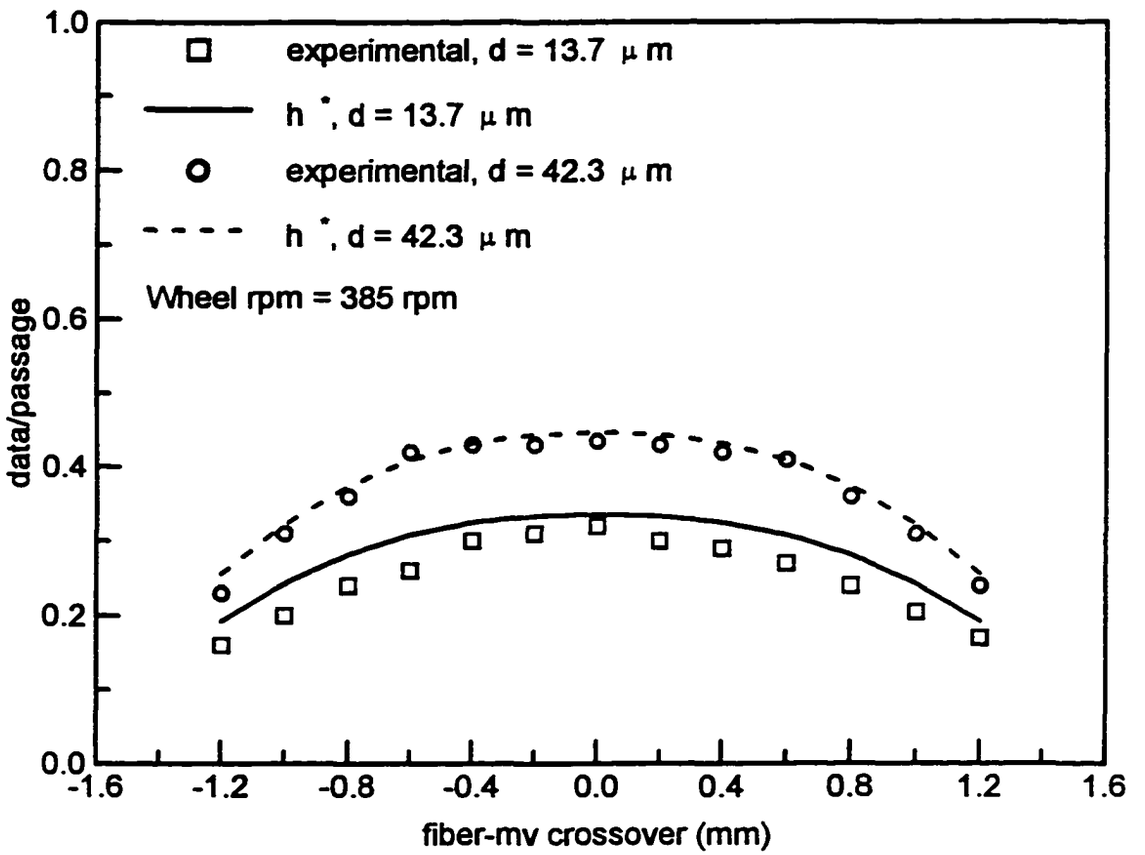

Figure AI.1 Effect of fiber diameter and measuring-volume position on data/passage in calibration wheel experiments. The solid and dotted lines are predicted from the fitted correlation of eq 2.3.

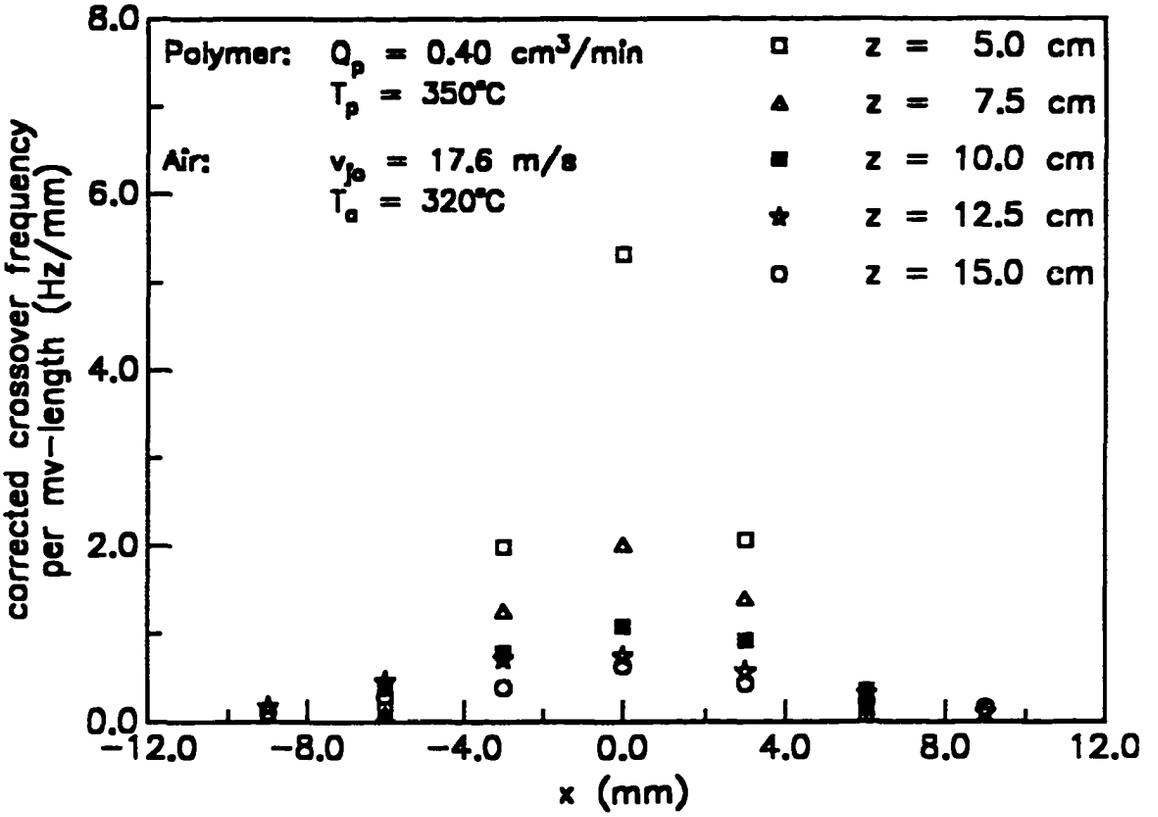

Figure AI.2 Fiber crossover frequency per unit length across the x axis for an air velocity v_{jo} = 17.6 m/s.

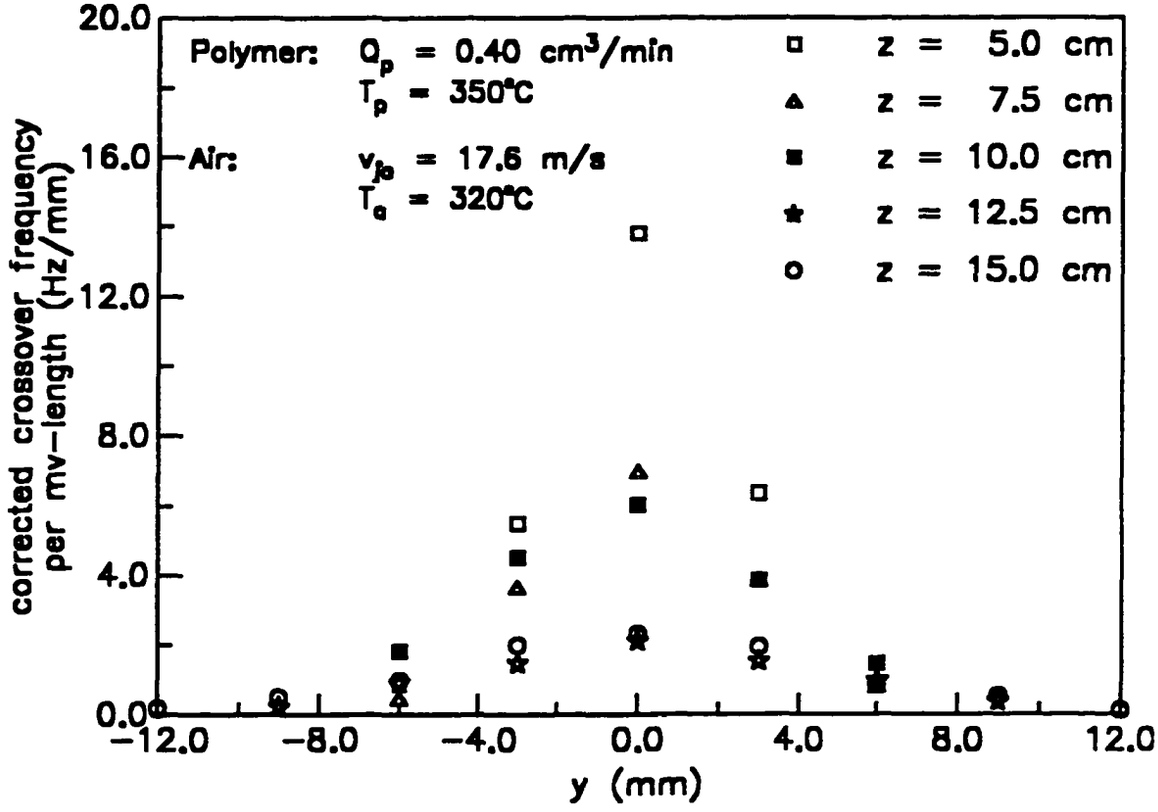

Figure AI.3 Fiber crossover frequency per unit length across the y axis for an air velocity v_{jo} = 17.6 m/s.

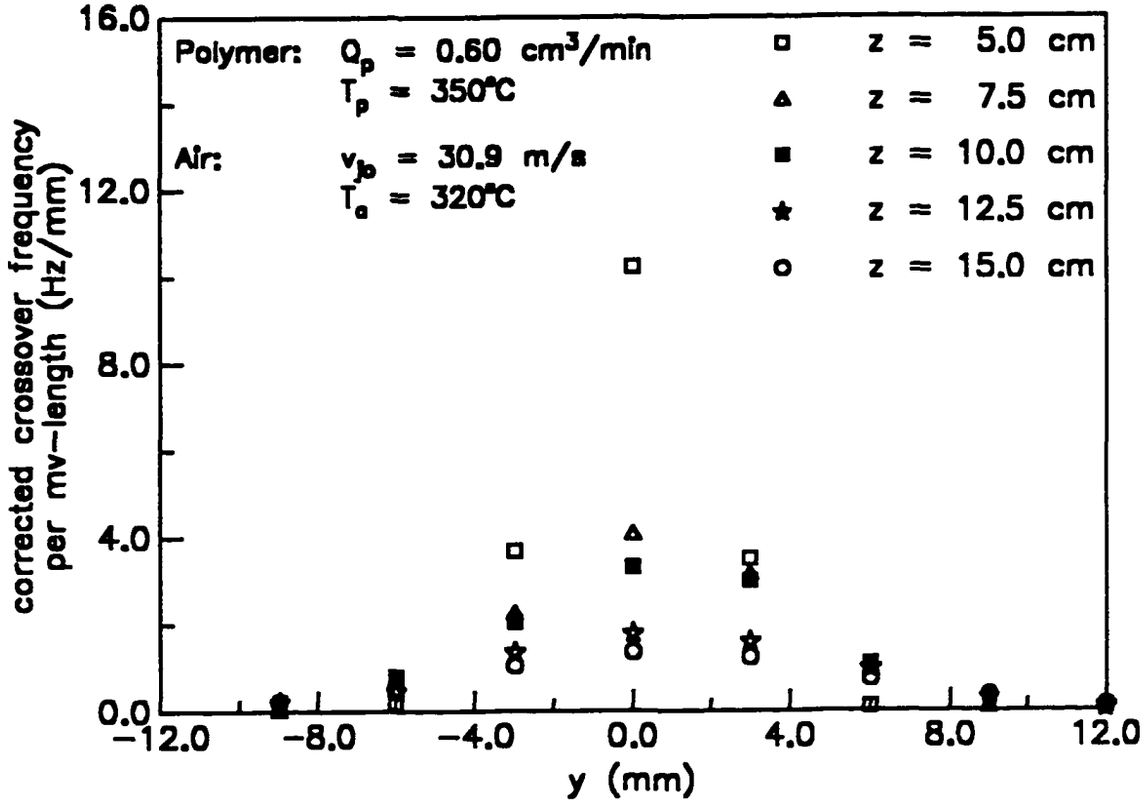

Figure AI.4 Fiber crossover frequency per unit length across the y axis for a polymer flow rate Q_p = 0.60 cm³/min.

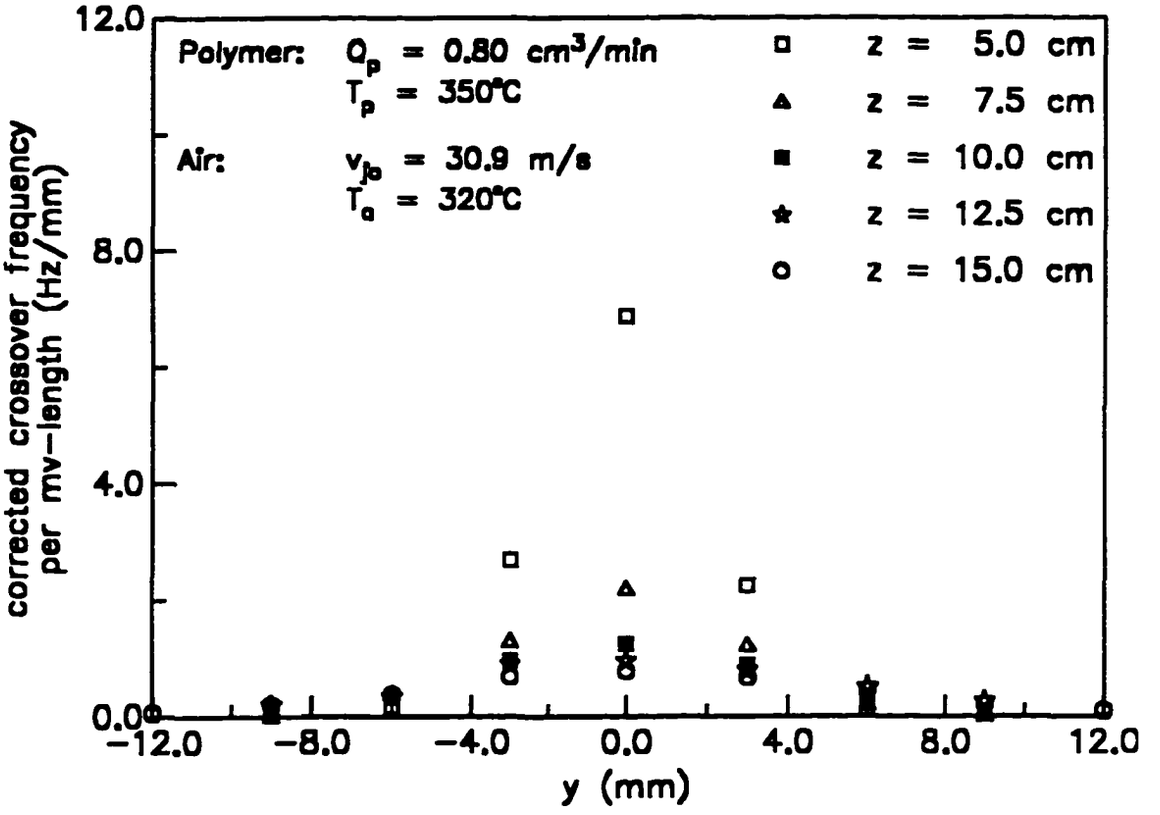

Figure AI.5 Fiber crossover frequency per unit length across the y axis for a polymer flow rate $Q_p = 0.80$ cm³/min.

Appendix II

A SUPPLEMENT TO CHAPTER 3

On the following pages, in this appendix, are the supplementary fiber density distribution surface plots which were not included in Chapter 3.

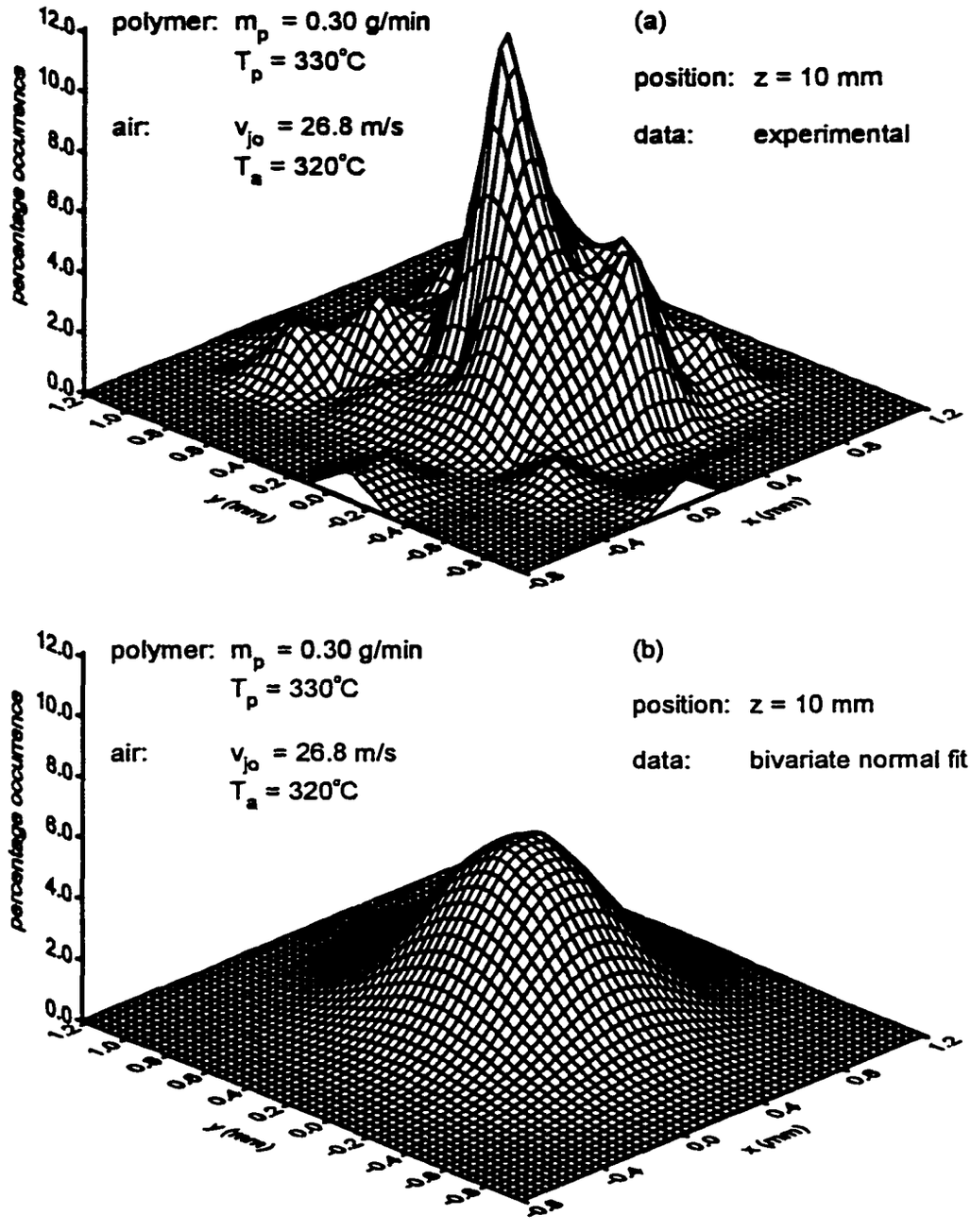

Figure AII.1 Surface plots of (a) experimental and (b) fitted fiber density distribution at z = 10 mm.

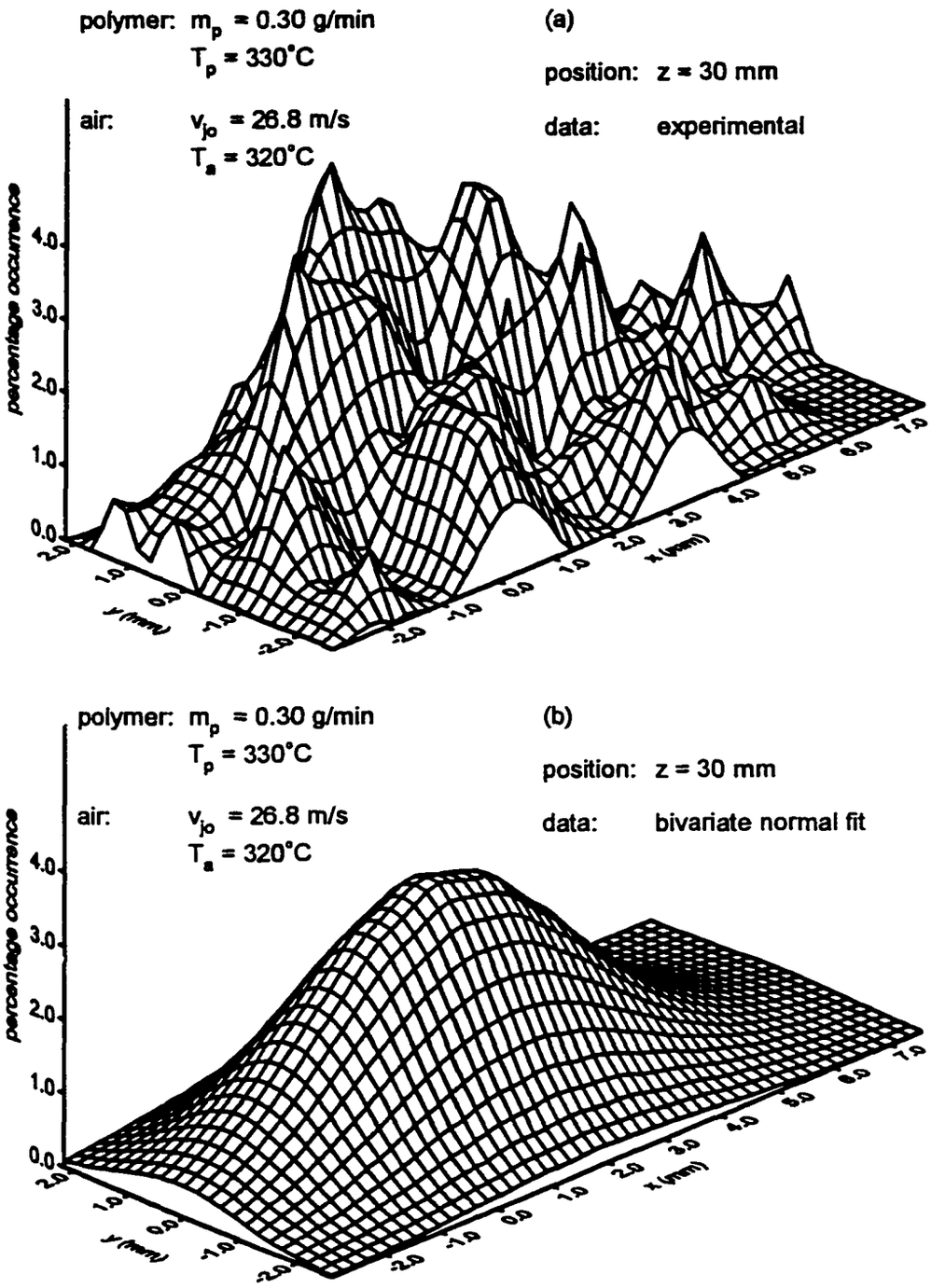

Figure AII.2 Surface plots of (a) experimental and (b) fitted fiber density distribution at z = 30 mm.

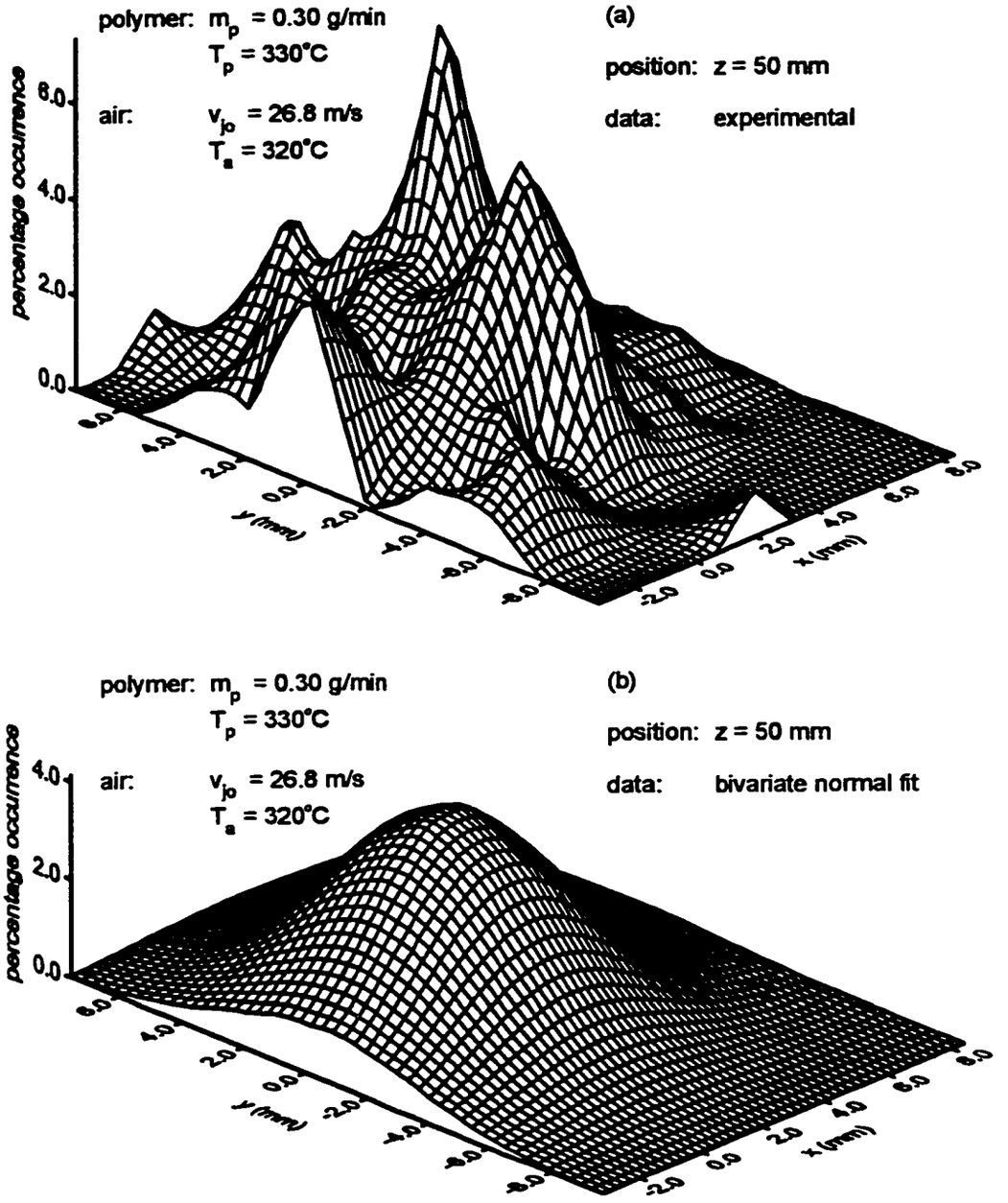

Figure AII.3 Surface plots of (a) experimental and (b) fitted fiber density distribution at z = 50 mm.

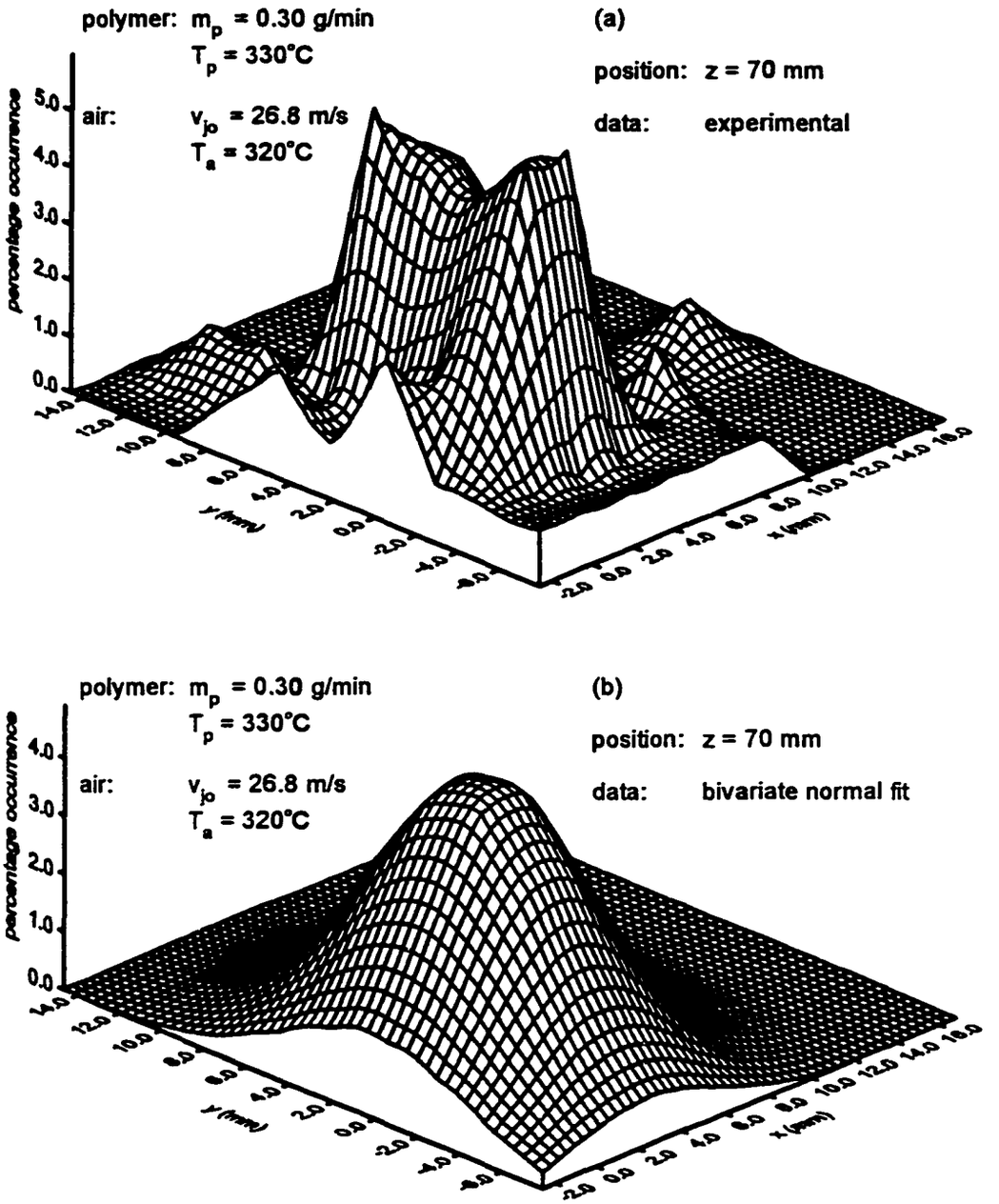

Figure AII.4 Surface plots of (a) experimental and (b) fitted fiber density distribution at $z = 70$ mm.

Appendix III

COMPUTER PROGRAM FOR EVALUATING THE WEB DISTRIBUTION USING ENTROPIC ANALYSIS

This appendix includes the computer program developed to analyze the web images as described in Chapter 4. The description of each variable and subroutine is present in the respective subroutine. To make the program self-explanatory and user-friendly, the comments for each module have been included.

```
CCCCCCCCCCCCCCCCCCCCCCCCCCCCCCCCCCCCCCCCCCCCCCCCCCCCCCCCCCCCCCCCCCCCCCCCCCCCCCC
C                                                                              C
C LANGUAGE: FORTRAN 77                                                         C
C FILENAME: entropy.f (main program)                                           C
C                                                                              C
C This program approximates the fiber presence probability density             C
C function using Kullback-Leibler entropy optimization principle of            C
C minimum information.  The observed distribution is evaluated                 C
C from 8-bit gray scale image of the laydown pattern.  The image is            C
C stored in PGM (Portable Gray Map) format with 256 gray levels.               C
C The program uses IMSL function BNRDF for evaluating probability              C
C integral for bivariate normal distribution as model fiber presence           C
C pdf.  For minimizing KL-information function, Simulated Annealing            C
C global minimization routine is used.                                         C
C                                                                              C
C EXTERNAL SUB-PROGRAMS CALLED IN ORDER:                                       C
C     CalStats (calstats.f)                                                    C
C     Minimize (minimize.f)                                                    C
C     PrintOut (entropy.f)                                                     C
C                                                                              C
CCCCCCCCCCCCCCCCCCCCCCCCCCCCCCCCCCCCCCCCCCCCCCCCCCCCCCCCCCCCCCCCCCCCCCCCCCCCCCC
```

```
C       PROGRAM Entropy
C       MAIN ROUTINE

C       **** DECLARATION OF VARIABLES ****

        INTEGER Wx, Wy, ndim
        PARAMETER (ndim=2)
        REAL Po(35,35), Pm(35,35), mu(ndim), sigma(ndim), sd(ndim),
       *      r, xbw(36), ybw(36), CF, t, rho
        DOUBLE PRECISION sdguess(ndim)

        EXTERNAL CalStats, Minimize, PrintOut

        COMMON /OBSERVED/ mu, r, Wx, Wy, Po, xbw, ybw, CF, t

C       **** DEFINITION OF VARIABLES ****

C       ---- INTEGER VARIABLES ----
C       Wx    : Number of windows set in X direction of the image
C       Wy    : Number of windows set in X direction of the image
C       ndim  : Number of dimensions in the problem - 2 in this case

C       ---- REAL VARIABLES ----
C       Po    : Array to store observed fiber presence pdf
C       Pm    : Array to store model (binormal) fiber presence pdf
C       mu    : Array to store means of distribution
C               mu(1) - X dimension mean
C               mu(2) - Y dimension mean
C       sd    : Array to store observed (image) standard deviations
C               sd(1) - observed X dimension standard deviation
C               sd(2) - observed Y dimension standard deviation
C       sigma : Array to store optimized standard deviations
C               sigma(1) - X dimension standard deviation
C               sigma(2) - Y dimension standard deviation
C       r     : observed correlation coefficient
C       rho   : optimized correlation coefficient
C       xbw   : array of X coordinates of NORTH boundaries of windows
C       ybw   : array of Y coordinates of WEST boundaries of windows
C       t     : orientation angle (in degrees) between major axis of
C               bivariate normal distribution ellipse and x-axis

C       **** DEFINITIONS OF SUB-PROGRAMS CALLED FROM MAIN ****

C       CalStats: Calculates the statistics of observed fiber presence
C                 pdf.  It calls a subroutine to read the image and
C                 then evaluates the statistics.
C       Minimize: Minimizes the KL-information function.  This routine
C                 calls the Simulated Annealing algorithm
C       PrintOut: Prints final statistical output of the program

C       ** CALLING ROUTINE TO EVALUATE STATISTICS FROM OBSERVED DATA **

        call CalStats(ndim, sd, sdguess)

C       ** CALLING SUBROUTINE TO MINIMIZE KL INFORMATION FUNCTION **

        call Minimize(ndim, sd, sdguess, sigma, rho)

C       ** CALLING SUBROUTINE TO PRINT OUT THE FINAL STATISTICS **

        call PrintOut(ndim, sd, sigma, rho)
```

```
      STOP
      END

*************************************************************************

      SUBROUTINE PrintOut(ndim, sd, sigma, rho)

C     **** DECLARATION OF VARIABLES ****
      CHARACTER infile*12, prob_dat*12, statfile*12
      INTEGER Wx, Wy, ndim
      REAL Po(35,35), mu(2), sigma(ndim), sd(ndim),
     +           r, xbw(36), ybw(36), CF, t, rho
      DOUBLE PRECISION ThetaFCN, KLF
      COMMON /OBSERVED/ mu, r, Wx, Wy, Po, xbw, ybw, CF, t
      COMMON /FILES/ infile, prob_dat, statfile
      COMMON /OPTIMIZED/ ThetaFCN, KLF

C     **** WRITING FINAL STATISTICS IN statfile ****
      open(unit=1, file=statfile, status='unknown')
      write(1,10)
 10   format(' This program approximated the fiber presence'/
     2    ' probability density function using Kullback-Leibler'/
     3    ' entropy optimization principle of minimum information.'/
     4    ' The observed distribution was evaluated from 8-bit gray'/
     5    ' scale image of the laydown pattern.  The image was stored'/
     6    ' in PGM (Portable Gray Map) format with 256 gray levels.'/
     7    ' The program used IMSL function BNRDF for evaluating'/
     8    ' probability integral for bivariate normal distribution as'/
     9    ' model fiber presence pdf.  For minimizing KL-information'/
     +    ' function, Simulated Annealing routine was used.'/)

      write(1,20) infile, Wx, Wy, KLF, (mu(j), mu(j), j=1,ndim),
     +                  (sd(i), sigma(i), i=1,ndim), r, rho
 20   format(1x,'ANALYZED IMAGE: ',A,/
     +        1x,'NUMBER OF X-DIRECTION WINDOWS: ',I2/
     +        1x,'NUMBER OF Y-DIRECTION WINDOWS: ',I2/
     +        1x,'MINIMUM VALUE OF KULLBACK-LEIBLER FUNCTION: ',e13.6//
     +        1x,'STATISTICAL PARAMETERS OF THE DISTRIBUTIONS:',/
     +        1x,'=============================================',/
     +        2x,'PARAMETER',10x,'OBSERVED',10x,'MODEL',/
     +        1x,'=============================================',/
     +        2x,'    mu(X)',10x, f8.4, 7x, f8.4,/
     +        2x,'    mu(Y)',10x, f8.4, 7x, f8.4,/
     +        2x,' sigma(X)',10x, f8.4, 7x, f8.4,/
     +        2x,' sigma(Y)',10x, f8.4, 7x, f8.4,/
     +        2x,'  rho(XY)',7x, e11.4, 4x, e11.4,/
     +    1x,'=============================================',//
     +        1x,'NOTE: mu AND sigma VALUES ARE IN mm')

      RETURN
      END

*************************************************************************
```

```
CCCCCCCCCCCCCCCCCCCCCCCCCCCCCCCCCCCCCCCCCCCCCCCCCCCCCCCCCCCCCCCCCCCCCCCCCC
C                                                                       C
C FILENAME: calstats.f                                                  C
C                                                                       C
C This file contains following subroutine(s):                           C
C                                                                       C
C SUBROUTINE  PARENT-ROUTINE  PARENT-RT-FILE  VARIABLES-RETURNED        C
C ~~~~~~~~~~  ~~~~~~~~~~~~~~  ~~~~~~~~~~~~~~  ~~~~~~~~~~~~~~~~~        C
C CalStats    Main            entropy.f       sd, mu, r, Wx, Wy,        C
C                                             and Po                    C
C                                                                       C
C Subroutine CalStats evaluates the grouped mean, standard deviations C
C and correlation coefficient from the windowed image.                  C
C                                                                       C
C Calstats CALLS EXTERNAL SUBROUTINE                                    C
C CalWinFreq (set_img.f)                                                C
C                                                                       C
CCCCCCCCCCCCCCCCCCCCCCCCCCCCCCCCCCCCCCCCCCCCCCCCCCCCCCCCCCCCCCCCCCCCCCCCCC
***************************************************************************

      SUBROUTINE CalStats(ndim, sd, sdguess)

C     **** DECLARATION OF ARGUMENT VARIABLES ****

      INTEGER Wx, Wy, ndim
      REAL Po(35,35), mu(2), sd(ndim), r, xbw(36), ybw(36), CF, t
      DOUBLE PRECISION sdguess(ndim)

      COMMON /OBSERVED/ mu, r, Wx, Wy, Po, xbw, ybw, CF, t

      EXTERNAL CalWinFreq

C     Subroutine CalWinFreq first reads the image pixel intensities
C     from (8-bit) 256 gray level image, then groups the image
C     pixels into W windows.  It, then, computes the normalized fiber
C     presence (fp) frequencies of the W windows and returns them as
C     observed fp-pdf array Po to the parent subroutine CalStats.

C     **** DECLARATION OF LOCAL VARIABLES ****

      INTEGER i, j
      REAL tan2t
      DOUBLE PRECISION uf, Ui, FiUi, FiU2i, Ux, Uy, fxy, PI
      PARAMETER (PI=3.14159265359)
C     ===================================================================

C     **** DEFINITION OF LOCAL VARIABLES ****

C     ---- REAL VARIABLE ----

C     CF    : Conversion factor from pixel to millimeter
C                (to be multiplied)

C     ---- DOUBLE PRECISION VARIABLES ----
C     uf    : Sum of normalized freq. in jth column or ith row
C     Ui    : Class mark of jth column or ith row
C     FiUi  : Sum of (uf*Ui)
C     FiU2i : Sum of (uf*Ui^2)
C     Ux    : Class mark of each row
C     Uy    : Class mark of each column
C     fxy   : Sum of (frequency*coordinates of center of cell)
```

```
C             or [Po(i,j)*Ux*Uy]
C     sdguess: Array containing initial guess values of standard
C             deviations to be used by optimization routine
C     ================================================================

C     **** CALLING THE SUBROUTINE TO READ AND GROUP IMAGE DATA ****

      call CalWinFreq(CF, Wx, Wy, Po, xbw, ybw, sdguess)

C     **** COMPUTING MEAN, SD, AND R FROM THE GROUPED DATA ****

      FiUi=0.0
      FiU2i=0.0

      print 5
 5    format(/5x,'X STATISTICS:')
      do 20 i=1,Wx
         uf=0.
         do 10 j=1,Wy
            uf=uf+Po(i,j)
 10      continue
         Ui=(xbw(i)+xbw(i+1)-1)*CF/2.0
         FiUi=FiUi + uf*Ui
         FiU2i=FiU2i + uf*(Ui**2.0)
C        print 15, Ui, uf, FiUi, FiU2i
C 15     format(1x,f6.4,3(1x,e11.4))
 20   continue
      mu(1)=FiUi
      sd(1)=sqrt(FiU2i-(mu(1)**2.0))
C     mu(1)=FiUi/sumPo
C     sd(1)=sqrt((FiU2i-(mu(1)**2.0)*sumPo)/(sumPo-1.0))
      print 30, mu(1), sd(1)
 30   format(7x,'mean =',f7.3,' mm;',2x,'s.d. =',f7.3,' mm')

      FiUi=0.0
      FiU2i=0.0

      print 35
 35   format(5x,'Y STATISTICS:')
      do 50 j=1,Wy
         uf=0.
         do 40 i=1,Wx
            uf=uf+Po(i,j)
 40      continue
         Ui=(ybw(j)+ybw(j+1)+1)*CF/2.0
         FiUi=FiUi + uf*Ui
         FiU2i=FiU2i + uf*(Ui**2.0)
C        print 15, Ui, uf, FiUi, FiU2i
 50   continue
      mu(2)=FiUi
      sd(2)=sqrt(FiU2i-(mu(2)**2.0))
C     mu(2)=FiUi/sumPo
C     sd(2)=sqrt((FiU2i-(mu(2)**2.0)*sumPo)/(sumPo-1.0))
      print 30, mu(2), sd(2)

C     ---- COMPUTING OBSERVED CORRELATION COEFFICIENT ----

      fxy=0.
      do 70 i=1,Wx
         Ux=(xbw(i)+xbw(i+1)-1)*CF/2.0
         do 60 j=1,Wy
```

```
            Uy=(ybw(j)+ybw(j+1)+1)*CF/2.0
            fxy=fxy+Po(i,j)*Ux*Uy
 60       continue
 70    continue
       r=(fxy-mu(1)*mu(2))/(sd(1)*sd(2))
       print 75, r
 75    format(5x,'CORRELATION COEFFICIENT:',/7x,'r = ',f7.4)

C      -- COMPUTING ANGLE BETWEEN MAJOR AXIS OF ELLIPSE AND X-AXIS --
       if (sd(1).EQ.sd(2)) then
          if (r.GT.0.0) then
             t=45.0
          else if (r.LT.0.0) then
             t=135.0
          else
             t=0.0
          end if
          tan2t=1.0E99
       else
          tan2t=2.0*r*sd(1)*sd(2)/(sd(1)**2.0-sd(2)**2.0)
          t=0.5*atan(abs(tan2t))
          if (r.GE.0.0) then
             if (sd(1).GT.sd(2)) then
                t=180.0*t/PI
             else
                t=180.0*(0.5-t/PI)
             end if
          else if (r.LT.0.0) then
             if (sd(1).GT.sd(2)) then
                t=180.0*(1.0-t/PI)
             else
                t=180.0*(0.5+t/PI)
             end if
          end if
       end if
       print 85, t
 85    format(5x,'ANGLE BETWEEN X-AXIS AND MAJOR AXIS OF ELLIPSE:',/
      +             7x,'t = ',f6.2,' degrees')

       RETURN
       END

*************************************************************************
```

```
CCCCCCCCCCCCCCCCCCCCCCCCCCCCCCCCCCCCCCCCCCCCCCCCCCCCCCCCCCCCCCCCCCCCCCCCCC
C                                                                       C
C FILENAME: set_img.f                                                   C
C                                                                       C
C This file contains following subroutines:                             C
C                                                                       C
C SUBROUTINE  PARENT-ROUTINE  PARENT-RT-FILE  VARIABLES-RETURNED        C
C ~~~~~~~~~~  ~~~~~~~~~~~~~~  ~~~~~~~~~~~~~~  ~~~~~~~~~~~~~~~~~~        C
C PixelInWin  CalWinFreq      calstats.f      Wx or Wy, and             C
C                                             nx_ptl or ny_ptl          C
C                                                                       C
C CalWinFreq  CalStats        calstats.f      Wx, Wy, Po, xbw,          C
C                                             and ybw                   C
C                                                                       C
C Subroutine PixelInWin calculates the total number of windows (full    C
C and partial) in a given direction.  It also finds out number of       C
C pixels in the given direction's partial window.                       C
C                                                                       C
C Subroutine CalWinFreq first reads the image pixel intensities from    C
C (8-bit) 256 gray level image, then groups the image pixels into       C
C W windows.  It, then, computes the normalized fiber presence (fp)     C
C frequencies of the W windows and returns them as observed fp-pdf      C
C array Po to the parent subroutine CalStats.                           C
C                                                                       C
C CalWinFreq CALLS EXTERNAL SUBROUTINE                                  C
C PixelInWin (set_img.f)                                                C
C                                                                       C
CCCCCCCCCCCCCCCCCCCCCCCCCCCCCCCCCCCCCCCCCCCCCCCCCCCCCCCCCCCCCCCCCCCCCCCCCC
************************************************************************

      SUBROUTINE CalWinFreq(CF, Wx, Wy, Po, xbw, ybw, sdguess)

C     **** DECLARATION OF ARGUMENT VARIABLES ****

      CHARACTER infile*12, prob_dat*12, statfile*12, sp_file*18
      INTEGER Wx, Wy
      REAL Po(35,35), xbw(36), ybw(36), CF
      DOUBLE PRECISION sdguess(2)
      LOGICAL print_flag, spatial_print

      COMMON /FILES/ infile, prob_dat, statfile, sp_file
      COMMON /PRINTING/ print_flag, spatial_print

C     **** DECLARATION OF LOCAL VARIABLES ****
      CHARACTER dummy*50, ans*3, gz_infile*15, command*30
      INTEGER d_lines, x, y, k, wd, ht, gmax, gmin, xo, yo, Wapprox,
     +              r_pix(0:900,0:900),pix(-550:550,-550:550), npix,
     +              nx_ptl, ny_ptl, xstart, xend, ystart, yend
      LOGICAL there, xo_found, yo_found
      DOUBLE PRECISION sumPo
      EXTERNAL PixelInWin, SYSTEM

C     **** DEFINITION OF LOCAL VARIABLES ****

C     ---- CHARACTER VARIABES ----
C     infile  : Image file name (12 characters allowed)
C     statfile: Final statistics' results file name
C     prob_dat: Probability output file name
C     sp_file : Spatial probability output file name
C     dummy : Dummy strings in image file (max. characters = 50)
C     ans   : Answer to questions asked to user
```

```
C     ---- INTEGER VARIABLES ----
C     d_lines: No. of dummy lines describing the creator program
C     wd     : Width of the image in pixels
C     ht     : Height of the image in pixels
C     gmax   : Maximum gray level intensity of a pixel in the image
C     gmin   : Minimum gray level intensity of a pixel in the image
C              It corresponds to complete fiber absence
C     x      : Index variable in X dimension (height-ways)
C     y      : Index variable in Y dimension (width-ways)
C     k      : File inquiry index
C     xo     : X axis zero position
C     yo     : Y axis zero position
C     pix    : 2-D array to store pixel intensity level.
C              Indices store position of pixel in web coordinate
C              system
C     r_pix  : 2-D array to read pixel intensity level from the file.
C              Indices store position of pixel in image coordinate
C              system
C     Wapprox: Approximate no. of windows in any direction of image
C     npix   : No. of pixels (odd no.) on each side of FULL window
C              >> It needs to be odd as center of a window has to be
C              >> a pixel position and not the edge of a pixel
C     nx_ptl: No. of pixels (odd no.) in X dir. partial window
C     ny_ptl: No. of pixels (odd no.) in Y dir. partial window
C     xstart: X dir. pixel position at NORTH end of each window
C     xend  : X dir. pixel position at SOUTH end of each window
C     ystart: Y dir. pixel position at WEST end of each window
C     yend  : Y dir. pixel position at EAST end of each window

C     ---- LOGICAL VARIABLES ----
C     there    : Indicates whether file exists
C     xo_found: Indicates whether X axis zero position is found
C     yo_found: Indicates whether Y axis zero position is found

C     ---- DOUBLE PRECISION VARIABLE ----
C     sumPo  : Sum of observed frequencies over all the windows
C              >> Needed for normalization of frequencies

C     **** READING IMAGE FILENAME ****

      k=0
  5   write(*,10)
 10   format(5x,'ENTER THE IMAGE FILE WITHOUT ".pgm" EXTENSION:')
      read 15, infile
 15   format(A)
C     infile='test93.pgm'

C     **** ADDING EXTENSIONS TO FILENAMES ****
      prob_dat=infile(:INDEX(infile,' ')-1)//'.dat'
      statfile=infile(:INDEX(infile,' ')-1)//'.stt'
      gz_infile=infile(:INDEX(infile,' ')-1)//'.pgm.gz'
      infile=infile(:INDEX(infile,' ')-1)//'.pgm'

C     **** CHECKING IF INPUT FILE EXISTS ****
      inquire(file=infile, exist=there)
      if(.NOT.there) then
         inquire(file=gz_infile, exist=there)
         if (there) then
            command='gunzip -v '//gz_infile//' \0'
            write(*,'(/5x,''INPUT FILE COMPRESSED!'',
     +                /5x,''UNCOMPRESSING INPUT FILE USING:''/5x,A)')
```

```
     +                    command
            write(*,*)
            i=SYSTEM(command)
         else
            print 16, infile
 16         format(5x,'**** INPUT FILE ',A,' DOES NOT EXIST! ****'/)
            k=k+1
C           >> ASK FOR NEW FILENAME ONLY THRICE
            if (k.GT.3) then
               write(*,*) '     FINALLY QUITTING'
               STOP
            end if
            go to 5
         end if
       end if

C      **** CHECKING IF INPUT FILE ALREADY ANALYZED ****
       there=.FALSE.
       inquire(file=prob_dat, exist=there)
       if (there) then
          write(*,17) infile
 17       format(/5x,'** IMAGE ',A,' HAS BEEN ANALYZED BEFORE! **',
     +           /5x,'DO YOU WISH TO RE-ANALYZE THE IMAGE? (y/n)')
          read(*,18) ans
 18       format(A)
          if ((ans(1:1).EQ.'n').OR.(ans(1:1).EQ.'N')) STOP
       end if

C      **** PRINTING THE FILENAMES ****
       write(*,19) infile, prob_dat, statfile
 19    format(/5x,'IMAGE FILE TO BE ANALYZED: ',A,
     +        /5x,'PROBABILITY OUTPUT TO BE STORED IN FILE: ',A,
     +        /5x,'FINAL STATISTICS TO BE STORED IN FILE: ',A)

C      **** READING IF USER WANTS TO PRINT SPATIAL PROBABILITIES ****
       write(*,'(/5x,''DO YOU WANT TO PRINT SPATIAL PROBABILITIES?'',
     +              '' (y/n)'')')
       read(*,'(A)') ans
       if ((ans(1:1).EQ.'n').OR.(ans(1:1).EQ.'N')) then
          spatial_print=.FALSE.
          write(*,'(5x,''>> YOU CHOSE NOT TO PRINT SPATIAL '',
     +          ''PROBABILITIES'')')
       else
          spatial_print=.TRUE.
          sp_file=infile(:INDEX(infile,'.')-1)//'.spa.tar'
          write(*,'(5x,''SPATIAL PROBABILITIES WILL BE STORED IN'',/
     +              5x,''24 FILES WHICH WILL BE tar AND gzipped'',/
     +              5x,''AND STORED AS: '',A,/
     +              5x,''THE FILES CAN BE RETREIVED BY EXECUTING:'',/
     +              5x,''gunzip -v '',A,'' ; tar -xvf '',A)')
     +              sp_file(:INDEX(sp_file,' ')-1)//'.gz',
     +              sp_file(:INDEX(sp_file,' ')-1)//'.gz', sp_file
       end if

       open(unit=1, file=infile, status='old')

C      **** READING FIRST LINE OF PGM IMAGE FILE ****
C      >> FIRST LINE DESCRIBES THE TYPE OF PGM FILE (ASCII OR BINARY)
C      >> SO IS STORED IN A DUMMY STRING AS FIRST DUMMY LINE

       read(1,20) dummy
```

```
 20   format(A50)
      d_lines=1

C     **** COUNTING LINES STARTING WITH '#' CHARACTER IN FILE ****
C     >> LINES STARTING WITH '#' DESCRIBE THE IMAGE CREATOR PROGRAM
C     >> THEIR NUMBER IS UNKNOWN AS EVERYTIME IMAGE IS TRANSFORMED
C     >> THE TRANSFORMING/CREATOR PROGRAM ADDS A LINE ABOUT ITSELF

 25   read(1,20) dummy
      d_lines=d_lines+1
      if (dummy(1:1).EQ.'#') then
         go to 25
      else
         d_lines=d_lines-1
      end if
C     write(*,*) 'dummy lines=',d_lines

C     **** REWINDING THE FILE ****
C     >> SO THAT DUMMY LINES CAN BE IGNORED WHEN RE-READING

      rewind(1)

C     **** RE-READING DUMMY LINES WITH KNOWN NO. OF DUMMY LINES ****
      do 30 i=1,d_lines
         read(1,20) dummy
C        print 20, dummy
 30   continue

C     **** READING WIDTH AND HEIGHT OF THE IMAGE FROM IMAGE FILE ****
      read(1,*) wd, ht

C     **** READING MAXIMUM GRAY LEVEL OF THE IMAGE ****
      read(1,*) gmax

C     **** READING MINIMUM GRAY LEVEL OF THE IMAGE FROM THE USER ****
      write(*,35)
 35   format(/5x,'ENTER THE MINIMUM GRAY LEVEL OF THE IMAGE:')
      read*, gmin
C     gmin=96
C     gmin=0
      write(*,37) gmin
 37   format(5x,'>> MINIMUM GRAY LEVEL OF THE IMAGE: ',I2)

C     **** READING CONVERSION FACTOR FROM PIXEL TO MM ****
      write(*,40)
 40   format(/5x,'ENTER THE NUMBER OF PIXELS IN ONE ACTUAL CM:')
      read*, CF
      write(*,42) CF
 42   format(5x,'>> NUMBER OF PIXELS IN ONE ACTUAL CM: ',F4.0)
      CF=10./CF

C     CF=0.62/320.       !for test7 image
C     CF=14.0/320.       !for test8 image
C     CF=10.0/37.0       !for test58, test9, and test10 images

C     **** READING INITIAL GUESS VALUES OF S.D. ****
      write(*,'(/5x,''ENTER INITIAL GUESS VALUES OF S.D. IN mm:'',/
     +           5x,''IF NOT SURE, ENTER ZERO FOR BOTH GUESSES.'',/
     +           5x,''IMAGE S.D.s WILL BE TAKEN AS GUESS VALUES:'')')
      read*, (sdguess(i), i=1,2)
      if (sdguess(2).EQ.sdguess(1).AND.sdguess(2).NE.0.) then
```

```
         write(*,'(5x,''>> TO AVOID DIVISION BY ZERO IN ANGLE '',
     +        ''CALCULATION,'',/8x,''sdguess(Y) IS REDUCED BY 0.01''/)')
         sdguess(2)=sdguess(2)-0.01
       end if
       write(*,'(5x,''ENTERED INITIAL GUESS VALUES OF S.D. ARE:''/,
     +          7x,''sdguess(X) = '',f5.2,'' mm''/,
     +          7x,''sdguess(Y) = '',f5.2,'' mm'')')(sdguess(i), i=1,2)


C      **** READING PIXEL POSITIONS AND INTENSITIES ****

       write(*,45) wd, ht
 45    format(/5x,'=============',/ 5x,'READING IMAGE',/
     +        5x,'=============',//5x,'IMAGE INFORMATION:',/
     +        7x,'width = ',I3,' pixels; height = ',I3,' pixels')
       read(1,*) ((r_pix(x,y), y=0,wd-1), x=0,ht-1)

C      **** FINDING ZERO POSITION OF THE WEB ****

       xo_found=.FALSE.
       yo_found=.FALSE.
       do 60 x=0,ht-1
          do 50 y=0,wd-1
             if (r_pix(x,y).EQ.gmax) then
                if ((.NOT.xo_found).AND.(y.EQ.0)) then
C                >> axis line is 3 pixel wide, middle pixel is xo
                   xo=x+1
                   xo_found=.TRUE.
                   write(*,46) xo
 46                format(7x,'x axis zero position = ',I3)
                else if (.NOT.yo_found) then
C                >> axis line is 3 pixel wide, middle pixel is yo
                   yo=y+1
                   yo_found=.TRUE.
                   write(*,47) yo
 47                format(7x,'y axis zero position = ',I3)
                end if
             end if
 50       continue
 60    continue

C      **** RESETING PIXEL POSITIONS ACCORDING TO WEB COORDINATES ****

       do 80 x=0,ht-1
          do 70 y=0,wd-1
             pix((x-xo),(yo-y))=r_pix(x,y)
C            if ((mod(x-xo,20).EQ.0).AND.(mod(yo-y,20).EQ.0)) then
C               print *, x-xo, yo-y, pix((x-xo),(yo-y))
C            end if
 70       continue
 80    continue

C      **** CREATING WINDOWS ****

       Wapprox=nint(sqrt(float(max(ht,wd))))
       npix=nint(min(ht,wd)/float(Wapprox))
       if (mod(npix,2).EQ.0) then
          npix=npix+1
       end if
C      print*, 'Wapprox=',Wapprox,'    npix=',npix
```

```
C     **** SUBROUTINE CALLS TO COUNT NO. OF WINDOWS IN EACH DIR. ****

      call PixelInWin(wd, npix, Wy, ny_ptl)
      call PixelInWin(ht, npix, Wx, nx_ptl)

C     print*, 'Wx=',Wx,'    nx_ptl=', nx_ptl
C     print*, 'Wy=',Wy,'    ny_ptl=', ny_ptl

      write(*,85) Wx, Wy, npix, nx_ptl, ny_ptl
 85   format(7x,'Windows in X-direction (heightwise), Wx = ',I2,/
     +       7x,'Windows in Y-direction (widthwise),  Wy = ',I2,/
     +       7x,'No. of pixels in each full window, npix = ',I2,/
     +       7x,'Pixels in X-direction partial window = ',I2,/
     +       7x,'Pixels in Y-direction partial window = ',I2)

C     **** CALCULATING FREQUENCIES OF THE WINDOWS ****

      xend=0-xo-1
      do 90 i=1,Wx
         xstart=xend+1

C        >> if xstart lies on x axis (3 pixels wide),
C        >> increment xstart by accordingly
C        >> axis line is to be ignored for probability calculation
C        >> as actual gray level at zero position is unknown

         if (xstart.EQ.-1) then
            xstart=xstart+3
         else if (xstart.EQ.0) then
            xstart=xstart+2
         else if (xstart.EQ.1) then
            xstart=xstart+1
         end if

         if ((i.EQ.Wx).AND.(nx_ptl.NE.0)) then
            xend=xstart+(nx_ptl-1)
C           >> xend is not allowed to exceed image boundary
            if (xend.GT.(wd-1-xo)) then
               xend=wd-1-xo
            end if
         else
            xend=xstart+(npix-1)
         end if

C        >> if axis lies somewhere in full window or on xend position
C        >> ignore it by incrementing xend accordingly. However, if
C        >> x axis is somewhere in the partial window, no need to
C        >> increase xend as axis position then has already been
C        >> taken into account

         if ((xstart.LT.-1.AND.xend.GE.1).AND.(i.NE.Wx)) then
            xend=xend+3
         end if

C        ---- setting lower boundary of window ----
         xbw(i)=float(xstart)

 90   continue
      xbw(Wx+1)=xend+1

      yend=yo+1
```

```
      do 100 j=1,Wy
         ystart=yend-1

C        >> if ystart lies on y axis (3 pixels wide),
C        >> decrement ystart by accordingly
C        >> axis line is to be ignored for probability calculation
C        >> as actual gray level at zero position is unknown

         if (ystart.EQ.1) then
            ystart=ystart-3
         else if (ystart.EQ.0) then
            ystart=ystart-2
         else if (ystart.EQ.-1) then
            ystart=ystart-1
         end if

         if ((j.EQ.Wy).AND.(ny_ptl.NE.0)) then
            yend=ystart-(ny_ptl-1)
C           >> yend is not allowed to exceed image boundary
            if (yend.LT.(yo-(ht-1))) then
               yend=yo-(ht-1)
            end if
         else
            yend=ystart-(npix-1)
         end if

C        >> if axis lies somewhere in full window or on xend position
C        >> ignore it by incrementing xend accordingly. However, if
C        >> y axis is somewhere in the partial window, no need to
C        >> increase xend as axis position then has already been
C        >> taken into account

         if ((ystart.GT.-1.AND.yend.LE.1).AND.(j.NE.Wy)) then
            yend=yend-3
         end if

         ybw(j)=float(ystart)

 100  continue
      ybw(Wy+1)=yend-1.

C     print*, '-------------------------------------------------'
C     print 102
C 102 format(3x,'i',3x,'j',2x,'xstr',2x,'xend',2x,'ystr',2x,'yend',
C     +            4x,'xbw',5x,'ybw')
C     print*, '-------------------------------------------------'

      sumPo=0.
C     --- i loop: traverses windows in +ve x dir. heightwise ---
      do 140 i=1,Wx
C        -- j loop: traverses windows in -ve y dir. widthwise --
         do 130 j=1,Wy
            Po(i,j)=0.
            xstart=xbw(i)
            xend=xbw(i+1)-1
            ystart=ybw(j)
            yend=ybw(j+1)+1

C           if (j.EQ.Wy.OR.i.EQ.1) then
C              print 105, i,j,xstart,xend,ystart,yend,xbw(i),ybw(j)
C 105          format(2(2x,I2),4(2x,I4),2(2x,F6.2))
```

```
C           end if

C           -- 2nd and 3rd inner loops: traverse pixels in windows --
C           -- while ignoring pixel positions lying on either axes --
C           -- Therefore, care must be taken when calculating Pm --

            do 120 x=xstart,xend,1
               do 110 y=ystart,yend,-1
                  if ((x.NE.-1.AND.x.NE.0.AND.x.NE.1).AND.
     +                    (y.NE.-1.AND.y.NE.0.AND.y.NE.1).AND.
     +                    (pix(x,y).GT.gmin)) then
                     Po(i,j)=Po(i,j)+(pix(x,y)-gmin)
                  end if
 110           continue
 120        continue

            sumPo=sumPo+Po(i,j)
 130     continue
 140  continue

C     **** NORMALIZING WINDOW FREQUENCIES TO FINALLY COMPUTE Po ****

      do 160 i=1,Wx
         do 150 j=1,Wy
            Po(i,j)=Po(i,j)/sumPo
 150     continue
 160  continue

C     print*, 'Normalized Po(1,1)=', Po(1,1)

      RETURN
      END

*************************************************************************

      SUBROUTINE PixelInWin(len, npix, Wx_or_y, n_ptl)

C     **** DECLARATION OF ARGUMENT VARIABLES ****

      INTEGER len, npix, Wx_or_y, n_ptl

C     **** CALCULATING NO. OF FULL WINDOWS IN GIVEN DIRECTION ****

C     >> THREE PIXELS ARE DECREMENTED TO ALLOW FOR AXIS LINE WIDTH

      Wx_or_y=(len-3)/npix

C     **** CALCULATING NO. OF PIXELS IN LEFT OVER PARTIAL WINDOW ****
      n_ptl=(len-3) - npix*Wx_or_y

C     >> SINCE LEFT OVER PARTIAL WINDOW IS ALSO A WINDOW, Wx_or_y
C     >> HAS TO BE INCREMENTED BY ONE.  ALSO, n_ptl HAS TO BE ODD.
C     >> THEREFORE, IT IS CHECKED IF IT IS ODD.  AS IT IS A COUNT
C     >> OF PIXELS IN LAST WINDOW, IT IS DECREASED BY ONE IF IT IS
C     >> EVEN (CAN'T HAVE AN EXTRA ROW/COLUMN OF PIXELS OUT OF IMAGE

      if (n_ptl.NE.0) then
         Wx_or_y=Wx_or_y+1
         if (mod(n_ptl,2).EQ.0) then
            n_ptl=n_ptl-1
         end if
```

```
      end if

      RETURN
      END
*****************************************************************************
```

```
CCCCCCCCCCCCCCCCCCCCCCCCCCCCCCCCCCCCCCCCCCCCCCCCCCCCCCCCCCCCCCCCCCCCCCCCCC
C                                                                       C
C FILENAME: minimize.f                                                  C
C USES SIMULATED ANNEALING FOR GLOBAL MINIMIZATION                      C
C                                                                       C
C This file contains following subroutine(s):                           C
C                                                                       C
C SUBROUTINE    PARENT-ROUTINE    PARENT-RT-FILE    VARIABLES-RETURNED  C
C ~~~~~~~~~~    ~~~~~~~~~~~~~~    ~~~~~~~~~~~~~~    ~~~~~~~~~~~~~~~~~~  C
C Minimize      Main              entropy.f         sigma, rho, KLF     C
C                                                                       C
C FCN           Minimize          minimize.f        FCNvalue, KLF,      C
C                                                   ThetaFCN            C
C                                                                       C
C Gp            FCN               minimize.f        Gp                  C
C                                                                       C
C KLFCN         FCN               minimize.f        KLFCN, KLF          C
C                                                                       C
C CDF           KLFCN             minimize.f        CDF                 C
C                                                                       C
C ModelFpProb   Minimize, FCN     minimize.f        Pm                  C
C                                                                       C
C ======================================================================= C
C                                                                       C
C Minimize subroutine manages the optimization procedure, prints the    C
C optimized values standard deviations of model fiber presence PDF,     C
C and fiber presence PDF in a file.  For minimization procedure, it     C
C calls the simulated annealing procedure, SIM_ANNEAL, which returns    C
C the optimized values of the objective function and variables (s.d.)   C
C Routine SIM_ANNEAL requires initial guess values of variables, the    C
C lower and the upper limits on variables and the number of variables   C
C to be optimized.                                                      C
C                                                                       C
C FCN is a double precision function that calculates the objective      C
C function to be minimized by simulated annealing.                      C
C ======================================================================= C
C                                                                       C
C Minimize CALLS FOLLOWING EXTERNAL SUBROUTINES:                        C
C SIM_ANNEAL      (anneal.f)                                            C
C FCN             (minimize.f - this file)                              C
C ModelFpProb     (minimize.f - this file)                              C
C SYSTEM          (UNIX Library)                                        C
C                                                                       C
C FCN CALLS FOLLOWING EXTERNAL SUBROUTINES:                             C
C ModelFpProb     (minimize.f - this file)                              C
C Gp              (minimize.f - this file)                              C
C                                                                       C
C KLFCN CALLS EXTERNAL SUBROUTINE:                                      C
C CDF             (minimize.f - this file)                              C
C SYSTEM          (UNIX Library)                                        C
C                                                                       C
C ModelFpProb CALLS EXTERNAL SUBROUTINE:                                C
C BNRDF           (IMSL Library)                                        C
C                                                                       C
CCCCCCCCCCCCCCCCCCCCCCCCCCCCCCCCCCCCCCCCCCCCCCCCCCCCCCCCCCCCCCCCCCCCCCCCCC

**************************************************************************

      SUBROUTINE Minimize(ndim, sd, stguess, sigma, rho)

C     **** DECLARATION OF ARGUMENT VARIABLES ****
```

```
      CHARACTER infile*12, prob_dat*12, statfile*12, sp_file*18
      INTEGER Wx, Wy, ndim
      REAL Po(35,35), mu(2), sd(1:ndim), sigma(1:ndim), r, xbw(36),
     +     ybw(36), CF, t
      DOUBLE PRECISION stguess(ndim)

      COMMON /OBSERVED/ mu, r, Wx, Wy, Po, xbw, ybw, CF, t
      COMMON /FILES/ infile, prob_dat, statfile, sp_file

C     **** DECLARATION OF LOCAL VARIABLES ****

      INTEGER i, nopt
      PARAMETER (nopt=2)

      CHARACTER command*80
      REAL rho, Pm(35,35), x, y
      DOUBLE PRECISION stat(nopt), LB(nopt), UB(nopt)
      DOUBLE PRECISION ThetaFCN, Fopt
      DOUBLE PRECISION KLF
      LOGICAL minimized, print_flag, spatial_print

      EXTERNAL FCN, SIM_ANNEAL, SYSTEM, ModelFpProb
      COMMON /OPTIMIZED/ ThetaFCN, KLF
      COMMON /PRINTING/ print_flag, spatial_print


C     ================================================================

C     **** DEFINITION OF LOCAL VARIABLES ****

C     ---- CHARACTER VARIABLES ----
C     command: variable to store archiving command to pass
C              to system

C     ---- INTEGER VARIABLES ----
C     nopt  : number of variables to be optimized (= 2)

C     ---- REAL VARIABLES ----
C     rho   : correlation coefficient of the model distribution
C     Pm    : array to store model fiber presence probabilities
C     x     : x dimension of the center of the window
C     y     : y dimension of the center of the window

C     ---- DOUBLE PRECISION VARIABLES ----
C     stat  : array of statistical parameters to be optimized (s.d.)
C     LB    : array of lower bound of variable optimization range
C     UB    : array of upper bound of variable optimization range
C     KLF   : Kullback-Leibler function to be optimized
C             (must be >= 0.0)
C     ThetaFCN: theta function constraint added to KL function
C             to be optimized.  It is equal to the square of
C             differences in tangents of model and observed
C             orientation angles of distribution ellipses
C     Fopt  : objective function to be optimized.  It is sum of
C             square of KLF and ThetaFCN

C     ---- LOGICAL VARIABLES ----
C     minimized:  flag to indicate completion of minimization
C     print_flag: flag to indicate whether to print spatial
C                 probabilities if user flags spatial_print to TRUE
C     spatial_print: user switch to indicate printing of spatial
```

```
C                  probabilities

C     ================================================================

C     **** COMPRESSING (gzip) THE IMAGE FILE TO SAVE DISK SPACE ****
      write(*,'(/5x,29(''-'')
     +          /5x,''COMPRESSING IMAGE FILE USING:''/5x,29(''-''))')
      command='gzip -v '//infile//' \0'
      write(*,'(5x,A/)') command
C     >> CALLING SYSTEM (unix) AND SENDING THE COMPRESSION COMMAND
      i=SYSTEM(command)
      write(*,*)
      print 5
 5    format(/5x,'=================================================',
     +       /5x,'MINIMIZING KULLBACK-LIEBLER INFORMATION FUNCTION',
     +       /5x,'=================================================')

C     **** SETTING print_flag TO FALSE BEFORE OPTIMIZATION ****
      print_flag=.FALSE.

C     **** SETTING LOWER AND UPPER BOUNDS ON stat VARIABLES ****
      do 10 i=1,nopt
         if (stguess(i).EQ.0.) stguess(i)=sd(i)
         LB(i)=sd(i)*0.85      !Decrease by 15%
         UB(i)=sd(i)*1.25      !Increase by 25%
C        stguess(i)=23.0       !sd(i)+1.0E-06
 10   continue

C     **** MAKING SURE THAT LB(1) AND UB(1) ARE GREATER THAN ****
C     **** LB(2) AND UB(2) RESPECTIVELY                     ****
      if (LB(1) .LT. LB(2)) then
         LB(2)=0.99*LB(1)
         UB(2)=0.99*UB(1)
        end if

C     **** MAKING SURE THAT stguess(X) > stguess(Y) ****
      if (stguess(1) .LT. stguess(2)) stguess(2)=stguess(1)*0.99

C     **** SETTING CORRELATION COEFF. FOR MODEL DISTRIBUTION ****
C     **** EQUAL TO THAT OF OBSERVED (IMAGE) DISTRIBUTION    ****
      rho=r

C     **** PRINTING GUESS VALUES OF stat ****
      write(*,25) (stguess(j),j=1,nopt)
 25   format(/5x,'GLOBAL MINIMIZATION WITH FOLLOWING GUESS VALUES:',
     +       /7x,'stguess(X) = ',e10.4,
     +       /7x,'stguess(Y) = ',e10.4/)

C     **** MINIMIZATION USING SIMULATED ANNEALING ****
      call SIM_ANNEAL(nopt, stguess, LB, UB, stat, Fopt)

C     **** EVALUATING THETA AND KL FUNCTIONS AT OPTIMUM stat(i) ****
      call FCN(nopt,stat,Fopt)

C     **** CONVERTING DOUBLE PRECISION stat TO SINGLE PRECISION ****
      do 30 j=1,nopt
         sigma(j)=stat(j)
 30   continue

C     **** PRINTING FINAL VALUES OF PARAMETERS AND FUNCTIONS ****
      print 280, (sd(i), sigma(i), i=1,ndim), r, rho,
```

```
     +                  Fopt, KLF, KLF**2., ThetaFCN
 280  format(//5x,'KULLBACK-LIEBLER FUNCTION MINIMIZED...',/
     +       5x,38('='),//
     +       5x,'STATISTICAL PARAMETERS OF THE DISTRIBUTIONS ARE:',/
     +       7x,'OBS. sd(X) =',f8.4,' mm; MODEL sigma(X) =',f8.4,' mm',/
     +       7x,'OBS. sd(Y) =',f8.4,' mm; MODEL sigma(Y) =',f8.4,' mm',/
     +       7x,'OBS.     r =',e11.4,'; MODEL      rho =',e12.4,/
     +       5x,'WHEN MINIMUM VALUE OF OBJECTIVE FUNCTION  = ',e13.6/,
     +       5x,'VALUE OF KL FUNCTION                      = ',e13.6/,
     +       5x,'VALUE OF SQUARE OF KL FUNCTION            = ',e13.6/,
     +       5x,'VALUE OF THETA FUNCTION                   = ',e13.6/)

C      **** PRINTING FINAL VALUES OF SPATIAL PDF ****
       if (spatial_print) then
          print_flag=.TRUE.
          call FCN(nopt,stat,Fopt)
       end if

C      **** PRINTING FINAL VALUES OF FIBER PRESENCE PDF ****
       call ModelFpProb(ndim, sigma, rho, Pm)
       open(unit=99, file=prob_dat, status='unknown')
       write(99,282)
 282   format(5x,'x',7x,'y',8x,'Po',10x,'Pm')
       do 300 i=1,Wx
          do 290 j=1,Wy
             x=(xbw(i)+xbw(i+1)-1)*CF/2.
             y=(ybw(j)+ybw(j+1)+1)*CF/2.
             write(99,285) x,y,Po(i,j),Pm(i,j)
 285         format(2(2x,f6.2),2(2x,e10.4))
 290      continue
 300   continue

       RETURN
       END

*************************************************************************

       SUBROUTINE FCN(nopt,stat,FCNvalue)

C      **** DECLARATION OF ARGUMENT VARIABLES ****

       INTEGER Wx, Wy, nopt
       REAL Po(35,35), mu(2), r, xbw(36), ybw(36), CF, t
       DOUBLE PRECISION FCNvalue, stat(2), ThetaFCN
       DOUBLE PRECISION KLF
       LOGICAL print_flag, spatial_print

       COMMON /OBSERVED/ mu, r, Wx, Wy, Po, xbw, ybw, CF, t
       COMMON /OPTIMIZED/ ThetaFCN, KLF
       COMMON /PRINTING/ print_flag, spatial_print

C      **** DECLARATION OF LOCAL VARIABLES ****

       INTEGER i, j, k, Kn, fltB(4)
       REAL Pm(35,35), pi(250), dp, PoMax, PoMax_ij, rho
       REAL NPo(35,35), NPm(35,35), sigma(2), x, y
       DOUBLE PRECISION Gp, PIvalue, KLFCN, var1, var2, diffvar
       PARAMETER (PIvalue= 3.14159265359)

       EXTERNAL Gp, KLFCN
```

```
      INTEGER no_fn_eval
      SAVE no_fn_eval, PoMax, dp, Kn, pi

      DATA no_fn_eval /0/

C     ================================================================

C     **** DEFINITION OF LOCAL VARIABLES ****

C     ---- INTEGER VARIABLES ----
C     Kn     : No. of outcome values assigned to computed fiber
C              presence observed and model probabilities (= 50)
C     no_fn_eval: No. of function evaluations done so far
C                 It is needed to avoid re-calculating PoMax, dp,
C                 Kn, pi.  These variables are calculated only first
C                 time.  It is also needed in printing status of
C                 program

C     ---- REAL VARIABLES ----
C     Pm     : Array to store model (binormal) fiber presence pdf
C     pi     : Array of Kn outcome values assigned to normalized
C              fiber presence observed and model probabilities
C     dp     : Delta p needed to compute spatial PDF using finite
C              difference numerical approximation of derivative
C     PoMax  : Maximum probability value of Po (fp observed) pdf
C     PoMax_ij: Maximum probability value of Po (fp observed) pdf
C              in any direction
C     rho    : Model correlation coefficient
C     NPo    : Array of normalized observed fiber presence pdf by
C              NPo(i,j) = Po(i,j)/PoMax
C     NPm    : Array of normalized model fiber presence pdf by
C              NPm(i,j) = Pm(i,j)/PoMax
C     sigma  : Array of single precision 'stat' variables passed
C              to subroutine evaluating model fp pdf
C     x      : X dimension coordinate of center of a window
C     y      : Y dimension coordinate of center of a window

C     ---- DOUBLE PRECISION VARIABLES ----
C     Gp     : External function to evaluate gradient of Po
C              values in a given direction
C     PIvalue: Value of PI (3.141592...)
C     KLFCN  : External function to evaluate square of KL function
C     var1   : X dimension variance [= sqr(stat(X))]
C     var2   : Y dimension variance [= sqr(stat(Y))]
C     diffvar: Difference in variances [var1 - var2]

C     ================================================================


C     ** CALLING ROUTINE TO COMPUTE MODEL FIBER PRESENCE PROB. **

      ndim=nopt
      sigma(1)=stat(1)
      sigma(2)=stat(2)
      rho=r
      call ModelFpProb(ndim, sigma, rho, Pm)

C     ** ASSIGNING FIBER PRESENCE PROBABILITIES AS Kn OUTCOMES **

C     -- FINDING MAXIMUM VALUE OF Po AT WHICH PROFILE GETS FLAT --
C     -- AND MARKING THE FLAT REGION --
```

```
      if (no_fn_eval.EQ.0) then

C        >> For Error Checking
C        open(unit=10,file='gradpox.dat',status='unknown')
C        do 5 i=2,Wx-1
C           do 3 j=2,Wy-1
C              x=(xbw(i)+xbw(i+1)-1)*CF/2.
C              y=(ybw(j)+ybw(j+1)+1)*CF/2.
C              write(10,2) x, y, Gp(i,j), Po(i,j)
C 2            format(2(2x,f6.2),2(2x,e10.4))
C 3         continue
C 5      continue
C        close(unit=10)

         print*
         print*, '    FINDING MAXIMUM VALUE OF Po AT WHICH PROFILE ',
     +           'GETS FLAT:'
         PoMax=0.
C        -- FINDING FIRST MAXIMUM IN INCREASING X-DIRECTION --
C        -- IGNORING FIRST AND LAST Y WINDOWS, AS THEY COULD --
C        -- HAVE ALL ZERO Po --
         PoMax_ij=0.
         do 20 j=2,Wy-1
            i=2
C           >> IF GRADIENT INCREASES, GO TO NEXT i
C           >> FIRST CHECK FOR GRADIENT INCREASE BETWEEN i AND i+1
 10         if (Gp(i+1,j,'x').GE.Gp(i,j,'x')) then
               i=i+1
               go to 10
C           >> IF GRADIENT DECREASES BETWEEN i AND i+1, THEN
C           >> CHECK FOR GRADIENT INCREASE BETWEEN i AND i+2 TO
C           >> AVOID ANY LOCAL MINIMA
            else if (Gp(i+2,j,'x').GE.Gp(i,j,'x')) then
               i=i+1
               go to 10
C           >> IF GRADIENT DECREASES, SELECT Po(i,j) AS MAXIMUM
C           >> AND MARK i AS X-DIR STARTING POSITION FOR FLAT REGION
            else
               if (Po(i,j).GE.PoMax_ij) then
                  PoMax_ij=Po(i,j)
                  fltB(1)=i+1
               end if
            end if

C           >> CHOOSE MAXIMUM OF ALL MAXIMA FROM ALL j
            PoMax=max(PoMax_ij,PoMax)
 20      continue
         print*, '      PoMax in increasing x-dir =', PoMax_ij

C        -- FINDING FIRST MAXIMUM IN DECREASING Y-DIRECTION --
C        -- AND INCREASING j, STARTING X FROM fltB(1) BOUNDARY --
         PoMax_ij=0.
         do 40 i=fltB(1),Wx-1
            j=2
C           >> IF GRADIENT INCREASES, GO TO NEXT j
C           >> FIRST CHECK FOR GRADIENT INCREASE BETWEEN j AND j+1
 30         if (Gp(i,j+1,'y').GE.Gp(i,j,'y')) then
               j=j+1
               go to 30
C           >> IF GRADIENT DECREASES BETWEEN j AND j+1, THEN
C           >> CHECK FOR GRADIENT INCREASE BETWEEN j AND j+2 TO
```

```
C           >> AVOID ANY LOCAL MINIMA
            else if (Gp(i,j+2,'y').GE.Gp(i,j,'y')) then
               j=j+1
               go to 30
C           >> IF GRADIENT DECREASES, SELECT Po(i,j) AS MAXIMUM
C           >> AND MARK j AS Y-DIR STARTING POSITION FOR FLAT REGION
            else
C              >> CHOOSE MAXIMUM OF ALL MAXIMA FROM ALL i
               if (Po(i,j).GE.PoMax_ij) then
                  PoMax_ij=Po(i,j)
                  fltB(3)=j+1
               end if
            end if

C           >> CHOOSE MAXIMUM OF ALL MAXIMA FROM ALL j
            PoMax=max(PoMax_ij,PoMax)
 40      continue
         print*, '      PoMax in decreasing y-dir =', PoMax_ij

C        -- FINDING SECOND MAXIMUM IN INCREASING Y-DIRECTION --
C        -- AND DECREASING j, STARTING X FROM fltB(1) BOUNDARY --
         PoMax_ij=0.
         do 60 i=fltB(1),Wx-1
            j=Wy-1
C           >> IF ABSOLUTE GRADIENT INCREASES, GO TO PREVIOUS j
C           >> FIRST CHECK FOR ABSOLUTE GRADIENT INCREASE BETWEEN
C           >> j AND j-1
 50         if (abs(Gp(i,j-1,'y')).GE.abs(Gp(i,j,'y'))) then
               j=j-1
               go to 50
C           >> IF ABSOLUTE GRADIENT DECREASES BETWEEN j AND j-1,
C           >> CHECK FOR ABSOLUTE GRADIENT INCREASE BETWEEN j AND j-2
C           >> TO AVOID ANY LOCAL MINIMA
            else if (abs(Gp(i,j-2,'y')).GE.abs(Gp(i,j,'y'))) then
               j=j-1
               go to 50
C           >> IF ABSOLUTE GRADIENT DECREASES, SELECT Po(i,j) AS MAX
C           >> AND MARK j AS Y-DIR ENDING POSITION FOR FLAT REGION
            else
C              >> CHOOSE MAXIMUM OF ALL MAXIMA FROM ALL i
               if (Po(i,j).GE.PoMax_ij) then
                  PoMax_ij=Po(i,j)
                  fltB(4)=j-1
               end if
            end if

C           >> CHOOSE MAXIMUM OF ALL MAXIMA FROM ALL j
            PoMax=max(PoMax_ij,PoMax)
 60      continue
         print*, '      PoMax in increasing y-dir =', PoMax_ij

C        -- FINDING SECOND MAXIMUM IN DECREASING X-DIRECTION --
C        -- STARTING Y FROM fltB(3) AND ENDING AT fltB(4) BOUNDARY --
         PoMax_ij=0.
         do 80 j=fltB(3),fltB(4)
            i=Wx-1
C           >> IF ABSOLUTE GRADIENT INCREASES, GO TO PREVIOUS i
C           >> FIRST CHECK FOR ABSOLUTE GRADIENT INCREASE BETWEEN
C           >> i AND i-1
 70         if (abs(Gp(i-1,j,'x')).GE.abs(Gp(i,j,'x'))) then
               i=i-1
```

```
                go to 70
C            >> IF ABSOLUTE GRADIENT DECREASES BETWEEN i AND i-1,
C            >> CHECK FOR ABSOLUTE GRADIENT INCREASE BETWEEN i AND i-1
C            >> TO AVOID ANY LOCAL MINIMA
             else if (abs(Gp(i-2,j,'x')).GE.abs(Gp(i,j,'x'))) then
                i=i-1
                go to 70
C            >> IF ABSOLUTE GRADIENT DECREASES, SELECT Po(i,j) AS MAX
C            >> AND MARK i AS X-DIR ENDING POSITION FOR FLAT REGION
             else
C               >> CHOOSE MAXIMUM OF ALL MAXIMA FROM ALL j
                if (Po(i,j).GE.PoMax_ij) then
                   PoMax_ij=Po(i,j)
                   fltB(2)=i-1
                end if
             end if

C            >> CHOOSE MAXIMUM OF ALL MAXIMA FROM ALL j
             PoMax=max(PoMax_ij,PoMax)
 80       continue
          print*, '       PoMax in decreasing x-dir =', PoMax_ij

          write(*,90) (fltB(i),i=1,4), PoMax
 90       format(7x,'fltB(X1,X2) = (',I2,',',I2,'); ',
     +                  'fltB(Y1,Y2) = (',I2,',',I2,')',
     +                /7x,'PoMax = ',e14.8)
          print*

C         open(unit=99, file='po58.out', status='unknown')
C         write(99,122)
C 122     format(5x,'x',7x,'y',6x,'Po',6x,'NPo',6x,'Pm',6x,'NPm')

       end if             !FINISHED FINDING PoMax


C      **** NORMALIZING FIBER PRESENCE PROBABILITIES TO AVOID ****
C      **** EVALUATION OF SPATIAL CO-OCCURENCE PROBALITIES IN ****
C      **** FLAT REGION                                       ****
       do 170 i=1,Wx
          do 160 j=1,Wy
             NPo(i,j)=Po(i,j)/PoMax
             NPm(i,j)=Pm(i,j)/PoMax
C            if (no_fn_eval.EQ.0) then
C               x=(xbw(i)+xbw(i+1)-1)*CF/2.
C               y=(ybw(j)+ybw(j+1)+1)*CF/2.
C               write(99,155) x,y,Po(i,j),NPo(i,j),Pm(i,j),NPm(i,j)
C 155           format(2(2x,f6.2),4(2x,f6.4))
C            end if
 160      continue
 170   continue

C      **** EVALUATING pi VALUES ONLY ON FIRST FUNCTION CALL ****
       if (no_fn_eval.LE.0) then
C         -- FINDING Kn, dp AND pi VALUES --
          Kn=50
          pi(Kn)=1.0
          dp=pi(Kn)/float(Kn)
C         print*, 'dp=',dp

C         print 175, no_fn_eval, Kn, pi(Kn)
 175      format(10x,I2,':  pi(',I3,')=',f7.5)
```

```
         do 180 k=Kn-1,1,-1
            pi(k)=pi(k+1)-dp
C           print 175, no_fn_eval, k, pi(k)
 180     continue

C        close(unit=99)
      end if

C     print*

C     **** CALLING FUNCTION TO EVALUATE SQUARED KL FUNCTION ****
      FCNvalue=KLFCN(NPo, NPm, Wx, Wy, pi, dp, Kn)

C     **** EVALUATING THETA FUNCTION ****
      var1=stat(1)**2.
      var2=stat(2)**2.
      diffvar=var1-var2
      ThetaFCN=2.*rho*stat(1)*stat(2)/diffvar
      ThetaFCN=(ThetaFCN-dtan(2.*t*PIvalue/180.))**2.

C     **** EVALUATING FINAL OBJECTIVE FUNCTION ****
      FCNvalue=FCNvalue+ThetaFCN

C     -- INCREMENTING FUNCTION CALL VARIABLE --
      no_fn_eval=no_fn_eval+1

C     **** PRINTING STATUS OF PROGRAM EVERY 40 FUNCTION CALLS ****
      if (.NOT.print_flag.AND.mod(no_fn_eval,40).EQ.0) then
         print 240, no_fn_eval
 240     format(/5x,42('-')
     +          /5x,'>> STATUS: ',I4,' FUNCTION EVALUATIONS DONE!'
     +          /5x,42('-'))

C        >> USED FOR ERROR CHECKING
C        print 250, no_fn_eval, (stat(i),i=1,nopt), FCN
 250     format(/5x,'INTERMEDIATE FUNCTION EVALUATION ',
     +          I3,':',/5x,40('-'),/
     +          7x,'sigma(X)       = ',e14.8,/
     +          7x,'sigma(Y)       = ',e14.8,/
     +          7x,'KLF VALUE      = ',e14.8/)
      end if


      RETURN
      END

*************************************************************************

      DOUBLE PRECISION FUNCTION Gp(i,j,dir)

C     **** DECLARATION OF ARGUMENT VARIABLES ****
      CHARACTER dir*1
      INTEGER i, j
      REAL Po(35,35), xbw(36), ybw(36), CF

C     **** DECLARATION OF LOCAL VARIABLES ****
      DOUBLE PRECISION dXi, dPo

C     ** UNUSED VARIABLES **
      INTEGER Wx, Wy
      REAL mu(2), r, t
```

```
      COMMON /OBSERVED/ mu, r, Wx, Wy, Po, xbw, ybw, CF, t

C     **** DEFINITION OF LOCAL VARIABLES ****
C     ---- DOUBLE PRECISION VARIABLES ----
C     dXi   : Central difference delta displacement
C     dPo   : Central difference delta probability


C     **** FINDING DELTA DISPLACEMENT AND PROBABILITY ****
      if (dir.EQ.'x') then
C        >> X VALUES INCREASE AS i INCREASES
         dXi=CF*(xbw(i+1)-xbw(i-1))
         dPo=Po(i+1,j)-Po(i-1,j)
      else
C        >> Y VALUES DECREASE AS j INCREASES
         dXi=CF*(ybw(j-1)-ybw(j+1))
         dPo=Po(i,j+1)-Po(i,j-1)
      end if

C     **** CENTRAL DIFFERENCE GRADIENT ****
      Gp=dPo/dXi


C     print 10, i, j, Po(i,j), dXi, dir, Gp
 10   format(7x,'Po(',I2,',',I2,') = ',e10.4,'; dXi = ',f6.2,
     +             '; Grad Po(',A1,') = ',e10.4)

      RETURN
      END

*****************************************************************************

      DOUBLE PRECISION FUNCTION KLFCN(NPo, NPm, Wx, Wy, pi, dp, Kn)

C     **** DECLARATION OF ARGUMENT VARIABLES ****
      CHARACTER infile*12, prob_dat*12, statfile*12, sp_file*18
      INTEGER Wx, Wy, Kn
      REAL NPo(35,35), NPm(35,35), pi(250), dp
      LOGICAL print_flag, spatial_print

      COMMON /FILES/ infile, prob_dat, statfile, sp_file

C     **** DECLARATION OF LOCAL VARIABLES ****
      INTEGER i, j, k, k1, k2, hx_i, hy_i, ufileno, ofileno
      INTEGER hx(12), hy(12)
      DATA hx /0,1,1, 1,-1,0,1,2,2,2, 2, 2/
      DATA hy /1,1,0,-1, 2,2,2,2,1,0,-1,-2/
C     DATA hx /0,1,1,1,-1,0,1,2,2,2,2,2,2,-2,-1,0,1,2,3,3,3,3,3,3,3/
C     DATA hy /1,1,0,-1,2,2,2,2,1,0,-1,-2,3,3,3,3,3,3,2,1,0,-1,-2,-3/
      CHARACTER filename*12, command*80
      REAL P1, P1_dP, P2, P2_dP, CDF, SpdfTol
      DOUBLE PRECISION f(30000), g, SpPDF, fINT(24), gINT(24),
     +                 SpoCDF, SpmCDF, KLFsum, dummy
      DOUBLE PRECISION KLF

      COMMON /OPTIMIZED/ dummy, KLF
      COMMON /PRINTING/ print_flag, spatial_print

      EXTERNAL CDF, SYSTEM

      INTEGER count
```

```
      SAVE f, count

      DATA SpdfTol /1.E-06/, count /0/

C     ================================================================

C     **** DEFINITION OF LOCAL VARIABLES ****

C     ---- CHARACTER VARIABLES ----
C     filename: Character array for storing spatial probability files
C     command : Command to archive spatial probability files

C     ---- INTEGER VARIABLES ----
C     k1    : Loop index for p values (for first window of pair)
C     k2    : Loop index for p' values (for second window of pair)
C     hx    : Array of X dimensions of the lag vectors
C     hy    : Array of Y dimensions of the lag vectors
C     hx_i  : X dimension of ith lag vector passed to CDF function
C     hy_i  : Y dimension of ith lag vector passed to CDF function
C     ufileno: Unit numbers of unoptimized spatial probability files
C     ofileno: Unit numbers of optimized spatial probability files
C     count : Counts number of function calls.  It is needed as
C             observed spatial co-occurrence probabilities are
C             computed only on first function call as they remain
C             constant for an image

C     ---- REAL VARIABLES ----
C     P1    : 1st window p value for which spatial PDF is computed
C     P1_dP : p+dp for finite difference numerical approximation of
C             derivative to compute spatial PDF
C     P2    : 2st window p' value for which spatial PDF is computed
C     P1_dP : p'+dp for finite difference numerical approximation
C             of derivative to compute spatial PDF
C     CDF   : External function to compute spatial CDF
C     SpdfTol: Spatial pdf tolerance.  It is the tolerance allowed
C             for SpPDF to become greater than 1.0 in case of
C             numerical instability caused due to finite difference
C             gradient approximation.  It is also used when SpPDF
C             becomes less than SpdfTol but greater than 0.0,
C             f or g is set to 0.0

C     ---- DOUBLE PRECISION VARIABLES ----
C     f     : Array of observed spatial co-occurrence PDF (computed
C             on first call only, saved for rest of the program)
C     g     : Model spatial co-occurrence PDF
C     SpPDF : Spatial PDF at each of p and p' value
C     fINT  : Array of integral of observed spatial PDF at each lag
C             distance, 'h'.  Each must be less than equal to 1.0
C             fINT = INTEGRAL ( INTEGRAL (f dp) dp')
C     gINT  : Array of integral of model spatial PDF at each lag
C             distance, 'h'.  Each must be less than equal to 1.0
C             gINT = INTEGRAL ( INTEGRAL (g dp) dp')
C     SpoCDF: Observed spatial CDF
C     SpmCDF: Model spatial CDF
C     KLFsum: Sum of KL functions over all Cartesian lag distances
C     dummy : Dummy variable corresponding to ThetaFCN evaluated
C             in FCN subroutine.  Since it is computed after calling
C             this function, its value from this function is
C             overwritten in FCN subroutine
C     KLF   : Value of KLF function (not squared) passed to
C             subroutine Minimize through 'OPTIMIZED' common block
```

```
C     ================================================================

C     ** SETTING FILENAMES AND OPENING FILES FOR SPATIAL PDF & CDF **
      if (spatial_print .AND. count.EQ.0) then
         ufileno=11
         do 10 i=1,12
            open(unit=90,status='scratch')
C           >> ATTACH LAG INDEX TO FILENAME & STORE IT IN SCRATCH FILE
            if (i.GE.10) then
               write(90,3) i
 3             format('spun_h',I2)
            else
             write(90,4) i
 4             format('spun_h',I1)
            end if
            rewind(90)
            read(90,5) filename
 5          format(A8)
            close(unit=90,status='delete')

C           >> ATTACH '.dat' EXTENSION TO SPATIAL FILENAME
            filename=filename(:INDEX(filename,' ')-1)//'.dat'
            open(unit=ufileno, file=filename, status='unknown')
            write(ufileno,8)
 8          format(4x,'p1',5x,'p2',7x,'f',6x,'SpoCDF',7x,'g',6x,
     +                    'SpmCDF')
            ufileno=ufileno+1
 10      continue
         ufileno=11
      end if

      if (spatial_print .AND. print_flag) then
         ofileno=31
         do 20 i=1,12
            open(unit=90,status='scratch')
C           >> ATTACH LAG INDEX TO FILENAME & STORE IT IN SCRATCH FILE
            if (i.GE.10) then
               write(90,12) i
 12            format('spop_h',I2)
            else
             write(90,14) i
 14            format('spop_h',I1)
            end if
            rewind(90)
            read(90,16) filename
 16         format(A8)
            close(unit=90,status='delete')

C           >> ATTACH '.dat' EXTENSION TO SPATIAL FILENAME
            filename=filename(:INDEX(filename,' ')-1)//'.dat'
            open(unit=ofileno, file=filename, status='unknown')
            write(ofileno,8)
            ofileno=ofileno+1
 20      continue
         ofileno=31
      end if

C     ** FOR EACH LAG VECTOR h=[hx,hy], COMPUTING KL-FUNCTION **

      KLFsum=0.0
      j=1
```

```
      do 80 i=1,12
         fINT(i)=0.
         gINT(i)=0.
         hx_i=hx(i)
         hy_i=hy(i)
C        print 25, hx(i), hy(i)
C 25     format(1x,'hx=',I2,'; hy=',I2)

C        -- SUMMING SPATIAL PDF OVER ALL pi VALUES FOR 1ST WIN --
         do 70 k1=1,Kn
            P1=pi(k1)

C           -- SUMMING SPATIAL PDF OVER ALL pi VALUES FOR 2ND WIN --
            do 60 k2=1,Kn
               P2=pi(k2)

               if (count.EQ.0) then
C                 -- COMPUTING OBSERVED SPATIAL PDF --
                  SpPDF=( CDF(NPo,(P1+dp),(P2+dp),hx_i,hy_i,Wx,Wy)
     +                        -CDF(NPo,(P1-dp),(P2+dp),hx_i,hy_i,Wx,Wy)
     +                        -CDF(NPo,(P1+dp),(P2-dp),hx_i,hy_i,Wx,Wy)
     +                        +CDF(NPo,(P1-dp),(P2-dp),hx_i,hy_i,Wx,Wy)
     +                        )/(4.0*dp**2.)

C                  >> IF SpPDF BECOMES GREATER THAN 1.0 DUE TO
C                  >> APPROXIMATION OF FINITE DIFFERENCE GRADIENT, SET
C                  >> SpPDF TO 1.0
                     if (SpPDF.GT.1.) then
                        if ((SpPDF-1.).LE.SpdfTol) then
                           print 30, SpPDF-1.,hx(i),hy(i),P1,P2
 30                        format(/4x,'SpPDF:Po > 1.0 by ',e9.4,/4x,
     +                           'at h=(',I2,1x,I2,'); P1=',f7.5,'; P2=',
     +                           f7.5/,4x,'** SpPDF set to 1.0 **')
                        end if
                        SpPDF=1.0
                     end if

                     f(j)=SpPDF
                     fINT(i)=fINT(i)+f(j)*(dp**2)

C                    >> IF f(j) IS GREATER THAN ZERO BY SpdfTol, f(j)=0.0
                     if (f(j).LT.SpdfTol.AND.f(j).NE.0.0) then
C                       print 35, f(j)
C 35                    format(8x,'f=',e10.4)
                        f(j)=0.0
                     end if

                  end if           !of if (count.EQ.0)

C                    -- COMPUTING MODEL SPATIAL PDF --
                     SpPDF=( CDF(NPm,(P1+dp),(P2+dp),hx_i,hy_i,Wx,Wy)
     +                       -CDF(NPm,(P1-dp),(P2+dp),hx_i,hy_i,Wx,Wy)
     +                       -CDF(NPm,(P1+dp),(P2-dp),hx_i,hy_i,Wx,Wy)
     +                       +CDF(NPm,(P1-dp),(P2-dp),hx_i,hy_i,Wx,Wy)
     +                      )/(4.0*dp**2.)

C                    >> IF SpPDF BECOMES GREATER THAN 1.0 DUE TO
C                    >> APPROXIMATION OF FINITE DIFFERENCE GRADIENT, SET
C                    >> SpPDF TO 1.0
                     if (SpPDF.GT.1.) then
                        if ((SpPDF-1.).LE.SpdfTol) then
```

```
                  print 40, SpPDF-1.,hx(i),hy(i),P1,P2
 40               format(/4x,'SpPDF:Pm > 1.0 by ',e9.4,/
     +                    4x,'at h=(',I2,1x,I2,'); P1=',f7.5,'; P2=',
     +                    f7.5/,4x,'** SpPDF set to 1.0 **')
               end if
               SpPDF=1.0
            end if

            g=SpPDF

            gINT(i)=gINT(i)+g*(dp**2)

C           >> IF g IS GREATER THAN ZERO BY SpdfTol, g = 0.0
            if (g.LT.SpdfTol.AND.g.NE.0.0) then
C              print 45, g
C 45           format(8x,'g=',e10.4)
               g=0.0
            end if

C           -- CALCULATING KL-FUNCTION --
            if (f(j).NE.0.0.AND.g.NE.0.0) then
               KLFsum=KLFsum+f(j)*dlog(f(j)/g)
            end if

C           -- PRINTING SPATIAL PDF AND CDF WHEN FLAGGED --
            if (spatial_print.AND.(count.EQ.0.OR.print_flag)) then
               SpoCDF=CDF(NPo,P1,P2,hx_i,hy_i,Wx,Wy)
               SpmCDF=CDF(NPm,P1,P2,hx_i,hy_i,Wx,Wy)
               if (count.EQ.0) then
                  write(ufileno,55) P1,P2,f(j),SpoCDF,g,SpmCDF
               else if (print_flag) then
                  write(ofileno,55) P1,P2,f(j),SpoCDF,g,SpmCDF
               end if
 55            format(2(2x,f5.3),4(2x,f8.6))
            end if

C           -- INCREMENTING INDEX FOR f(j) --
            j=j+1
 60         continue
 70      continue

C        -- INCREMENTING SPATIAL FILE UNIT NOS. --
         if (spatial_print.AND.(count.EQ.0.OR.print_flag)) then
            ufileno=ufileno+1
            ofileno=ofileno+1
         end if
C        print*, '---------------------------------'
 80   continue

C     **** AVERAGING KL FUNCTION OVER 12 LAG DISTANCES ****
      KLF=KLFsum/12.

C     ** SQUARING KL FUNCTION AS REQUIRED FOR OBJECTIVE FUNCTION **
      KLFCN=KLF**2.

C     ** CLOSING SPATIAL PDF AND CDF FILES WHEN FLAGGED **
      if (spatial_print .AND. count.EQ.0) then
         ufileno=11
         do 110 i=1,12
            close(unit=ufileno)
            ufileno=ufileno+1
```

```
 110     continue
      end if

      if (spatial_print .AND. print_flag) then
         ofileno=31
         do 120 i=1,12
            close(unit=ofileno)
            ofileno=ofileno+1
 120     continue
         write(*,'(5x,''ARCHIVING, THEN REMOVING SPATIAL FILES '',
     +                 ''USING:'')')
         command='tar -cv -f '//sp_file(:INDEX(sp_file,' ')-1)
     +          //' sp*.dat; gzip -fv '//sp_file(:INDEX(sp_file,' ')-1)
     +          //'; rm sp*.dat\0'
         write(*,'(5x,A/)') command
         i=SYSTEM(command)
      end if

C     **** INCREMENTING FUNCTION EVALUATION COUNT ****
      count=count+1

      RETURN
      END

*************************************************************************

      REAL FUNCTION CDF(P, Pa, Pb, hi, hj, Wx, Wy)

C     **** DECLARATION OF ARGUMENT VARIABLES ****

      INTEGER hi, hj, Wx, Wy
      REAL P(35,35), Pa, Pb

C     **** DECLARATION OF LOCAL VARIABLES ****

      INTEGER x, y, x_h, y_h
      REAL Pxy, Pxy_h, no_pairs, total_pairs, n_win

C     **** VARIABLE USED FOR PRINTING WHILE DEBUGGING ****
      INTEGER counter, i
      SAVE counter, i
      DATA counter,i /2*0/

C     ================================================================

C     **** DEFINITION OF LOCAL VARIABLES ****

C     ---- INTEGER VARIABLES ----
C     x      : Index of windows in X dimension
C     y      : Index of windows in Y dimension
C     x_h    : Index of (x+hi) lagged window in X dimension
C     y_h    : Index of (y+hj) lagged window in Y dimension
C     counter: Function evaluation counter (error checking)
C     i      : Counter for function evaluations when CDF = 1.0

C     ---- REAL VARIABLES ----
C     Pxy    : Normalized fiber presence probability of (x,y) window
C     Pxy_h  : Normalized fp probability of (x+hi, y+hj) window
C     n_win  : Total number of windows in the image
C     total_pairs: Total number of pairs that can be possibly
C              selected from n_win windows, Combinatorial(n_win,2)
```

```
C     no_pairs: Number of pairs of windows in the image with 1st
C               window having fp probability < = Pa and the 2nd
C               window, lagging from 1st window by given vector
C               (hi,hj),having fp probability < = Pb.  Both windows
C               have to be in the image to be considered

C     ================================================================

      n_win=float(Wx*Wy)
      total_pairs=n_win*(n_win-1.)/2.
      no_pairs=0.
      do 20 x=1,Wx
         x_h=x+hi
         do 10 y=1,Wy
            Pxy_h=0.
            y_h=y+hj

C           >> If second window of the pair [x+hi, y+hj] is out of
C           >> image, then the pair is ignored

            if (x_h.LE.Wx.AND.y_h.LE.Wy.AND.y_h.GE.0) then
               Pxy=P(x,y)
               Pxy_h=P(x_h, y_h)

C              -- CHECKING IF (Pxy <= Pa) AND (Pxy_h <= Pb) --
               if ((Pxy.LE.Pa).AND.(Pxy_h.LE.Pb)) then
                  no_pairs=no_pairs+1.
               end if

C              ---- ERROR CHECKING ----
C              if (counter.EQ.0.AND.x.EQ.1.AND.y.EQ.Wy-1) then
C                     print 5, Pxy, Pxy_h, hi, hj
C 5                 format(1x,'Pxy=',f6.4,'; Pxy_h=',f6.4,'; h=',I2,
C     +                       1x,I2)
C              end if
            end if
 10      continue
 20   continue

C     **** EVALUATING CDF FUNCTION ****
      CDF=no_pairs/total_pairs

      counter=counter+1

C     **** ERROR CHECKING ****
C     if (mod(counter,100).EQ.0.OR.no_pairs.EQ.total_pairs) then
C     if (no_pairs.EQ.total_pairs) then
C        i=i+1
C        print 30, i, hi, hj, no_pairs, total_pairs
C 30     format(1x,I8,': h=(',I2,1x,I2,'); np=',f7.0,'; tp=',f7.0)
C     end if

      RETURN
      END

*************************************************************************

      SUBROUTINE ModelFpProb(ndim, sigma, rho, Pm)

C     **** DECLARATION OF ARGUMENT VARIABLES ****
```

```
      INTEGER Wx, Wy, ndim
      REAL Po(35,35), mu(2), sigma(2), rho, xbw(36), ybw(36), CF,
     +           Pm(35,35), r, t

      COMMON /OBSERVED/ mu, r, Wx, Wy, Po, xbw, ybw, CF, t

C     **** DECLARATION OF LOCAL VARIABLES ****

      INTEGER i, j
      LOGICAL x0_exists, y0_exists
      REAL zx(36), zy(36), zxlt0, zxgt0, zylt0, zygt0

C     ================================================================

C     **** DEFINITION OF LOCAL VARIABLES ****

C     ---- INTEGER VARIABLES ----
C     i     : Window index in X dimension
C     j     : Window index in Y dimension

C     ---- LOGICAL VARIABLES ----
C     x0_exists: Indicates whether x axis exists in a window.
C     y0_exists: Indicates whether y axis exists in a window.
C        Needed for a situation when x and y axes cross in a
C        window.  The fp probability is not to be evaluated
C        for the width of the axes.  To avoid the
C        subtraction of cross-over region of the axes twice
C        from the calculations, logical variables are required.

C     ---- REAL VARIABLES ----
C     zx    : Array of normalized X coordinates of windows
C     zy    : Array of normalized Y coordinates of windows
C     zxlt0 : Normalized X dimension position calculated as 1.5
C             pixel lengths less than zero position (axes are
C             3 pixels wide and are to be ignored)
C     zxgt0 : Normalized X dimension position calculated as 1.5
C             pixel lengths greater than zero position
C     zylt0 : Normalized Y dimension position calculated as 1.5
C             pixel lengths less than zero position
C     zygt0 : Normalized Y dimension position calculated as 1.5
C             pixel lengths greater than zero position

C     ================================================================


C     **** CALCULATING BIVARIATE NORMAL DISTRIBUTION ****

C     -- NORMALIZING CELL BOUNDARIES --

C     print 5
C 5   format(6x,'bw',7x,'z')
      do 10 i=1,Wx+1
         zx(i)=(xbw(i)*CF-mu(1))/sigma(1)
C        print 25, xbw(i)*CF, zx(i)
 10   continue

C     print*
      do 20 j=1,Wy+1
         zy(j)=(ybw(j)*CF-mu(2))/sigma(2)
C        print 25, ybw(j)*CF, zy(j)
 20   continue
```

```
C     -- NORMALIZING X-BOUNDARIES OF 3 PIXELS WIDE X AXIS LINE --
      zxlt0=((0.-3.*CF/2.)-mu(1))/sigma(1)
      zxgt0=((0.+3.*CF/2.)-mu(1))/sigma(1)
C     print*
C     print 25, zxlt0, zxgt0

C     -- NORMALIZING Y-BOUNDARIES OF 3 PIXELS WIDE Y AXIS LINE --
      zylt0=((0.-3.*CF/2.)-mu(2))/sigma(2)
      zygt0=((0.+3.*CF/2.)-mu(2))/sigma(2)
C     print 25, zylt0, zygt0
C 25  format(2(2x,f7.4))

C     -- EVALUATING PROBABILITY INTEGRAL USING IMSL ROUTINE BNRDF --

      do 40 i=1,Wx
         do 30 j=Wy,1, -1
            x0_exists=.FALSE.
            y0_exists=.FALSE.

            Pm(i,j)= BNRDF(zx(i+1), zy(j), rho)
     +              -BNRDF(zx(i+1), zy(j+1), rho)
     +              -BNRDF(zx(i), zy(j), rho)
     +              +BNRDF(zx(i), zy(j+1), rho)

C           >> X axis line is 3 pixels wide and is to be ignored
C           >> for evaluating binormal probabilty integral of cell
            if (xbw(i).LT.0.0.AND.xbw(i+1).GT.0.0) then
               Pm(i,j)=Pm(i,j)-( BNRDF(zxgt0, zy(j), rho)
     +                 -BNRDF(zxgt0, zy(j+1), rho)
     +                 -BNRDF(zxlt0, zy(j), rho)
     +                 +BNRDF(zxlt0, zy(j+1), rho) )
               x0_exists=.TRUE.
            end if

C           >> Y axis line is 3 pixels wide and is to be ignored
C           >> for evaluating binormal probabilty integral of cell
            if (ybw(j+1).LT.0.0.AND.ybw(j).GT.0.0) then
               Pm(i,j)=Pm(i,j)-( BNRDF(zx(i+1), zygt0, rho)
     +                 -BNRDF(zx(i+1), zylt0, rho)
     +                 -BNRDF(zx(i), zygt0, rho)
     +                 +BNRDF(zx(i), zylt0, rho) )
               y0_exists=.TRUE.
            end if

C           >> if both X axis and Y axis exist in a cell and both
C           >> have been ignored, the pixel width corresponding to
C           >> actual zero position is ignored twice.  Therefore,
C           >> probability integral of the pixel has to added
            if (x0_exists.AND.y0_exists) then
               Pm(i,j)=Pm(i,j)+( BNRDF(zxgt0,zygt0,rho)
     +            -BNRDF(zxgt0,zylt0,rho)-BNRDF(zxlt0,zygt0,rho)
     +            +BNRDF(zxlt0,zylt0,rho) )
            end if
 30      continue
 40   continue

C     **** ERROR CHECKING ****
C     print*, 'Po Integral'
C     do 50 i=1,Wx
C        print 65, (Po(i,j), j=1,Wy)
C 50  continue
```

```
C     print*
C     print*, 'Pm Integral'
C     do 60 i=1,Wx
C        print 65, (Pm(i,j), j=1,Wy)
C 60  continue
C
C 65  format(17(1x,f6.4))

      RETURN
      END
```

****

```
cccccccccccccccccccccccccccccccccccccccccccccccccccccccccccccccccccccccc
C                                                                      C
C FILENAME: anneal.f                                                   C
C [Modified form of the routine developed by Goffe et al. (1994)]      C
C                                                                      C
C ABSTRACT:                                                            C
C Simulated annealing is a global optimization method that             C
C distinguishes between different local optima. Starting from an       C
C initial point, the algorithm takes a step and the function is        C
C evaluated. When minimizing a function, any downhill step is          C
C accepted and the process repeats from this new point. An uphill      C
C step may be accepted. Thus, it can escape from local optima. This    C
C uphill decision is made by the Metropolis criteria. As the           C
C optimization process proceeds, the length of the steps decline and   C
C the algorithm closes in on the global optimum. Since the algorithm   C
C makes very few assumptions regarding the function to be optimized,   C
C it is quite robust with respect to non-quadratic surfaces. The       C
C degree of robustness can be adjusted by the user. In fact,           C
C simulated annealing can be used as a local optimizer for difficult   C
C functions.                                                           C
C                                                                      C
C This implementation of simulated annealing was used in "Global       C
C Optimization of Statistical Functions with Simulated Annealing,"     C
C Goffe, Ferrier and Rogers, Journal of Econometrics, vol. 60,         C
C no. 1/2, Jan./Feb. 1994, pp.65-100. Briefly, we found it             C
C competitive, if not superior, to multiple restarts of conventional   C
C optimization routines for difficult optimization problems.           C
C                                                                      C
C For more information on this routine, contact its author:            C
C Bill Goffe, bgoffe@whale.st.usm.edu                                  C
C                                                                      C
C To understand the algorithm, the documentation for SA on lines 236-  C
C 484 should be read along with the parts of the paper that describe   C
C simulated annealing. Then the following lines will aid the user      C
C in becomming proficient with this implementation of simulated        C
C annealing.                                                           C
C                                                                      C
C Learning to use SA:                                                  C
C Use the sample function from Judge with the following suggestions    C
C to get a feel for how SA works. When you've done this, you should    C
C be ready to use it on most any function with a fair amount of        C
C expertise.                                                           C
C 1. Run the program as is to make sure it runs okay. Take a look at   C
C    the intermediate output and see how it optimizes as temperature   C
C    (T) falls. Notice how the optimal point is reached and how        C
C    falling T reduces VM.                                             C
C 2. Look through the documentation to SA so the following makes a     C
C    bit of sense. In line with the paper, it shouldn't be that hard   C
C    to figure out. The core of the algorithm is described on          C
C    pp. 68-70 and on pp. 94-95. Also see Corana et al. pp. 264-9.     C
C 3. To see how it selects points and makes decisions about uphill     C
C    and downhill moves, set IPRINT = 3 (very detailed intermediate    C
C    output) and MAXEVL = 100 (only 100 function evaluations to limit  C
C    output).                                                          C
C 4. To see the importance of different temperatures, try starting     C
C    with a very low one (say T = 10E-5). You'll see (i) it never      C
C    escapes from the local optima (in annealing terminology, it       C
C    quenches) & (ii) the step length (VM) will be quite small. This   C
C    is a key part of the algorithm: as temperature (T) falls, step    C
C    length does too. In a minor point here, note how VM is quickly    C
C    reset from its initial value. Thus, the input VM is not very      C
```

```
C     important. This is all the more reason to examine VM once the    C
C     algorithm is underway.                                           C
C  5. To see the effect of different parameters and their effect on    C
C     the speed of the algorithm, try RT = .95 & RT = .1. Notice the   C
C     vastly different speed for optimization. Also try NT = 20. Note  C
C     that this sample function is quite easy to optimize, so it will C
C     tolerate big changes in these parameters. RT and NT are the      C
C     parameters one should adjust to modify the runtime of the        C
C     algorithm and its robustness.                                    C
C  6. Try constraining the algorithm with either LB or UB.            C
C                                                                      C
CCCCCCCCCCCCCCCCCCCCCCCCCCCCCCCCCCCCCCCCCCCCCCCCCCCCCCCCCCCCCCCCCCCCCCCCC

**************************************************************************

      SUBROUTINE SIM_ANNEAL(N, X, LB, UB, XOPT, FOPT)

      PARAMETER (NEPS = 4)

      DOUBLE PRECISION  LB(N), UB(N), X(N), XOPT(N), C(N), VM(N),
     1                  FSTAR(NEPS), XP(N), T, EPS, RT, FOPT

      INTEGER  NACP(N), NS, NT, NFCNEV, IER, ISEED1, ISEED2,
     1         MAXEVL, IPRINT, NACC, NOBDS

      LOGICAL  MAX

      EXTERNAL FCN

C  Set underflows to zero on IBM mainframes.
C     CALL XUFLOW(0)

C  Set input parameters.
      MAX = .FALSE.
      EPS = 1.0D-5
      RT = .5
      ISEED1 = 1
      ISEED2 = 2
      NS = 20
      NT = 2
      MAXEVL = 3500
      IPRINT = 2
      DO 10, I = 1, N
         C(I) = 2.0
10    CONTINUE

C  Set input values of the input/output parameters.
      T = 5.0
      DO 20, I = 1, N
         VM(I) = 1.0
 20   CONTINUE

      WRITE(*,1000) N, T, RT, EPS, NS, NT, NEPS, MAXEVL

      CALL PRTVEC(X,N,'STARTING VALUES')
      CALL PRTVEC(VM,N,'INITIAL STEP LENGTH')
      CALL PRTVEC(LB,N,'LOWER BOUND')
      CALL PRTVEC(UB,N,'UPPER BOUND')
      CALL PRTVEC(C,N,'C VECTOR')
      WRITE(*,'(/,5x,''**** END OF DRIVER ROUTINE OUTPUT ****''
     1          /,5x,''**** BEFORE CALL TO SA.           ****'')')
```

```
      CALL SA(N,X,MAX,RT,EPS,NS,NT,NEPS,MAXEVL,LB,UB,C,IPRINT,ISEED1,
     1         ISEED2,T,VM,XOPT,FOPT,NACC,NFCNEV,NOBDS,IER,
     2         FSTAR,XP,NACP)

      WRITE(*,'(/,5x,''****   RESULTS AFTER SA   ****   '')')
      CALL PRTVEC(XOPT,N,'SOLUTION')
      CALL PRTVEC(VM,N,'FINAL STEP LENGTH')
      WRITE(*,1001) FOPT, NFCNEV, NACC, NOBDS, T, IER

1000  FORMAT(/,5x,38('-'),
     1       /,5x,'STARTING SIMULATED ANNEALING ALGORITHM',
     2       /,5x,38('-')/,
     3       /,5x,'NUMBER OF PARAMETERS:       ',I1,
     4       /,5x,'INITIAL TEMP:             ',F5.1,
     5       /,5x,'TEMP REDUCTION FACTOR, RT: ',F5.2,
     6       /,5x,'EPS:                        ',E10.4,
     7       /,5x,'NO OF CYCLES, NS:         ',I3,
     8       /,5x,'NO OF ITERATIONS, NT:      ',I2,
     9       /,5x,'NEPS:                       ',I2,
     +       /,5x,'MAXEVL:                   ',I5/)

1001  FORMAT(/5x,50('='),
     +       /5x,'OPTIMAL FUNCTION VALUE:              ',E14.4,
     1       /5x,'NUMBER OF FUNCTION EVALUATIONS:      ',I5,
     2       /5x,'NUMBER OF ACCEPTED EVALUATIONS:      ',I5,
     3       /5x,'NUMBER OF OUT OF BOUND EVALUATIONS: ',I5,
     4       /5x,'FINAL TEMP:                          ',E14.4,
     5       /5x,'IER:                                 ',I5,
     6       /5x,50('='))

      RETURN
      END

*************************************************************************

      SUBROUTINE SA(N,X,MAX,RT,EPS,NS,NT,NEPS,MAXEVL,LB,UB,C,IPRINT,
     1              ISEED1,ISEED2,T,VM,XOPT,FOPT,NACC,NFCNEV,NOBDS,IER,
     2              FSTAR,XP,NACP)

C  Synopsis:
C  This routine implements the continuous simulated annealing global
C  optimization algorithm described in Corana et al.'s article
C  "Minimizing Multimodal Functions of Continuous Variables with the
C  "Simulated Annealing" Algorithm" in the September 1987 (vol. 13,
C  no. 3, pp. 262-280) issue of the ACM Transactions on Mathematical
C  Software.
C
C  A very quick (perhaps too quick) overview of SA:
C     SA tries to find the global optimum of an N dimensional function.
C  It moves both up and downhill and as the optimization process
C  proceeds, it focuses on the most promising area.
C     To start, it randomly chooses a trial point within the step length
C  VM (a vector of length N) of the user selected starting point. The
C  function is evaluated at this trial point and its value is compared
C  to its value at the initial point.
C     In a maximization problem, all uphill moves are accepted and the
C  algorithm continues from that trial point. Downhill moves may be
C  accepted; the decision is made by the Metropolis criteria. It uses T
C  (temperature) and the size of the downhill move in a probabilistic
```

```
C  manner. The smaller T and the size of the downhill move are, the more
C  likely that move will be accepted. If the trial is accepted, the
C  algorithm moves on from that point. If it is rejected, another point
C  is chosen instead for a trial evaluation.
C     Each element of VM periodically adjusted so that half of all
C  function evaluations in that direction are accepted.
C     A fall in T is imposed upon the system with the RT variable by
C  T(i+1) = RT*T(i) where i is the ith iteration. Thus, as T declines,
C  downhill moves are less likely to be accepted and the percentage of
C  rejections rise. Given the scheme for the selection for VM, VM falls.
C  Thus, as T declines, VM falls and SA focuses upon the most promising
C  area for optimization.
C
C  The importance of the parameter T:
C     The parameter T is crucial in using SA successfully. It influences
C  VM, the step length over which the algorithm searches for optima. For
C  a small intial T, the step length may be too small; thus not enough
C  of the function might be evaluated to find global optima. The user
C  should carefully examine VM in the intermediate output (set IPRINT =
C  1) to make sure that VM is appropriate. The relationship between the
C  initial temperature and the resulting step length is function
C  dependent.
C     To determine the starting temperature that is consistent with
C  optimizing a function, it is worthwhile to run a trial run first. Set
C  RT = 1.5 and T = 1.0. With RT > 1.0, the temperature increases and VM
C  rises as well. Then select the T that produces a large enough VM.
C
C  For modifications to the algorithm and many details on its use,
C  (particularly for econometric applications) see Goffe, Ferrier
C  and Rogers, "Global Optimization of Statistical Functions with
C  Simulated Annealing," Journal of Econometrics, vol. 60, no. 1/2,
C  Jan./Feb. 1994, pp. 65-100.
C
C  In this description, SP is single precision, DP is double precision,
C  INT is integer, L is logical and (N) denotes an array of length n.
C  Thus, DP(N) denotes a double precision array of length n.
C
C  Input Parameters:
C    Note: The suggested values generally come from Corana et al. To
C          drastically reduce runtime, see Goffe et al., pp. 90-1 for
C          suggestions on choosing the appropriate RT and NT.
C    N - Number of variables in the function to be optimized. (INT)
C    X - The starting values for the variables of the function to be
C        optimized. (DP(N))
C    MAX - Denotes whether the function should be maximized or
C          minimized. A true value denotes maximization while a false
C          value denotes minimization. Intermediate output (see IPRINT)
C          takes this into account. (L)
C    RT - The temperature reduction factor. The value suggested by
C         Corana et al. is .85. See Goffe et al. for more advice. (DP)
C    EPS - Error tolerance for termination. If the final function
C          values from the last neps temperatures differ from the
C          corresponding value at the current temperature by less than
C          EPS and the final function value at the current temperature
C          differs from the current optimal function value by less than
C          EPS, execution terminates and IER = 0 is returned. (EP)
C    NS - Number of cycles. After NS*N function evaluations, each
C         element of VM is adjusted so that approximately half of
C         all function evaluations are accepted. The suggested value
C         is 20. (INT)
C    NT - Number of iterations before temperature reduction. After
```

```
C         NT*NS*N function evaluations, temperature (T) is changed
C         by the factor RT. Value suggested by Corana et al. is
C         MAX(100, 5*N). See Goffe et al. for further advice. (INT)
C    NEPS - Number of final function values used to decide upon termi-
C           nation. See EPS. Suggested value is 4. (INT)
C    MAXEVL - The maximum number of function evaluations. If it is
C             exceeded, IER = 1. (INT)
C    LB - The lower bound for the allowable solution variables. (DP(N))
C    UB - The upper bound for the allowable solution variables. (DP(N))
C         If the algorithm chooses X(I) .LT. LB(I) or X(I) .GT. UB(I),
C         I = 1, N, a point is from inside is randomly selected. This
C         This focuses the algorithm on the region inside UB and LB.
C         Unless the user wishes to concentrate the search to a par-
C         ticular region, UB and LB should be set to very large positive
C         and negative values, respectively. Note that the starting
C         vector X should be inside this region. Also note that LB and
C         UB are fixed in position, while VM is centered on the last
C         accepted trial set of variables that optimizes the function.
C    C - Vector that controls the step length adjustment. The suggested
C        value for all elements is 2.0. (DP(N))
C    IPRINT - controls printing inside SA. (INT)
C             Values: 0 - Nothing printed.
C                     1 - Function value for the starting value and
C                         summary results before each temperature
C                         reduction. This includes the optimal
C                         function value found so far, the total
C                         number of moves (broken up into uphill,
C                         downhill, accepted and rejected), the
C                         number of out of bounds trials, the
C                         number of new optima found at this
C                         temperature, the current optimal X and
C                         the step length VM. Note that there are
C                         N*NS*NT function evalutations before each
C                         temperature reduction. Finally, notice is
C                         is also given upon achieveing the termination
C                         criteria.
C                     2 - Each new step length (VM), the current optimal
C                         X (XOPT) and the current trial X (X). This
C                         gives the user some idea about how far X
C                         strays from XOPT as well as how VM is adapting
C                         to the function.
C                     3 - Each function evaluation, its acceptance or
C                         rejection and new optima. For many problems,
C                         this option will likely require a small tree
C                         if hard copy is used. This option is best
C                         used to learn about the algorithm. A small
C                         value for MAXEVL is thus recommended when
C                         using IPRINT = 3.
C             Suggested value: 1
C             Note: For a given value of IPRINT, the lower valued
C                   options (other than 0) are utilized.
C    ISEED1 - The first seed for the random number generator RANMAR.
C             0 .LE. ISEED1 .LE. 31328. (INT)
C    ISEED2 - The second seed for the random number generator RANMAR.
C             0 .LE. ISEED2 .LE. 30081. Different values for ISEED1
C             and ISEED2 will lead to an entirely different sequence
C             of trial points and decisions on downhill moves (when
C             maximizing). See Goffe et al. on how this can be used
C             to test the results of SA. (INT)
C
C  Input/Output Parameters:
```

```
C     T - On input, the initial temperature. See Goffe et al. for advice.
C         On output, the final temperature. (DP)
C     VM - The step length vector. On input it should encompass the
C          region of interest given the starting value X. For point
C          X(I), the next trial point is selected is from X(I) - VM(I)
C          to  X(I) + VM(I). Since VM is adjusted so that about half
C          of all points are accepted, the input value is not very
C          important (i.e. is the value is off, SA adjusts VM to the
C          correct value). (DP(N))
C
C  Output Parameters:
C    XOPT - The variables that optimize the function. (DP(N))
C    FOPT - The optimal value of the function. (DP)
C    NACC - The number of accepted function evaluations. (INT)
C    NFCNEV - The total number of function evaluations. In a minor
C             point, note that the first evaluation is not used in the
C             core of the algorithm; it simply initializes the
C             algorithm. (INT).
C    NOBDS - The total number of trial function evaluations that
C            would have been out of bounds of LB and UB. Note that
C            a trial point is randomly selected between LB and UB.
C            (INT)
C    IER - The error return number. (INT)
C          Values: 0 - Normal return; termination criteria achieved.
C                  1 - Number of function evaluations (NFCNEV) is
C                      greater than the maximum number (MAXEVL).
C                  2 - The starting value (X) is not inside the
C                      bounds (LB and UB).
C                  3 - The initial temperature is not positive.
C                  99 - Should not be seen; only used internally.
C
C  Work arrays that must be dimensioned in the calling routine:
C       RWK1 (DP(NEPS))  (FSTAR in SA)
C       RWK2 (DP(N))     (XP    "  " )
C       IWK  (INT(N))    (NACP  "  " )
C
C  Required Functions (included):
C    EXPREP - Replaces the function EXP to avoid under- and overflows.
C             It may have to be modified for non IBM-type main-
C             frames. (DP)
C    RMARIN - Initializes the random number generator RANMAR.
C    RANMAR - The actual random number generator. Note that
C             RMARIN must run first (SA does this). It produces uniform
C             random numbers on [0,1]. These routines are from
C             Usenet's comp.lang.fortran. For a reference, see
C             "Toward a Universal Random Number Generator"
C             by George Marsaglia and Arif Zaman, Florida State
C             University Report: FSU-SCRI-87-50 (1987).
C             It was later modified by F. James and published in
C             "A Review of Pseudo-random Number Generators." For
C             further information, contact stuart@ads.com. These
C             routines are designed to be portable on any machine
C             with a 24-bit or more mantissa. I have found it produces
C             identical results on a IBM 3081 and a Cray Y-MP.
C
C  Required Subroutines (included):
C    PRTVEC - Prints vectors.
C    PRT1 ... PRT10 - Prints intermediate output.
C    FCN - Function to be optimized. The form is
C             SUBROUTINE FCN(N,X,F)
C             INTEGER N
```

```
C            DOUBLE PRECISION  X(N), F
C            ...
C            function code with F = F(X)
C            ...
C            RETURN
C            END
C          Note: This is the same form used in the multivariable
C          minimization algorithms in the IMSL edition 10 library.
C
C  Machine Specific Features:
C    1. EXPREP may have to be modified if used on non-IBM type main-
C       frames. Watch for under- and overflows in EXPREP.
C    2. Some FORMAT statements use G25.18; this may be excessive for
C       some machines.
C    3. RMARIN and RANMAR are designed to be protable; they should not
C       cause any problems.

C  Type all external variables.
      DOUBLE PRECISION  X(*), LB(*), UB(*), C(*), VM(*), FSTAR(*),
     1                  XOPT(*), XP(*), T, EPS, RT, FOPT
      INTEGER  NACP(*), N, NS, NT, NEPS, NACC, MAXEVL, IPRINT,
     1         NOBDS, IER, NFCNEV, ISEED1, ISEED2
      LOGICAL  MAX

C  Type all internal variables.
      DOUBLE PRECISION  F, FP, P, PP, RATIO
      INTEGER  NUP, NDOWN, NREJ, NNEW, LNOBDS, H, I, J, M
      LOGICAL  QUIT

C  Type all functions.
      DOUBLE PRECISION  EXPREP
      REAL  RANMAR

C  Initialize the random number generator RANMAR.
      CALL RMARIN(ISEED1,ISEED2)

C  Set initial values.
      NACC = 0
      NOBDS = 0
      NFCNEV = 0
      IER = 99

      DO 10, I = 1, N
         XOPT(I) = X(I)
         NACP(I) = 0
10    CONTINUE

      DO 20, I = 1, NEPS
         FSTAR(I) = 1.0D+20
20    CONTINUE

C  If the initial temperature is not positive, notify the user and
C  return to the calling routine.
      IF (T .LE. 0.0) THEN
         WRITE(*,'(/,5x,''  THE INITIAL TEMPERATURE IS NOT POSITIVE. ''
     1             /,5x,''  RESET THE VARIABLE T. ''/)')
         IER = 3
         RETURN
      END IF

C  If the initial value is out of bounds, notify the user and return
```

```
C  to the calling routine.
      DO 30, I = 1, N
         IF ((X(I) .GT. UB(I)) .OR. (X(I) .LT. LB(I))) THEN
            CALL PRT1
            IER = 2
            RETURN
         END IF
30    CONTINUE

C  Evaluate the function with input X and return value as F.
      CALL FCN(N,X,F)

C  If the function is to be minimized, switch the sign of the function.
C  Note that all intermediate and final output switches the sign back
C  to eliminate any possible confusion for the user.
      IF(.NOT. MAX) F = -F
      NFCNEV = NFCNEV + 1
      FOPT = F
      FSTAR(1) = F
      IF(IPRINT .GE. 1) CALL PRT2(MAX,N,X,F)

C  Start the main loop. Note that it terminates if (i) the algorithm
C  succesfully optimizes the function or (ii) there are too many
C  function evaluations (more than MAXEVL).
100   NUP = 0
      NREJ = 0
      NNEW = 0
      NDOWN = 0
      LNOBDS = 0

      DO 400, M = 1, NT
         DO 300, J = 1, NS
            DO 200, H = 1, N

C  Generate XP, the trial value of X. Note use of VM to choose XP.
               DO 110, I = 1, N
                  IF (I .EQ. H) THEN
                     XP(I) = X(I) + (RANMAR()*2.- 1.) * VM(I)
                  ELSE
                     XP(I) = X(I)
                  END IF

C  If XP is out of bounds, select a point in bounds for the trial.
                  IF((XP(I) .LT. LB(I)) .OR. (XP(I) .GT. UB(I))) THEN
                    XP(I) = LB(I) + (UB(I) - LB(I))*RANMAR()
                    LNOBDS = LNOBDS + 1
                    NOBDS = NOBDS + 1
                    IF(IPRINT .GE. 3) CALL PRT3(MAX,N,XP,X,FP,F)
                  END IF
110            CONTINUE

C  If XP(1) [sigma(X)] is less than XP(2) [sigma(2)], set new XP(2)
C  New XP(2) is to lie somewhere between LB(2) and XP(1).
C  IT IS ASSUMED THAT LB(2) IS LESS THAN LB(1)
C  EPS is subtracted to make sure XP(2) is always less than XP(1)

 112            IF (XP(1) .LT. XP(2)) THEN
               XP(2) = LB(2) + (XP(1) - LB(2) - EPS)*RANMAR()
               GO TO 112
                END IF
```

```
C  Evaluate the function with the trial point XP and return as FP.
                CALL FCN(N,XP,FP)
                IF(.NOT. MAX) FP = -FP
                NFCNEV = NFCNEV + 1
                IF(IPRINT .GE. 3) CALL PRT4(MAX,N,XP,X,FP,F)

C  If too many function evaluations occur, terminate the algorithm.
                IF(NFCNEV .GE. MAXEVL) THEN
                   CALL PRT5
                   IF (.NOT. MAX) FOPT = -FOPT
                   IER = 1
                   RETURN
                END IF

C  Accept the new point if the function value increases.
                IF(FP .GE. F) THEN
                   IF(IPRINT .GE. 3) THEN
                      WRITE(*,'(5x,''POINT ACCEPTED'')')
                   END IF
                   DO 120, I = 1, N
                      X(I) = XP(I)
120                CONTINUE
                   F = FP
                   NACC = NACC + 1
                   NACP(H) = NACP(H) + 1
                   NUP = NUP + 1

C  If greater than any other point, record as new optimum.
                   IF (FP .GT. FOPT) THEN
                   IF(IPRINT .GE. 3) THEN
                      WRITE(*,'(5x,''NEW OPTIMUM'')')
                   END IF
                      DO 130, I = 1, N
                         XOPT(I) = XP(I)
130                   CONTINUE
                      FOPT = FP
                      NNEW = NNEW + 1
                   END IF

C  If the point is lower, use the Metropolis criteria to decide on
C  acceptance or rejection.
                ELSE
                   P = EXPREP((FP - F)/T)
                   PP = RANMAR()
                   IF (PP .LT. P) THEN
                      IF(IPRINT .GE. 3) CALL PRT6(MAX)
                      DO 140, I = 1, N
                         X(I) = XP(I)
140                   CONTINUE
                      F = FP
                      NACC = NACC + 1
                      NACP(H) = NACP(H) + 1
                      NDOWN = NDOWN + 1
                   ELSE
                      NREJ = NREJ + 1
                      IF(IPRINT .GE. 3) CALL PRT7(MAX)
                   END IF
                END IF

200          CONTINUE
300       CONTINUE
```

```
C  Adjust VM so that approximately half of all evaluations are accepted.
         DO 310, I = 1, N
            RATIO = DFLOAT(NACP(I)) /DFLOAT(NS)
            IF (RATIO .GT. .6) THEN
               VM(I) = VM(I)*(1. + C(I)*(RATIO - .6)/.4)
            ELSE IF (RATIO .LT. .4) THEN
               VM(I) = VM(I)/(1. + C(I)*((.4 - RATIO)/.4))
            END IF
            IF (VM(I) .GT. (UB(I)-LB(I))) THEN
               VM(I) = UB(I) - LB(I)
            END IF
310      CONTINUE

         IF(IPRINT .GE. 2) THEN
            CALL PRT8(N,VM,XOPT,X)
         END IF

         DO 320, I = 1, N
            NACP(I) = 0
320      CONTINUE

400   CONTINUE

      IF(IPRINT .GE. 1) THEN
         CALL PRT9(MAX,N,T,XOPT,VM,FOPT,NUP,NDOWN,NREJ,LNOBDS,NNEW)
      END IF

C  Check termination criteria.
      QUIT = .FALSE.
      FSTAR(1) = F
      IF ((FOPT - FSTAR(1)) .LE. EPS) QUIT = .TRUE.
      DO 410, I = 1, NEPS
         IF (ABS(F - FSTAR(I)) .GT. EPS) QUIT = .FALSE.
410   CONTINUE

C  Terminate SA if appropriate.
      IF (QUIT) THEN
         DO 420, I = 1, N
            X(I) = XOPT(I)
420      CONTINUE
         IER = 0
         IF (.NOT. MAX) FOPT = -FOPT
         IF(IPRINT .GE. 1) CALL PRT10
         RETURN
      END IF

C  If termination criteria is not met, prepare for another loop.
      T = RT*T
      DO 430, I = NEPS, 2, -1
         FSTAR(I) = FSTAR(I-1)
430   CONTINUE
      F = FOPT
      DO 440, I = 1, N
         X(I) = XOPT(I)
440   CONTINUE

C  Loop again.
      GO TO 100

      END
```

```
************************************************************************

      FUNCTION  EXPREP(RDUM)
C  This function replaces exp to avoid under- and overflows and is
C  designed for IBM 370 type machines. It may be necessary to modify
C  it for other machines. Note that the maximum and minimum values of
C  EXPREP are such that they has no effect on the algorithm.

      DOUBLE PRECISION  RDUM, EXPREP

      IF (RDUM .GT. 174.) THEN
         EXPREP = 3.69D+75
      ELSE IF (RDUM .LT. -180.) THEN
         EXPREP = 0.0
      ELSE
         EXPREP = EXP(RDUM)
      END IF

      RETURN
      END

************************************************************************

      subroutine RMARIN(IJ,KL)
C  This subroutine and the next function generate random numbers. See
C  the comments for SA for more information. The only changes from the
C  orginal code is that (1) the test to make sure that RMARIN runs first
C  was taken out since SA assures that this is done (this test didn't
C  compile under IBM's VS Fortran) and (2) typing ivec as integer was
C  taken out since ivec isn't used. With these exceptions, all following
C  lines are original.

C This is the initialization routine for the random number generator
C     RANMAR()
C NOTE: The seed variables can have values between:    0 <= IJ <= 31328
C                                                      0 <= KL <= 30081
      real U(97), C, CD, CM
      integer I97, J97
      common /raset1/ U, C, CD, CM, I97, J97
      if( IJ .lt. 0  .or.  IJ .gt. 31328  .or.
     *    KL .lt. 0  .or.  KL .gt. 30081 ) then
          print '(A)', ' The first random number seed must have a value
     *between 0 and 31328'
          print '(A)',' The second seed must have a value between 0 and
     *30081'
            stop
      endif
      i = mod(IJ/177, 177) + 2
      j = mod(IJ    , 177) + 2
      k = mod(KL/169, 178) + 1
      l = mod(KL,     169)
      do 2 ii = 1, 97
         s = 0.0
         t = 0.5
         do 3 jj = 1, 24
            m = mod(mod(i*j, 179)*k, 179)
            i = j
            j = k
            k = m
            l = mod(53*l+1, 169)
            if (mod(l*m, 64) .ge. 32) then
```

```
                s = s + t
              endif
              t = 0.5 * t
3          continue
           U(ii) = s
2       continue
        C = 362436.0 / 16777216.0
        CD = 7654321.0 / 16777216.0
        CM = 16777213.0 /16777216.0
        I97 = 97
        J97 = 33
        return
        end

*************************************************************************

        function ranmar()
        real U(97), C, CD, CM
        integer I97, J97
        common /raset1/ U, C, CD, CM, I97, J97
           uni = U(I97) - U(J97)
           if( uni .lt. 0.0 ) uni = uni + 1.0
           U(I97) = uni
           I97 = I97 - 1
           if(I97 .eq. 0) I97 = 97
           J97 = J97 - 1
           if(J97 .eq. 0) J97 = 97
           C = C - CD
           if( C .lt. 0.0 ) C = C + CM
           uni = uni - C
           if( uni .lt. 0.0 ) uni = uni + 1.0
           RANMAR = uni
        return
        END

*************************************************************************

        SUBROUTINE PRT1
C   This subroutine prints intermediate output, as does PRT2 through
C   PRT10. Note that if SA is minimizing the function, the sign of the
C   function value and the directions (up/down) are reversed in all
C   output to correspond with the actual function optimization. This
C   correction is because SA was written to maximize functions and
C   it minimizes by maximizing the negative a function.

        WRITE(*,'(/,7x,''THE STARTING VALUE (X) IS OUTSIDE THE BOUNDS ''
       1          /,7x,''(LB AND UB). EXECUTION TERMINATED WITHOUT ANY''
       2          /,7x,''OPTIMIZATION. RESPECIFY X, UB OR LB SO THAT  ''
       3          /,7x,''LB(I) .LT. X(I) .LT. UB(I), I = 1, N. ''/)')

        RETURN
        END

*************************************************************************

        SUBROUTINE PRT2(MAX,N,X,F)

        DOUBLE PRECISION  X(*), F
        INTEGER  N
        LOGICAL  MAX
```

```
      WRITE(*,'(5x,''  '')')
      CALL PRTVEC(X,N,'INITIAL X')
      IF (MAX) THEN
         WRITE(*,'(5x,''INITIAL F: '',/,7x,G25.18)') F
      ELSE
         WRITE(*,'(5x,''INITIAL F: '',/,7x,G25.18)') -F
      END IF

      RETURN
      END

*****************************************************************************

      SUBROUTINE PRT3(MAX,N,XP,X,FP,F)

      DOUBLE PRECISION  XP(*), X(*), FP, F
      INTEGER  N
      LOGICAL  MAX

      WRITE(*,'(5x,''  '')')
      CALL PRTVEC(X,N,'CURRENT X')
      IF (MAX) THEN
         WRITE(*,'(5x,''CURRENT F: '',G24.18)') F
      ELSE
         WRITE(*,'(5x,''CURRENT F: '',G24.18)') -F
      END IF
      CALL PRTVEC(XP,N,'TRIAL X')
      WRITE(*,'(5x,''POINT REJECTED SINCE OUT OF BOUNDS'')')

      RETURN
      END

*****************************************************************************

      SUBROUTINE PRT4(MAX,N,XP,X,FP,F)

      DOUBLE PRECISION  XP(*), X(*), FP, F
      INTEGER  N
      LOGICAL  MAX

      WRITE(*,'(5x,''  '')')
      CALL PRTVEC(X,N,'CURRENT X')
      IF (MAX) THEN
         WRITE(*,'(5x,''CURRENT F: '',2x,G24.18)') F
         CALL PRTVEC(XP,N,'TRIAL X')
         WRITE(*,'(5x,''RESULTING F: '',G24.18)') FP
      ELSE
         WRITE(*,'(5x,''CURRENT F: '',2x,G24.18)') -F
         CALL PRTVEC(XP,N,'TRIAL X')
         WRITE(*,'(5x,''RESULTING F: '',G24.18)') -FP
      END IF

      RETURN
      END

*****************************************************************************

      SUBROUTINE PRT5

      WRITE(*,'(/,5x,''TOO MANY FUNCTION EVALUATIONS; CONSIDER ''
     1          /,5x,''INCREASING MAXEVL OR EPS, OR DECREASING ''
```

```
     2          /,5x,''NT OR RT. THESE RESULTS ARE LIKELY TO BE ''
     3          /,5x,''POOR.'',/)')

      RETURN
      END

*****************************************************************************

      SUBROUTINE PRT6(MAX)

      LOGICAL  MAX

      IF (MAX) THEN
         WRITE(*,'(5x,''THOUGH LOWER, POINT ACCEPTED'')')
      ELSE
         WRITE(*,'(5x,''THOUGH HIGHER, POINT ACCEPTED'')')
      END IF

      RETURN
      END

*****************************************************************************

      SUBROUTINE PRT7(MAX)

      LOGICAL  MAX

      IF (MAX) THEN
         WRITE(*,'(5x,''LOWER POINT REJECTED'')')
      ELSE
         WRITE(*,'(5x,''HIGHER POINT REJECTED'')')
      END IF

      RETURN
      END

*****************************************************************************

      SUBROUTINE PRT8(N,VM,XOPT,X)

      DOUBLE PRECISION  VM(*), XOPT(*), X(*)
      INTEGER  N

      WRITE(*,'(/,5x,
     1  ''INTERMEDIATE RESULTS AFTER STEP LENGTH ADJUSTMENT'',/)')
      CALL PRTVEC(VM,N,'NEW STEP LENGTH (VM)')
      CALL PRTVEC(XOPT,N,'CURRENT OPTIMAL X')
      CALL PRTVEC(X,N,'CURRENT X')
      WRITE(*,'(5x,'' '')')

      RETURN
      END

*****************************************************************************

      SUBROUTINE PRT9(MAX,N,T,XOPT,VM,FOPT,NUP,NDOWN,NREJ,LNOBDS,NNEW)

      DOUBLE PRECISION  XOPT(*), VM(*), T, FOPT
      INTEGER  N, NUP, NDOWN, NREJ, LNOBDS, NNEW, TOTMOV
      LOGICAL  MAX
```

```
      TOTMOV = NUP + NDOWN + NREJ

      WRITE(*,'(/,5x,
     1  ''INTERMEDIATE RESULTS BEFORE NEXT TEMPERATURE REDUCTION'',/)')
      WRITE(*,'(5x,''CURRENT TEMPERATURE:                  '',E12.5)') T
      IF (MAX) THEN
         WRITE(*,'(7x,''MAX FUNCTION VALUE SO FAR:     '',E16.5)') FOPT
         WRITE(*,'(7x,''TOTAL MOVES:                  '',I8)') TOTMOV
         WRITE(*,'(7x,''   UPHILL:                    '',I8)') NUP
         WRITE(*,'(7x,''   ACCEPTED DOWNHILL:        '',I8)') NDOWN
         WRITE(*,'(7x,''   REJECTED DOWNHILL:        '',I8)') NREJ
         WRITE(*,'(7x,''OUT OF BOUNDS TRIALS:        '',I8)') LNOBDS
         WRITE(*,'(7x,''NEW MAXIMA THIS TEMPERATURE:'',I8)') NNEW
      ELSE
         WRITE(*,'(7x,''MIN FUNCTION VALUE SO FAR:     '',E16.5)') -FOPT
         WRITE(*,'(7x,''TOTAL MOVES:                  '',I8)') TOTMOV
         WRITE(*,'(7x,'' DOWNHILL:                    '',I8)')  NUP
         WRITE(*,'(7x,''   ACCEPTED UPHILL:           '',I8)')  NDOWN
         WRITE(*,'(7x,''   REJECTED UPHILL:           '',I8)')  NREJ
         WRITE(*,'(7x,''TRIALS OUT OF BOUNDS:         '',I8)')  LNOBDS
         WRITE(*,'(7x,''NEW MINIMA THIS TEMPERATURE:'',I8)')  NNEW
      END IF
      CALL PRTVEC(XOPT,N,'CURRENT OPTIMAL X')
      CALL PRTVEC(VM,N,'STEP LENGTH (VM)')
      WRITE(*,'(5x,'' '')')

      RETURN
      END

*****************************************************************************

      SUBROUTINE PRT10

      WRITE(*,'(/,5x,''SIMULATED ANNEALING ACHIEVED'',
     1          '' TERMINATION CRITERION OF IER = 0'',/)')

      RETURN
      END

*****************************************************************************

      SUBROUTINE PRTVEC(VECTOR,NCOLS,NAME)
C  This subroutine prints the double precision vector named VECTOR.
C  Elements 1 thru NCOLS will be printed. NAME is a character variable
C  that describes VECTOR. Note that if NAME is given in the call to
C  PRTVEC, it must be enclosed in quotes. If there are more than 10
C  elements in VECTOR, 10 elements will be printed on each line.

      INTEGER NCOLS
      DOUBLE PRECISION VECTOR(NCOLS)
      CHARACTER *(*) NAME

      WRITE(*,1001) NAME

      IF (NCOLS .GT. 10) THEN
         LINES = INT(NCOLS/10.)

         DO 100, I = 1, LINES
            LL = 10*(I - 1)
            WRITE(*,1000) (VECTOR(J),J = 1+LL, 10+LL)
  100    CONTINUE
```

```
         WRITE(*,1000) (VECTOR(J),J = 11+LL, NCOLS)
      ELSE
         WRITE(*,1000) (VECTOR(J),J = 1, NCOLS)
      END IF

 1000 FORMAT(7x, 10(G12.5,1X))
 1001 FORMAT(/,5x,A)

      RETURN
      END

*************************************************************************

#Makefile for linking and compiling all the files of the program

FTN=/usr/bin/f77
LIBS=-limsl
OBJS=entropy.o calstats.o set_img.o minimize.o anneal.o
EXEC=entropy

$(EXEC): $(OBJS)
      $(FTN) -o $(EXEC) $(OBJS) $(LIBS)

#Compile Files
anneal.o: anneal.f
      $(FTN) -c anneal.f

minimize.o: minimize.f
      $(FTN) -c minimize.f

set_img.o: set_img.f
      $(FTN) -c set_img.f

calstats.o: calstats.f
      $(FTN) -c calstats.f

entropy.o: entropy.f
      $(FTN) -c entropy.f

#Remove *.o files that have changed
clean :
      /bin/rm -f core $(EXEC) *.o

#*************************************************************************
```